

Partial response techniques and robustness in data equalization

Citation for published version (APA):

Bergmans, J. W. M. (1987). *Partial response techniques and robustness in data equalization*. [Phd Thesis 1 (Research TU/e / Graduation TU/e), Electrical Engineering]. Technische Universiteit Eindhoven.
<https://doi.org/10.6100/IR270153>

DOI:

[10.6100/IR270153](https://doi.org/10.6100/IR270153)

Document status and date:

Published: 01/01/1987

Document Version:

Publisher's PDF, also known as Version of Record (includes final page, issue and volume numbers)

Please check the document version of this publication:

- A submitted manuscript is the version of the article upon submission and before peer-review. There can be important differences between the submitted version and the official published version of record. People interested in the research are advised to contact the author for the final version of the publication, or visit the DOI to the publisher's website.
- The final author version and the galley proof are versions of the publication after peer review.
- The final published version features the final layout of the paper including the volume, issue and page numbers.

[Link to publication](#)

General rights

Copyright and moral rights for the publications made accessible in the public portal are retained by the authors and/or other copyright owners and it is a condition of accessing publications that users recognise and abide by the legal requirements associated with these rights.

- Users may download and print one copy of any publication from the public portal for the purpose of private study or research.
- You may not further distribute the material or use it for any profit-making activity or commercial gain
- You may freely distribute the URL identifying the publication in the public portal.

If the publication is distributed under the terms of Article 25fa of the Dutch Copyright Act, indicated by the "Taverne" license above, please follow below link for the End User Agreement:

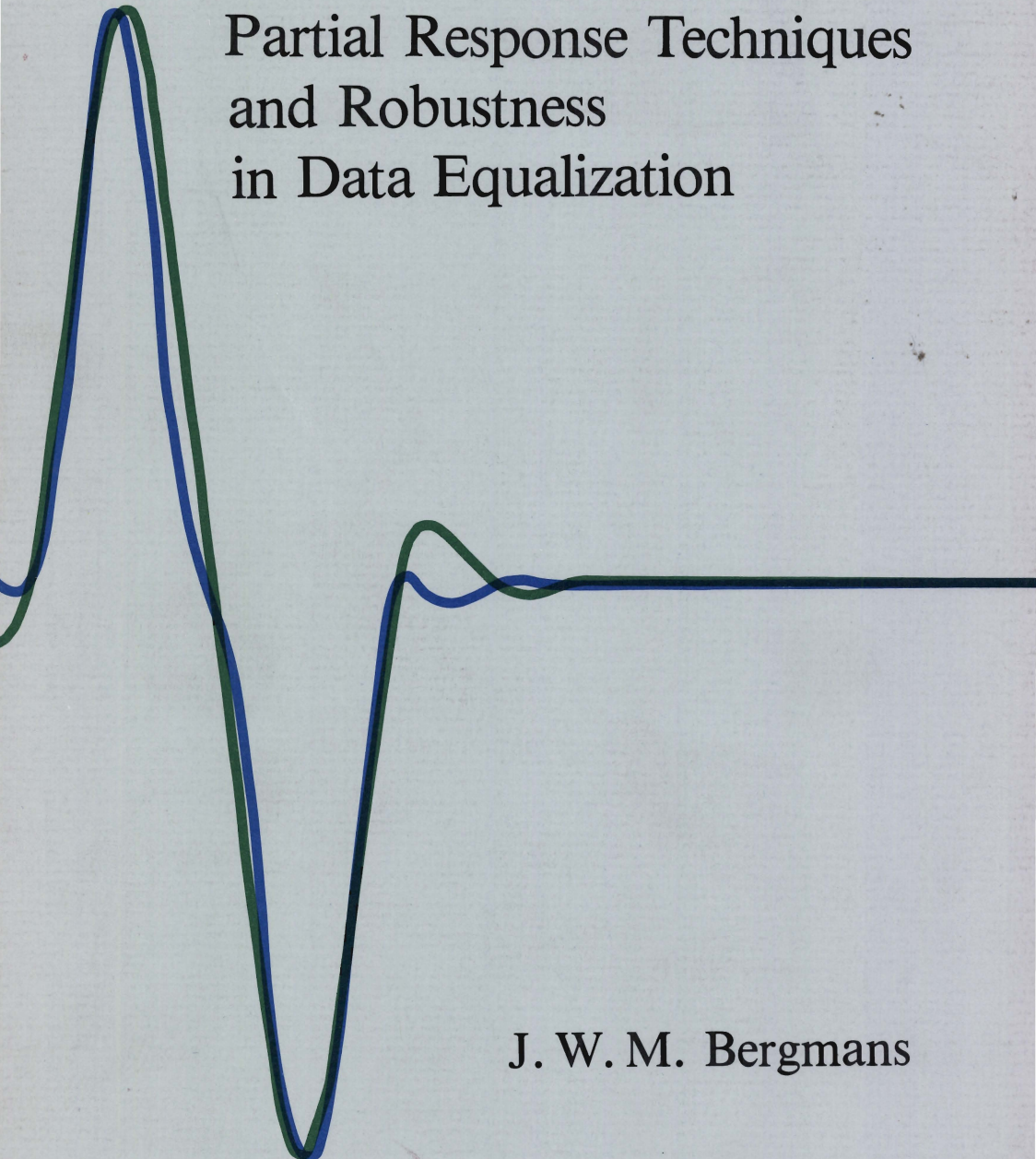
www.tue.nl/taverne

Take down policy

If you believe that this document breaches copyright please contact us at:

openaccess@tue.nl

providing details and we will investigate your claim.



Partial Response Techniques
and Robustness
in Data Equalization

J. W. M. Bergmans

Partial Response Techniques and Robustness in Data Equalization

J. W. M. Bergmans

Partial Response Techniques and Robustness in Data Equalization

Proefschrift

ter verkrijging van de graad van doctor aan de
Technische Universiteit Eindhoven, op gezag van
de rector magnificus, prof. dr. F. N. Hooge,
voor een commissie aangewezen door het college
van dekanen in het openbaar te verdedigen op
dinsdag 8 september 1987 te 14.00 uur

door

Johannes Wilhelmus Maria Bergmans

geboren te Tilburg

This thesis was approved by the promotor
Prof. Dr. Ir. J.P.M. Schalkwijk and Prof. Dr. J.K. Wolf

Summary	vii
Acknowledgement	viii
1. Introductory chapter	1
2. Discrete-time models for digital magnetic recording	14
3. Partial response equalization	42
4. A simulation study of intersymbol interference cancellation	79
5. Performance consequences of timing errors in digital magnetic recording	88
6. A method of designing robust linear partial response equalizers	115
7. Robust data equalization, fractional tap spacing and the Zak transform	146
Biography	193
Samenvatting	194

Chapters 2,3 and 5-7 are reprinted from Philips Journal of Research. Chapter 4 is reprinted from AEÜ (Electronics and Communication). Chapters 4 and 7 are co-authored by Y.C. Wong and A.J.E.M. Janssen, respectively. Parts of this material were also published in Proc. ICC'86, Toronto, Canada, 176 (1986), IEEE Trans. Magn. **22**, 157 (1986), and Proc. MTNS'87, Phoenix, Arizona, 1987.

SUMMARY

Data equalizers serve to combat the intersymbol interference (ISI) and noise which arise in digital transmission and recording systems. They comprise one or more filters, whose combined action causes an estimate of the transmitted data sequence to arise, from which decisions are extracted by means of a detector.

This thesis explores the application of partial reponse techniques in data equalization. These techniques involve the introduction of a controlled amount of ISI and the detection of a correlated data sequence with an increased number of amplitude levels, from which the original transmitted data sequence can be recovered by means of a deterministic inverse mapping. Among other things, it is shown that this indirect approach may lead to advantages in terms of noise immunity and error propagation.

The scope is then extended to the robustness of data equalizers, i.e. their ability to function properly in the presence of variations of the system parameters. This property is particularly important for non-adaptive implementations, as applied at high data rates or when the admissible power consumption is restricted. After analyzing the robustness of various equalization and detection methods in a conventional dimensioning, the optimally robust versions of the most commonly used equalizers are derived relative to a mean-square measure of performance.

The analytical results of the thesis are illustrated by means of performance comparisons for a class of digital magnetic recording systems, for which a simple discrete-time characterization is first derived. Apart from conventional versions of the equalizers under study, these comparisons also cover maximum-likelihood sequence detection and a recently introduced method called ISI cancellation.

ACKNOWLEDGEMENT

I am indebted to the management of Philips Research Laboratories for giving me the opportunity to prepare this Ph.D. thesis.

It is a pleasure to thank Prof. J.P.M. Schalkwijk for his effort spent on yet another external customer, and to thank Prof. J.K. Wolf for accepting the second promotorship and for undertaking the consequential journey. I am also grateful to Prof. W.F.G. Mecklenbräuker for his careful review of a preliminary version of the thesis.

The work presented here has been influenced appreciably by the characteristic ideas of Kees Schouhamer Immink, whose constructive criticism has been very helpful to me. In preparing the thesis, I have also appreciated the competent and ever available mathematical and linguistic advice of Guido Janssen. Among the influences of other colleagues implicit here, I especially wish to accredit the useful comments and suggestions of Peter van der Wurf.

Finally, I thank my Polish treasure for her assistance and endurance.

INTRODUCTORY CHAPTER

1. Equalization methods

In the unfolding information society¹⁾, transportation of information (in place or time) takes place at any level between the global (radio, cable and satellite) communication networks that are already covering the world like spiderwebs, down to the growing arrays of electronic equipment that fill the homes of nearly every individual. Increasingly, information of any sort (voice, audio and TV signals serving as examples) is first translated into a digital form before it is transported as a sequence of discrete message elements in a process which is commonly referred to as data transmission²⁾. Not only does this discrete form suit the nature of existing technology well, but it also allows communication to become more reliable, as the intrinsic uncertainty associated with the distinction between a continuum of possible messages is avoided by discretization³⁾. Historically confined to such fields as radio and telephone modems⁴⁾, the application area of data transmission is now entering a phase of rapid diversification, covering e.g. satellite communications⁵⁾, fibre optics⁶⁾ and the emerging Integrated Services Digital Network (ISDN)⁷⁾, wherein vast amounts of high-speed digital data traverse the subscriber cables in the local telephone network. Perhaps less obvious, aspects of data transmission are also central to digital magnetic and optical recording systems, where digital streams of information are stored as patterns of magnetization and chains of shallow deflections, respectively^{8,9)}. Until recently applied almost exclusively for the background storage of computer-related data, digital recording now holds out great promise for the storage of audio and video information, Compact Disc being only a forerunner of upcoming generations of equipment of this kind^{9,10)}.

Central to the data transmission process, the analog channels across which information is conveyed generally deliver corrupted and transformed versions of their input waveforms. Among the possible transmission impairments, noise and interference between neighbouring message elements (referred to as Inter-

Symbol Interference or ISI) are almost always predominant, because reasons of economy designate signal power and bandwidth to be scarce commodities¹¹⁾. Also, nonlinearities and variations of the channel parameters may be present²⁾. Among the various (and often conjunctively applicable) methods available to handle these transmission problems, equalization methods play an important and conspicuous role^{2,4)}. In a general definition^{4,12)}, a data equalizer is a constellation of one or more filters applied at the receiving end of the system, whose purpose it is to mitigate the combined effect of ISI and noise. By proper instrumentation, data equalizers can additionally serve to counter channel parameter variations and channel nonlinearities²⁾.

This thesis presents a number of theoretical extensions to the state of the art in data equalization. Originally motivated by the equalization problems that arise in high-density digital magnetic recording, these extensions are presented and analyzed here in a general form, and their virtues are quantified by means of numerical recurrences to their source of inspiration. Before the contents of the thesis are described in more detail, the following section first establishes a suitable base of reference by sketching a historical perspective of data equalization and some closely related concepts, and by tracing the development of digital magnetic recording back in time, with emphasis on the aspects that are relevant to data equalization.

2. A historical perspective of data equalization

2.1. Linear equalization

The earliest roots of data equalization lie in the annals of telegraphy^{13,14)}. After Heaviside's analysis in 1887 of the properties of transmission lines¹⁵⁾, implicit forms of equalization emerged in the form of adding inductance to long (e.g. submarine) cables so as to improve their frequency response¹¹⁾. In the twenties of this century, Küpfmüller and Nyquist were perhaps first in pointing out the capabilities of a linear filter to mitigate the harmful effects of intersymbol interference^{16,17,18)}. According to Nyquist's classical first criterion for distortionless transmission¹⁸⁾, all ISI can be eliminated prior to detection by means of a linear filter which essentially equalizes the characteristics of the channel across a certain frequency range which, for a low-pass channel, extends from zero to somewhat beyond half of the signalling rate. Reflecting the nature of the cable networks that were used as transmission media in those days, Nyquist refrained from considering a second disturbance which sets a fundamental limit to the attainable data throughput, viz. noise. Although some important notions with regard to this disturbance were already put forward by Hartley around that time¹⁹⁾, nearly two decades elapsed before it was recog-

nized that in single pulse transmission, i.e. in the absence of ISI, noise can be optimally suppressed by a filter whose impulse response is the time inverse of the channel impulse response^{20,21}). Having an amplitude-frequency characteristic equal to that of the channel, this so-called matched filter is in a sense the opposite of the linear equalizer, which approximates the reciprocal of the channel characteristics over a certain frequency range. Hence, although both ISI and noise can be optimally suppressed by means of a linear filter when occurring individually, their combined suppression poses conflicting requirements, whose disparity is proportional to the amplitude distortion arising in the channel. Explained here heuristically, this insight emerged analytically in the early sixties, when the structure, dimensioning and performance of the optimum linear equalizer in the presence of a mixture of ISI and noise were first derived^{22,23,24}). In later years, a mainstream of work has been directed towards the achievement of noise suppression figures which more closely approach the matched filter ideal by treating ISI in a different manner. This is possible by making use of its strong structural properties, some of which have actually been recognized very early in history. These methods and their underlying concepts will now be discussed in order of increasing performance (and, unavoidably, complexity).

2.2. Partial response techniques

Already in the late nineteenth century it was observed that, relative to the maximum operating speed at which telegraph signals could be clearly received "doubling the dotting speed" would result in a received signal assuming three (as opposed to the regular two) values: positive, negative and zero (ref. 11, pp. 123-124). By using a suitable (manual and later mechanical) decoding procedure, the transmitted data could in principle be unambiguously reconstructed from this ternary signal. After various recurrences to the topic^{18,11}), this concept was generalized in the sixties into what is nowadays known as 'partial response techniques'^{25,26,27,28}). Involving the use of an integer-valued system impulse response which extends over a small number of symbol intervals, partial response techniques entail the occurrence of a controlled quantity of ISI, thus causing a received signal with a somewhat increased number of amplitude levels to arise, from which the original data can be recovered by means of a simple (symbol-by-symbol) decoding procedure. In order for this procedure to be memoryless so as to prevent error propagation from occurring, a simple pre-coding operation must be added at the transmitting end of the system, which changes neither the statistics nor the alphabet of the data sequence²⁷). Traditionally thought of as allowing an increased information

throughput in exchange for a reduced margin against noise^{4,11,29}), partial response techniques can also be viewed as a means of providing additional freedom of equalization by allowing a well-defined quantity of ISI to remain untackled before detection, thereby potentially reducing noise enhancement. As it no longer entails a spectral smoothing operation, the common term "equalization" is strictly speaking inappropriate to designate the conditioning of ISI that takes place here. This historical abuse prevails even more strongly in the case of the decision feedback equalizer (DFE), which will now be considered.

2.3. Decision feedback equalization

Like partial response techniques, the historical origins of decision feedback equalization can also be traced back into the pre-Nyquist era^{30,31,32}), when it was recognized that reception of cable telegraph signals was mainly hampered by interference due to symbols that had already been detected. By feeding these "past" digits into a properly adjusted feedback filter (FBF), an estimate would be formed of this post-cursive ISI, that could next be subtracted from the incoming signal. Accuracy of compensation being an important prerequisite for the success of this technique, the immature state of technology precluded it from becoming widely applied until adaptive filtering methods became available in the late sixties. Also, considerable time elapsed before it was recognized that the technique, when combined with an additional prefilter, would enable a significant improvement in noise suppression relative to the linear equalizer³³). Conceptually, the optimum prefilter acts as a low-pass phase equalizer, transforming all pre-cursive ISI into post-cursive ISI that can in turn be removed by the FBF^{34,35,36}). Having a smooth amplitude-frequency characteristic across the band of interest and hence causing essentially no noise enhancement, this prefilter in a sense takes the middle between the inverse modelling (with associated noise enhancement) performed by the linear equalizer, and the duplication of the channel amplitude-frequency characteristics (with associated noise reduction) realized by the matched filter. Designated Decision Feedback Equalization³⁷) (although again no spectral smoothing is involved), this method achieves its noise advantage at the cost of allowing decision errors to induce further errors through the backward coupling of the FBF. Although this error propagation process is difficult to analyze, theoretical considerations and practical experience have shown that, on typical channels, error propagation is not catastrophic and in fact degrades the achieved transmission quality only slightly^{12,37,38}). Now that its performance benefits are no longer disputed, the DFE is currently evolving into a major equalization workhorse. This applies in

particular for ISDN transmission systems, where advantage is taken of the natural suitability of the FBF to adaptive, digital implementation⁸⁹).

2.4. ISI cancellation

As the DFE prefilter achieves the largest possible noise suppression subject to the condition of suppressing all pre-cursive ISI, a further improvement of noise suppression is only feasible at the cost of allowing such ISI to arise. Although its influence can intrinsically not be undone by means of a feedback filter, pre-cursive ISI can be intentionally removed by means of an additional ("forward") filter which is excited by preliminary decisions that have been produced beforehand using a separate (e.g. decision feedback) equalizer. Although its roots date back nearly two decades⁴⁰), the fully fledged version of this concept, referred to as ISI cancellation or data-aided equalization, has only recently been established and elaborated^{41,42,43}). Subject to the assumption that all arising ISI is perfectly eliminated by the combined action of the forward and feedback filters, the prefilter need only be concerned with noise and hence ideally equals a matched filter^{41,42}). Unfortunately, simulations reveal that erroneous preliminary decisions which propagate through the forward filter cause decision errors in the final detection stage to be far more likely than anticipated on the basis of the naive assumption of perfect ISI elimination⁴³). For this reason, the precise merits of ISI cancellation are yet to be uncovered.

2.5. Maximum-Likelihood Sequence Detection (MLSD)

In all equalization methods, ISI is regarded as a nuisance whose effect has to be attacked by some means. For the sake of completeness, we shall now also trace the development of an alternative approach called Maximum Likelihood Sequence Detection (MLSD), which does not entail linear filtering, although it is often applied in conjunction with equalization.

In MLSD, ISI is essentially regarded as an implicit form of coding, causing the incoming data sequence to be transformed into an "encoded" signal with a well-defined, highly specific correlation structure. From this point of view, optimum detection in the presence of ISI and additive noise amounts to choosing the data sequence whose "encoded" version most closely matches the received signal. As according to this MLSD perspective ISI becomes in a sense invisible, the attained performance basically corresponds to that of the matched filter in single pulse transmission⁴⁸). Only for channels with very severe amplitude distortion is confusion likely between candidate sequences which differ in more than one position, in which case a loss relative to optimum isolated pulse transmission is incurred²). Through explained easily, MLSD

requires in its straightforward implementation the calculation of a likelihood or distance metric for all possible data sequences. Already for short message lengths, the exploding cardinality of this set renders this approach absolutely prohibitive. The earliest breakthrough in MLSD occurred halfway through the sixties, when it became obvious that this exponential dependence can actually be brought down to linear proportions by carrying MLSD out in a sequential fashion⁴⁴). Still involving an intimidating workload, the algorithm concerned was followed in the early seventies by the Viterbi algorithm, an offspring from methods in dynamic programming^{45,46,47,48,49}). Having a complexity which is independent of the message length and which grows exponentially with the extent of the ISI (i.e. the channel memory duration expressed in symbol intervals), the Viterbi detector finally rendered MLSD practicable for systems at low speeds and suffering from ISI with a restricted extent. Nevertheless, in many instances the fully fledged Viterbi algorithm is still orders of magnitude more complicated than the equalizers discussed above. For this reason, subsequent research has aimed at establishing further complexity reductions, thereby inevitably sacrificing some performance⁵⁰). Apart from reduced-state Viterbi detection^{51,52}), wherein the number of sequences kept track of is dramatically reduced, channel memory truncation^{53,54}) has proved to be an effective means to this end. Involving the use of linear^{53,54}) or decision feedback^{55,56}) equalization, the latter collection of methods transforms the impulse response of the channel into a substantially shorter Desired Impulse Response (DIR), which has to be chosen appropriately in order to keep the performance degradation in terms of noise suppression and/or error propagation as small as possible. By choosing a DIR among the class of integer-valued responses discussed previously, this approach can alternatively be viewed as a substitution of the memoryless threshold detector normally used in partial response equalization by a relatively simple MLSD, thus establishing an improvement of the effective signal-to-noise ratio, which ranges up to about 3 dB for the commonly used pseudoternary class of partial responses⁴⁵).

2.6. Parameter variations

If no special measures are taken, serious performance degradations may be incurred if an equalizer or detector has been dimensioned to perform well for the nominal characteristics of the channel, while the actual characteristics exhibit a deviation^{11,78}). Because this sensitivity problem is generally greater for the advanced equalization methods than for the simpler ones (as will be illustrated in later chapters of this thesis), it has undoubtedly delayed the development and application of the former category. As a first step to its

solution, early work has sought an improvement of the resistance of the linear equalizer to parameter variations, at the expense of some performance in the nominal situation⁵⁷).

Only two decades ago, theory and technology were ripe for the emergence of the most natural solution to the parameter variation problem, viz. adaptive techniques. These techniques enable the dimensioning of the equalizer (or detector) to be adapted according to an estimate of the actual channel parameters which is extracted dynamically from the received signal. Particularly the Least-Mean-Square (LMS) algorithm^{58,59}) and many derivatives thereof⁶⁰) have become widely applied. Recently, more powerful adaptation methods have been appearing whose merits basically lie in an improved convergence speed, mostly achieved at a substantial expense to hardware complexity^{60,61}).

Even in the presence of an adaptation mechanism it may be difficult to counter specific variations due to inherent restrictions set by the structure of the equalizer or detector used. For example, the occurrence of timing errors can only partly be compensated by the symbol interval-spaced transversal equalizers that were commonly applied up to the mid seventies¹²). By that time, it became clear that fractionally-spaced equalizers, whose tap spacing is (often considerably) smaller than a symbol interval, are so much more flexible than the symbol interval-spaced equalizer, that their adaptive versions can effectively counter variations (notably timing errors) that were formerly beyond grasp^{62,63}). For this reason, adaptive equalizers are nowadays often equipped with this feature¹²).

2.7. Nonlinearities

Although ISI normally stems from linear interaction between transmitted symbols, it may happen that a channel causes an additional nonlinear portion of ISI to arise. In their basic forms, the methods discussed before can withstand no more than a restricted quantity of nonlinear interference. During the last decade, several adaptive methods have been proposed to overcome this shortcoming. For the linear equalizer, the addition of appropriately (and adaptively) dimensioned quadratic and third order nonlinearities (Volterra kernels) has proved to be an effective, though hardware-expensive, approach⁶⁴). By contrast, the use of a table lookup feedback filter enables the DFE to handle nonlinearities of the trailing type as a natural consequence of the ability of this filter structure to handle any nonlinear input-output relation⁶⁵). Apart from being faster, the table lookup filter is in fact less complicated than its transversal counterpart for the short feedback filter lengths that are often applied in practice. Analogously, by implementing both the forward and the feedback

filter of the ISI canceller in a (preferably combined) table lookup structure, this equalizer manifests itself as a powerful tool for coping with a wide class of nonlinearities⁶⁶).

3. A historical perspective of digital magnetic recording

The origin of magnetic recording can be traced back to its first description by Smith in 1888⁶⁷), and to its first embodiment in 1898 by Poulsen in the form of his "Telegraphone"⁶⁸), for which he received the Grand Prix at the 1900 Paris World Exhibition. Originally intended for the storage and reproduction of analog signals, soon after the first world war the (U.S.) military authorities recognized the value of the magnetic storage medium (which at that time took the form of steel wire) for the recording at increased speeds of telegraph signals, thereby giving birth to digital magnetic recording. After a period of slow evolution, the advent and rapid growth of digital computing in the second half of the forties ushered digital magnetic recording into the data storage scene. Supported by the need to provide random data access, the initially developed tape machines were followed in 1956 by the first magnetic disk drive, IBM's RAMAC 350⁶⁹). Since then, an ever-growing stream of new magnetic data storage equipment has flooded the market, culminating in the present generations of equipment where storage capacities, data reliability and information densities have increased by several orders of magnitude over their earliest predecessors^{8,10}). In the near future, confirming the maturity of the discipline, digital magnetic recording will form the heart of several systems for the storage of high-quality audio and video signals^{70,71}).

In the course of this commercial development, increasingly general and refined models have been constructed to describe the magnetic recording process. For systems using longitudinal magnetization and a replay head of the differentiating (coil pick-up) type, foundations were laid in the fifties by Wallace and Karlqvist, who studied the influence of the spacing of the recording medium and the replay head, the gap size of the replay head and the thickness of the medium upon the transfer characteristics of the system^{72,73}). In later years, a plethora of refinements and extensions (for e.g. perpendicular magnetization and magneto-resistive heads) to their baseline models has pervaded the technical literature^{8,74}). Remarkably, although magnetic materials and mechanical constructions have greatly changed since then, the models of Karlqvist and Wallace still appear to be a good description of the major transfer impairments encountered in much present-day equipment^{8,74,75}). Although the noise arising in the recording channel can generally be considered as additive and Gaussian, its precise characteristics are often hard to predict because of its

many constituents, of which only some (e.g. the medium-induced noise) have been modelled in a general fashion⁸).

4. Outline of the thesis

Following the preceding historical review, the contents of this thesis can now be previewed in more detail. As a comprehensive illustration of the origins of the disturbances that equalization methods are expected to deal with, chapter 2 is concerned with an important practical category of digital magnetic recording systems, whose representatives are used in all later chapters to judge the merits of distinct equalization methods. The chapter opens by describing the mechanisms in the recording process that give rise to ISI and noise, and by summarizing the continuous-time models that have been conceived in the last decades (on the basis of physical and electromagnetic considerations) to describe these phenomena analytically⁸). Making use of a well-known sufficient statistic of the resulting equalizer input signal³), the remainder of the chapter translates these models into discrete-time models which are equivalent in the sense of detection theory. As a canonic representation of the information transfer that takes place across the recording channel, these discrete-time models are closely related to the optimum performances of all possible equalizer types²). Their remarkably simple form moreover provides direct insight into the influence of several system parameters upon the transmission quality and upon the equalization problems that are to be expected, and this insight can in turn be used as a guideline for the system designer.

Following this baseline work, chapter 3 is devoted to the use of partial response techniques^{26,27,28}) in equalization. Viewing them as being essentially embodied in the equalizer only, the chapter complements their traditional interpretation as a "signalling" or "coding" method^{29,76}). For the linear equalizer, a mean-square analysis that is carried through on the basis of this novel perspective reveals that the use of partial response techniques may be beneficial for the transmission quality. This finding contradicts the belief^{4,11,29}) that partial response techniques unavoidably entail a lower transmission quality, in return for their capability of rendering data transmission at the Nyquist rate practicable. Expanding upon their traditional use in conjunction with linear equalization, the chapter proceeds by showing that partial response techniques can also be combined with the more sophisticated decision-feedback method of equalization³⁷). Sharply contrasting with the linear equalizer situation, it is found that no mean-square performance advantages can originate from applying partial response techniques here, leaving only potential advantages in the domain of error propagation. Concluding the chapter, the developed theory

is verified by applying it to the equivalent models derived in chapter 2, and by validating the so-obtained quantitative equalizer rankings by means of Monte Carlo simulations.

Although the angle of incidence taken and the extensions studied in chapter 3 are new, the basic methods treated are traditional, and their merits and characteristics are well understood²). By contrast, chapter 4 is concerned with the relatively new concept of ISI cancellation, whose performance merits, as noted before, have been the subject of both theoretical speculations^{41,42}) and preliminary numerical investigations⁴³). By carrying out an extensive and refined set of simulations for several of the recording channels of chapter 2, chapter 4 establishes a number of important new insights relating to ISI cancellation. For example, it is shown that the existing theoretical predictions^{41,42}) are grossly optimistic in accrediting a performance level to the canceller equal to or exceeding that of the most powerful receiver type known to date, viz. the Maximum-Likelihood Sequence Detector (MLSD). Furthermore, a broad category of channels is demarcated for which the ISI canceller essentially parallels the decision feedback equalizer (DFE) in performance and hence disqualifies itself from application in view of its more involved implementation.

The remainder of the thesis centers around the robustness of equalizers, i.e. their ability to withstand variations of system parameters. In recent years, a renewed interest can be observed in this topic in the context of digital recording, where rapid parameter variations, high data rates and power consumption restrictions may preclude adaptation methods from being either beneficial or at all applied⁷⁸). To place the subject in perspective, chapter 5 presents an analysis of the sensitivity to timing errors of conventional equalization and detection methods when applied to the category of digital magnetic recording systems of chapter 2. This analysis is comprehensive in that it covers the vast majority of methods existing to date, and because it is largely cast in a general form which makes specialization to other types of systems and variations a straightforward undertaking. Complying with experimental observations⁷⁷), the performance calculations and Monte Carlo simulations which are carried out at the end of the chapter to validate the anticipated sensitivity behaviour, indicate that all methods studied may already induce serious performance degradations in the presence of relatively small timing errors. The rate of degradation generally depends strongly upon both the nominal system parameters and the applied equalization or detection method. Furthermore, variation of other parameters, such as the system gain (whose influence is studied in passing in chapter 3), may lead to a different sensitivity ranking. Thus, it is a priori difficult, if not impossible, to make more than the global prediction that,

in a conventional dimensioning, the simplest equalization methods are frequently the least sensitive ones. Clearly, more control over the robustness of equalizers would be desirable. To this end, chapter 6 derives a general solution to this dimensioning problem for the linear equalizer, thereby extending more fragmentary work which dates back to the pre-adaptive era⁵⁷⁾. More in particular, for both the partial and the full response situation, this chapter derives the structure, dimensioning and performance of the equalizer which is optimum relative to a mean-square performance measure that takes account of parameter variations. Also, it outlines an efficient numerical method for calculating this dimensioning. The potential of the so-identified design method is then illustrated by a recurrence to the recording environment of chapter 5, for which in many instances significant improvements of the timing margin are found to be within reach at a modest expense to the nominal performance.

In a treatment which also covers several of the results of the preceding chapters, the final chapter of the thesis applies a novel tool to the signal processing stage in order to be able to identify the optimally robust decision feedback equalizer (DFE). This tool is the Zak transform, a linear time-frequency signal representation originating from quantum mechanics, which is in between the Fourier integral for continuous-time signals and the Fourier series for discrete-time ones.* As such, it is in a natural way capable of reflecting both the continuous- and the discrete-time aspects inherent in data transmission, where a data stream is converted into a continuous-time signal and decisions are taken at discrete, equidistant moments. While progressing towards its main result, the chapter ascertains the merits of the Zak transform as a tool for use in data transmission by re-deriving several classical results in this field in a general and compact way. The chapter concludes by performing a numerical comparison of the optimally robust DFE and its conventional counterpart for the recording environment of the preceding two chapters.

REFERENCES

- 1) J. Naisbitt, *Megatrends*, Warner Books, New York, 1982.
- 2) J. Proakis, *Digital Communications*, McGraw-Hill, New York, 1983.
- 3) J. Zencraft and I. Jacobs, *Principles of Communication Engineering*, Wiley, New York, 1965.
- 4) R. W. Lucky, J. Salz and E. J. Weldon, Jr., *Principles of Data Communication*, McGraw-Hill, New York, 1968.
- 5) V. K. Bhargawa, D. Haccoun, B. Matyas and P. P. Nuspl, *Digital Communications by Satellite*, New York, Wiley, 1981.
- 6) J. M. Senior, *Optical Fiber Communications*, Prentice-Hall, Englewood-Cliffs, N.J., 1985.
- 7) *IEEE Communications Magazine*, Vol. 24, no. 3, March 1986.
- 8) J. C. Mallinson, *Proc. IEEE* 64, 196 (1976).

* The use of the Zak transform for deriving the optimally robust DFE was suggested by A. J. E. M. Janssen, who also co-authored the chapter.

- 9) G. Bouwhuis, J. Braat, A. Huiser, J. Pasman, G. van Rosmalen and K. Schouhamer Immink, Principles of Optical Disc Systems, Adam Hilger Ltd., Bristol and Boston, 1985.
- 10) R. W. Wood, Proc. IEEE 74, 1557 (1986).
- 11) W. R. Bennett and J. R. Davey, Data Transmission, McGraw-Hill, New York, 1965.
- 12) S. U. Qureshi, Proc. IEEE 73, 1349 (1985).
- 13) G. B. Prescott, History, Theory and Practice of the Electric Telegraph, Ticknor and Fields, Boston, 1866.
- 14) J. W. Freebody, Telegraphy, Sir Isaac Pitman & Sons. Ltd., London, 1958.
- 15) O. Heaviside, Electrical Papers, MacMillan & Co., Ltd., London, 1892.
- 16) K. Küpfmüller, Elek. Nachr.-Techn. 1, 124 (1924).
- 17) H. Nyquist, Bell Syst. Tech. J. 3, 324 (1924).
- 18) H. Nyquist, Trans. AIEE (Commun. Electron.) 47, 617 (1928).
- 19) R. V. L. Hartley, Bell Syst. Tech. J. 7, 535 (1928).
- 20) D. O. North, Rept. PTR-6C, RCA Laboratories, June 1943.
- 21) J. Van Vleck and D. Middleton, J. Appl. Phys. 17, 940 (1946).
- 22) D. W. Tufts, Proc. IEEE 53, 248 (1965).
- 23) J. W. Smith, Bell Syst. Tech. J. 44, 2263 (1965).
- 24) M. R., Aaron and D. W. Tufts, IEEE Trans. Inform. Theory IT-22, 26 (1966).
- 25) M. R. Aaron, Bell Syst. Tech. J. 41, 99 (1962).
- 26) A. Lender, IEEE Trans. Commun. Electron. 82, 214 (1963).
- 27) P. J. van Gerwen, Philips Res. Rept. 20, 469 (1965).
- 28) E. R. Kretzmer, IEEE Trans. Commun. Technol. COM-14, 67 (1966).
- 29) P. Kabal and S. Pasupathy, IEEE Trans. Commun. CO-23, 921 (1975).
- 30) R. C. Mathes, U. S. Patent 1 295 553, Feb. 25, 1919.
- 31) A. A. Clokey, Bell Syst. Tech. J. 6, 402 (1927).
- 32) W. R. Bennett, 1955 Proc. of the Symposium on Modern Network Synthesis, pp. 45-61.
- 33) M. E. Austin, M. I. T. Res. Lab. Electron., Cambridge, Mass., Quart. Progr. Rept. 84, pp. 227-243, April 1967. Also Sc. D. Dissertation, M.I.T., Cambridge, Mass., May 1967.
- 34) P. Mosen, IEEE Trans. Inform. Theory IT-17, 56 (1971).
- 35) R. Price, in Rec. ICC-72, pp. 22.12-22.17, Philadelphia, PA, 1972.
- 36) J. Salz, Bell Syst. Tech. J. 52, 1341 (1973).
- 37) C. A. Belfiore and J. H. Park, Jr., Proc. IEEE 67, 1143 (1979).
- 38) D. L. Duttweiler, J. E. Mazo and D. G. Messerschmitt, IEEE Trans. Inform. Theory IT-20, 490 (1974).
- 39) K. J. Wouda, S. J. M. Tol, P. Zuidweg and O. Reingruber, Proc. ISSLS'86, pp. 250-255, Tokyo, Japan, 1986.
- 40) J. G. Proakis, IEEE Symp. on Adaptive Processes, Decision and Control, pp. XV.2.1-5, 1970.
- 41) A. Gersho and T. Lim, Bell Syst. Tech. J. 60, 1997 (1981).
- 42) S. Mueller and J. Salz, Bell Syst. Tech. J. 60, 2023 (1981).
- 43) K. Wesolowski, IEEE Trans. Commun. COM-33, 425 (1985).
- 44) R. W. Chang and J. C. Hancock, IEEE Trans. Inform. Theory IT-12, 463 (1966).
- 45) H. Kobayashi, IBM J. Res. Develop. 15, 64 (1971).
- 46) H. Kobayashi, IEEE Trans. Inform. Theory IT-17, 586 (1971).
- 47) J. K. Omura, Inform. Sci. 3, 243, (1971).
- 48) G. D. Forney, Jr., IEEE Trans. Inform. Theory IT-18, 363 (1972).
- 49) G. D. Forney, Jr., Proc. IEEE 61, 268 (1973).
- 50) A. D. Fagan, F. D. O'Keane, IEE Proc. 133, Pt. F., 535 (1986).
- 51) F. L. Vermeulen and M. E. Hellman, in Proc. ICC-74, pp. 37B.1-37B.9, Minneapolis, MN, 1974.
- 52) G. J. Foschini, IEEE Trans. Inform. Theory IT-23, 605 (1977).
- 53) S. U. H. Qureshi and E. E. Newhall, IEEE Trans. Inform. Theory IT-19, 448 (1973).
- 54) D. D. Falconer and F. R. Magee, Jr., Bell Syst. Tech. J. 52, 1541 (1973).
- 55) W. U. Lee and F. S. Hill, IEEE Trans. Commun. COM-25, 971 (1977).
- 56) A. Duel and C. Heegard, Proc. 23rd Annual Allerton Conf. on Communication, Control and Computing, 1985.
- 57) R. A. Gonsalves and D. W. Tufts, IEEE Trans. Commun. Technol. COM-16, 375 (1968).
- 58) B. Widrow and M. Hoff, Jr., IRE WESCON Convention Record, Pt. 4, pp. 96-104, 1960.
- 59) R. W. Lucky, Bell Syst. Tech. J. 44, 547 (1965).

- ⁶⁰⁾ B. Widrow and S. D. Stearns, *Adaptive Signal Processing*, Prentice-Hall, Englewood Cliffs, N.J., 1984.
- ⁶¹⁾ C. F. N. Cowan and P. M. Grant, *Adaptive Filters*, Prentice-Hall, Englewood Cliffs, N. J. 1985.
- ⁶²⁾ L. Guidoux, *L'Onde Electronique* **55**, 9 (1975).
- ⁶³⁾ G. Ungerboeck, *IEEE Trans. Commun.* **COM-24**, 856 (1976).
- ⁶⁴⁾ D. D. Falconer, *Bell Syst. Tech. J.* **57**, 2589 (1977).
- ⁶⁵⁾ P. J. v. Gerwen, N. A. M. Verhoeckx and T. A. C. M. Claasen, *IEEE J. Select. Areas Commun.* **SAC-2**, 314 (1984).
- ⁶⁶⁾ E. Biglieri, A. Gersho, R. D. Gitlin and T. L. Lim, *IEEE J. Select. Areas Commun.* **SAC-2**, 765 (1984).
- ⁶⁷⁾ O. Smith, *Electrical World*, pp. 116-117, 1888.
- ⁶⁸⁾ V. Poulsen, *Ann. Phys.* **3**, 754 (1900).
- ⁶⁹⁾ T. Noyes and W. E. Dickinson, *Proc. Western Joint Computer Conf.*, pp. 42-44, San Fransico, 1956.
- ⁷⁰⁾ H. Nakajima and M. Kosaka, *IEEE Trans. Cons. Electr.* **CE-32**, 404 (1986).
- ⁷¹⁾ L. M. H. E. Driessen, W. A. L. Heijnemans, E. de Niet, J. H. Peters and A. M. A. Rijckaert, *IEEE Trans. Cons. Electr.* **CE-32**, 362 (1986).
- ⁷²⁾ R. L. Wallace, Jr., *Bell Syst. Tech. J.* **30**, 1145 (1951).
- ⁷³⁾ O. Karlqvist, *Trans. Royal Institute of Technology, Stockholm, Sweden*, No. 86, 1954.
- ⁷⁴⁾ N. Yeh, *IEEE Trans. Magn.* **MAG-21**, 1338 (1985).
- ⁷⁵⁾ H. Osawa, S. Tazaki and S. Ando, *IEEE Trans. Magn.* **MAG-22**, 253 (1986).
- ⁷⁶⁾ H. Kobayashi and D. Tang, *IBM J. Res. Develop.* **14**, 368 (1970).
- ⁷⁷⁾ S. Nakagawa, K. Yokoyama and H. Katayama, *IEEE Trans. Magn.* **MAG-16**, 104 (1980).
- ⁷⁸⁾ K. A. Schouhamer Immink, *Philips J. of Res.* **41**, 410 (1986).

DISCRETE-TIME MODELS FOR DIGITAL MAGNETIC RECORDING

Abstract

Using a fundamental result from detection theory, this paper translates the most popular continuous-time models for digital magnetic recording into simple discrete-time models which are equivalent from an information transfer point of view, and which are closely related to the optimum performances of all commonly applied receiver types. The models take account of the head-to-medium spacing, medium thickness, playback head gap size, tape speed, transmission code and information density, and are valid for both longitudinally and perpendicularly magnetized media.

1. Introduction

It has long been known (see e.g. ref. 1, ch. 4) that any continuous-time noisy dispersive channel which transports pulse-amplitude-modulated digital data can be translated into a discrete-time form which is equivalent from an information transfer point of view. This characterization goes without the redundancy which implicitly resides in the continuous-time description, and is as such more convenient to handle both analytically and numerically. It is moreover closely related to the optimum performances of all commonly applied receiver types (see e.g. ref. 2, ch. 6), and hence facilitates the analysis and design of the communications system. Unfortunately, many real world channels (e.g. voiceband telephone connections, wire pairs, optical storage media, radio links) are so complex in nature that it seems in general to be impossible to establish manageable analytical forms for the equivalent discrete-time channel. This paper presents, however, an exception to this rule. Building upon the most popular continuous-time models for digital magnetic recording it derives simple closed-form expressions for the equivalent discrete-time channels, which uncover many of the intimate ties that exist between the communications properties of the recording system and its physical parameters.

A companion paper⁸) uses a subclass of the derived models to compare several (both traditional and less conventional) equalization methods, and may as such serve to further demonstrate the usefulness of the characterization under study.

The paper starts with the presentation of a general continuous-time model for digital magnetic recording which captures the parameters of interest, commenting in passing upon the validity of some of the assumptions embodied in it. The theoretical background underlying the equivalent discrete-time characterization is next presented in both time- and frequency-domain terms, followed by a discussion of the basic properties of a canonic factorized form of the characterization which is particularly useful for simulation purposes and for the analysis of certain receiver types. Subsequent sections actually derive the models equivalent to increasingly general subsets of the category of recording systems studied, with special emphasis on their spectral properties and on the received energy per recorded bit, a quantity of particular relevance in communications engineering. For the classical and most restricted Lorentzian model, which assumes longitudinal magnetization, a vanishing medium thickness, and a playback head with a very narrow gap, exact and remarkably simple equivalent descriptions are established, and two canonic factorizations are identified. Two generalizations of the Lorentzian model, relieving the medium thickness and gap size restrictions, respectively, are then subjected to analysis. Although it appears to be feasible to establish exact equivalent time-domain characterizations, their rather unpalatable form and their non-amenability to Fourier transformation call for simple yet accurate approximations to the true equivalent characteristics, which are successfully identified. After showing that all derived models remain valid for perpendicular and mixed modes of magnetization, a concluding section finally summarizes the major insights gained.

2. The digital magnetic recording process

The recording of digital information on magnetic information carriers is conventionally a two-level process: according to the value of a binary digit a_k a position on the medium is magnetized (to saturation) in one direction or in the opposite direction. The finite dimensions of the recording and playback head, as well as the spatial dispersion on the information carrier, together give rise to intersymbol interference which may extend over many bit intervals. The most widely applied playback head is of the gapped-ring core type⁴), in which a pick-up coil translates flux changes into a proportional output voltage. A suitable conceptual model for a recording system that uses this type of head is depicted in fig. 1. A (possibly pre-coded or modulated) incoming binary data

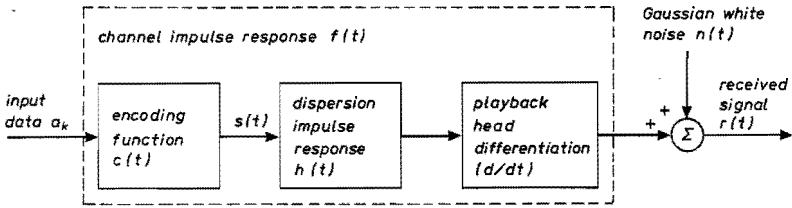


Fig. 1. Continuous-time channel model for a digital magnetic recording system employing a differentiating playback head.

sequence $a_k \in \{-1, 1\}$ is translated by means of an encoding function $c(t)$ into a two-level continuous-time data signal $s(t)$ of the form

$$s(t) = \sum_{k=-\infty}^{\infty} a_k c(t - kT), \quad (1)$$

which is applied to the recording head. In this formula, T represents the time separation of successive bits. The encoding function $c(t)$ depends upon the transmission code used. For the widely applied class of NRZ-like codes (comprising e.g. NRZ⁵, NRZI⁶, 8-to-10⁶), $c(t)$ equals

$$c(t) = \begin{cases} 1, & 0 \leq t < T, \\ 0, & \text{else.} \end{cases} \quad (2)$$

A second popular encoding function is associated with the Bi-phase transmission code⁵) (which is also referred to as Manchester code or as phase modulation). It is given by

$$c(t) = \begin{cases} 1, & 0 \leq t < \frac{1}{2}T, \\ -1, & \frac{1}{2}T \leq t < T, \\ 0, & \text{else.} \end{cases} \quad (3)$$

The recording head, tape and playback head together cause dispersion which can be modelled as an impulse response $h(t)$. Conforming to the majority of practical systems encountered to date, we will initially assume the medium to be longitudinally magnetized, which causes $h(t)$ to be symmetrical⁴). At the end of the paper we will show that the equivalent discrete-time models derived on the basis of this assumption are also valid for longitudinal and mixed modes of magnetization. In the case that both the medium thickness and the gap width of the playback head are small (this notion will be made more precise later on), the classical Lorentzian model^{5,7}) is applicable, for which $h(t)$ takes the form

$$h(t) = \frac{Kv \delta(a + d)}{(vt)^2 + (a + d)^2}. \quad (4)$$

In this expression, v , δ , a and d represent the relative head-medium velocity, the effective thickness of the medium (or, equivalently, the effective depth of recording), the transition width of recorded pulses, and the effective medium-to-head spacing, respectively, while K is a proportionality constant depending on the head efficiency factor, the track width, the system of units employed, and several other factors. Typically, δ , a and d range between roughly 0.25 and 2.5 μm ^{4,7-9}).

The influence of the thickness δ of the medium was first studied in detail by Wallace¹⁰), who generalized eq. 4 into the frequency-domain version of the expression^{8,11})

$$h(t) = \frac{Kv}{2} \ln \frac{(vt)^2 + (d+a+\delta)^2}{(vt)^2 + (d+a)^2}, \quad (5)$$

which is valid for arbitrary δ . By making a power series expansion in δ and neglecting the quadratic and higher order terms, eq. 5 is seen to degenerate into eq. 4 for small medium thicknesses.

The second extension of eq. 4 to be considered is due to Karlqvist¹²). It again has a bearing on thin recording media (for which $\delta \ll d+a$), but additionally accounts for the presence of a gap of size g in the playback head. The associated dispersion impulse response equals

$$h(t) = \frac{Kv\delta}{g} \cdot \left[\arctan \left(\frac{vt + \frac{g}{2}}{a+d} \right) - \arctan \left(\frac{vt - \frac{g}{2}}{a+d} \right) \right]. \quad (6)$$

The gap size g is usually of the same order of magnitude as the aforementioned parameters^{4,7-9}). It should be stressed that eqs 4, 5 and 6 are compatible models related to the same recording system. In fact the three can be combined into one frequency domain expression⁴)

$$H_c(f) = \frac{\pi K \delta}{(a+d)} \cdot \frac{1 - \exp\left(\frac{-2\pi\delta|f|}{vT}\right)}{\left(\frac{2\pi\delta|f|}{vT}\right)} \cdot \exp\left(\frac{-2\pi(a+d)|f|}{vT}\right) \cdot \frac{\sin\left(\frac{\pi gf}{vT}\right)}{\left(\frac{\pi gf}{vT}\right)}, \quad (7)$$

where the Fourier transform $H_c(f)$ of $h(t)$ is defined as

$$H_c(f) \triangleq \int_{-\infty}^{\infty} h(t) \exp\left(\frac{-j2\pi ft}{T}\right) dt. \quad (8)$$

This somewhat unconventional definition, with f dimensionless, has been chosen because in the remainder this turns out to simplify the equations. The

three frequency-dependent factors appearing from the left to the right in the RHS of eq. 7 are referred to as thickness loss, spacing loss, and gap loss, respectively^{4,10}).

As the flux-to-voltage conversion in the playback head is essentially a differentiation, the overall impulse response of the recording channel (see fig. 1) amounts to

$$f(t) \triangleq \frac{d}{dt} (c * h)(t), \quad (9)$$

where '*' indicates linear convolution. The output signal $r(t)$ of the reproduce head can now be described as

$$r(t) = \sum_{k=-\infty}^{\infty} a_k f(t - kT) + n(t), \quad (10)$$

where $n(t)$ accounts for the presence of additive noise. Accurate and universally applicable models describing all relevant noise sources are not available to the author's knowledge, although it seems reasonable to assume $n(t)$ to be Gaussian^{4,5}. Among the major components of $n(t)$ are medium noise (with spectral characteristics that depend to a large extent on the magnetic material used and on whether the medium is particulate^{13,14} or metallic¹⁵), head noise¹⁶, surface roughness noise¹⁷, and preamplifier noise¹⁷⁻²⁰. The latter three categories are becoming more important because of the trend of track sizes to decrease in favour of larger areal information densities^{20,21}. In view of this plethora of mainly ill-predictable constituents of $n(t)$ a first-order approximation has been made. This implies that we shall resort to a white noise assumption, which is not uncommon^{5,20} and in many instances reflects the net reality reasonably well¹⁷⁻¹⁹. It should be recognized, though, that the applicability of the models derived hereafter depends on the extent to which this assumption is realistic. A similar remark applies to the linear form of eq. 10, which is somewhat suggestive as it relies upon the validity of the superposition principle. Despite the nonlinear nature of the magnetic storage process, it appears that for the particular class of (binary) input signals $s(t)$ under study superposition is mostly well approximated in practice, particularly when the recording densities are not extreme^{11,22,23}).

3. An equivalent discrete-time characterization

We proceed by feeding the received signal $r(t)$ into a filter matched to $f(t)$, the output of which is sampled at the rate $1/T$ (see fig. 2). This is an information lossless procedure (ref. 1, ch. 4). Thus the sampled output sequence u_k of the matched filter is a sufficient statistic for the optimum estimation of the information sequence a_k . Mathematically, u_k can be denoted as

$$u_k = (a * x)_k + v_k, \quad (11)$$

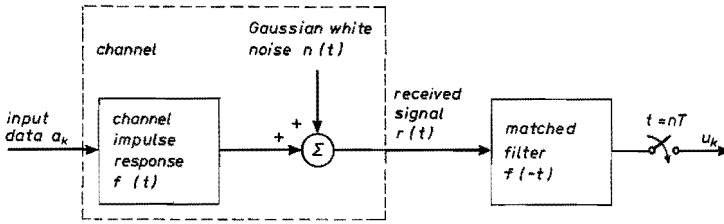


Fig. 2. Continuous-time model of a noisy dispersive channel followed by a matched filter and a sampler.

where x_k represents the sampled autocorrelation function of $f(t)$, i.e.

$$x_k \triangleq \int_{-\infty}^{\infty} f(t) f(t + kT) dt, \tag{12}$$

and v_k is the sampled additive noise sequence at the output of the matched filter, i.e.

$$v_k \triangleq \int_{-\infty}^{\infty} n(t) f(t - kT) dt. \tag{13}$$

This sequence has an autocorrelation function $E[v_k v_l]$ which equals

$$E[v_k v_l] = N_0 x_{k-l}, \tag{14}$$

where N_0 represents the spectral density of $n(t)$. The (fully discrete-time) model described by eqs 12 to 14 is depicted in fig. 3. Defining the autocorrelation function $z(t)$ of $h(t)$ as

$$z(t) \triangleq \int_{-\infty}^{\infty} h(v) h(v + t) dv, \tag{15}$$

and making use of eqs 2, 3 and 10 we see that x_k can be expressed in terms of $z(t)$ as

$$x_k = -z(kT + T) + 2z(kT) - z(kT - T) \tag{16}$$

for NRZ-like codes, and as

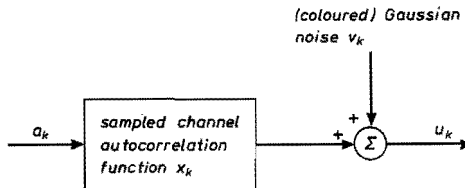


Fig. 3. Equivalent discrete-time model of the continuous-time system depicted in fig. 2.

$$x_k = z(kT + T) - 4z\left(kT + \frac{T}{2}\right) + 6z(kT) - 4z\left(kT - \frac{T}{2}\right) + z(kT - T) \quad (17)$$

for Bi-phase. Defining the Fourier transform $X(\Omega)$ of x_k as

$$X(\Omega) \triangleq \sum_{k=-\infty}^{\infty} x_k \exp(-j 2\pi \Omega k), \quad (18)$$

we can translate eq. 16 into the frequency-domain expression

$$X(\Omega) = 4 \sin^2(\pi \Omega) Z(\Omega), \quad (19)$$

where $Z(\Omega)$ is the Fourier transform of the sampled autocorrelation sequence

$$z_k \triangleq z(kT). \quad (20)$$

As appendix A shows, the frequency-domain equivalent of eq. 17 reads

$$X(\Omega) = 8 \sin^4\left(\frac{\pi \Omega}{2}\right) \hat{Z}\left(\frac{\Omega}{2}\right) + 8 \cos^4\left(\frac{\pi \Omega}{2}\right) \hat{Z}\left(\frac{\Omega - 1}{2}\right), \quad (21)$$

where $\hat{Z}(\Omega)$ is the Fourier transform of the sampled autocorrelation sequence

$$\hat{z}_k \triangleq z\left(\frac{kT}{2}\right). \quad (22)$$

Comparing eqs 22 and 20, we see that an analytic expression for $\hat{Z}(\Omega)$ can be obtained by substituting T by $\frac{1}{2}T$ in a given expression for $Z(\Omega)$.

The sampled system autocorrelation function x_k and its Fourier transform $X(\Omega)$ are closely related to the optimum performances of all known receiver types²). In the sequel of this paper we will capture z_k and $Z(\Omega)$ in analytic forms. By applying the above time- or frequency-domain relations the corresponding functions x_k or $X(\Omega)$, and hence the associated receiver performances, are then readily determined.

4. Spectral factorization

Because x_k is a real-valued autocorrelation sequence it can be factored as the convolution of a real-valued sequence f_k and its time-reversed version f_{-k} (ref. 2, ch. 6). Introducing the notation

$$(f-)_k \triangleq f_{-k}, \quad \text{for all } k, \quad (23)$$

it follows that x_k can be represented as

$$x_k = (f- * f)_k. \quad (24)$$

This equation can be transformed to the frequency domain, and then reads

$$X(\Omega) = |F(\Omega)|^2, \quad (25)$$

where $F(\Omega)$ represents the Fourier transform of f_k . From eqs 14 and 24, we see that the correlation structure of the sampled noise sequence v_{-k} can be thought of as being brought about by filtering a white noise sequence n_k by a filter with an impulse response f_{-k} . This observation leads us to the canonic system model of fig. 4, which is equivalent to our original continuous-time model with regard

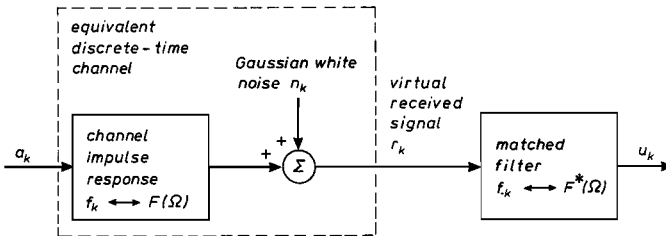


Fig. 4. Canonic equivalent discrete-time model of the continuous-time system depicted in fig. 2.

to the optimum attainable transmission quality. It comprises a discrete-time noisy dispersive channel, which transforms the input data sequence a_k into a ‘received’ sequence r_k of the form

$$r_k = (a * f)_k + n_k, \quad (26)$$

where n_k is a zero mean white Gaussian noise sequence having variance N_0 . The output signal of the equivalent discrete-time channel has been named r_k to stress the similarity with the continuous-time model of fig. 1. It should be borne in mind, however, that r_k is, in general, not a sampled version of $r(t)$.

The canonic representation of eq. 26 clearly reveals that for every recorded bit a_k a signal energy $(f_{-} * f)_0 = x_0$ is received. As the performance of any applied receiver is directly governed by the signal-to-noise ratio of the received signal, which is in turn proportional to the received energy per bit, we will devote special consideration in the forthcoming sections to the behaviour of x_0 as a function of the system parameters.

Although the knowledge of x_k or $X(\Omega)$ suffices to evaluate the performance of any receiver type, it can be useful, e.g. for simulation purposes, to have an analytic description of f_k or $F(\Omega)$ as well. Without further constraints the knowledge of x_k or $X(\Omega)$ does not suffice to identify a unique function f_k or $F(\Omega)$, since the factorization of x_k allows the phase characteristics of f_k to be chosen at liberty. A useful constraint, particularly when the receiver is of the decision feedback equalizer or Viterbi detector type²), is that f_k be minimum

phase. In view of the complexity of the problem we will restrict our factorization efforts in this paper to an important and tractable subclass of the considered recording systems, employing an NRZ-like transmission code and conforming to the Lorentzian or Wallace dispersion characterization. For this subclass we will be able to identify two distinct analytical (but unfortunately non-minimum phase) factorizations.

5. The discrete-time Lorentzian model

We now concentrate upon the derivation of the equivalent discrete-time Lorentzian model, for which the dispersion impulse response $h(t)$ is given by eq. 4. This (symmetrical) impulse response has a spatial width pw_{50} at half of its maximum amplitude $h(0)$ which equals (ref. 8)

$$\text{pw}_{50} = 2(a + d). \quad (27)$$

This motivates the introduction of a normalized information density D as

$$D \triangleq \frac{2(a + d)}{v T}. \quad (28)$$

According to eq. 28, changes in D can be brought about by changing the time separation of bits T (which leads to a different bit frequency and changing requirements for the hardware operating speed), the head-to-medium spacing d , the transition width of recording pulses a , and finally by changing the medium velocity v , which from a physical point of view is the most direct density control mechanism. For this reason we are motivated to attribute changes in D to changes of the medium velocity v , which will be explicitly reflected in the constant gain factors appearing in the forthcoming formulas. Further defining a normalized medium thickness Δ as

$$\Delta \triangleq \frac{\delta}{2(a + d)}, \quad (29)$$

we see that the Lorentzian impulse response, eq. 4, can be written as

$$h(t) = \frac{4K \Delta (a + d)}{D T} \cdot \frac{1}{\left(\frac{2t}{D T}\right)^2 + 1}. \quad (30)$$

The Fourier transform of $h(t)$ equals

$$H_c(f) = 2\pi K \Delta (a + d) \exp(-\pi D |f|), \quad (31)$$

in accordance with eq. 7. Applying Parseval's theorem to eq. 31, we see that

the sampled autocorrelation function $z_k = z(kT)$ of $h(t)$ can be expressed as

$$\begin{aligned} z_k &= \frac{1}{T} \int_{-\infty}^{\infty} |H_c(f)|^2 \exp(j 2\pi f k) df \\ &= \frac{2[2\pi K \Delta(a+d)]^2}{T} \int_0^{\infty} \exp(-2\pi D f) \cos(2\pi f k) df \\ &= \frac{A}{\pi} \cdot \frac{D}{D^2 + k^2}, \end{aligned} \quad (32)$$

where the constant of proportionality A is given by

$$A \triangleq \frac{[2\pi K \Delta(a+d)]^2}{T}. \quad (33)$$

Thus the (sampled) autocorrelation function of $h(t)$ also has a Lorentzian shape. The Fourier transform

$$Z(\Omega) \triangleq \sum_{i=-\infty}^{\infty} z_k \exp(-j 2\pi \Omega k) \quad (34)$$

of z_k is given by (ref. 24, p. 138)

$$Z(\Omega) = A \cdot \frac{\cosh(2\pi D(0.5 - \Omega))}{\sinh(\pi D)}. \quad (35)$$

As the Fourier transform $F(\Omega)$ of any real-valued sequence f_k has a Hermitian symmetry about zero and is periodic with period 1²⁶), it suffices to consider frequencies in the interval $[0, 0.5]$. Eq. 35 and all forthcoming expressions in Ω are valid in this interval, outside which the appropriate extension applies. Combining eq. 35 with eqs 19 and 21 we arrive at the system transfer functions

$$X(\Omega) = 4A \cdot \frac{\sin^2(\pi \Omega) \cosh(2\pi D(0.5 - \Omega))}{\sinh(\pi D)} \quad (36)$$

for NRZ, and

$$\begin{aligned} X(\Omega) &= 16A \cdot \frac{\cos^4\left(\frac{\pi \Omega}{2}\right) \cosh(2\pi D \Omega) + \sin^4\left(\frac{\pi \Omega}{2}\right) \cosh(2\pi D(1 - \Omega))}{\sinh(2\pi D)} \\ &= 2A \left[(3 + \cos(2\pi \Omega)) \frac{\cosh\left[\pi D\left(1 - \frac{\Omega}{2}\right)\right]}{\sinh(\pi D)} - 4 \cos(\pi \Omega) \frac{\sinh\left[\pi D\left(1 - \frac{\Omega}{2}\right)\right]}{\cosh(\pi D)} \right] \end{aligned}$$

for Bi-phase. These functions are plotted in figs 5 and 6 with the normalized

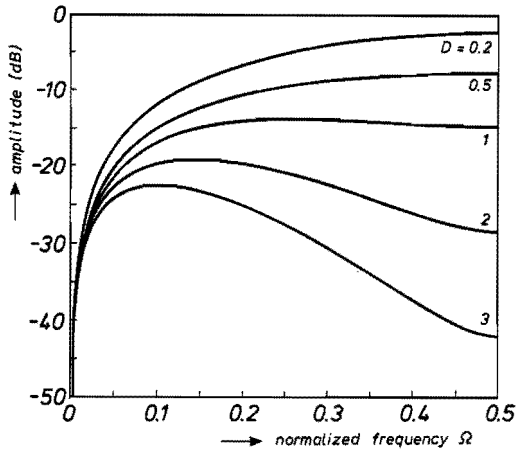


Fig. 5. Equivalent channel amplitude-frequency characteristics for a system applying an NRZ-like transmission code and conforming to the Lorentzian dispersion model.

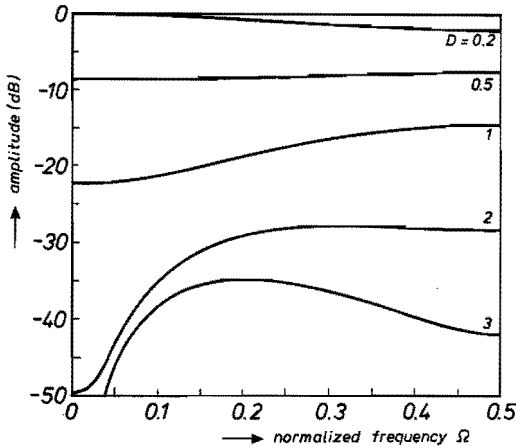


Fig. 6. Equivalent channel amplitude-frequency characteristics for a system applying the Bi-phase transmission code and conforming to the Lorentzian dispersion model.

information density D as parameter. The 0 dB levels in both figures coincide, so that a direct comparison is allowed. It is easily verified from eqs 36 and 37 that the $\Omega = 0.5$ values of $X(\Omega)$ for NRZ and Bi-phase are equal. As can be observed from fig. 5, the equivalent NRZ system transfer function suffers from severe amplitude distortion in the vicinity of dc, which causes the performance of particularly the conventional linear equalizer to deteriorate strongly (ref. 2, ch. 6). Due to its nonzero spectral content at the bit frequency (which folds back onto dc by eq. 21), the Bi-phase transfer function turns out to be much

smoother, although the favourably reduced amplitude distortion goes beyond effective densities of roughly 0.5 at the expense of a strongly decreased received signal power (or, equivalently, a worse signal-to-noise ratio), which again tilts the net performance balance in favour of NRZ. Thus Bi-phase may be considered a good choice at low densities, but is definitely inferior to NRZ-like codes for high-density applications. This conclusion can be strengthened by considering the received energy per bit x_0 , which directly governs the performance of any receiver incorporated in the system under study. Combining eq. 32 with eqs 16 and 17, we find that

$$x_0 = \frac{2A}{\pi} \cdot \frac{1}{D(D^2 + 1)} \tag{38}$$

for NRZ-like codes, and

$$x_0 = \frac{6A}{\pi} \cdot \frac{1}{D(4D^2 + 1)(D^2 + 1)} \tag{39}$$

for Bi-phase. These two functions are shown in fig. 7 (the 0 dB level coincides with $16A/5\pi$, corresponding to the parameter choice $D = 0.5$ for NRZ). Comparing both curves we see that for densities D below roughly 0.5 the Bi-phase received energy per bit clearly exceeds the corresponding NRZ entity (for small D by a factor of 3, i.e. 4.77 dB, reflecting the full profit of the threefold average number of flux reversals per second), whereas the opposite holds beyond $D = 0.5$, confirming our view regarding the applicability of both codes. It is seen that for both NRZ and Bi-phase the received energy per bit

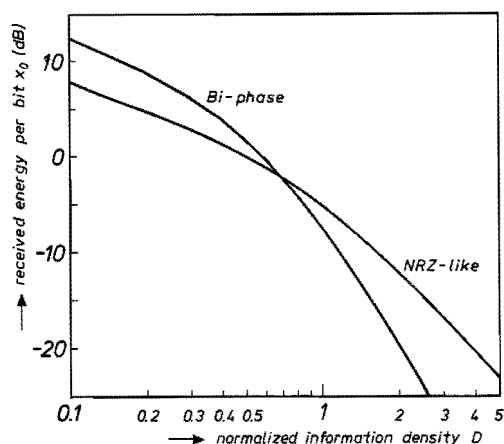


Fig. 7. Received energy per bit x_0 versus normalized information density D for systems employing NRZ-like and Bi-phase transmission codes and conforming to the Lorentzian dispersion model.

initially degrades relatively slowly as D increases, but that beyond a critical density in the order of magnitude of 1 it suddenly decreases at a dramatic rate (proportional to the third or even fifth power of D). This severe penalty for density increments discourages attempts to achieve effective signal-to-noise ratio improvements by means of channel coding techniques, as the increased information density which accompanies their use (the application of more data levels to accommodate redundancy is, to say the least, nontrivial) is likely to induce a degradation of received signal power which outweighs the established noise immunity improvements.

We proceed by considering the problem of factorizing the autocorrelation function x_k as the convolution of a real discrete-time sequence f_k and its time-reversed version f_{-k} . For convenience we confine our attention to the NRZ class of transmission codes. According to eq. 19 we then see that the Fourier transform $X(\Omega)$ of x_k can be written as

$$X(\Omega) = |G(\Omega) \cdot H(\Omega)|^2, \quad (40)$$

where

$$G(\Omega) = 1 - \exp(-j 2\pi \Omega), \quad (41)$$

and $H(\Omega)$ is a root of the Lorentzian dispersion spectrum $Z(\Omega)$ according to eq. 35, i.e.

$$|H(\Omega)|^2 = Z(\Omega). \quad (42)$$

In time-domain notation eq. 41 reads

$$g_k = \delta_k - \delta_{k-1}, \quad (43)$$

so that g_k is obviously a real-valued function. Our problem therefore reduces to the identification of a real-valued root h_k of the dispersion autocorrelation function z_k , so that the desired equivalent discrete-time system impulse response

$$f_k = (g * h)_k \quad (44)$$

is also real-valued.

Writing the Lorentzian dispersion spectrum eq. 35 as

$$Z(\Omega) = A \cdot \frac{1 + 2 \sinh^2(\pi D(0.5 - \Omega))}{\sinh(\pi D)}, \quad (45)$$

and defining two real-valued functions $H_e(\Omega)$ and $H_o(\Omega)$ as

$$H_e(\Omega) \triangleq \left(\frac{A}{\sinh(\pi D)} \right)^{\frac{1}{2}} \quad (46)$$

and

$$H_o(\Omega) \triangleq \left(\frac{2A}{\sinh(\pi D)} \right)^{\frac{1}{2}} \sinh(\pi D(0.5 - \Omega)), \quad (47)$$

we see from eq. 45 that $Z(\Omega)$ can be expressed as

$$Z(\Omega) = [H_e(\Omega) + j H_o(\Omega)] [H_e(\Omega) - j H_o(\Omega)]. \quad (48)$$

Comparing eqs 48 and 42 we now see that the function

$$H(\Omega) \triangleq H_e(\Omega) + j H_o(\Omega) \quad (49)$$

is apparently a factor of $Z(\Omega)$. Since both $H_e(\Omega)$ and $j H_o(\Omega)$ correspond to real-valued sequences (having an even and odd symmetry about zero, respectively), the sequence h_k corresponding to $H(\Omega)$ is real-valued, as desired. Performing the inverse transformation of eq. 49 (the transform of $H_o(\Omega)$ can e.g. be found in ref. 24, p. 138), we find that h_k equals

$$h_k = \frac{A^{\frac{1}{2}}}{\pi} \left[\frac{\pi \delta_K}{(\sinh(\pi D))^{\frac{1}{2}}} + \frac{k \left[\tanh\left(\frac{\pi D}{2}\right) \right]^{\frac{1}{2}}}{k^2 + \left(\frac{D}{2}\right)^2} \right]. \quad (50)$$

An alternative factorization can be performed by writing $Z(\Omega)$ as

$$Z(\Omega) = A \cdot \frac{\cosh^2(\pi D(0.5 - \Omega)) + \sinh^2(\pi D(0.5 - \Omega))}{\sinh(\pi D)}, \quad (51)$$

which, after a derivation along the same lines, leads to a root h_k of the more compact form

$$h_k = \frac{\left[2A \tanh\left(\frac{\pi D}{2}\right) \right]^{\frac{1}{2}}}{2\pi} \cdot \frac{k + \frac{D}{2}}{k^2 + \left(\frac{D}{2}\right)^2}, \quad (52)$$

which is, as eq. 50, neither causal nor symmetric. The equivalent discrete-time channel model conforming to eqs 43 and 50/52 is depicted in fig. 8. The strong functional symmetries between fig. 8 and the continuous-time model of fig. 1

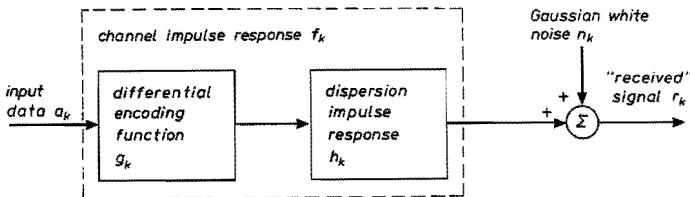


Fig. 8. Discrete-time channel model for a system employing an NRZ-like transmission code and conforming to the Lorentzian dispersion model.

are immediately apparent. The encoding function and the playback head differentiation have their counterpart in the differential encoding function g_k , whereas the dispersion impulse response $h(t)$ is reflected in a discrete-time impulse response h_k in which a (non-symmetrical) Lorentzian tendency still prevails. Interestingly, it is easy to show that a dispersion factor h_k with a fully (symmetrical) Lorentzian shape can never satisfy condition 42, so that the equivalent discrete-time model can never be completely similar in form to its continuous-time ancestor.

6. The influence of the medium thickness

This section focusses upon the model due to Wallace, conforming to eq. 5. Making use of the normalizations 28 and 29, eq. 5 can equivalently be denoted as

$$h(t) = \frac{K(a+d)}{DT} \ln \frac{\left(\frac{2t}{DT}\right)^2 + (1+2\Delta)^2}{\left(\frac{2t}{DT}\right)^2 + 1}. \quad (53)$$

The Fourier transform of $h(t)$ equals (ref. 25, vol. 1, p. 18)

$$H_c(f) = \frac{K(a+d)}{D|f|} \cdot [1 - \exp(-2\pi \Delta D|f|)] \exp(-\pi D|f|), \quad (54)$$

in accordance with eq. 7. Making use of this transform, it is easy to find the associated autocorrelation sequence z_k defined in eqs 15 and 20 (see appendix B). Using the shorthand notation

$$U(k, \Delta) \triangleq -\frac{k}{D} \cdot \arctan\left(\frac{k}{D(1+\Delta)}\right) + \frac{1+\Delta}{2} \ln\left((1+\Delta)^2 + \left(\frac{k}{D}\right)^2\right), \quad (55)$$

z_k can, according to appendix B, be expressed as

$$z_k = \frac{A}{\pi D} [U(k, 0) - 2U(k, \Delta) + U(k, 2\Delta)], \quad (56)$$

where the constant of proportionality A has been defined in eq. 33 (it should be noted that A is proportional to the square of Δ and hence may not be considered constant in the context of this section). Combining eqs 56 and 16 yields the desired expression for x_k for NRZ-like transmission codes (which is not reproduced here in view of its size). Substituting T by $\frac{1}{2}T$ and D by $2D$ in eq. 56 yields the sequence \hat{z}_k defined in eq. 21, which can be combined with eq. 17 to yield the corresponding Bi-phase expression for x_k (which is omitted

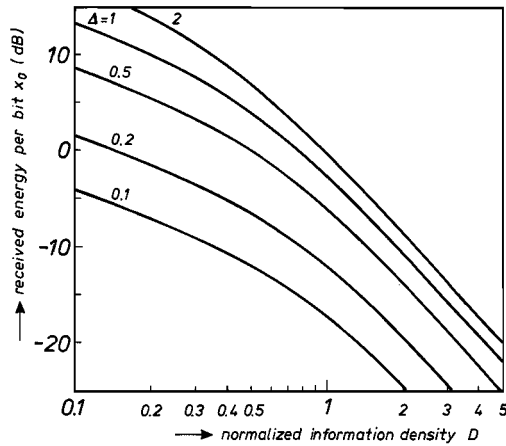


Fig. 9. Received energy per bit x_0 versus normalized information density D with normalized medium thickness Δ as parameter for a system employing an NRZ-like transmission code.

for the same reason). The received energy per bit x_0 as a function of the information density D , calculated on the basis of the foregoing expressions, is displayed in figs 9 and 10, with Δ as parameter. The 0 dB level in both figures corresponds to the parameter choice $D = \Delta = 0.5$ for NRZ. For small Δ the curves closely resemble their Lorentzian counterparts displayed in fig. 7, as was to be expected. Irrespective of Δ , in the high-density region beyond $D = 1$ the received energy per bit is again seen to deteriorate at a rate which increasingly disqualifies any coding technique from establishing there effective signal-

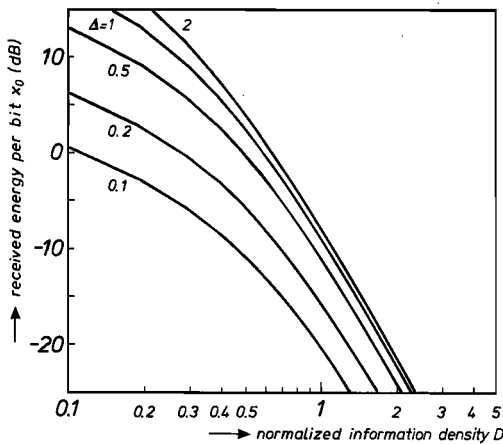


Fig. 10. Received energy per bit x_0 versus normalized information density D with normalized medium thickness Δ as parameter for a system employing the Bi-phase transmission code.

to-noise ratio increments. It can be observed that the received energy per bit grows rapidly with Δ up to about $\Delta = 1$, after which a saturation effect occurs, accompanied (and partly caused) by a rapid increase of the system dispersion, as will become apparent shortly.

Although the foregoing expressions take exact account of the medium thickness, they have a rather complicated form and hence are relatively difficult to interpret. Moreover, their Fourier transform cannot easily (and more likely not at all) be expressed in closed form. We are thus led to proceed along a somewhat indirect line which, as will become apparent later, will culminate in a simple and yet accurate approximation of the exact characterization.

From eqs 54 and 15 it follows that the Fourier transform

$$Z_c(f) \triangleq \int_{-\infty}^{\infty} z(t) \exp\left(\frac{-j 2\pi f t}{T}\right) dt \quad (57)$$

of $z(t)$ equals with A from eq. 33

$$\begin{aligned} Z_c(f) &= \frac{[K(a+d)]^2}{(D|f|)^2} \cdot [1 - \exp(-2\pi \Delta D|f|)]^2 \cdot \exp(-2\pi D|f|) \\ &= AT \cdot \frac{\sinh^2(\pi \Delta D|f|)}{(\pi \Delta D|f|)^2} \cdot \exp(-2\pi D(1 + \Delta)|f|). \end{aligned} \quad (58)$$

The Fourier transform $Z(\Omega)$ of z_k (which has been defined in eq. 34) is according to the sampling theorem (see e.g. ref. 26, ch. 2) related to $Z_c(f)$ as

$$Z(\Omega) = \frac{1}{T} \sum_{n=-\infty}^{\infty} Z_c(\Omega - n). \quad (59)$$

Combining eqs 58 and 59 we now have that

$$Z(\Omega) = A \cdot \sum_{n=-\infty}^{\infty} \frac{\sinh^2(\pi \Delta D|\Omega - n|)}{(\pi \Delta D|\Omega - n|)^2} \cdot \exp(-2\pi D(1 + \Delta)|\Omega - n|). \quad (60)$$

The $\sinh^2(x)/x^2$ factor encountered in eq. 60 is reminiscent of the Fourier transform of a triangular time sequence. This similarity shows up explicitly in the identity

$$\frac{1}{a} \int_{-a}^a \left(1 - \frac{|x|}{a}\right) \exp(2\pi \Omega x) dx = \frac{\sinh^2(\pi a \Omega)}{(\pi a \Omega)^2}, \quad (61)$$

which can easily be verified by applying standard identities. Using eq. 61,

eq. 60 can be written as

$$Z(\Omega) = \frac{A}{\Delta D} \int_{-\Delta D}^{\Delta D} \left(1 - \frac{|x|}{\Delta D}\right) \sum_{n=-\infty}^{\infty} \exp(-2\pi(D(1 + \Delta) - x)|\Omega - n|) dx. \quad (62)$$

This expression contains a series of the form

$$G(a, \Omega) \triangleq \sum_{n=-\infty}^{\infty} \exp(-a|n - \Omega|), \quad (63)$$

which can be seen to equal

$$G(a, \Omega) = \frac{\cosh(a(0.5 - \Omega))}{\sinh(\frac{1}{2}a)} \quad (64)$$

by decomposing it into two semi-infinite geometric series, summing each of these series individually, and adding the results. Applying this result to eq. 62, we find that

$$Z(\Omega) = \frac{A}{\Delta D} \int_{-\Delta D}^{\Delta D} \left(1 - \frac{|x|}{\Delta D}\right) \cdot \frac{\cosh(2\pi(D(1 + \Delta) - x)(0.5 - \Omega))}{\sinh(\pi(D(1 + \Delta) - x))} dx. \quad (65)$$

In spite of its relatively simple form, it does not appear feasible to evaluate analytically the integral contained in eq. 65. It is, however, relatively straightforward to approximate it accurately by noting that the function

$$F(x) \triangleq \frac{\cosh(2\pi(D(1 + \Delta) - x)(0.5 - \Omega))}{\sinh(\pi(D(1 + \Delta) - x))}, \quad \text{for } |x| \leq \Delta D, \quad (66)$$

contained in the integrand is convex- \cup for all Ω in $[0, 0.5]$ and $D > 0$. Thus we can bound $F(x)$ from above by a straight line between the two boundary values $F(-\Delta D)$ and $F(\Delta D)$, and from below by the tangent of $F(x)$ in the midpoint $x = 0$. Doing so, we find that $Z(\Omega)$ is bounded as

$$Z_l(\Omega) \leq Z(\Omega) \leq Z_u(\Omega), \quad (67)$$

where

$$Z_u(\Omega) \triangleq \frac{A}{2} \cdot \left[\frac{\cosh(2\pi D(0.5 - \Omega))}{\sinh(\pi D)} + \frac{\cosh(2\pi D(1 + 2\Delta)(0.5 - \Omega))}{\sinh(\pi D(1 + 2\Delta))} \right], \quad (68)$$

and

$$Z_l(\Omega) \triangleq A \cdot \frac{\cosh(2\pi D(1 + \Delta)(0.5 - \Omega))}{\sinh(\pi D(1 + \Delta))}. \quad (69)$$

Because of the convexity of $F(x)$ the midpoint approximation is better than the one involving its two boundary values. Moreover the triangular weighting

function contained in eq. 65 emphasizes the vicinity of $x = 0$, for which the midpoint approximation of $F(x)$ is most accurate. Therefore we may expect $Z_I(\Omega)$ to be a good approximation of $Z(\Omega)$. Some insight into the accuracy of $Z_I(\Omega)$ can be obtained by defining an inaccuracy figure E as

$$E \triangleq 10 \cdot \log \left[\frac{\int_0^{0.5} Z(\Omega) d\Omega}{\int_0^{0.5} Z_I(\Omega) d\Omega} \right], \quad (70)$$

which compares $Z(\Omega)$ and $Z_I(\Omega)$ over the entire frequency interval of interest, weighing all frequencies equally strongly. By means of numerical techniques we found that E is nearly independent of the information density D . The relation between E and the normalized medium thickness Δ is displayed in fig. 11. It is seen that E depends nearly linearly upon Δ , and that it does not exceed 0.3 dB for any thickness Δ smaller than 1.5. According to eq. 69, the net effect of increasing the medium thickness is not only a (favourable) multiplicative increment of the amplitude of $Z(\Omega)$ (recall that A is proportional to the square of Δ), but also an increment by a factor $(1 + \Delta)$ of the system dispersion, which is clearly less desirable in view of the resulting performance degradation of most conventional receiver types (ref. 2, ch. 6).

Since eq. 69 fully conforms to the Lorentzian model, all the results of the preceding section apply to this approximation, provided that the appropriate modifications are made to the constant gain factor and/or dispersion. In particular, we found that the simple approximations to the received energy per bit

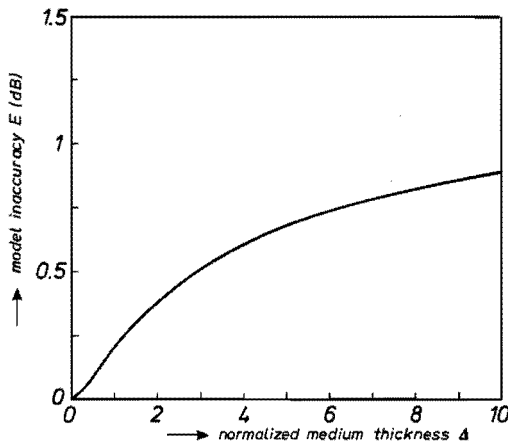


Fig. 11. Model inaccuracy E versus normalized medium thickness Δ for the approximate dispersion spectrum according to eq. 69.

which are obtained in this way (identical in form to eqs 38 and 39) comply within 1 dB with the true behaviour depicted in figs 9 and 10 for normalized medium thickness up to 1 and 0.5, respectively.

7. The influence of the gap size

Applying the definitions 28 and 29, we see that the impulse response $h(t)$ according to eq. 6 assumes the normalized form

$$h(t) = \frac{2K \Delta (a + d)}{D T G} \cdot \left[\arctan \left(\frac{2t}{D T} + G \right) - \arctan \left(\frac{2t}{D T} - G \right) \right], \quad (71)$$

where the normalized gap size G is defined as

$$G \triangleq \frac{g}{2(a + d)}. \quad (72)$$

The determination of the sampled autocorrelation sequence z_k of $h(t)$ is straightforward though somewhat lengthy, and is reproduced in appendix C. There it is shown that z_k can be expressed in the shorthand notations A and $U(k, \Delta)$ defined in eqs 33 and 55 as

$$z_k = \frac{A}{\pi D G^2} \cdot [-U(k - G D, 0) + 2U(k, 0) - U(k + G D, 0)]. \quad (73)$$

It is worth noting the similarity of eqs 73 and 56. Combining eq. 73 with eqs 16 and 17, we again find analytical expressions for the received energy per bit x_0 for NRZ-like and Bi-phase transmission codes, respectively, which are displayed in figs 12 and 13. The 0 dB level in both figures corresponds to the para-

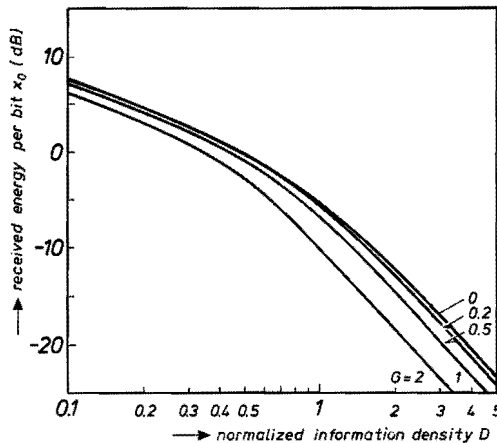


Fig. 12. Received energy per bit x_0 versus normalized information density D with normalized gap size G as parameter for a system employing an NRZ-like transmission code.

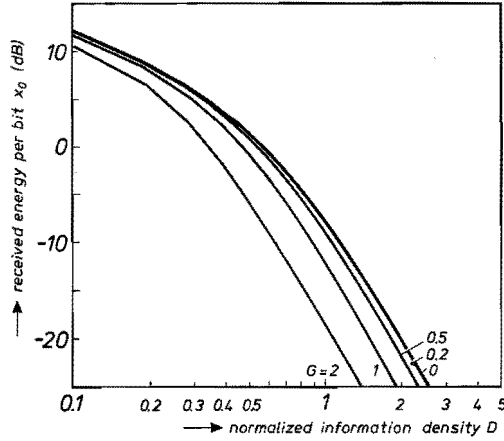


Fig. 13. Received energy per bit x_0 versus normalized information density D with normalized gap size G as parameter for a system employing the Bi-phase transmission code.

meter choice ($D = 0.5, G = 0$) for NRZ. We see that a non-zero gap size leads to a loss in received signal energy which slowly increases with the information density D , and which exceeds 1 dB for normalized gap sizes beyond roughly 0.5. It should be noted that both figures assume A to be constant, and hence do not account for the dependence of the head efficiency factor on the gap size⁸).

Though being exact, expression eq. 73 is again too complicated to allow its Fourier transform to be evaluated analytically. For this reason we again proceed towards an approximation. According to appendix C, the Fourier transform $Z_c(f)$ of the autocorrelation function $z(t)$ of $h(t)$ equals

$$Z_c(f) = A T \cdot \frac{\sin^2(\pi G D |f|)}{(\pi G D |f|)^2} \cdot \exp(-2\pi D |f|). \quad (74)$$

Combining eqs 74 and 59 we now have that

$$Z(\Omega) = A \cdot \sum_{n=-\infty}^{\infty} \frac{\sin^2(\pi G D |\Omega - n|)}{(\pi G D |\Omega - n|)^2} \cdot \exp(-2\pi D |\Omega - n|). \quad (75)$$

A straightforward upper bound for $Z(\Omega)$ can be obtained by replacing the $\sin^2(x)/x^2$ form contained in eq. 75 by its largest ($n = 0$) term. This yields

$$\begin{aligned} Z(\Omega) &\leq A \cdot \frac{\sin^2(\pi G D \Omega)}{(\pi G D \Omega)^2} \cdot \sum_{n=-\infty}^{\infty} \exp(-2\pi D |\Omega - n|) \\ &= A \cdot \frac{\sin^2(\pi G D \Omega)}{(\pi G D \Omega)^2} \cdot \frac{\cosh(2\pi D(0.5 - \Omega))}{\sinh(\pi D)} \triangleq Z_u(\Omega). \quad (76) \end{aligned}$$

This bound is nearly tight when D is relatively large (say, $D > 1$), so that the sum in eq. 75 converges rapidly. Alternatively, when G is small, it is also quite accurate since then the $\sin^2(x)/x^2$ term decreases relatively slowly, so that its substitution by 1 is legitimate. We can obtain insight into the accuracy of eq. 76 by again defining a model inaccuracy figure E as

$$E \triangleq 10 \cdot 10 \log \left[\frac{\int_0^{0.5} Z_u(\Omega) d\Omega}{\int_0^{0.5} Z(\Omega) d\Omega} \right]. \quad (77)$$

Fig. 14 shows E as a function of D , with G as parameter. Unlike the Wallace case, it is seen that E now depends upon both parameters involved. As expected, the model is very accurate for both small G and large D . Only in the region ($D \leq 0.5, G \geq 1$) E exceeds 0.3 dB. In this region z_k normally has only

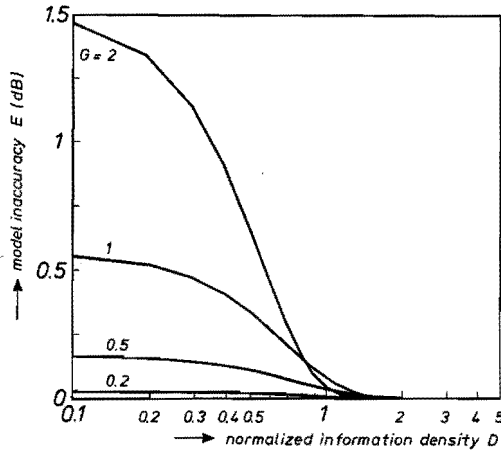


Fig. 14. Model inaccuracy E versus normalized information density D for the approximate dispersion spectrum according to eq. 76.

a few terms which differ relevantly from zero. Truncating its Fourier series to include only these terms and making use of the symmetry of z_k , we get an alternative approximation for $Z(\Omega)$ which reads

$$Z(\Omega) \cong z_0 + 2 \sum_{k=1}^L z_k \cos(2\pi \Omega k), \quad (78)$$

where z_k is given explicitly by eqs 73 and 55. The truncation length L can be determined by requiring all disregarded coefficients z_k to be less than $\epsilon \cdot z_0$ in magnitude, where ϵ is a predetermined constant. For instance for $\epsilon = 0.02$,

numerical calculations indicate that values of G up to 3 in conjunction with values of D up to 0.2 and 0.5 allow L to be chosen as small as 1 and 3, respectively.

Applying the results of the previous section, it is easy to show that eq. 76 can be extended to include the effect of the medium thickness by substituting D by $D(1 + \Delta)$ in the arguments of the contained hyperbolic functions. Outside the region ($D \leq 0.5$, $G \geq 1$) this gives an accurate approximation to the true dispersion spectrum for normalized medium thicknesses Δ up to about 1.5.

8. Perpendicular magnetization

So far we have been exclusively concerned with longitudinally magnetized media, characteristic for the majority of systems in current use. In the present section we present a brief digression on perpendicular magnetization. This subject is interesting in itself, its application being pursued intensively^{21,27}), and it also merits attention because the two modes of magnetization more often than not appear to occur in conjunction, causing noticeable deviations from the ideally expected symmetrical (or asymmetrical) playback waveforms^{11,28}).

The continuous-time dispersion transfer function $H_p(f)$ for perpendicularly magnetized media is the Hilbert transform of its longitudinal counterpart $H_c(f)$ ⁴), i.e.

$$H_p(f) = \begin{cases} j H_c(f), & f < 0 \\ -j H_c(f), & f > 0. \end{cases} \quad (79)$$

From eq. 79 we see at once that

$$|H_p(f)| = |H_c(f)|, \quad \text{all } f, \quad (80)$$

so that according to the frequency domain version of eq. 15 the dispersion autocorrelation function for perpendicular magnetization is simply equal to the corresponding longitudinal function, implying that the equivalent discrete-time characterizations are also equal. This observation reflects the well-known fact that phase distortion does not affect the optimum attainable performance of any receiver type²). Using eq. 79 and the real-valuedness of $H_c(f)$, it can easily be verified that mixed modes of magnetization also induce equivalent discrete-time characterizations which are (apart from a constant gain factor) identical to the ones derived before.

9. Conclusion

This paper has translated the most commonly employed continuous-time models for digital magnetic recording into discrete-time characterizations

which are equivalent from an information transfer point of view. Apart from being simpler to interpret and to handle numerically, these characterizations are closely related to the optimum performances of all known digital receiver types. Therefore they provide valuable criteria to assess both the influences of specific system parameters on the attainable performance, and the effects of important trade-offs which are involved in the system design. This rewarding aspect is exemplified in a companion paper³⁾, in which a subclass of the derived models serves as a basis for the comparison of several (linear and decision feedback) equalization methods.

For the classical Lorentzian model, which presupposes that both the medium thickness and the gap size of the playback head are small, we have established compact equivalent characterizations in both the time and the frequency domain, and we were able to translate these into a simple canonic form which bears close resemblance to its continuous-time predecessor. These descriptions indicate that the received energy per bit, which directly governs the signal-to-noise ratio and therewith the performance of any receiver connected to the recording system, depends strongly upon both the information density on the recording medium and the applied transmission code. More in particular, we have classified the Bi-phase transmission code to be superior to NRZ-like codes at low densities: to be precise there is a 4.77 dB signal-to-noise ratio advantage. In contrast, at high densities the signal-to-noise ratio balance clearly reverses, designating Bi-phase to be distinctly inferior. The received energy per bit was initially found to decrease only linearly with the information density, whereas beyond a (well defined) critical density it suddenly deteriorates at a dramatic rate. This effect discourages attempts to achieve effective signal-to-noise ratio improvements at high densities by means of channel coding techniques, since the increased information density which accompanies their use is likely to cause a degradation of received signal power which outweighs the achieved noise immunity improvements.

As a first extension to the Lorentzian model we have removed the constraint on the medium thickness. For the (more complex) continuous-time characterization which arises in this way we have established a comparably complex equivalent discrete-time characterization, as well as alternative characterizations which are considerably simpler, though at the sacrifice of some accuracy. We found that an increment of the medium thickness gives rise to an initially fairly rapid, but beyond a well defined critical thickness practically negligible growth of received signal power. At the same time the system dispersivity (or, equivalently, the channel amplitude distortion) increases rapidly, in a manner which closely resembles the effect of an information density enlargement. Our efforts relating to the extension of the Lorentzian model which elucidates the

role of the gap size of the playback head have also resulted in a rather complex exact equivalent characterization as well as in simple but accurate approximations thereof. These descriptions revealed a nearly Lorentzian behaviour up to a well defined critical gap size, beyond which substantial dispersion losses are incurred.

Though initially established for longitudinally magnetized media, all derived models were found to be valid for perpendicular and mixed modes of magnetization as well.

Appendix A. Bi-phase spectral mapping

This appendix expresses the Fourier transform $X(\Omega)$ of the sampled dispersion autocorrelation function x_k according to eq. 17 in terms of the Fourier transform $\hat{Z}(\Omega)$ of the sampled dispersion autocorrelation sequence

$$\hat{z}_k \triangleq z\left(\frac{kT}{2}\right). \quad (\text{A1})$$

Rewriting eq. 17, we see that x_k and \hat{z}_k are interrelated as

$$x_k = (y * \hat{z})_{2k}, \quad (\text{A2})$$

in which the sequence y_k is defined as

$$y_k \triangleq \delta_{k+2} - 4\delta_{k+1} + 6\delta_k - 4\delta_{k-1} + \delta_{k-2}. \quad (\text{A3})$$

The Fourier transform of y_k is

$$Y(\Omega) = 16 \sin^4(\pi \Omega). \quad (\text{A4})$$

Applying the multirate signal processing theory developed in ref. 26 to eq. A2 and making use of eq. A4 we now find that

$$\begin{aligned} X(\Omega) &= \frac{1}{2} \left[Y\left(\frac{\Omega}{2}\right) \hat{Z}\left(\frac{\Omega}{2}\right) + Y\left(\frac{\Omega-1}{2}\right) \hat{Z}\left(\frac{\Omega-1}{2}\right) \right] \\ &= 8 \sin^4\left(\frac{\pi \Omega}{2}\right) \hat{Z}\left(\frac{\Omega}{2}\right) + 8 \cos^4\left(\frac{\pi \Omega}{2}\right) \hat{Z}\left(\frac{\Omega-1}{2}\right). \end{aligned} \quad (\text{A5})$$

Appendix B. The Wallace autocorrelation function

This appendix derives the Wallace autocorrelation function $z(t)$ defined as

$$z(t) \triangleq \int_{-\infty}^{\infty} h(v) h(v+t) dv, \quad (\text{B1})$$

where the Fourier transform $H_c(f)$ of $h(t)$ is given by

$$H_c(f) = \frac{K(a+d)}{D|f|} \cdot [1 - \exp(-2\pi \Delta D|f|)] \exp(-\pi D|f|). \quad (\text{B2})$$

Making use of Parseval's identity we can write $z(t)$ as

$$\begin{aligned}
 z(t) &= \frac{1}{T} \int_{-\infty}^{\infty} |H_c(f)|^2 \exp\left(\frac{j 2\pi f t}{T}\right) df \\
 &= \frac{(K(a+d))^2}{D^2 T} \int_{-\infty}^{\infty} \frac{1}{f^2} [1 - \exp(-2\pi \Delta D|f|)]^2 \exp(-2\pi D|f|) \\
 &\quad \exp\left(\frac{j 2\pi f t}{T}\right) df. \quad (B3)
 \end{aligned}$$

This expression is hard to evaluate directly. We therefore resort to an indirect approach, differentiating $z(t)$ two times with respect to t , so that the square of f in the denominator of eq. B3 vanishes. Additionally making use of the symmetry of $H_c(f)$, we see that $z''(t)$ equals

$$\begin{aligned}
 z''(t) &= -\frac{2[2\pi K(a+d)]^2}{D^2 T^3} \int_0^{\infty} [1 - \exp(-2\pi \Delta Df)]^2 \exp(-2\pi Df) \cos\left(\frac{2\pi f t}{T}\right) df \\
 &= \frac{\pi(2K(a+d))^2}{(DT)^3} \left[-\frac{1}{1 + \left(\frac{t}{DT}\right)^2} + \frac{2(1+\Delta)}{(1+\Delta)^2 + \left(\frac{t}{DT}\right)^2} \right. \\
 &\quad \left. - \frac{1+2\Delta}{(1+2\Delta)^2 + \left(\frac{t}{DT}\right)^2} \right]. \quad (B4)
 \end{aligned}$$

Integrating this expression two times with respect to t and making use of the a priori knowledge that $z'(0) = z(\infty) = 0$, we find after some algebra that

$$z(t) = \frac{4\pi K^2(a+d)^2}{DT} \left[U\left(\frac{t}{T}, 0\right) - 2U\left(\frac{t}{T}, \Delta\right) + U\left(\frac{t}{T}, 2\Delta\right) \right], \quad (B5)$$

where the shorthand notation $U(k, \Delta)$ stands for

$$U(k, \Delta) \triangleq -\frac{k}{D} \cdot \arctan\left[\frac{k}{D(1+\Delta)}\right] + \frac{1+\Delta}{2} \ln\left[(1+\Delta)^2 + \left(\frac{k}{D}\right)^2\right]. \quad (B6)$$

Appendix C. The Karlqvist autocorrelation function

This appendix is concerned with the derivation of the autocorrelation function $z(t)$ of the Karlqvist impulse response $h(t)$ given by

$$h(t) = \frac{2K\Delta(a+d)}{GDT} \cdot \left[\arctan\left(\frac{2t}{DT} + G\right) - \arctan\left(\frac{2t}{DT} - G\right) \right]. \quad (C1)$$

The Fourier transform $H_c(f)$ of $h(t)$ equals⁴⁾

$$H_c(f) = \frac{2K\Delta(a+d)}{GD|f|} \exp(-\pi D|f|) \sin(\pi GD|f|). \quad (C2)$$

Applying Parseval's relationship, we can write $z(t)$ as

$$\begin{aligned} z(t) &= \frac{1}{T} \int_{-\infty}^{\infty} |H_c(f)|^2 \exp\left(\frac{j2\pi ft}{T}\right) df \\ &= 2 \frac{[2K\Delta(a+d)]^2}{(GD)^2 T} \int_0^{\infty} \frac{1}{f^2} \exp(-2\pi Df) \sin^2(\pi GDf) \cos\left(\frac{2\pi ft}{T}\right) df, \quad (C3) \end{aligned}$$

in which use was made of the symmetry properties of $z(t)$. This expression is again hard to evaluate directly. Differentiating two times with respect to t , we find that the second derivative $z''(t)$ of $z(t)$ equals

$$\begin{aligned} z''(t) &= -2 \frac{(4\pi K\Delta(a+d))^2}{(GD)^2 T^3} \int_0^{\infty} \exp(-2\pi Df) \sin^2(\pi GDf) \cos\left(\frac{2\pi ft}{T}\right) df \\ &= \frac{(4\pi K\Delta(a+d))^2}{(GD)^2 T^3} \int_0^{\infty} \exp(-2\pi Df) \left[-\cos\left(\frac{2\pi ft}{T}\right) + \right. \\ &\quad \left. + \frac{1}{2} \cos\left(2\pi f\left(\frac{t}{T} + GD\right)\right) + \frac{1}{2} \cos\left(2\pi f\left(\frac{t}{T} - GD\right)\right) \right] df. \\ &= \frac{2\pi [2K\Delta(a+d)]^2}{G^2 (DT)^3} \left[-\frac{1}{1 + \left(\frac{t}{DT}\right)^2} + \right. \\ &\quad \left. + \frac{1}{2} \cdot \frac{1}{1 + \left(\frac{t}{DT} - G\right)^2} + \frac{1}{2} \cdot \frac{1}{1 + \left(\frac{t}{DT} + G\right)^2} \right]. \quad (C4) \end{aligned}$$

Integrating two times with respect to t and making use of the (a priori) knowledge that $z'(0) = z'(\infty) = 0$, we finally obtain $z(t)$ as

$$z(t) = \frac{4\pi[K\Delta(a+d)]^2}{D T G^2} \left[-U\left(\frac{t}{T} - GD, 0\right) + 2U\left(\frac{t}{T}, 0\right) - U\left(\frac{t}{T} + GD, 0\right) \right], \quad (C5)$$

where, as before, the shorthand notation $U(k, \Delta)$ stands for

$$U(k, \Delta) \triangleq -\frac{k}{D} \cdot \arctan \left[\frac{k}{D(1+\Delta)} \right] + \frac{1+\Delta}{2} \ln \left[(1+\Delta)^2 + \left(\frac{k}{D} \right)^2 \right]. \quad (C6)$$

Acknowledgement

I am indebted to Dr Ir A. J. E. M. Janssen for his valuable suggestions, many of which have been adopted in this paper.

REFERENCES

- ¹⁾ J. Wozencraft and I. Jacobs, Principles of communication engineering, New York, Wiley, 1965.
- ²⁾ J. Proakis, Digital communications, New York, McGraw Hill, 1983.
- ³⁾ J. W. M. Bergmans, Philips J. of Res., to appear (1987).
- ⁴⁾ J. C. Mallinson, Proc. of the IEEE **64**, 196 (1976).
- ⁵⁾ T. Schonhof and R. Price, Proc. Int. Conf. Communications (Denver, C), 2.1.1, 1981.
- ⁶⁾ K. Schouhamer Immink, Philips J. of Res. **40**, 22 (1985).
- ⁷⁾ R. Comstock and M. Williams, IEEE Trans. Magn. **MAG-9**, 342 (1973).
- ⁸⁾ D. E. Speliotis and J. R. Morrison, IBM J. Res. and Dev. **10**, 233 (1966).
- ⁹⁾ J. Harker, D. W. Brede, R. E. Pattison, G. R. Santana and L. G. Taft, IBM J. Res. and Dev. **25**, 677 (1981).
- ¹⁰⁾ R. L. Wallace, Jr., Bell System Techn. J. **30**, 1145 (1951).
- ¹¹⁾ B. Middleton and P. Wisely, IEEE Trans. Magn. **MAG-14**, 1043 (1978).
- ¹²⁾ O. Karlqvist, Trans. Roy. Inst. Technol. Stockholm **86** (1954).
- ¹³⁾ J. Mallinson, IEEE Trans. Magn. **MAG-5**, 182 (1969).
- ¹⁴⁾ L. Thurlings, IEEE Trans. Magn. **MAG-19**, 84 (1983).
- ¹⁵⁾ N. Belk, P. K. George and G. S. Mowry, IEEE Trans. Magn. **MAG-21**, 1350 (1985).
- ¹⁶⁾ H. Watanbe, IEEE Trans. Magn. **MAG-10**, 903 (1974).
- ¹⁷⁾ M. Maeda, S. Ishida, T. Suenaga and S. Ogawa, J. Appl. Phys. **53**, 2573 (1982).
- ¹⁸⁾ R. Wood, S. Ahlgrim, K. Hallamasek and R. Stenerson, IEEE Trans. Magn. **MAG-20**, 698 (1984).
- ¹⁹⁾ C. Yamamitsu, K. Suesada, I. Ogura and A. Iketani, Proc. 6th Intern. Conf. on Video, Audio and Data Recording, 113, Brighton, U.K., 1986.
- ²⁰⁾ S. Nakagawa, K. Yokoyama and H. Katayama, IEEE Trans. Magn. **MAG-16**, 104 (1980).
- ²¹⁾ D. Tjaden, IEEE Trans. Magn. **MAG-9**, 331 (1973).
- ²²⁾ J. C. Mallinson and C. Steele, Proc. INTERMAG, Amsterdam, The Netherlands, 186, 1969.
- ²⁴⁾ L. B. W. Jolley, Summation of series, Chapman Publishing Co., London, England, 1925.
- ²⁶⁾ A. Erdelyi, W. Magnus, F. Oberhettinger and F. G. Tricomi, Tables of integral transforms, McGraw Hill book company, New York, 1954.
- ²⁶⁾ R. E. Crochiere and L. R. Rabiner, Multirate digital signal processing, Prentice-Hall Inc., Englewood Cliffs, New Jersey 07632, 1983.
- ²⁷⁾ C. S. Chi, K. A. Frey, R. A. Johnson and W. T. Maloney, IEEE Trans. Magn. **MAG-19**, 1608 (1983).
- ²⁸⁾ N. Yeh, IEEE Trans. Magn. **MAG-21**, 1338 (1985).

PARTIAL RESPONSE EQUALIZATION

Abstract

Supplementing their traditional view as a signalling or coding method, this paper elaborates a reception perspective of partial response techniques. It treats the data equalization problem that arises when an a priori selected partial response is secluded from a noisy dispersive communication channel and the equalization effort is exclusively directed to its remainder. For a given subdivision of the channel, and relative to a mean-square quality measure, it derives the optimum linear and decision-feedback equalizers, their performances and their sensitivity to gain variations. These results indicate that the linear equalizer greatly benefits from an appropriate selection of the partial response. In contrast, the performance of the optimum decision feedback equalizer turns out to be essentially independent of the applied subdivision, leaving only potential advantages in the domain of error propagation. The results are quantified for a class of digital magnetic recording channels, revealing a pre-eminent influence of the information density upon the relative merits of distinct partial response / equalizer combinations.

1. Introduction

Partial response techniques involve the introduction of a controlled amount of intersymbol interference and the detection of a correlated data sequence with an increased number of amplitude levels, from which the original transmitted data sequence can be recovered by means of a deterministic transformation¹⁻³). Compared to full response signalling, in which all intersymbol interference is eliminated prior to detection, their use generally increases the complexity of the system and not rarely decreases its margin against noise, but in return offers potential advantages in domains like spectrum control, spectral efficiency, sensitivity to timing errors and to changes of the data rate, error monitoring, and, last but not least, attainable data throughputs⁴⁻⁷). Embodiments of partial response techniques are encountered in digital magnetic recording systems^{8,9}) and in a variety of transmission systems using e.g. pulse amplitude modulation¹⁻⁵), phase-shift keying¹⁰) and quadrature-amplitude modulation¹¹). A survey of the application area is provided in ref. 7.

Focused upon the objectives just mentioned, most theoretical studies of the subject have viewed partial response techniques as a signalling or coding method^{1, 5, 7, 9, 11, 12}). The biased nature of this perspective may explain the scant recognition of the fact that, for a given transmission environment and at a fixed data rate, partial response techniques may also serve to achieve an improved transmission quality relative to full-response signalling. The present paper elaborates this hitherto under-exposed objective. In particular, it studies the situation where a linear equalizer is applied to transform the output signal of a noisy dispersive channel into one with controlled intersymbol interference, suitable for handling by a symbol-by-symbol multilevel threshold detector. Accordingly, partial response techniques are treated as primarily taking shape in the receiver. This unorthodox viewing angle is sometimes more natural, and throws new light upon the merits and characteristics of the concept under study. The paper further extends the state of the partial response art by exploring the merits of the decision feedback equalizer (DFE) as a more powerful substitute for its linear counterpart. Although a theoretical study hereof has to the author's knowledge not previously been undertaken, the use of decision-feedback equalization in a partial-response mode of operation has recently been considered for experimental ISDN transmission systems^{13, 14}).

The paper is organized as follows. After sketching the historical development and interpretation of partial response techniques, an alternative viewing angle is outlined according to which a noisy dispersive channel is conceptually subdivided into a predefined partial response and a residual channel upon which all equalization effort is concentrated. For a given partial response, and relative to a mean-square performance measure, the optimum linear equalizer and its performance are then derived, showing that distinct noise immunity advantages may accrue from partial rather than full response equalization. In contrast, a similar analysis that is next carried through reveals that for the DFE such advantages are essentially beyond reach, and that the optimum mean-square partial response DFE may in its straightforward configuration be even seriously hampered by error propagation. Among the three methods that are outlined to counter this problem, the most promising one, involving a modified (and in fact simplified) configuration, is subjected to a more detailed error propagation analysis. The sensitivity of both this modified DFE and the linear equalizer to channel gain variations, a factor of particular relevance in (e.g. recording) systems in which variations beyond the tracking speed of adaptation algorithms occur, is subsequently captured in analytic forms. To exemplify the developed body of theory, a comparison is finally presented of the mean-square performances and bit error characteristics achieved by various partial response/equalizer combinations for a class of digital magnetic recording systems of

practical relevance, for which a canonic discrete-time characterization has been derived in a companion paper¹⁵).

2. Partial response techniques

Historically, a prevailing incentive for the use of partial response techniques has been their capability to support a higher transmission rate on a given channel than feasible by means of full-response signalling^{6,3}). The first (avant-la-lettre) instance hereof originated in cable telegraphy midway the Victorian age, when it was discovered that 'doubling the dotting speed' relative to the maximum signalling rate at which transmitted symbols were clearly intelligible, would result in a received signal assuming 3 (rather than the transmitted 2) data levels, continually reflecting the sum of two adjacent transmitted symbols⁶). In the absence of past decision errors, the transmitted data could be unambiguously reconstructed from this received signal by means of a recursive decoding procedure. In return for the doubled signalling rate, discrimination between three rather than two possible signal values within the same range would be required, resulting in a (6 dB) reduction of the margin against noise.

In the sixties of this century, the modern version of this telegraph trick became known as duobinary signalling¹). Mathematically, duobinary signalling involves the reception of a signal b_k that is related to the signal a_k actually transmitted as

$$b_k = (a * g)_k, \tag{1}$$

where '*' represents linear convolution, while g_k is the duobinary response, whose \mathcal{D} -transform

$$g(\mathcal{D}) \triangleq \sum_{k=-\infty}^{\infty} g_k \mathcal{D}^k \tag{2}$$

equals

$$g(\mathcal{D}) = 1 + \mathcal{D}. \tag{3}$$

The serious problem of error propagation, originating from the recursive nature of the decoding procedure, was solved by adding a suitable data transformation (which normally takes the form of a so-called precoder²) at the transmitting end of the system, thus enabling the decoder to become memoryless. The term 'partial response techniques' emerged for the general idea of tolerating or deliberately introducing a controlled amount of intersymbol interference

in pursuit of an increased data throughput, spectrum control or related objectives^{3,12}). Central to the applicability of partial response techniques, the existence of simple pre- and decoding schemes was first demonstrated for simple, integer-valued partial responses, of which the category

$$g(\mathcal{D}) = (1 - \mathcal{D})^m (1 + \mathcal{D})^n \text{ with } m, n \geq 0 \text{ and } m + n \geq 1. \quad (4)$$

has come to dominate the partial response application scene^{2,3,5}). Later, precoding and symbol-wise decoding schemes were uncovered for increasingly more general classes of responses^{12,16}). As they involve the unravelling of 'controlled' intersymbol interference with a more complicated nature, these schemes are generally more involved than the ones applicable to eq. (4). Also, it was recognized that the correlation present in the received signal could be exploited to perform error monitoring, and even to establish an improved transmission quality (e.g. by 'null zone detection'¹⁷) or 'ambiguity zone detection'¹⁸). The ultimate improvement in this respect was brought in the early seventies by the Viterbi detector, the first practicable instance of a maximum-likelihood sequence detector (MLSD), and as such capable of making a maximum-likelihood estimate of the transmitted data sequence. As the precise structure of the intersymbol interference is immaterial to its applicability, the Viterbi detector in a sense blurred the distinction between the by then well established partial response discipline and the world outside it. To minimize this confusion, we shall in this paper essentially restrict consideration to responses of the category eq. (4)*). Also, we will assume the use of a conventional symbol-wise threshold detector throughout, although some concluding remarks will be devoted to its substitution by a Viterbi detector.

Supplementing their prevailing signalling or coding connotation, briefly addressed in the preceding lines, one can also consider partial response techniques as a method that aims at noise immunity improvements over full response signalling. This alternative viewing-angle will now be outlined in more detail.

3. A reception perspective of partial response techniques

Although data transmission across analog channels is a continuous-time process, its basic features can in principle be represented in a discrete-time fashion. More in particular, when pulse amplitude modulation is used and when the channel causes only linear intersymbol interference and additive Gaussian noise to arise (as we will assume in the present paper), then the

*) Nevertheless, many of the results obtained hereafter (especially those established in the appendices) have a more general applicability.

information transfer which takes place across the channel can be cast in the canonic discrete-time form

$$r_k = (a * f)_k + n_k, \quad (5)$$

where r_k is the equivalent discrete-time received signal, a_k is the data sequence to be conveyed, f_k is the equivalent discrete-time impulse response of the channel, '*' represents linear convolution, and n_k is an additive white Gaussian noise sequence having variance N_0 ¹⁹). The equivalent received signal r_k can be uniquely determined from the continuous-time signal $r(t)$ actually received through the application of a so-called whitened matched filter²⁰). This filter, which maps $r(t)$ into r_k , consists of a matched filter, a symbol-rate sampler and a discrete-time noise whitening filter. It is information-lossless, and can be regarded as a constituent of any receiver in an optimum dimensioning²⁰). Consequently, when optimizing distinct receiver types, attention may be confined to their discrete-time part, i.e. to the sequence of operations which they perform upon r_k . For the sake of compactness and clarity, we will take this approach in this paper. For the same reason, we will assume a_k to be drawn from the alphabet $\{-1, +1\}$, to be uncorrelated and to be statistically independent of n_k . Without changing the nature of the results derived hereafter, most of these assumptions can be easily relaxed²¹). Also, spectral colouration of n_k can be easily accounted for⁴). The well-defined nature of the whitened matched filter enables the equivalent discrete-time impulse f_k to be uniquely calculated from the actual continuous-time channel parameters^{19, 20, 22}). Although this calculation can mostly be made numerically only, it is sometimes possible to determine f_k or its amplitude characteristics analytically. This applies in particular to the class of digital recording systems which is used in a later section to compare distinct partial response/equalizer combinations.

The intersymbol interference and noise reflected in eq. (5) are normally dealt with by means of equalization methods. Using one or more linear filters, an equalizer attempts to form an accurate estimate of a_k (or, as we shall see, of a simple linear transformation thereof), which is then applied to a detector whose decisions are normally made in a memoryless (symbol-by-symbol) fashion*). Particularly the simpler and hence less powerful equalizers encounter severe difficulties (notably excessive noise enhancement) in directly estimating the transmitted data sequence a_k whenever the channel impulse response f_k exhibits

*) Apart from the conventional multilevel threshold detector, assumed throughout this paper, there exists a second symbol-by-symbol detector type employing decision feedback and a binary decision device^{3, 5}). Apart from its error propagation behaviour, this detector is identical in performance to its multilevel threshold counterpart for the category of responses (4)^{3, 5, 23}).

much amplitude distortion, i.e. when its amplitude spectrum contains zeros or deep depressions^{4, 19}). To cope with these problems, f_k may be factored into a predefined partial response g_k , $0 \leq k \leq K - 1$, which captures the major part of the amplitude distortion of f_k , and a residual response h_k which can be equalized without severe noise enhancement. This factorization can be denoted as

$$f_k = (g * h)_k. \tag{6}$$

With the aid of eq. (6), eq. (5) can be written as

$$r_k = (b * h)_k + n_k, \tag{7}$$

where

$$b_k \triangleq (a * g)_k \tag{8}$$

is a correlated data sequence taking on at most 2^K (and generally less) values. Fig. 1 depicts the model described by eqs. (7) and (8). The choice for g_k is

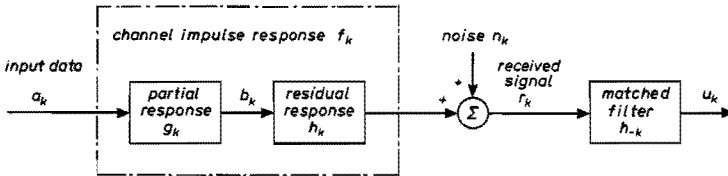


Fig. 1. Discrete-time factorized model of a data transmission system.

explicitly visible only in the receiver, which now attempts to reconstruct the (virtual) data sequence b_k rather than the original data sequence a_k . This is a less demanding task because of the relatively small amplitude distortion of the residual response h_k . The factorization of the channel impulse response can be governed by both performance considerations and engineering convenience (e.g. by the acceptable number of data levels of b_k). Whenever g_k represents an invertible operation, the estimate of b_k can be translated into a unique estimate of the original data sequence a_k by means of a deterministic transformation. In order for the estimate of the transformed data sequence b_k to be detectable by means of a simple symbol-by-symbol multilevel threshold detector, b_k should assume no more than a small number of amplitude levels. This prerequisite is (for small m and n) met by the important practical class of responses of eq. (4).

For future use, we now develop some notation. We shall denote the time-

reversal of a sequence by means of the subscript '-'. Using this notation, the autocorrelation functions x_k , y_k and z_k of f_k , g_k and h_k can be represented as

$$x_k = (f * f_-)_k, \quad (9)$$

$$y_k = (g * g_-)_k \quad (10)$$

and

$$z_k = (h * h_-)_k, \quad (11)$$

respectively. These functions play an important role in the following sections. Defining the Fourier transform $V(\Omega)$ of a sequence v_k as

$$V(\Omega) \triangleq \sum_{k=-\infty}^{\infty} v_k \exp(-j2\pi\Omega k), \quad (12)$$

eqs (9) to (11) can equivalently be represented in frequency domain notation as

$$X(\Omega) = |F(\Omega)|^2, \quad (13)$$

$$Y(\Omega) = |G(\Omega)|^2, \quad (14)$$

and

$$Z(\Omega) = |H(\Omega)|^2, \quad (15)$$

where $X(\Omega) \dots H(\Omega)$ denote the Fourier transforms of $x_k \dots h_k$, respectively. Before considering the equalization problem in more detail we augment the channel with a filter matched to the residual response h_k (see fig. 1). This is an information-lossless procedure (ref. 19, ch. 6), intended to simplify the forthcoming formulas. Applying eqs (5) and (11), we see that the output sequence u_k of the matched filter equals

$$u_k = (r * h_-)_k = (b * z)_k + (n * h_-)_k. \quad (16)$$

4. Optimum partial response linear equalizer

The linear equalizer, shown in fig. 2, is a discrete-time filter (having an impulse response c_k , $-\infty < k < \infty$) which operates on the matched filter output signal u_k . It is dimensioned to suppress intersymbol interference and noise as

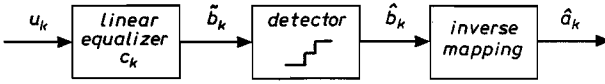


Fig. 2. Partial response linear equalizer.

well as possible, producing estimates \hat{b}_k of the (virtual) data sequence b_k . After a detection operation that maps \tilde{b}_k onto a detected sequence of digits \hat{b}_k , a subsequent inverse mapping produces an intentional replica \hat{a}_k of the original data sequence a_k . It can be noted that responses according to (4) have all their zeros (in the \mathcal{Z} -domain) on the unit circle, so that they strictly speaking cannot be inverted. For this reason, the inverse mapping which is needed to reconstruct a_k from its detected transformation \hat{b}_k is plagued by error propagation. In order to circumvent this problem, one normally adds a precoder at the transmitting end of the system in order for the inverse mapping to be memoryless. Since they are well documented and understood^{2, 3, 7, 9)} and do not affect the results presented hereafter, we will not account for the presence of these measures in the sequel of this paper.

As a quality measure for the decisions produced by the detector we will employ the mean-square error ε between \tilde{b}_k and b_k , defined as

$$\varepsilon \triangleq E[(\tilde{b}_k - b_k)^2], \quad (17)$$

in which E denotes mathematical expectation. Unlike the somewhat more relevant probability of error, this measure has the advantage of being analytically tractable, while it also underlies the most frequently used equalizer adaptation algorithms^{4, 19)}. To enable a meaningful comparison in mean-square error terms of the merits of distinct partial responses $g(\mathcal{D})$, it is necessary that the responses are normalized in amplitude such that identical mean-square errors indicate identical or at least comparable error probabilities. When its threshold levels are spaced halfway adjacent data levels of b_k , and when the error signal $\tilde{b}_k - b_k$ predominantly consists of Gaussian noise (with variance $\sigma^2 = \varepsilon$), the symbol error rate achieved by a multilevel symbol-wise threshold detector is, at high signal-to-noise ratios, linearly proportional to $Q(d/2\sigma) = Q(d/2\sqrt{\varepsilon})$, where d represents the smallest distance between adjacent data levels of b_k , while²⁴⁾

$$Q(x) \triangleq \frac{1}{\sqrt{2\pi}} \int_x^\infty e^{-y^2/2} dy. \quad (18)$$

Hence, an appropriate scaling is obtained when distinct partial responses $g(\mathcal{D})$ cause identical values of d . Using eq. (8) it can be observed that the responses cf. eq. (4) conform to this prerequisite with $d = 2$.

We now focus upon the minimum mean-square error ε_{\min} achieved by the partial response linear equalizer for given responses f_k and g_k and a given noise variance N_0 . Due to the correlated nature of both \tilde{b}_k and b_k the solution to this problem, reproduced in appendix A, is somewhat more complicated than in the conventional uncorrelated case. From appendix A it follows that the optimum transfer function $\hat{C}(\Omega)$ of the equalizer is given by the remarkably simple expression

$$\hat{C}(\Omega) = \frac{Y(\Omega)}{X(\Omega) + N_0} = \frac{|G(\Omega)|^2}{|F(\Omega)|^2 + N_0}, \quad (19)$$

while the minimum mean-square error ε_{\min} is given by

$$\varepsilon_{\min} = N_0 c_0 = N_0 \int_{-0.5}^{0.5} \frac{Y(\Omega)}{X(\Omega) + N_0} d\Omega = N_0 \int_{-0.5}^{0.5} \frac{|G(\Omega)|^2}{|F(\Omega)|^2 + N_0} d\Omega. \quad (20)$$

By performing direct detection of the transmitted data sequence a_k rather than of a linear transformation thereof (which corresponds to $G(\Omega) = Y(\Omega) = 1$), eqs (19) and (20) are seen to reduce to the familiar expressions for optimum mean-square full-response linear equalization (see ref. 19, ch. 6).

We illustrate the optimum dimensioning specified by eq. (19) by means of a simple example. Taking the partial response $g(\mathcal{D}) = 1 - \mathcal{D}$ (which leads to a ternary sequence b_k) and an ideal residual response (for which $H(\Omega) = Z(\Omega) = X(\Omega)/Y(\Omega) = 1$), it follows from eq. (19) that in the absence of noise ($N_0 = 0$) no equalization is needed. If N_0 substantially differs from zero, however, then eq. (19) specifies an optimum dimensioning in which some residual intersymbol interference is allowed in exchange for an improved noise suppression. For $N_0 = 1$ (corresponding to an unrealistically small signal-to-noise ratio x_0/N_0 of 3 dB, chosen to show more clearly the effects of interest) fig. 3 depicts the optimum system impulse response $(z * c)_k = c_k$ that results in this way. The system apparently suffers from severe intersymbol interference due to the large values of $(z * c)_{-1}$ and $(z * c)_1$, so that in combination with the relatively small sampling moment amplitude $(z * c)_0$ the quality of the decision variables \tilde{b}_k appears to be very poor. However, due to the correlated nature of b_k it is readily apparent that the actual quality of the decision variable \tilde{b}_k is much better than predicted by this heuristic reasoning.

Noting that

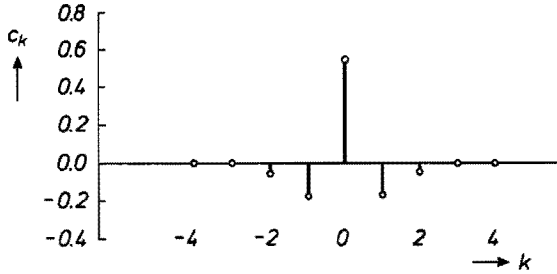


Fig. 3. Optimum linear equalizer impulse response for system having $g(\mathcal{D}) = 1 - \mathcal{D}$ and $Z(\Omega) = N_0 = 1$.

$$\tilde{b}_k \simeq -0.17b_{k+1} + 0.55b_k - 0.17b_{k-1} + (n * c)_k \quad (21)$$

and that

$$b_k = a_k - a_{k-1}, \quad (22)$$

it is easily verified that \tilde{b}_k can equivalently be expressed as

$$\tilde{b}_k = 0.72b_k - 0.17(a_{k+1} - a_{k-2}) + (n * c)_k \quad (23)$$

so that \tilde{b}_k resembles b_k considerably better than predicted by sole consideration of the system impulse response.

It is seen from this example that partial response systems can in principle take advantage of both pre-cursive and post-cursive intersymbol interference for establishing the beste possible transmission quality. This trait of character is greatly at variance with the non partial response case, in which intersymbol interference inevitably degrades system performance. In the following section, in which decision feedback equalization for partial response systems is studied, it will consequently be found that the conventional interpretation of the DFE as a canceller of all post-cursive intersymbol interference is suboptimum; since this cancellation would involve the removal of information which could be helpful in establishing a better transmission quality.

5. Optimum partial response decision feedback equalizer

Apart from a forward filter that suppresses noise and conditions pre-cursive intersymbol interference, the decision feedback equalizer (see fig. 4) also contains a feedback filter (FBF) which allows previous decisions to assist in the

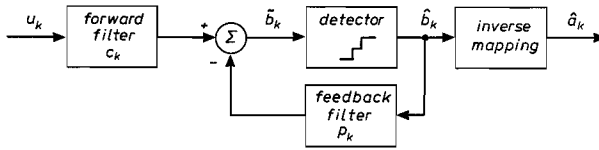


Fig. 4. Partial response decision feedback equalizer.

detection of subsequent symbols. The presence of an FBF designates the DFE to be intrinsically more powerful than the linear equalizer. To enable its performance to be analysed, one usually postulates that all previous decisions which affect the FBF output signal are correct²³), and hence neglects error propagation effects. Although we will not deviate from this approach in this paper, we will explore the error propagation problem in some detail in later sections. Under the mentioned assumption, the DFE is capable of removing all intersymbol interference of the trailing type if the impulse response of the FBF is chosen to be an exact replica of the trailing part of the system impulse response. In the conventional (non-partial response) case this replication is known to be optimum for the overall system performance^{23, 25}), and one might expect the same to be true for the situation under investigation. Surprisingly, the analysis that appendix B carries through demonstrates that this is not the case. More specifically, whenever the partial response g_k is causal and has minimum-phase, the optimum forward and feedback filters are found to satisfy in frequency domain notation

$$C(\Omega) = \frac{g_0}{\gamma_0} \cdot \frac{G^*(\Omega)}{\Gamma^*(\Omega)} \tag{24}$$

and

$$P(\Omega) = \frac{g_0}{\gamma_0} \cdot \frac{\Gamma(\Omega)}{G(\Omega)} - 1, \tag{25}$$

respectively, where $\Gamma(\Omega)$ represents the (unique) causal minimum phase factor of $X(\Omega) + N_0 = |F(\Omega)|^2 + N_0$ ^{25, 26}). Appendix B presents a recurrence relation by means of which $\Gamma(\Omega)$ (or, more precisely, the corresponding time domain sequence $\gamma_k, k \geq 0$) can be calculated from $X(\Omega) + N_0$. The restriction to causal and minimum-phase partial responses (which will henceforth be implied) entails little loss of practicality, as it does not exclude the important class of responses $g(\mathcal{Z}) = (1 - \mathcal{Z})^m(1 + \mathcal{Z})^n$. According to eqs (24) and

25), every spectral zero of the partial response g_k induces an identically located zero and pole of c_k and p_k , respectively. For all responses $g(\mathcal{D})$ of the form $(1 - \mathcal{D})^m(1 + \mathcal{D})^n$ this implies that the FBF impulse response p_k will have an infinite extent, so that one decision error influences subsequent decisions ad infinitum, which is clearly highly undesirable. We further conclude from eq. (24) that the total filtering in the forward path of the receiver performed by the cascade of the matched filter and the forward filter, is independent of the partial response used ($H^*(\Omega)C(\Omega)$ is, according to (24), completely determined by $\Gamma(\Omega)$ and $H^*(\Omega)G^*(\Omega) = F^*(\Omega)$, neither of which depend on $G(\Omega)$). Therefore, the FBF assumes the exclusive responsibility for tailoring the decision variable \hat{b}_k in such a way that it matches a predefined correlation structure (i.e. partial response).

As in the full-response case, the optimum forward filter c_k is again anticausal (naturally allowing a causal implementation by the introduction of an appropriate delay), and its optimum 'central' (i.e. last non-zero) coefficient value c_0 is related to the minimum mean square error ϵ_{\min} of the equalizer by

$$\epsilon_{\min} = N_0 c_0. \quad (26)$$

The following simple expression relates ϵ_{\min} explicitly to the known system parameters:

$$\epsilon_{\min} = g_0^2 \exp \left\{ \int_{-0.5}^{0.5} \ln \frac{N_0}{X(\Omega) + N_0} d\Omega \right\}. \quad (27)$$

For partial responses $g(\mathcal{D})$ of the form $(1 - \mathcal{D})^m(1 + \mathcal{D})^n$ we have $g_0 = 1$, so that eq. (27) reduces to the expression describing the optimum mean-square error in the non-partial response situation²⁵). In other words: irrespective of the channel characteristics, the added complexity incurred by applying this type of partial response is never rewarded in terms of a mean-square performance improvement! This remarkable result is in complete contrast with the linear equalizer situation just studied, in which the system performance invariably benefits from an appropriate selection of the partial response. As the presence of an FBF causes the partial response DFE to be intrinsically more powerful than its linear counterpart, this finding also asserts the performance superiority of the conventional full-response DFE over any partial response linear equalizer having $g(\mathcal{D}) = (1 - \mathcal{D})^m(1 + \mathcal{D})^n$ and followed by a symbol-by-symbol multilevel threshold detector.

We will address the interpretational aspects related to eqs (24) and (25) by means of the same example that we considered before in the context of linear equalization. Fig. 5 depicts the optimum forward and feedback filter impulse

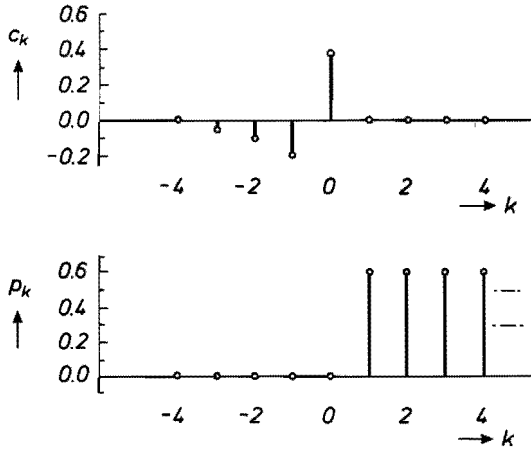


Fig. 5. Optimum DFE impulse responses for system having $g(\mathcal{D}) = 1 - \mathcal{D}$ and $Z(\Omega) = N_0 = 1$. Unconstrained feedback filter.

responses ($c_k = (c * z)_k$ and p_k , respectively) as described by (24) and (25) for a system having $g(\mathcal{D}) = 1 - \mathcal{D}$ and $H(\Omega) = Z(\Omega) = N_0 = 1$. It is seen that the FBF impulse response indeed has an infinite duration. Unlike the non-partial response situation, it no longer replicates the optimum system impulse response, which is zero inside its span. This seemingly strange behaviour can be understood by recalling that the sequence b_k is correlated, so that any decision \hat{b}_{k-1} regarding the symbol b_{k-1} contains some information about the following symbol b_k . As we have assumed previous decisions to be correct, this information is noise-free. Of course the optimum equalizer will try to invoke as much noise-free information regarding b_k in the decision variable \hat{b}_k as possible, thus allowing the 'direct' but undesirably noisy information about b_k (entering through the forward filter) to be smaller in magnitude. Due to this effect the first few feedback filter coefficients (i.e. the coefficients p_k within the span of the partial response g_k) will have a relatively large non-zero value. The remaining coefficients are then determined by the requirement that the disturbing influence of the corresponding older decisions (which are uncorrelated with b_k) should be minimum. This leads p_j to have a (nearly) zero transfer at those frequencies where g_k (and hence b_k) has its largest spectral density and vice versa. For instance, in the present example for which $g(\mathcal{D}) = 1 - \mathcal{D}$ the infinitely long feedback filter approaches an ideal integrator, which has an infinite transfer only at dc, being the only frequency for which g_k has zero spectral content. More quantitatively it is seen that the decision variable \hat{b}_k approximately equals

$$\begin{aligned} \tilde{b}_k &\approx -0.1b_{k+2} - 0.23b_{k+1} + 0.39b_k - 0.6(b_{k-1} + b_{k-2} + \dots) \\ &= 0.8b_k - 0.15(a_{k+1} + a_k + a_{k-1}) + (n * c)_k, \end{aligned} \quad (28)$$

in which use has been made of the correlation structure brought about by the partial response g_k of eq. (22). Unlike the linear equalizer case, the residual intersymbol interference is now correlated with b_k , but its total effect is only comparably large. Thus, due to the smaller noise transfer of the forward filter (caused by the reduced magnitude of its coefficients), the resulting mean-square error is favourable over the minimum linear equalizer error ($\epsilon_{\min} = N_0 c_0 = 0.39$, versus $\epsilon_{\min} = N_0 c_0 = 0.55$ for the linear equalizer).

The apparent impracticality of the feedback filter solution described by eq. (25) can be circumvented by restricting the length of the feedback filter to some finite value N , so that a decision error can affect no more than N subsequent decisions. Of course, optimization of the DFE subject to this restriction entails some increment of the minimum mean-square error. A straightforward extension of the first part of appendix B reveals that the optimum forward and feedback filter coefficients $c_j, j \neq 1 \dots N$, and $p_j, 1 \leq j \leq N$, solve the infinite set of equations

$$(c * (x + N_0 \delta))_j = ((p + \delta) * y)_j \quad \text{for all } j, \quad (29)$$

where δ_k denotes the Kronecker delta-function. The forward filter is here no longer anticausal, but rather has a gap within the span of the feedback filter. It can be observed that for the linear equalizer (for which $N = 0$) the right-hand side of eq. (29) degenerates into y_j , so that the time-domain version of eq. (19) remains.

A second possibility that exists for improving the practicality of the optimum feedback filter is to invoke the conventional condition that the feedback filter coefficients must be a replica of the trailing part of the system impulse response. Appendix C derives a semi-infinite set of equations describing both the DFE which solves this constrained optimization problem and its mean-square performance. The greatly differing nature of this solution with the unconstrained one can be visualized by returning to the example considered before. Fig. 6 depicts the optimum forward and feedback filter impulse responses resulting from a zero trailing intersymbol interference constraint for a system having $g(\mathcal{D}) = 1 - \mathcal{D}$, $z_k = \delta_k$ and $N_0 = 1$. The most striking feature of fig. 6 concerns the optimum feedback filter, of which all coefficients turn out to be zero. Using equation (C5) it is easy to show, incidentally, that this feedback filter solution is in fact optimum for all partial responses and irrespective of N_0 whenever

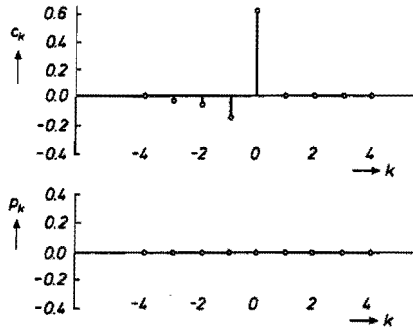


Fig. 6. Optimum DFE impulse responses for system having $g(\mathcal{D}) = 1 - \mathcal{D}$ and $Z(\Omega) = N_0 = 1$. Feedback filter constrained to remove all trailing intersymbol interference.

$z_k = \delta_k$; moreover in this specific case it again holds that ϵ_{\min} simply equals $N_0 c_0$. The minimum mean-square error ϵ_{\min} is seen to equal $N_0 c_0 = 0.63$, which is inferior to both solutions considered before, indicating that in specific cases the (less complex) optimum partial response linear equalizer can outperform its DFE counterpart when the latter is subjected to a zero trailing intersymbol interference constraint.

The two methods just described for diminishing FBF error propagation problems are beyond doubt effective, yet render the minimum mean-square error of the DFE interior to the performance achieved by the full-response DFE, which is moreover simpler to implement. In contrast, we will now consider an alternative approach, involving a modification of the DFE configuration, which essentially goes without these disadvantages.

6. An alternative decision feedback equalizer configuration and its error propagation behaviour

Fig. 7 depicts a simple modification to the DFE configuration considered so far which reduces both the implementational complexity and the error propagation problems without loss in minimum mean-square error. Rather than by the detected virtual sequence \hat{b}_k the feedback filter is now excited by the final estimate \hat{a}_k of the original data sequence a_k^* . The binary (as opposed to

*) For expositional simplicity, fig. 7 neglects the practical necessity of using a precoder at the transmitting end in order for the inverse mapping to be memoryless. Its presence dictates an additional precoder to be incorporated just before the feedback filter so as to feed it with an estimate of the precoded input data, to which the received signal is linearly related. Forming the modulo 2 sum of a current input and past output bit, the precoder produces a correct output bit whenever an even (or zero) total number of erroneous bits have been applied to it. This effect (which will be quantified for the recording system of sec. 8) causes error propagation to be slightly more serious than estimated in the present section, since it lengthens bursts so as to contain an even number of errors.

multilevel) nature of its new input signal obviously simplifies the digital implementation of the FBF. In the configuration of fig. 7, the impulse response

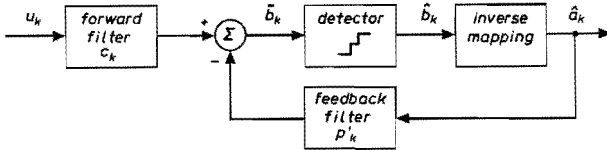


Fig. 7. Partial response DFE employing a binary feedback filter input signal.

p'_k of the FBF must also account for the relation

$$\hat{b}_k = (\hat{a} * g)_k \tag{30}$$

which exists between its former and present excitation. Invoking eq. (25), this implies that p'_k equals

$$p'_k = (g * p)_k = g_0 \left[\frac{\gamma_k}{\gamma_0} - \frac{g_k}{g_0} \right], \tag{31}$$

so that the FBF no longer possesses poles.

If the partial response adequately stylizes the amplitude distortion of the channel and if moreover N_0 is not too large, then γ_k will resemble g_k closely, so that the coefficients p'_k become small, and error propagation may be even less than in the non-partial response case, for which the FBF will have larger coefficients. We may take the FBF L_1 -norm

$$\mathcal{N} \triangleq \sum_{i=1}^{\infty} |p'_i| \tag{32}$$

to be a rough but simple indicator for the severity of error propagation^{27, 28)} (more accurate measures are, regrettably, conspicuous for their restricted tractability^{27, 28)}). For the class of partial responses $g(\mathcal{D}) = (1 - \mathcal{D})^m (1 + \mathcal{D})^n$, eq. (32) becomes

$$\mathcal{X} = \sum_{i=1}^{\infty} \left| \frac{\gamma_i}{\gamma_0} - g_i \right|, \quad (33)$$

where the sequence γ_i , $i \geq 0$, can be calculated by means of the procedure outlined in appendix B. Values of \mathcal{X} below 0.5 indicate that error propagation vanishes at high signal-to-noise ratios²⁷⁾. Conversely, values of \mathcal{X} in excess of roughly 1 indicate a relevant amount of error propagation, since the adverse FBF effect on the decision variable \tilde{b}_k caused by an erroneous decision then significantly exceeds the distance between adjacent data levels of b_k , so that further decision errors are likely. In such a situation it will often be advisable to choose a DFE dimensioning which leads to a shorter effective duration of the system impulse response, therewith exchanging a slight noise immunity degradation for a favourable reduction of error propagation²²⁾. Apart from being an indicator for error extension effects, the (full-response) FBF L_1 -norm \mathcal{X} also plays an important role in the sensitivity of the DFE to gain variations, as we will now see.

7. Sensitivity to gain variations

In spite of the static characterization which is usually adopted, it may happen that a communication channel exhibits variations, possibly at a rate beyond the tracking capabilities of commonly used adaptation mechanisms^{4, 19, 29)}. As an example, magnetic recording systems are subject to the influence of local tape defects and rapid tape-head contact fluctuations^{30, 31)}. A major effect of such variations is a decrease of the channel gain, which can be modelled by incorporating a marginal gain misadjustment factor α , so that the received signal takes on the form $(1 - \alpha)r_k$ rather than r_k . (We feel that a scaling of the entire received signal is more appropriate than a scaling of only the signal component $(a * f)_k$ of r_k , since in the present situation any receiver performance degradation can only be attributed to a mismatch and by no means to a signal-to-noise ratio change.) This will lead to a performance degradation due to the erroneous assumptions which the receiver now embodies about the actual channel characteristics, not having adapted its dimensioning to the decreased channel gain.

Since we are primarily interested in the order of magnitude of the effect, we will facilitate its analysis by restricting consideration to partial responses $g(\mathcal{D})$ of the form $(1 - \mathcal{D})^m(1 + \mathcal{D})^n$, in conjunction with a staircase multilevel symbol-by-symbol detector, the thresholds of which are spaced halfway between adjacent nominal data levels. For the sake of simplicity we will moreover make the not unusual assumption (see ref. 4, pp. 76-77) that, in

the absence of a gain misadjustment, the error signal $\tilde{b}_k - b_k$ consists predominantly of Gaussian noise (having variance $\sigma^2 = \epsilon_{\min}$). As a consequence, the symbol error rate achieved by the detector is asymptotically (i.e. for high signal-to-noise ratios) linearly proportional to $Q(d/2\sigma)$, where $Q(\cdot)$ has been defined in eq. (18), while $d/2 = 1$ is the minimum distance between any possible value of b_k and the nearest detector threshold level²⁴).

In the presence of a gain misadjustment α , the asymptotic error rate will be linearly proportional to $Q(d(\alpha)/[2(1 - \alpha)\sigma])$, where $d(\alpha)/2$ denotes the smallest distance between any possible value of $(1 - \alpha)b_k$ and the nearest detector threshold level²⁴). For this reason we are led to define an effective mean-square error $\epsilon_{\text{eff}}(\alpha)$ as

$$\epsilon_{\text{eff}}(\alpha) \triangleq \frac{4(1 - \alpha)^2}{d^2(\alpha)} \epsilon_{\min}, \quad (34)$$

so that ϵ_{eff} is a direct measure of the asymptotic symbol error rate achieved by the detector and compatible with ϵ_{\min} for $\alpha = 0$.

It is easily verified that for a partial response which gives rise to an L -level virtual data sequence b_k , the linear equalizer has

$$\frac{d(\alpha)}{2} = 1 - (L - 1)\alpha \quad \text{for } L \geq 2, \quad (35)$$

provided that α does not exceed $1/(L - 1)$. For the DFE we have to take account of the independence of the feedback filter output signal of α . This leads to a residual quantity of trailing intersymbol interference, the largest magnitude whereof determines $d(\alpha)$. Making use of eq. (25), it follows that for both $L = 2$ and $L = 3$,

$$\frac{d(\alpha)}{2} = 1 - \alpha \sum_{i=0}^{\infty} \left| \frac{\gamma_i}{\gamma_0} \right|. \quad (36)$$

It is worth noting that $d(\alpha)$ is intimately related to the full-response FBF L_1 -norm \mathcal{N} according to eq. (33). Combining eqs (34), (35) and (36) we now have that

$$\epsilon_{\text{eff}}(\alpha) = \frac{(1 - \alpha)^2}{[1 - (L - 1)\alpha]^2} \epsilon_{\min} \quad (37)$$

for the linear equalizer, and

$$\varepsilon_{\text{eff}}(\alpha) = \frac{(1 - \alpha)^2}{\left[1 - \frac{\alpha}{\gamma_0} \sum_{i=0}^{\infty} |\gamma_i|\right]^2} \varepsilon_{\text{min}} \quad (38)$$

for the ($L = 2$ and $L = 3$) DFE. Since neither γ_i nor ε_{min} depend upon the partial response used, eq. (38) reveals that the full-response DFE and its $L = 3$ partial response counterparts are all equally vulnerable to gain variations. In contrast, the full-response linear equalizer (for which $L = 2$) is judged to be completely insensitive to gain variations by eq. (37), whereas the partial response linear equalizer does suffer a performance loss in the presence of a gain misadjustment. According to eq. (38), the DFE sensitivity depends strongly upon the number of coefficients γ_i , $i > 0$, with a magnitude comparable to γ_0 and hence, roughly speaking, upon the dispersivity of the channel. Translated into magnetic recording vocabulary, we may expect DFE sensitivity figures comparable or favourable to the partial response linear equalizer at low information densities, and a very high sensitivity at the other end of the density spectrum. The next section will validate this conjecture.

8. Performance comparison for a digital magnetic recording system

To illustrate the foregoing results, we choose a digital magnetic recording system employing an NRZ (Non-Return to Zero) -like transmission code, longitudinal magnetization and a gapped-ring core playback head. When both the thickness of the recording medium and the gap width of the playback head are sufficiently small, this system can be characterized by the remarkably simple expression

$$X(\Omega) = 4A \sin^2(\pi\Omega) \frac{\cosh 2\pi D(0.5 - \Omega)}{\sinh \pi D}, \quad (39)$$

where D is a linear measure of the information density on the recording medium and A is a constant of proportionality without further relevance to the comparison. We refer to a companion paper¹⁵⁾ for a derivation of this expression and more detailed explanations. According to this paper, a generic channel decomposition for the transfer characteristic under study is

$$g(\mathcal{D}) = 1 - \mathcal{D} \quad (40)$$

in conjunction with the residual response

$$h_k = \frac{\sqrt{A}}{2} \sqrt{\arctan \frac{\pi D}{2}} \cdot \frac{k + \frac{D}{2}}{k^2 + (\frac{D}{2})^2}. \quad (41)$$

It can be observed from these expressions that g_k embodies a spectral zero at dc (which originates from the differentiation involved in the flux-to-voltage conversion of the playback head), while for small information densities D the residual response h_k closely resembles a Kronecker delta function and hence exhibits little amplitude distortion. Reception on the basis of this natural channel subdivision is usually referred to as amplitude detection of NRZI detection in magnetic recording jargon⁸). It may be expected to yield good results at low or moderate information densities, beyond which an alternative channel subdivision, designated partial response class IV detection⁸), becomes more appropriate. This subdivision corresponds to the choice

$$g(\mathcal{D}) = (1 - \mathcal{D})(1 + \mathcal{D}) = 1 - \mathcal{D}^2 \quad (42)$$

and also leads to a residual response h_k without a spectral zero at dc and a ternary sequence b_k , so that the added complexity over full-response detection (i.e. $g(\mathcal{D}) = 1$, normally referred to as integrated detection by the magnetic recording community⁸)), remains modest. In addition we will study the partial response

$$g(\mathcal{D}) = (1 - \mathcal{D})(1 + \mathcal{D})^2 = 1 + \mathcal{D} - \mathcal{D}^2 - \mathcal{D}^3, \quad (43)$$

which resembles the system impulse response at high information densities, and which leads to a 5-level virtual data sequence b_k .

A most useful reference for the comparison of reception methods is the so-called matched filter bound (see ref. 19, ch. 6). This bound stems from consideration of the transmission of only one isolated bit (as opposed to the continuous bit stream actually transmitted), so that intersymbol interference vanishes. In this (hypothetical) situation noise is the only remaining disturbance. Since a filter matched to the channel impulse response f_k is known to optimize the signal-to-noise ratio, the corresponding mean-square error can be considered as a (not necessarily attainable) bound to the performance of any receiver. Optimizing over a constant gain factor following the matched filter (which does not affect the signal-to-noise ratio) we obtain a mean-square error ϵ_{MFB} of the form

$$\varepsilon_{\text{MFB}} = \frac{N_0}{x_0 + N_0} \quad (44)$$

which obviously cannot be improved upon by any type of receiver. It is worth noting that ε_{MFB} depends exclusively upon the signal-to-noise ratio x_0/N_0 of the received signal, without involving any more detailed channel knowledge. For the recording system considered here, the received energy per bit x_0 equals¹⁵⁾

$$x_0 = \frac{2A}{\pi} \cdot \frac{1}{D(D^2 + 1)} \quad (45)$$

One important consequence of this expression is that beyond $D = 1$ even small increments of the information density lead to a dramatic reduction of the received energy per bit, a corresponding increment of ε_{MFB} , and a strong decrement of the performance of even the most powerful receiver. The information density improvements feasible by applying more sophisticated reception methods than the full response linear equalizer are explored in some depth in ref. 32.

Motivated by the foregoing considerations, we are led to introduce the following figure of merit \mathcal{L}

$$\mathcal{L} \triangleq \frac{\varepsilon_{\text{eff}}(\alpha)}{\varepsilon_{\text{MFB}}} \bigg|_{\frac{x_0}{N_0} = 20 \text{ dB}} \geq 1, \quad (46)$$

which assesses the mean-square performance loss relative to the matched filter bound of a given receiver operating with a given gain misadjustment α , assuming a realistic signal-to-noise ratio x_0/N_0 . It should be noted that for most receiver types \mathcal{L} does not depend strongly upon the precise value of the signal-to-noise ratio used. Figs 8 and 9, calculated on the basis of the foregoing theory, depict the dependence of \mathcal{L} on the information density D for various receivers operating without and with a gain misadjustment, respectively.

Looking at fig. 8, we see that the performance of the optimum linear equalizer depends strongly upon the partial response used. The performance balance is moreover strongly affected by the information density, a fact already recognized by other researchers⁸⁾. At low information densities ($D < 0.5$), amplitude detection ($g(\mathcal{D}) = 1 - \mathcal{D}$) appears to be better than the other alternatives. In contrast, and in agreement with the findings of ref. 8, both integrated detection ($g(\mathcal{D}) = 1$) and partial response class IV detection (for which $g(\mathcal{D}) = 1 - \mathcal{D}^2$) appear to be favourable at medium to high densities ($D > 1$), the former being preferable for complexity reasons. Finally, the partial response $g(\mathcal{D}) = 1 + \mathcal{D} - \mathcal{D}^2 - \mathcal{D}^3$ apparently outperforms the

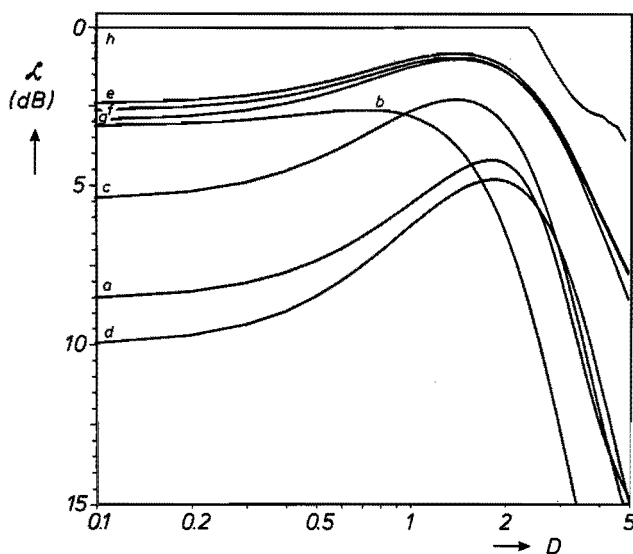


Fig. 8. Mean-square loss \mathcal{L} versus normalized information density D for various receivers in the absence of a gain misadjustment.

a. Full-response linear equalizer ($g(\mathcal{D}) = 1$); b. Bipolar linear equalizer ($g(\mathcal{D}) = 1 - \mathcal{D}$); c. Modified duobinary linear equalizer ($g(\mathcal{D}) = 1 - \mathcal{D}^2$); d. Linear equalizer having $g(\mathcal{D}) = 1 + \mathcal{D} - \mathcal{D}^2 - \mathcal{D}^3$; e. Unrestricted DFE; f. Bipolar DFE having a feedback filter with a ternary input signal and an impulse response restricted to a length $N = 5$; g. Bipolar DFE having a feedback filter with a ternary input signal, constrained to remove all trailing intersymbol interference; h. Maximum-likelihood sequence detector (MLSD).

other considered partial responses at the highest information densities ($D > 3$), where it apparently resembles the system impulse response quite well. In a previous section we have shown that the optimum performance of the unconstrained DFE is insensitive to the partial response $g(\mathcal{D})$ used (provided that it is a product of $(1 + \mathcal{D})$ and $(1 - \mathcal{D})$ terms). For this reason fig. 8 contains only one curve to describe the unconstrained DFE. Fig. 8 also visualizes the performance degradations that arise from a restriction of the feedback filter length to 5 bit intervals as well as from a zero trailing intersymbol interference constraint, in both cases assuming a partial response $g(\mathcal{D}) = 1 - \mathcal{D}$ and a ternary FBF input signal. It is seen that over the entire range of densities considered a feedback filter length of 5 bit intervals suffices to approximate the performance of the unconstrained DFE within 0.5 dB. In the low-density range the residual impulse response h_k approaches a delta function, so that the system under consideration comes to bear as close resemblance to the system considered before by way of example. The DFE which removes all trailing intersymbol interference is here seen to perform marginally better than the optimum $1 - \mathcal{D}$ linear equalizer. However, a small increment of the noise level already clearly

reverses the performance balance, in accordance with our previous findings. To put the comparison on a somewhat more global basis, fig. 8 displays the effective signal-to-noise ratio loss incurred by the most powerful type of receiver, viz. the maximum-likelihood sequence detector (MLSD), calculated using the theory developed in ref. 19. It is seen that the DFE approximates the MLSD performance to within 1 dB for all densities between roughly 1 and 2.5, so that the significant additional complexity of the MLSD is here unlikely to be justified by its performance benefits. By equipping the DFE with an additional provision (which does not greatly increase the complexity) to cope with pre-cursive intersymbol interference, its performance can be further improved in the vicinity of $D = 2$ by about 0.5 dB³³).

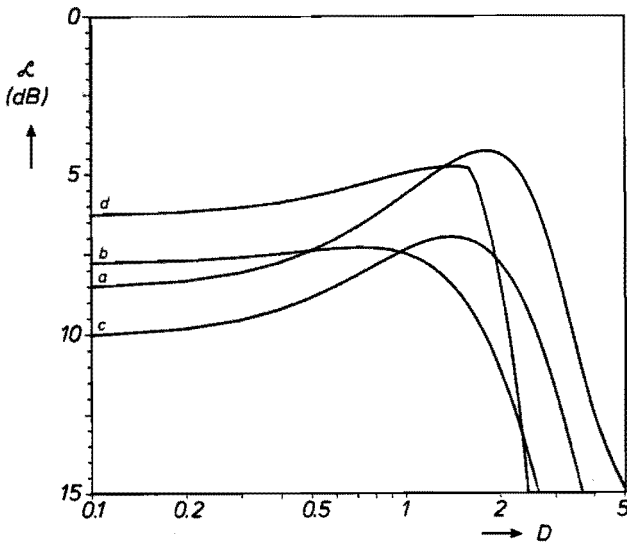


Fig. 9 Mean-square loss \mathcal{L} versus normalized information density D for various partial response equalizers in the presence of a gain misadjustment of 3 dB.
 a. Full-response linear equalizer ($g(\mathcal{D}) = 1$); b. Bipolar linear equalizer ($g(\mathcal{D}) = 1 - \mathcal{D}$);
 c. Modified duobinary linear equalizer ($g(\mathcal{D}) = 1 - \mathcal{D}^2$); d. DFE.

Fig. 9 compares several equalizers in the presence of a gain misadjustment of 3 dB (corresponding to $\alpha = 0.292$). With the exception of the full-response linear equalizer, which according to eq. (37) is completely insensitive to gain variations, all equalizers incur a significant performance loss, amounting to 4.6 dB for the partial response linear equalizers, and, as anticipated, even greatly exceeding this quantity at high densities for the DFE. The relevance of these sensitivity results should of course be judged against the factual occurrence of gain variations and the possibility to counter them adaptively.

The error propagation properties of the feedback equalizers considered are assessed in fig. 10 in terms of their FBF L_1 -norm \mathcal{N} . As was to be expected,

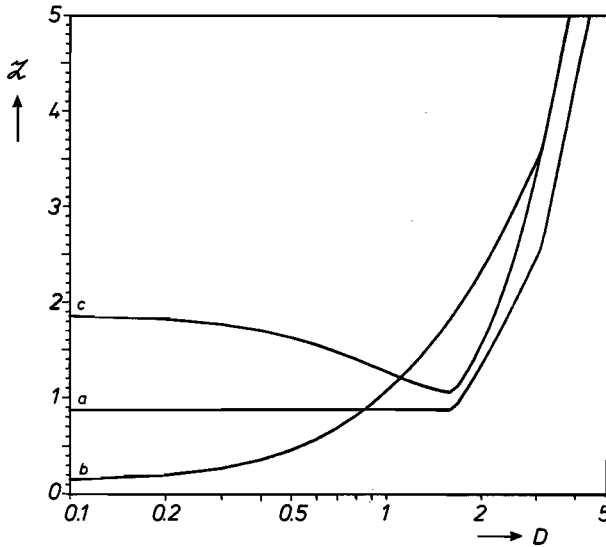


Fig. 10. Feedback filter L_1 -norm \mathcal{N} versus normalized information density D for 3 partial response decision feedback equalizers that use a binary feedback filter input signal. a. Full-response DFE ($g(\mathcal{D}) = 1$); b. Bipolar DFE ($g(\mathcal{D}) = 1 - \mathcal{D}$); c. Modified Duobinary DFE ($g(\mathcal{D}) = 1 - \mathcal{D}^2$).

the $1 - \mathcal{D}$ DFE turns out to operate with negligible values of \mathcal{N} at low densities, ranging up to about $D = 0.5$. The full-response DFE uniformly possesses an FBF L_1 -norm favourable to the $1 - \mathcal{D}^2$ DFE, which seems to be most applicable around $D = 1.5$. Finally, beyond roughly $D = 3$ not even the full response DFE seems capable any longer of maintaining a satisfactory error propagation behaviour. In this range a reduction of the effective system impulse response duration (and hence feedback filter length) is probably rewarding²²).

9. Simulation results

As a proof of the mean-square pudding we have performed a representative set of Monte Carlo simulations. In these simulations, the applied (transversal) linear equalizers were chosen to have 33 coefficients centered around 0, while the decision feedback equalizers were equipped with an FBF of length 12 and a forward filter of length 33, centered around zero and with the first 12 causal coefficients equal to zero. The equalizer coefficients were calculated on the basis of eqs (19) and (29), respectively. All equalizers were furnished with a staircase symbol-by-symbol detector with thresholds spaced halfway between

adjacent nominal data levels, followed by a memoryless square-law inverse mapping (serving to circumvent the singularity problems previously mentioned), and complemented at the transmitting end by a suitable precoder⁵). As they have the alternative configuration described in sec. 6, the partial response DFE's also incorporated a precoder just before the feedback filter. As explained earlier, the presence in the feedback loop of a precoder induces error bursts to contain an even number of errors. With the exception of the bipolar $(1 - \mathcal{D})$ DFE at low densities, whose FBF coefficients are so small that even a continuous stream of past decision errors does not completely ruin the detection margin for subsequent decisions, we have indeed consistently observed this interesting phenomenon, as a result of which bursts also tend to become somewhat longer than for the full response DFE. The latter effect is illustrated in table I.

TABLE I.
DFE burst error statistics measured at a bit error rate of 10^{-4} .

DFE type	average burst length (no. of bit intervals)			average no. of errors inside a burst		
	$D = 0.5$	$D = 2$	$D = 3$	$D = 0.5$	$D = 2$	$D = 3$
$g(\mathcal{D}) = 1$	10.8	9.5	12.9	2.8	1.2	3.1
$g(\mathcal{D}) = 1 - \mathcal{D}$	11.4	10.7	13.1	1.6	2.6	2.5
$g(\mathcal{D}) = 1 - \mathcal{D}^2$	12.8	11.5	16.0	3.2	2.2	4.7

In spite of their larger duration, table I indicates that bursts may on the average contain a smaller number of errors, resulting in a better overall performance. The actual error propagation behaviour of the equalizers is seen to comply well with the mutual ranking predicted in fig. 10, confirming e.g. the anticipated superiority of the Bipolar $(1 - \mathcal{D})$ DFE at low information densities over its full-response counterpart. Partly due to its relatively large FBF impulse response extent, the modified duobinary $(1 - \mathcal{D}^2)$ DFE shows up somewhat more negatively than anticipated^{27,28}). Nevertheless, as it exhibits no more than a modest number of errors inside a burst, even for this DFE error propagation is not a significant problem.

A more extensive digest of the performed simulations is collected in figs 11 to 13. At $D = 0.5$ (fig. 11), the full-response linear equalizer is found to lag slightly behind its predicted performance. This is due to its required integrating nature, which cannot accurately be approximated by a transversal filter having

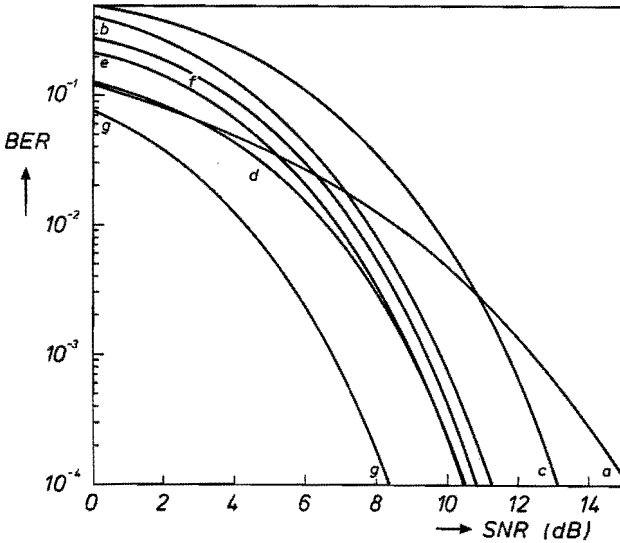


Fig. 11. Bit error rate (BER) vs. signal to noise ratio (SNR) for various receivers at $D = 0.5$ and in the absence of a gain misadjustment. a. Full-response linear equalizer ($g(\mathcal{S}) = 1$); b. Bipolar linear equalizer ($g(\mathcal{S}) = 1 - \mathcal{S}$); c. Modified duobinary linear equalizer ($g(\mathcal{S}) = 1 - \mathcal{S}^2$); d. Full-response DFE; e. Bipolar DFE using a binary feedback filter input signal; f. Modified duobinary DFE using a binary feedback filter input signal; g. Maximum-likelihood sequence detector (MLSD).

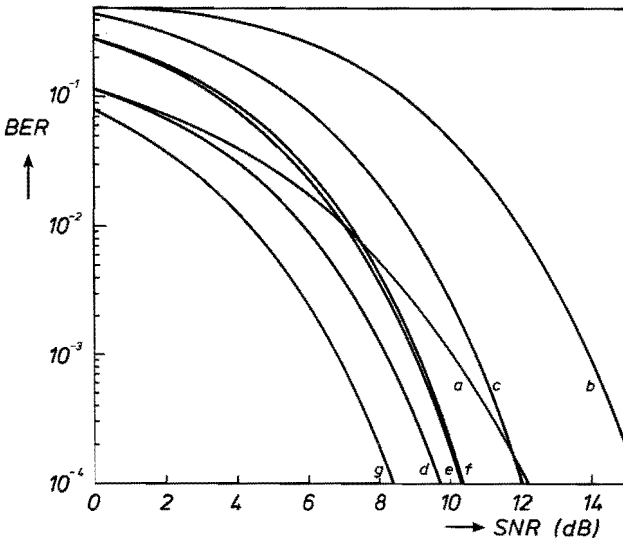


Fig. 12. Bit error rate (BER) vs. signal to noise ratio (SNR) for various receivers at $D = 2$ and in the absence of a gain misadjustment. a. Full-response linear equalizer ($g(\mathcal{S}) = 1$); b. Bipolar linear equalizer ($g(\mathcal{S}) = 1 - \mathcal{S}$); c. Modified duobinary linear equalizer ($g(\mathcal{S}) = 1 - \mathcal{S}^2$); d. Full-response DFE; e. Bipolar DFE using a binary feedback filter input signal; f. Modified duobinary DFE using a binary feedback filter input signal; g. Maximum-likelihood sequence detector (MLSD).

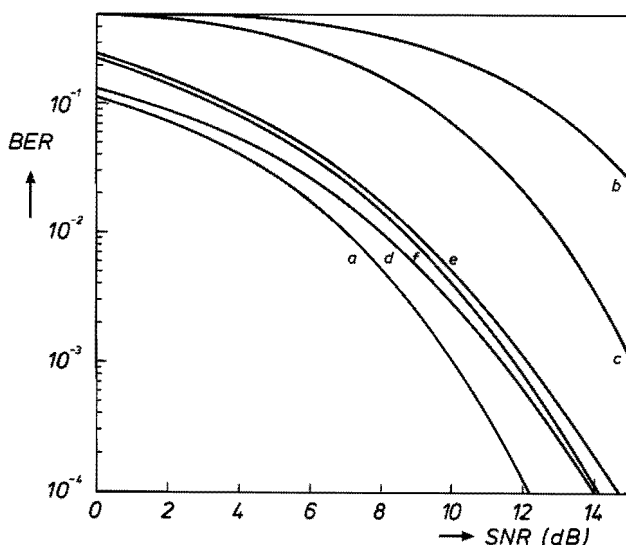


Fig. 13. Bit error rate (BER) vs. signal to noise ratio (SNR) for various partial response equalizers at $D = 2$ and in the presence of a gain misadjustment of 3 dB. a. Full-response linear equalizer ($g(\mathcal{D}) = 1$); b. Bipolar linear equalizer ($g(\mathcal{D}) = 1 - \mathcal{D}$); c. Modified duobinary linear equalizer ($g(\mathcal{D}) = 1 - \mathcal{D}^2$); d. Full-response DFE; e. Bipolar DFE using a binary feedback filter input signal; f. Modified duobinary DFE using a binary feedback filter input signal.

only 33 taps. All other equalizers are seen to achieve their predicted performances. In particular, the $1 - \mathcal{D}$ DFE outperforms both the $1 - \mathcal{D}^2$ and (at high signal-to-noise ratios) the full-response DFE, while in the category of linear equalizers the $1 - \mathcal{D}$ variant also stands out best. Without adding further comments, we remark that figs 12 and 13, depicting error characteristics which were measured at $D = 2$ without and with a gain misadjustment of 3 dB, respectively, again validate our performance expectations.

10. Concluding remarks

This paper has explored the merits and characteristics of the linear and decision feedback equalizer when applied to transform the output signal of a noisy dispersive channel into one with controlled intersymbol interference, suitable for handling by a symbol-by-symbol multilevel threshold detector. Relative to a suitably normalized mean-square error measure, it has derived the linear and decision feedback equalizers whose output signals optimally match an intersymbol interference structure defined by a given partial response. The performance of the optimum linear equalizer was shown to benefit greatly from an appropriate selection of the partial response, essentially depending upon

the extent to which its amplitude-frequency characteristics stylize the amplitude distortion introduced by the channel. In contrast, the optimum DFE performance as well as its forward path dimensioning were shown to be independent of the applied partial response whenever the \mathcal{D} -transform of the response is the usual product of $(1 + \mathcal{D})$ and $(1 - \mathcal{D})$ terms. As a consequence, for partial responses of this form the linear equalizer can never surpass the full response DFE in performance.

A notable finding of the DFE analysis is that, unlike the non-partial response case, the optimum feedback filter coefficients are not a replica of the overall system impulse response, but rather cause a well-defined amount of trailing intersymbol interference to arise which allows previous decisions to contribute constructively in the detection of subsequent symbols. We observed that the optimum feedback filter impulse response is potentially unacceptable from the point of view of error propagation, as it may extend over an infinite time-interval. Among the conceivable methods to overcome this problem we have studied a restriction of the feedback filter length and the use of a zero trailing intersymbol interference constraint, both of which were judged to be less practical as they increase the noise enhancement of the DFE, thereby ranking it behind the full-response DFE in terms of both performance and complexity. A third alternative however, involving a modification of the DFE configuration, entailed digital hardware savings in conjunction with a significant reduction of error propagation, without increasing the noise enhancement. Requiring only marginally more hardware, this alternative achieves better error propagation figures than the full-response DFE in specific environments, for which its application is consequently worth considering.

Quantifying the developed body of theory for a class of digital magnetic recording systems in which an NRZ-like transmission code is used in conjunction with differentiating playback heads, we have observed that the information density strongly affects the behaviour and the relative merits of the distinct equalizers. Among the category of linear equalizers, the bipolar $(1 - \mathcal{D})$ variant was found to achieve superior performances at low information densities, beyond which application of the class IV $(1 - \mathcal{D}^2)$ partial response becomes advantageous. The most conspicuous advantage of the full-response linear equalizer appeared to be its robustness, allowing it to withstand gain variations considerably better than its partial response relatives, though at the expense of an inferior nominal performance. Especially at medium and high densities, the optimum DFE was found to improve significantly (typically some 2dB) upon the best linear equalizer type. Beyond a (relatively high) critical density the DFE sensitivity to gain variations suddenly increases rapidly, however, and therefore its successful high-density application will rely

largely upon the absence of such variations or the possibility to combat them by adaptive means. Although relevant differences were observed in the error propagation behaviour of the feedback equalizers considered, it seems that for all but the highest densities error propagation is an insignificant problem, slightly favouring the $1 - \mathcal{D}$ DFE at low densities, beyond which the full-response DFE establishes a modest advantage.

It is worth spending some final remarks to the substitution of the symbol-wise multilevel threshold detector assumed in this paper by the more powerful maximum-likelihood sequence detector (MLSD), usually implemented as a Viterbi detector²⁰). For the linear equalizer, the resulting configuration has been considered before in the context of the channel memory length reduction and consequential substantial simplifications of the MLSD which partial response equalization affords^{34, 35}). The associated performance can be appraised in quadratic terms by evaluating a distance function which takes account of the noise colouration introduced by the equalizer. For the category of recording systems considered before, such an analysis reveals that the performance improvement of the MLSD over its symbol-wise counterpart is largest (up to about 3 dB for the bipolar and class IV partial responses) when the symbol-wise detector also functions best (judged relative to the matched filter bound). Conversely, the improvement decreases to negligible proportions whenever the symbol-wise detector incurs a large performance loss relative to the matched filter bound, i.e. whenever much equalization effort has to be spent to transform the intersymbol interference structure of the channel into the one prescribed by the partial response. Mutatis mutandis, similar (albeit smaller) improvements probably result for the partial response DFE whenever its error propagation is not too severe.

Appendix A. Minimum mean-square error partial response linear equalization

This appendix is concerned with the derivation of the minimum mean-square error dimensioning and performance of the partial response linear equalizer. The equalizer, having coefficients c_k , $-\infty < k < \infty$, transforms its input signal u_k into a sequence of decision variables \tilde{b}_k which intentionally resembles the original (virtual) sequence b_k as well as possible. From eq. (12) and fig. 1 we see immediately that \tilde{b}_k is given by

$$\tilde{b}_k = (b * z * c)_k + (n * h_* * c)_k, \quad (\text{A.1})$$

in which ‘*’ denotes linear convolution, z_k represents the autocorrelation

function of the discrete-time residual response h_k , and the subscript ‘ \cdot ’ indicates time-reversal. The mean-square error ε achieved by the equalizer is defined as

$$\varepsilon \triangleq E[(\tilde{b}_k - b_k)^2], \quad (\text{A.2})$$

in which $E[.]$ denotes mathematical expectation. It is possible to express ε in terms of the known system parameters by noting that b_k depends on a_k as

$$b_k = (a * g)_k, \quad (\text{A.3})$$

(where g_k represents the selected partial response), and that a_k is an uncorrelated binary sequence having unit power. Using eqs (A.3) and (A.1), the fact that n_k is a white noise process with variance N_0 statistically independent of a_k , and the fact that a_k is uncorrelated, eq. (A.2) can be written as

$$\begin{aligned} \varepsilon &= E[(b * (z * c - \delta) + (n * h_{\cdot} * c))_k^2] \\ &= E[(a * g * (z * c - \delta))_k^2] + E[(n * h_{\cdot} * c)_k^2] \\ &= \sum_{k=-\infty}^{\infty} (g * (z * c - \delta))_k^2 + N_0 \sum_{k=-\infty}^{\infty} (h_{\cdot} * c)_k^2, \end{aligned} \quad (\text{A.4})$$

where δ_k denotes the Kronecker delta function. By Parseval’s relationship it follows from eq. (A.4) that

$$\varepsilon = \int_{-0.5}^{0.5} \{|G(\Omega)[Z(\Omega)C(\Omega) - 1]|^2 + N_0 Z(\Omega)|C(\Omega)|^2\} d\Omega. \quad (\text{A.5})$$

The right-hand side of eq. (A.5) can conveniently be minimized over all $C(\Omega)$ by means of the calculus of variations technique. To this end, $\hat{C}(\Omega)$ is written as $\hat{C}(\Omega) + \mu V(\Omega)$, where $\hat{C}(\Omega)$ and $V(\Omega)$ represent the linear equalizer transfer function and an arbitrary deviation thereof, respectively. The requirement

$$\frac{\partial \varepsilon}{\partial \mu} \Big|_{\mu=0} = 0 \quad \text{for all } V(\Omega) \quad (\text{A.6})$$

then serves to identify the optimum transfer function $\hat{C}(\Omega)$. Using standard differentiation rules it is readily verified that

$$\frac{\partial \varepsilon}{\partial \mu} \Big|_{\mu=0} = 2 \operatorname{Re} \left\{ \int_{-0.5}^{0.5} Z(\Omega) V^*(\Omega) [Y(\Omega)(Z(\Omega)\hat{C}(\Omega) - 1) + N_0\hat{C}(\Omega)] d\Omega \right\}. \quad (\text{A.7})$$

Hence, provided that $Z(\Omega)$ is nonsingular it is required in order for eq. (A.6) to be fulfilled that the quantity in square brackets in eq. (A.7) equals zero for all Ω . Thus the optimum linear equalizer transfer function is given by

$$\hat{C}(\Omega) = \frac{Y(\Omega)}{X(\Omega) + N_0}. \quad (\text{A.8})$$

By substituting eq. (A.8) into eq. (A.5) the minimum mean-square error ε_{\min} is found to equal

$$\varepsilon_{\min} = \int_{-0.5}^{0.5} \frac{N_0 Y(\Omega)}{X(\Omega) + N_0} d\Omega = N_0 c_0. \quad (\text{A.9})$$

Appendix B. Minimum mean-square error partial response decision feedback equalization

In this appendix we derive the optimum partial response DFE dimensioning and performance, relative to a mean-square quality measure. The problem at hand involves the joint optimization of two filters, viz. the equalizers' forward and feedback filter, having impulse responses c_k ($-\infty < k < \infty$) and p_k ($1 \leq k < \infty$), respectively. As causality and anticausality, being typical time-domain concepts, play an important role in the derivation we shall, in contrast to appendix A, adopt a time domain-oriented approach. We set out by considering the decision variable \tilde{b}_k produced by the DFE. Making the usual assumption that all previous decisions which affect the output of the feedback filter are correct²³), it follows that \tilde{b}_k equals

$$\tilde{b}_k = (b * (z * c - p))_k + (n * h_- * c)_k. \quad (\text{B.1})$$

Using eq. (B.1), the mean-square error ε , defined as

$$\varepsilon \triangleq E[(\tilde{b}_k - b_k)^2], \quad (\text{B.2})$$

can be expressed as

$$\begin{aligned}
 \varepsilon &= E[(b * (z * c - p - \delta) + n * h * c)_k^2] \\
 &= E[(a * g * (z * c - p - \delta))_k^2] + E[(n * h * c)_k^2] \\
 &= ((z * c - p - \delta)_- * y * (z * c - p - \delta))_0 + N_0(c_- * z * c)_0, \quad (\text{B.3})
 \end{aligned}$$

provided that the input data and noise sequences are statistically independent, uncorrelated, and have variance 1 and N_0 , respectively.

We first focus upon the optimum setting of the feedback filter coefficients p_j . Differentiating eq. (B.3) with respect to p_j , $1 \leq j < \infty$, and requiring all partial derivatives to be zero, it follows that

$$\frac{\partial \varepsilon}{\partial p_j} = -2(y * (z * c - p - \delta))_j = 0 \quad \text{for } 1 \leq j < \infty. \quad (\text{B.4})$$

In the conventional (non partial response) case, $g_j = y_j = \delta_j$, so that according to eq. (B.4) the optimum feedback filter coefficients are the familiar replica of the impulse response $(z * c)_j$, $1 \leq j < \infty$. However, if $y_j \neq \delta_j$, then the solution to eq. (B.4) becomes more complicated, and the feedback filter impulse response p_j may no longer be expected to resemble the impulse response $(z * c)_j$ with complete fidelity.

Differentiating eq. (B.3) with respect to the forward filter coefficients c_j , $-\infty < j < \infty$, we find that

$$\begin{aligned}
 \frac{\partial \varepsilon}{\partial c_j} &= 2((y * z * (z * c - p - \delta))_j + 2N_0(z * c)_j) \\
 &= 2(z * [y * (z * c - p - \delta) + N_0 c])_j \quad \text{for all } j. \quad (\text{B.5})
 \end{aligned}$$

Whenever z_k is non-singular, eq. (B.5) can only be zero for all j if the expression within square brackets equals zero, i.e.

$$(y * (z * c - p - \delta))_j + N_0 c_j = 0 \quad \text{for all } j. \quad (\text{B.6})$$

Using eq. (B.4) in eq. (B.6) we see at once that

$$c_j = 0 \quad \text{for } 1 \leq j < \infty, \quad (\text{B.7})$$

so that, as in the non-partial response case, the optimum forward filter is anticausal. Rearranging terms in eq. (B.6) and realizing that eq. (B.7) must

hold, we arrive at a set of equations in the variables c_j , $-\infty < j \leq 0$, and p_j , $1 \leq j < \infty$, which can in principle be solved:

$$(c * (x + N_0 \delta))_j - (p * y)_j = y_j \text{ for all } j. \quad (\text{B.8})$$

Directing our attention to the minimum attainable mean-square error ε_{\min} , we see by substituting eq. (B.6) into eq. (B.3) that

$$\varepsilon_{\min} = N_0 [(p_- + \delta) * c]_0, \quad (\text{B.9})$$

and realizing that $p_{-j} = c_j = 0$, $j \geq 1$, eq. (B.9) reduces to

$$\varepsilon_{\min} = N_0 c_0. \quad (\text{B.10})$$

For mathematical convenience we now make the assumption that the partial response g_k is causal and has minimum-phase, so that its convolutional inverse g_k^{-1} is both stable and causal*). Responses within this category that have zeros on the unit circle are accommodated by moving the zeros a small distance from the unit circle and performing a limiting operation at the end of the derivation. In addition, we factor the sequence $x_k + N_0 \delta_k$ as the convolution of a causal minimum-phase sequence γ_k and its anticausal image γ_{-k} , i.e.

$$(x + N_0 \delta)_k = (\gamma_- * \gamma)_k \text{ for all } k, \quad (\text{B.11})$$

According to Doob (ref. 26, pp. 159-161) this factorization is unique, and exists under mild regularity conditions (the most stringent of which is the Paley-Wiener condition, requiring that $\ln[X(\Omega) + N_0]$ be integrable, which is implied by $N_0 > 0$). The sequence γ_k can be expressed recursively in its $k = 0$ value, which equals

$$\gamma_0 = \exp \left\{ 0.5 \int_{-0.5}^{0.5} \ln[X(\Omega) + N_0] d\Omega \right\}. \quad (\text{B.12})$$

The recursion relation is³⁶⁾

$$\gamma_k = \frac{2}{k} \sum_{i=0}^{k-1} (k-i)r_{k-i} \gamma_i \text{ for } k \geq 1, \quad (\text{B.13})$$

*) From a practical point of view, this assumption is hardly restrictive since it does not exclude the important category of responses $g(\mathcal{S}) = (1 - \mathcal{S})^m (1 + \mathcal{S})^n$.

where the coefficients r_k , $k \geq 1$, are defined as

$$r_k = \int_0^{0.5} \ln[X(\Omega) + N_0] \cos(2\pi k \Omega) d\Omega. \quad (\text{B.14})$$

By convolving both sides of eq. (B.8) by $(\gamma^{-1} * g^{-1})_k$ (where the superscript '-1' indicates the convolutional inverse operator) and making use of eqs (B.11) and (10) we find that

$$(c * g^{-1} * \gamma^{-1})_k = ((p + \delta) * g * \gamma^{-1})_k \text{ for all } k. \quad (\text{B.15})$$

The right- and left-hand sides of this expression are (by construction) causal and anti-causal, respectively. Since eq. (B.15) requires them to be equal, they can be nonzero for $k = 0$ only, and then assume the (right hand side) value $(g * \gamma^{-1})_0$ because $p_0 = 0$. By expressing γ_k^{-1} in Z-transform notation and making use of the fact that $\Gamma(Z)$ has no zeros outside the unit circle, this value is seen to equate to g_0/γ_0 . We therefore conclude that

$$c_k = \frac{g_0}{\gamma_0} (g * \gamma^{-1})_k \text{ for all } k, \quad (\text{B.16})$$

and

$$p_k = \frac{g_0}{\gamma_0} (g^{-1} * \gamma)_k - \delta_k \text{ for all } k. \quad (\text{B.17})$$

An immediate consequence of eqs (B.16) and (B.17) is that every spectral zero of g_k induces an identically located zero and pole of c_k and p_k , respectively. Combining eqs (B.10), (B.12) and (B.16) we finally arrive at the desired closed-form expression for ϵ_{\min} :

$$\epsilon_{\min} = N_0 \frac{g_0^2}{\gamma_0^2} = g_0^2 \exp \left\{ \int_{-0.5}^{0.5} \ln \frac{N_0}{X(\Omega) + N_0} d\Omega \right\}. \quad (\text{B.18})$$

Appendix C. Minimum mean-square error partial response decision feedback equalization subject to a zero trailing intersymbol interference constraint

This appendix is concerned with the derivation of the mean-square optimum decision feedback equalizer and its performance in a partial response mode of

operation, subject to the constraint that the feedback filter removes all trailing intersymbol interference. The constraint can be denoted as

$$p_k = \begin{cases} 0, & k \leq 0, \\ (z * c)_k, & k \geq 1. \end{cases} \quad (\text{C.1})$$

Defining a sequence U_k as

$$U_k = \begin{cases} (z * c - \delta)_k, & k \leq 0, \\ 0, & k \geq 1, \end{cases} \quad (\text{C.2})$$

it follows with the aid of eq. (C.1) that the mean-square error ε conforming to eq. (B.2) can be written as

$$\varepsilon = (U_- * y * U)_0 + N_0(c_- * z * c)_0. \quad (\text{C.3})$$

Our aim is the minimization of ε over all c_k . A first step towards this objective can be made by observing that

$$\frac{\partial U_j}{\partial c_n} = \begin{cases} z_{j-n}, & j \leq 0, \\ 0, & j \geq 1, \end{cases} \quad (\text{C.4})$$

so that

$$\frac{\partial \varepsilon}{\partial c_n} = 2 \sum_{i=-\infty}^0 \sum_{j=-\infty}^0 U_i y_{i-j} z_{j-n} + 2N_0(z * c)_n. \quad (\text{C.5})$$

Requiring this derivative to equal zero yields the following set of necessary and sufficient conditions:

$$\sum_{j=-\infty}^0 (U * y)_{j-z_{j-n}} + N_0(z * c)_n = 0 \quad \text{for all } n. \quad (\text{C.6})$$

By invoking eq. (C.2), we see that eq. (C.6) reduces to the following set of equations in only c_n , $-\infty < n < \infty$:

$$\sum_{k=-\infty}^0 c_k \left[\sum_{i=-\infty}^0 \sum_{j=-\infty}^0 z_{i-k} y_{i-j} z_{j-n} + N_0 z_{n-k} \right] = - \sum_{j=-\infty}^0 y_j z_{n-j}, \quad (\text{C.7})$$

which can in principle be solved. Multiplying both sides of eq. (C.6) by c_n and summing over all n we get:

$$\sum_{j=-\infty}^0 (U * y)_j (z * c)_j + N_0 (c * z * c)_0 = 0, \quad (\text{C.8})$$

or, invoking eq. (C.2),

$$(U * y * U)_0 + (U * y)_0 + N_0 (c * z * c)_0 = 0. \quad (\text{C.9})$$

Comparing eq. (C.9) and eq. (C.3) we see that the minimum mean-square error ε_{\min} can be expressed in the optimum sequence U_k as follows:

$$\varepsilon_{\min} = -(U * y)_0. \quad (\text{C.10})$$

Finally, by multiplying eq. (C.6) by y_{k-n} , $k \leq 0$, invoking eq. (C.2), and summing over all nonpositive n it follows that

$$\sum_{j=-\infty}^0 (U * y)_j \left[\sum_{n=-\infty}^0 y_{k-n} z_{j-n} + N_0 \delta_{k-j} \right] = -N_0 y_k, \quad (\text{C.11})$$

from which $(U * y)_j$, $j \leq 0$, can in principle be solved. $-(U * y)_0$ then specifies, according to eq. (C.10), the minimum mean-square error ε_{\min} .

REFERENCES

- 1) A. Lender, IEEE Trans. Commun. Electron., **52**, 214 (1963).
- 2) P. J. van Gerwen, Philips Res. Rept., **20**, 469 (1965).
- 3) E. Kretzmer, 1965 IEEE Communications Convention, Boulder, Colorado, pp. 451-455; also: IEEE Trans. Commun. Technol., **COM-14**, 67 (1966).
- 4) R. W. Lucky, J. Salz and E. J. Weldon, Jr., Principles of Data Communication, McGraw-Hill, New York, 1968.
- 5) P. Kabal and S. Pasupathy, IEEE Trans. Commun. Technol., **COM-23**, 921 (1975).
- 6) W. R. Bennett and J. R. Davey, Data Transmission, McGraw-Hill, New York, 1965.
- 7) H. Kobayashi, IEEE Trans. Commun. Technol., **COM-19**, 1087 (1971).
- 8) S. Nakagawa, K. Yokoyama and H. Katayama, IEEE Trans. Magn., **MAG-16**, 104 (1980).
- 9) H. Kobayashi and D. Tang, IBM J. Res. Develop., **14**, 368 (1970).
- 10) A. Lender, IEEE Spectrum, **3**, 104 (1966).
- 11) P. J. van Gerwen, IEEE Trans. Commun. Technol., **COM-16**, 108 (1968).
- 12) A. M. Gerrish and R. D. Hawson, in Conf. Rec., 1967 IEEE Int. Conf. Communications, Minneapolis, 186, 1967.

- 13) M. G. Vry, Proc. ISSLS'84, Nice, 259, 1984.
- 14) C. A. Ehrenbard and M. F. Tompsett, Proc. 1982 Globecom, Miami. pp. D8.4.1-D8.4.5.
- 15) J. W. M. Bergmans, Philips J. Res., **41**, 531 (1986).
- 16) H. Harashima and H. Miyakawa, IEEE Trans. Commun. Technol., **COM-20**, 774 (1972).
- 17) J. W. Smith, IEEE Trans. Commun. Technol., **COM-16**, 825 (1968).
- 18) H. Kobayashi and D. T. Tang, IEEE Trans. Commun. Technol. **COM-19**, 467 (1971).
- 19) J. Proakis, Digital Communications, McGraw Hill, New York, 1983.
- 20) G. Forney, Jr., IEEE Trans. Inform. Theory, **IT-18**, 363 (1972).
- 21) D. W. Tufts and T. Berger, IEEE Trans. Inform. Theory, **IT-13**, 196 (1967).
- 22) D. Messerschmitt, Rec. Int. Conf. Communications, **ICC-74**, Minneapolis, pp. 37D1-37D5.
- 23) C. Belfiore and J. Park, Proc. IEEE, **67**, 1143 (1979).
- 24) F. E. Glave, IEEE Trans. Inform. Theory, **IT-18**, 356 (1972).
- 25) J. Salz, Bell Syst. Tech. J., **52**, 1341 (1973).
- 26) J. L. Doob, Stochastic Processes, John Wiley and Sons, New York, 1967.
- 27) D. L. Duttweiler, J. E. Mazo and D. G. Messerschmitt, IEEE Trans. Inform. Theory, **IT-20**, 490 (1974).
- 28) O. Duarte and J. O'Reilly, IEE Proc., pt.F, **132**, 567 (1985).
- 29) K. Mueller, Bell Syst. Tech. J. **54**, 143 (1975).
- 30) J. Mallinson, Proc. IEEE, **64**, 196 (1976).
- 31) G. Sonu, IEEE Trans. Magn., **MAG-21**, 1392 (1985).
- 32) J. W. M. Bergmans, IEEE Trans. Magn. **MAG-22**, 157 (1986).
- 33) J. W. M. Bergmans and Y. C. Wong, Electronics and Communications, **41**, 33 (1987).
- 34) D. D. Falconer and F. R. Magee, Bell Syst. Tech. J., **52**, 1541 (1973).
- 35) A. D. Fagan and F. D. O'Keane, IEE Proc. pt.F, **133**, 535, (1986).
- 36) D. Messerschmitt, Bell Syst. Tech. J., **52**, 1521 (1973).

A SIMULATION STUDY OF INTERSYMBOL INTERFERENCE CANCELLATION

Abstract

The canceller of intersymbol interference is compared with its two main competitors in two distinct and representative environments. It is found that the canceller consistently lags behind the Viterbi detector in performance, and no longer improves upon the decision feedback equalizer in environments which predominantly give rise to multiple bit errors. The effects of filter length reduction and of the stacking of several canceller stages are investigated. Large reductions appear to be tolerable without notably degrading performance, and stacking of several canceller stages can improve the transmission quality whenever single bit errors prevail.

1. Introduction

The idea of using preliminary decisions to assist in the detection of a transmitted data sequence dates back nearly two decades¹⁾. During the last few years a growing consensus can be observed to designate its embodiment as a 'canceller of intersymbol interference'^{2,3)}. Various authors have studied performance aspects related to the canceller^{2,4)}, the operation of which is now understood to the extent that a description of its optimal dimensioning and performance is available in which the influence of error propagation has been neglected^{2,4)}. We will refer to a canceller that has been dimensioned in conformity with this description as ideal. The performance predicted for the ideal canceller corresponds to optimal isolated-pulse transmission quality^{2,4)}, which is well known to be beyond the reach of even the most powerful type of receiver (viz. the Maximum-Likelihood Sequence Estimator, in its most popular disguise as a Viterbi Detector) for certain classes of very dispersive channels^{5,6)}. Not surprisingly, simulations indicate that the transmission quality actually achieved by the ideal canceller drops far below the predictions, though still improving upon the decision feedback equalizer³⁾. The simulations that have so far been carried out³⁾ have concentrated upon channels for which

a Viterbi detector predominantly produces single bit errors (and thus essentially achieves optimal isolated pulse transmission quality⁷). We will in this paper also study (considerably worse) channels for which the Viterbi detector produces strongly correlated error sequences. Specifically for the latter type of channel it appears to be impossible to achieve relevant performance improvements over the DFE, even if a rather involved canceller optimization procedure is followed which takes account of the influence of erroneous preliminary decisions, and which leads to dimensionings that differ significantly from the ideal ones.

The paper sets out with a description of a (discrete-time) system model that suits the problem at hand. A subsequent section reports on a numerical assessment of the performance of the canceller and its "nested" extensions as well as of the DFE and the Viterbi detector for two distinct channels stemming from the area of digital magnetic recording. A concluding section finally attempts to recapitulate the essence of the acquired insights.

2. System Model

Fig. 1 depicts a model of a data transmission system employing intersymbol interference cancellation. This model can be regarded as the canonical equivalent discrete-time representation of a corresponding continuous-time system, from which it can be uniquely determined⁷). Its operation can be described as follows. An input sequence b_k consisting of uncorrelated binary digits drawn from the alphabet $\{-1, +1\}$ is applied to a discrete-time filtered signal channel having an impulse response f_k . The received signal r_k can be described as

$$r_k = (b * f)_k + n_k, \tag{1}$$

in which ' $*$ ' denotes linear convolution and n_k is an additive white Gaussian noise sequence having variance N_0 . The received signal r_k is fed into both a receiver which produces preliminary decisions and a canceller stage. Such a

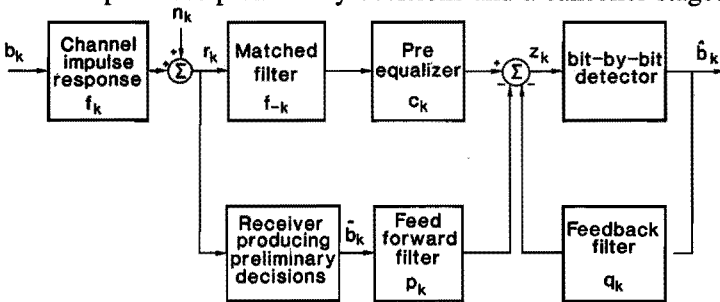


Fig. 1. Discrete-time model of a system employing intersymbol interference cancellation.

stage is composed around three filters, which more or less independently combat noise, pre-cursive and post-cursive intersymbol interference. The receiving filter suppresses noise in the incoming signal r_k as well as possible, and provides in addition a signal delay that suffices for the receiver which produces preliminary decisions to carry out its task (for mathematical convenience we shall not consider this causality constraint in the sequel). It consists of a matched filter (having an impulse response f_{-k}) cascaded by a preequalizer having an impulse response c_k (for the ideal canceller the preequalizer degenerates, and noise suppression becomes its only objective). Pre- and post-cursive intersymbol interference are intentionally removed by means of feedforward and feedback filters (FFF and FBF) of length M and N , respectively. To this end their impulse responses p_k , $-M \leq k \leq -1$, and q_k , $1 \leq k \leq N$, must satisfy the condition

$$\begin{aligned} p_k &= (x * c)_k, & -M \leq k \leq 1, \\ q_k &= (x * c)_k, & 1 \leq k \leq N, \end{aligned} \quad (2)$$

in which x_k represents the channel autocorrelation function, i.e.

$$x_k = (f * f_{-})_k \quad \text{all } k, \quad (3)$$

and where $(f_{-})_k \triangleq f_{-k}$, all k . Complete removal of intersymbol interference requires moreover that M and N are sufficiently large and that all preliminary and final decisions \hat{b}_k and \hat{b}_k propagating in the FFF and FBF are correct.

The combined action of the filters comprised in the canceller stage gives rise to a sequence of decision variables z_k given by

$$z_k = (b * x * c)_k - (\tilde{b} * p)_k - (\hat{b} * q)_k + (n * f_{-} * c)_k, \quad (4)$$

which is fed into the bit-by-bit detector. Under the usual assumptions that b_k and n_k are statistically independent and that all relevant preliminary and final decisions are correct, the mean-square error ε , defined as

$$\varepsilon \triangleq \text{E} \{(z_k - b_k)^2\}, \quad (5)$$

is easily seen to equal

$$\varepsilon = [(x * c - p - q - \delta)_{-} * (x * c - p - q - \delta)]_0 + N_0(c_{-} * x * c)_0, \quad (6)$$

in which δ_k represents the Kronecker delta function, and in which the subscript

'_' again denotes time reversal. The FFF and FBF impulse responses which minimize this expression satisfy eqs. 2, while the optimizing receiving filter $(f_* * c)_k$ approaches a matched filter when M and N tend to infinity⁴).

It is possible to arrive at a more realistic estimate for the mean-square error by extending eq. 6 with two terms which explicitly account for preliminary decision errors and their correlation with the noise sequence n_k . The involved auto- and cross correlation sequences can be estimated by performing either measurements or an approximative theoretical analysis. Reformulating the so-obtained expression for ϵ in matrix terms and performing a minimization, one arrives in a relatively straightforward fashion at the associated optimal impulse responses c_k , p_k and q_k . When comparing this solution with the ideal canceller, several differences can be observed, including in particular a strong ('causal') asymmetry in the overall system impulse response $(x * c)_k$ and a nonperfect match between the overall system and FFF impulse response. Unfortunately, we found these sizable changes in dimensioning to result in performance improvements which are at best marginal. For this reason we shall not dwell on further details of this approach.

The performance comparisons presented in this paper have a bearing upon a discrete-time channel impulse response of which the spectral density $X(\Omega) = |F(\Omega)|^2$ equals

$$X(\Omega) = 4 \sin^2 \pi \Omega \frac{\cosh 2\pi D(\frac{1}{2} - |\Omega|)}{\sinh \pi D}, \quad |\Omega| \leq \frac{1}{2}. \quad (7)$$

This model naturally arises in an important class of digital magnetic recording systems⁸). The parameter D characterizes the spatial information density on the magnetic medium, and ranges roughly from 0.1 to 3 in present systems. Fig. 2 depicts two typical (minimum-phase) impulse responses f_k which conform to this characterization. The associated amplitude-frequency characteristics are shown in Fig. 3. The response of Fig. 2a corresponds to an information density $D = 2.0$, for which the Viterbi detector still achieves optimal isolated pulse transmission quality, and hence predominantly produces single bit errors^{7,9}). Using standard mean-square performance results (see e.g. ref. 7, ch. 6), the performance loss relative to the matched filter bound which the MMSE DFE incurs can be estimated as 1.4 dB at a signal-to-noise ratio x_0/N_0 of 20 dB and in the absence of error propagation. The response of Fig. 2b characterizes the system at an information density which is some 65 percent larger than the density assumed in Fig. 2a, viz. for $D = 3.3$. For this density both the DFE and the Viterbi detector incur a significant performance loss relative to the matched filter bound, estimated as 4.4 dB (at a signal-to-noise

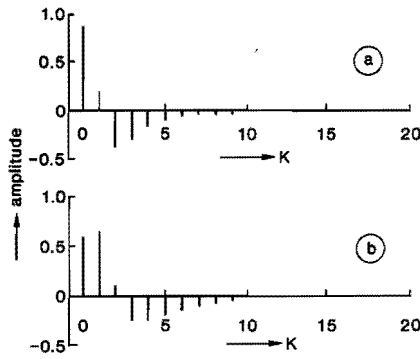


Fig. 2. Impulse response of (a) $D = 2.0$ channel, (b) $D = 3.3$ channel.

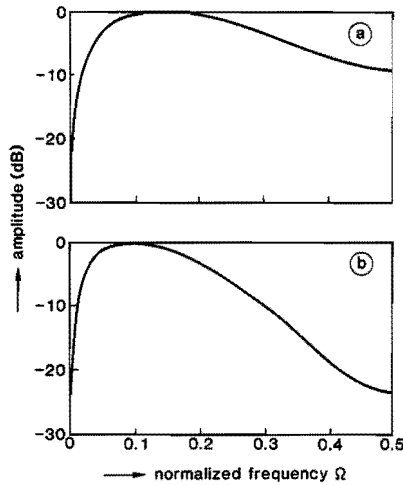


Fig. 3. Amplitude-frequency characteristics of (a) $D = 2.0$ channel, (b) $D = 3.3$ channel.

ratio of 20 dB and neglecting error propagation) and to 2.1 dB, respectively⁹).

3. Simulations

The preliminary decisions \tilde{b}_k can be produced by a receiver of any convenient type. Because of the preponderant influence upon the overall transmission quality of errors in the feedforward filter input signal we have in our simulations restricted attention to either the (MMSE) DFE or a preceding canceller stage

(thus allowing a 'nesting' of several stages) for providing the preliminary decisions. The filters of all DFEs and cancellers considered hereafter have been optimized with respect to the mean-square error measure of eq. 6. Moreover, we have consistently applied a preequalizer with a generous length of 16 bit intervals before and after the central tap, thereby virtually achieving infinite preequalizer length performance for all considered environments.

The enormous amount of trellis states resulting from the long duration of the system impulse response forced us to apply a reduced state Viterbi detector. The reduction is achieved by maintaining a stack of a predetermined maximum size (in our case equalling 32), in which only the best surviving paths are stored. Whenever much noise is present there is a considerable probability that the correct path will drop outside the stack, which explains the poor performance of the detector at low signal-to-noise ratios. At high signal-to-noise ratios a restriction of the stack size is much less problematical, and the detector is seen to approach its full stack size performance rapidly.

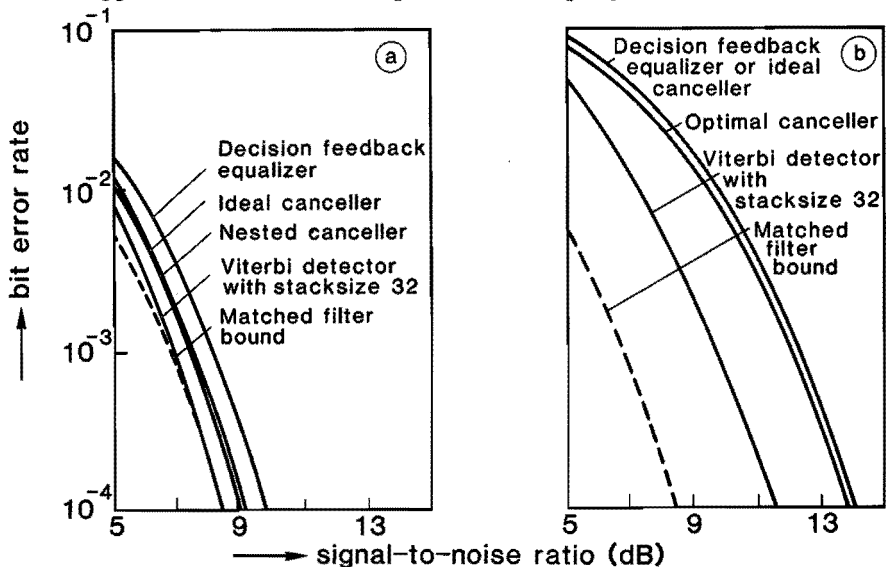


Fig. 4. Receiver performance characteristics for (a) $D = 2.0$ channel, (b) $D = 3.3$ channel.

We now consider the simulation results for the $D = 2.0$ recording system according to Fig. 2a. The associated performance curves have been collected in Fig. 4a. Focussing upon the DFE curve it is seen that the predicted loss of 1.4 dB relative to the matched filter bound is a realistic assessment of the true loss at $\text{SNR} = 10$ dB. The detrimental effects of error propagation are consequently at most marginal, even though the feedback filter length N has not been restricted. When this DFE is used to provide the preliminary decisions for a

subsequent canceller stage the overall transmission quality improves significantly, as can be observed from Fig. 4a. We observed that considerable reductions of particularly the FFF length (or, equivalently, complexity savings) were allowable without any notable degradation of the transmission quality. In fact, using an FFF and FBF of length 1 and 4, respectively, we obtained performances which were virtually indistinguishable from the (unrestricted FFF and FBF size) ones depicted in Fig. 4a. When the canceller is augmented with an additional, identical stage the resulting performance exhibits a further improvement of approximately 0.3 dB. Since the receiving filters of both stages are identical and operate upon the same signal there is no need to duplicate their hardware. Taking also the allowable small FFF and FBF sizes into account, it follows that a 'nested' canceller design need not be significantly more complex than a 'basic' canceller comprising only one stage. We found that still deeper nestings do not cause any significant further performance improvement.

Unlike the $D = 2.0$ channel, the errors produced by all the receivers for the $D = 3.3$ channel are highly correlated, as Table I illustrates for a signal-to-noise ratio x_0/N_0 of 12 dB.

It is seen in Table I that the error sequence $\{1 - 1\}$ predominates in all receivers, as should be expected on the basis of Euclidean distance considerations⁷). The average number of errors inside a burst comes close to the average burst length, indicating that error-free positions within a burst are rare. This is also reflected in the lower part of Table I, in which the cumulative error sequence distributions are presented.

TABLE I
Error statistics for $D = 3.3$ channel at SNR = 12 dB.

	DFE	Ideal canceller	Optimal canceller	Viterbi detector
Bit error rate	1.2×10^{-3}	1.2×10^{-3}	1.0×10^{-3}	8.6×10^{-5}
Average burst length	4.8	4.5	4.4	4.3
Average no. of errors inside a burst	3.7	3.7	3.6	3.4
Cumulative error sequence distribution (%)				
{1}	9	2	5	11
{1-1}	7	13	15	0
{1-1 1}	50	59	57	71
{1-1 1-1 1}	11	12	10	2
{others}	23	14	13	16

The measured performance curves for the $D = 3.3$ channel are depicted in Fig. 4b. The DFE feedback filter has been shortened to a length of 6 bit intervals, thereby exchanging a slight noise immunity degradation for a favourable improvement in error propagation¹⁰). The combined influence of error propagation and extra noise enhancement causes the DFE performance curve to be separated approximately 1 dB further from the matched filter bound than predicted. The Viterbi detector also suffers a (0.8 dB) larger loss than expected, which we attribute to the relatively small stack size used and to the increased average length of error events. Using a canceller that has been optimized with regard to the mean-square error measure given by eq. 6 it is impossible to attain a performance improvement over the DFE for any combination of FFF and FBF lengths. Only by applying the more involved optimization procedure outlined after eq. 6 are notable improvements feasible, the most favourable result of which is shown in Fig. 4b. We expect that the highly correlated error structure will prevent any bit-by-bit detection scheme from doing significantly better.

4. Conclusions

Although in this concise text we were not able to focus upon more than two distinct channels, we have actually performed simulations for a larger variety of environments, which all validate the following conclusive remarks. The canceller can achieve significant performance improvements over the DFE for all channels which predominantly give rise to single bit errors. For such channels, the augmentation of the canceller by one additional stage (which does not significantly increase complexity) gives rise to modest further improvements. Provided that the canceller is dimensioned appropriately it is feasible to reduce the length of its feedforward and feedback filters considerably (down to as little as 1 and approximately 4 bit intervals, respectively) at virtually no expense to the optimal performance. In contrast, channels which cause strongly correlated error sequences to arise appear to be essentially unsuitable for the application of the canceller. Contradicting the existing asymptotic predictions^{2,4}), the canceller consistently lags behind the Viterbi detector in performance.

REFERENCES

- 1) J. Proakis, Adaptive nonlinear filtering technique for data transmission. Proc. IEEE Symp. Adaptive Processes, Decision and Control, 1970, pp. XV.2.1 – XV.2.5.
- 2) A. Gersho and T. Lim, Adaptive cancellation of intersymbol interference for data transmission. Bell. Syst. techn. J. **60** (1981), 1997 – 2021.
- 3) K. Wesolowski, On the performance and convergence of the adaptive canceller of intersymbol interference in data transmission. Transact. IEEE COM-33 (1985), 425 – 432.
- 4) S. Mueller and J. Salz, A unified theory of data-aided equalization. Bell Syst. techn. J. **60** (1981), 2023 – 2038.
- 5) G. Forney, Jr., Maximum-likelihood sequence estimation of digital sequences in the presence of intersymbol interference. Transact. IEEE IT-18 (1972), 363 – 378.
- 6) D. Messerschmitt, A geometric theory of intersymbol interference – Part II: Performance of the maximum-likelihood detector. Bell. Syst. techn. J. **52** (1973), 1521 – 1539.
- 7) J. Proakis, Digital communications. McGraw-Hill Book Co., New York 1983.
- 8) J. Bergmans, Density improvements in digital magnetic recording by decision feedback equalization. Transact. IEEE MAG-22 (1986), 157 – 162.
- 9) J. Bergmans, Partial response equalization. Philips J. Res., vol. **42**, no. 2, (1987), pp. 131 – 172.
- 10) D. Messerschmitt, Design of a finite impulse response for the Viterbi algorithm and decision feedback equalizer. Record ICC-74, June 17 – 19, 1974, pp. 37D1 – 37D5. Minneapolis, MN, USA.

PERFORMANCE CONSEQUENCES OF TIMING ERRORS IN DIGITAL MAGNETIC RECORDING

Abstract

In digital magnetic recording systems, timing errors may arise during playback due to e.g. tape speed fluctuations, particularly at the high information densities encountered in the newest consumer-grade equipment. This paper studies the consequential performance degradations incurred by the most commonly used equalization and detection schemes, including the decision-feedback equalizer and the powerful maximum-likelihood sequence detector (MLSD). For all methods studied, it is found that even relatively small timing errors may already induce serious performance degradations. Although the simplest methods are on the average somewhat less sensitive than the more powerful ones, the precise ranking depends strongly upon the information density.

1. Introduction

The advent of digital VLSI technology has enabled the development of high-density digital magnetic recording systems for e.g. digital audio ¹⁾, digital consumer-grade video ²⁾, digital professional video ³⁾ and high-definition digital television ⁴⁾. The registration process in these systems proceeds at data rates of tens or even hundreds of megabits per second. At such rates it may be anything but simple to recover accurately the timing of the recorded waveform upon playback. This timing may fluctuate appreciably due to e.g. tape-head rubbing, tape tension variations, and, perhaps most importantly, fluctuations of the relative velocity of the (usually rotating) head and the registration medium ⁵⁾. As a result, the (conventionally linear and fixed) receiver operating on the playback signal may suffer a serious performance degradation relative to the situation of perfect timing recovery, as both experiments ⁶⁾ and simulations ^{7, 8)} indicate. These fragmentary findings, illustrating the apparent importance of the effect, underscore the desirability of establishing more structural

knowledge regarding the sensitivity to timing errors of the equalization and detection methods used in digital magnetic recording. The present paper is devoted to this topic. Apart from several variants of the traditional linear equalizer, it also considers two more powerful methods that currently attract much interest, viz. the decision-feedback equalizer (DFE) ⁹⁻¹² and the maximum-likelihood sequence detector (MLSD) ^{13,14}. In contrast to the linear and decision-feedback equalizer, the MLSD has an inherent decision delay, which complicates the accurate tracking (and therefore compensation) of timing jitter ^{15,16}.

The paper is constructed as follows. First, for an important practical class of digital magnetic recording systems, an equivalent discrete-time model is derived which takes account of the effect of static sampling phase errors. Next, the performance of the methods considered is analysed in the situation where they have been dimensioned to perform optimally for the nominal channel characteristics, while the actual characteristics exhibit a given deviation thereof. (It can be noted that this approach implicitly assumes fixed or at most slowly adaptive receivers, and hence provides a pessimistic estimate of the true sensitivities in the presence of an adaptation mechanism which (partly) compensates for parameter variations ¹⁷). This theoretical framework is finally specialized to the derived model and captured in numerical terms, revealing sensitivity figures which nearly invariably require sophisticated clock recovery schemes in order to allow full advantage to be taken of capabilities of the reception method used. As a large degree of generality is retained in the analysis of the distinct receivers, specialization of the results to other filter types of systems or variations should be a relatively straightforward undertaking.

2. A discrete-time representation of the influence of sampling phase errors

To illustrate their origin, fig. 1 depicts a part of a data transmission system suffering from timing errors.

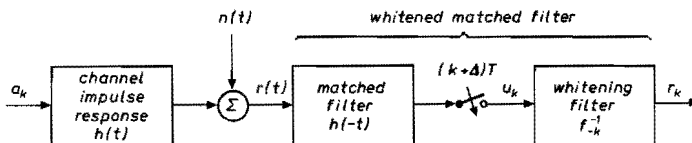


Fig. 1. Continuous-time model of a noisy dispersive channel followed by a matched filter, sampler and whitening filter.

A binary data sequence $a_k \in \{-1, 1\}$, whose symbols are spaced T seconds apart, is applied to a continuous-time noisy dispersive channel, which transforms a_k into an output signal

$$r(t) = \sum_{k=-\infty}^{\infty} a_k h(t - kT) + n(t), \quad (1)$$

where $h(t)$ is the impulse response of the channel, while $n(t)$ is an additive white Gaussian noise signal with power spectral density N_0 . For mathematical convenience, a_k is assumed to be uncorrelated and statistically independent of $n(t)$.

In many instances, the digital magnetic recording process can be well approximated by the model of eq. (1) in conjunction with the mentioned (explicit and implicit) assumptions¹⁸). This is true in particular for the important practical category of systems where use is made of an NRZ-like (e.g. 8-to-10¹⁹) transmission code, longitudinal magnetization and a differentiating (gapped-ring core) playback head. For these systems, provided that the medium thickness and the gap size of the playback head are sufficiently small, the Fourier transform

$$H(f) \triangleq \int_{-\infty}^{\infty} h(t) \exp\left(\frac{-j2\pi ft}{T}\right) dt \quad (2)$$

of $h(t)$ is, apart from a constant of proportionality without relevance to the present problem, given by

$$H(f) = T^{\frac{1}{2}} (1 - \exp(-j2\pi f)) \exp(-\pi D|f|), \quad (3)$$

where D is a normalized measure of the information density on the recording medium, ranging between approximately 0.1 and 3 in current systems¹⁸). The somewhat unconventional Fourier transform definition (with f dimensionless) is chosen here in order to simplify the following formulas.

The received signal $r(t)$ is fed into a filter matched to $h(t)$, and sampled at the symbol rate. In the absence of sampling phase errors, this is an information lossless procedure²⁰), which can be considered to form part of any receiver with an optimum dimensioning in e.g. the mean-square sense²²). Obviously, further linear processing needs to involve only discrete-time (transversal) filtering. In a practical (non-adaptive) implementation, the characteristics of the matched filter and all cascaded discrete-time (transversal) filters are usually combined into one continuous-time filter, the output of which is sampled at the symbol rate. As an interchange of the order of sampling and transversal filtering does not affect the resulting discrete-time output signal, it follows

that the sensitivity figures for such a configuration are identical to those obtained for the somewhat less practical (but theoretically more convenient) sampler position of fig. 1.

In the presence of a normalized sampling phase error Δ , the sampler output u_k can be denoted as

$$u_k = (a * x + n * h_-)((k + \Delta)T), \quad (4)$$

where ' $*$ ' and ' $_-$ ' denote linear convolution and time reversal, respectively, and $x(t)$ is the autocorrelation function of $h(t)$, i.e.

$$x(t) \triangleq (h * h_-)(t) = \frac{1}{T} \int_{-\infty}^{\infty} |H(f)|^2 \exp\left(\frac{j2\pi ft}{T}\right) df. \quad (5)$$

The filtered noise component $v_k \triangleq (n * h_-)((k + \Delta)T)$ contained in u_k has an autocorrelation function

$$E[v_i v_j] = N_0 x((i - j)T), \quad (6)$$

where N_0 is the spectral density of $n(t)$. Per transmitted bit, an energy

$$E_b = \int_{-\infty}^{\infty} h^2(t) dt = x(0) \quad (7)$$

is received. Using eq. (3) in eq. (5) it follows that ¹²⁾

$$x(0) = \frac{2}{\pi} \frac{1}{D(D^2 + 1)}. \quad (8)$$

The energy received per bit therefore decreases with the information density, particularly rapidly beyond $D = 1$. We now introduce the (discrete-time) notation

$$x_k^A \triangleq x((k + \Delta)T) = (h * h_-)((k + \Delta)T) \quad (9)$$

and define a sequence f_k to be the causal minimum-phase factor of x_k^0 . This sequence is unique and can be easily determined from the log power spectrum of x_k^0 (21). It satisfies

$$x_k^0 = (f * f_-)_k, \quad (10)$$

where ‘*’ and ‘.’ again indicate linear convolution and time-reversal, this time in their discrete-time forms. By making use of eqs (9) and (10), we can equivalently write eq. (4) as

$$u_k = (a * x^{\Delta})_k + (n * f)_k, \quad (11)$$

where n_k is a white Gaussian noise sequence having variance N_0 . According to eqs (11) and (10), the autocorrelation function of the noise component of u_k equals $N_0 x_k^0$, and hence adequately describes the noise colouration by the matched filter cf. eq. (6). By denoting the convolutional inverse operator by means of the superscript ‘ -1 ’, we see that the noise component of u_k can be whitened by means of a filter having an impulse response f_k^{-1} (fig. 1). This yields a signal r_k of the form

$$r_k = (a * x^{\Delta} * f_k^{-1})_k + n_k. \quad (12)$$

(The notation r_k has been chosen here in order to stress the similarity with the continuous-time received signal $r(t)$, which is also corrupted by white noise. It should be borne in mind, though, that r_k is, in general, not a sampled version of $r(t)$.) The cascade of matched filter, sampler and whitening filter is referred to as a whitened matched filter¹³). In the absence of timing errors, its output is a sufficient statistic for the optimum detection of a_k ¹³), and, in view of eq. (10), assumes the canonic form

$$r_k = (a * f)_k + n_k. \quad (13)$$

The minimum-phase causal root f_k of x_k^0 hence serves as an equivalent nominal discrete-time response for the system under consideration. In the sequel, we will find it useful to describe the effect of sampling phase errors in terms of a convolutional deviation from f_k . To this end, we introduce a deviation impulse response e_k^{Δ} , and write r_k as

$$r_k = (a * f * (\delta + e^{\Delta}))_k + n_k, \quad (14)$$

where δ_k denotes the Kronecker delta function. By comparing eqs (14) and (12) we see that e_k^{Δ} and x_k^{Δ} are interrelated as

$$(x^0 * e^{\Delta})_k = x_k^{\Delta} - x_k^0. \quad (15)$$

Hence e_k^{Δ} can be uniquely determined from x_k^{Δ} , e.g. by means of Fourier

transform techniques. Figure 2 depicts the system model conforming to eq. (14).

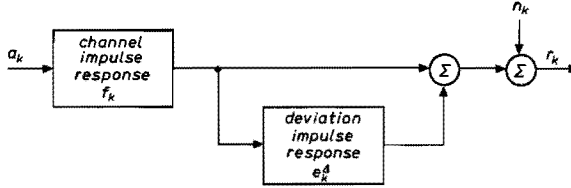


Fig. 2. Equivalent discrete-time model of the system in fig. 1.

For the class of recording systems under study, we will now derive the Fourier transforms of both x_k^d and e_k^d , from which x_k^d , e_k^d and f_k can be easily calculated numerically.

3. Transfer function of the equivalent discrete-time channel

We define the Fourier transform $X^d(\Omega)$ of x_k^d as

$$X^d(\Omega) \triangleq \sum_{k=-\infty}^{\infty} x_k^d \exp(-2\pi \Omega k) \quad \text{for all } \Omega. \quad (16)$$

$X^d(\Omega)$ is periodic with period 1, and furthermore has a Hermitian symmetry because of the fact that x_k^d is real-valued²¹). Hence it can be uniquely determined for all Ω from its behaviour in $[0, \frac{1}{2}]$, which we will now consider. Applying Poisson's summation formula²¹) to eq. (9), $X^d(\Omega)$ and $H(f)$ (cf. eq. (2)) are found to be interrelated as

$$X^d(\Omega) = \frac{1}{T} \sum_{n=-\infty}^{\infty} |H(\Omega + n)|^2 \exp(j2\pi \Delta(\Omega + n)). \quad (17)$$

By distinguishing between negative and non-negative values of n , the series contained in eq. (17) can be split in two semi-infinite geometric series, which can each be summed to yield for $\Omega \in [0, \frac{1}{2}]$:

$$X^d(\Omega) = 4 \sin^2 \pi \Omega \left[\frac{\exp(-2\pi(D + j\Delta)(1 - \Omega))}{1 - \exp(-2\pi(D + j\Delta))} + \frac{\exp(-2\pi(D - j\Delta)\Omega)}{1 - \exp(-2\pi(D - j\Delta))} \right]. \quad (18)$$

By combining both terms and applying elementary hyperbolic and trigonome-

tric identities, this expression can equivalently be written as

$$\begin{aligned}
 X^{\Delta}(\Omega) &= \\
 4 \sin^2 \pi \Omega &\frac{\exp(j 2 \pi \Delta \Omega) \sinh (2 \pi(1-\Omega) D)+\exp(-j 2 \pi \Delta(1-\Omega)) \sinh (2 \pi \Omega D)}{\cosh 2 \pi D-\cos 2 \pi \Delta} \\
 &= 8 \sin^2 \pi \Omega \exp(-j 2 \pi \Delta(\frac{1}{2}-\Omega))\left[\frac{\cos \pi \Delta \sinh \pi D \cosh 2 \pi D(\frac{1}{2}-\Omega)}{\cosh 2 \pi D-\cos 2 \pi \Delta}\right. \\
 &\quad \left.+j \frac{\sin \pi \Delta \cosh \pi D \sinh 2 \pi D(\frac{1}{2}-\Omega)}{\cosh 2 \pi D-\cos 2 \pi \Delta}\right]. \tag{19}
 \end{aligned}$$

In the absence of sampling phase errors, this rather unmanageable form simplifies to

$$X^0(\Omega)=4 \sin ^2 \pi \Omega \frac{\cosh 2 \pi D(\frac{1}{2}-\Omega)}{\sinh \pi D}, \tag{20}$$

in accordance with the results of refs 10 and 12. We now focus upon the Fourier transform $E^{\Delta}(\Omega)$ of the deviation impulse response e_k^{Δ} . The frequency-domain version of eq. (15) reads

$$E^{\Delta}(\Omega)=\frac{X^{\Delta}(\Omega)-X^0(\Omega)}{X^0(\Omega)}. \tag{21}$$

By inserting eqs (19) and (20) in eq. (21), we obtain a lengthy expression for $E^{\Delta}(\Omega)$, which can be simplified for small Δ by expanding the Δ -dependent factors in a Taylor series and retaining only the constant and linear terms. Provided that D is not too small, so that the denominator of eq. (19) does not approach zero, this yields for $\Omega \in [0, \frac{1}{2}]$:

$$E^{\Delta}(\Omega) \approx j 2 \pi \Delta\left\{\Omega-\frac{\sinh 2 \pi \Omega D}{2 \sinh \pi D \cosh 2 \pi D(\frac{1}{2}-\Omega)}\right\}, \tag{22}$$

the approximation error being of the order $O(\Delta^2)$. When D is also close to zero, expansion of $E^{\Delta}(\Omega)$ gives the even simpler and frequency-independent approximation

$$E^A(\Omega) \approx - \frac{\Delta^2}{D^2 + \Delta^2}. \quad (23)$$

Numerical calculations reveal that this approximation complies within 4 and 15 percent in modulus with the true function for densities D up to 0.1 and 0.2, respectively, provided that $|\Delta| \leq 0.5$, and irrespective of Ω . Expression (23) indicates a gain mismatch, which may lead to severe sensitivity problems when Δ is as large or larger than D , as we will see later on.

4. Sensitivity of the linear equalizer

In this section we consider a number of linear reception methods which all involve the use of a forward linear filter in conjunction with a (two- or three-level) symbol-by-symbol detector.

4.1. Full-response equalizer

The full-response equalizer, depicted in fig. 3, is a discrete-time filter (having an impulse response c_k for $-\infty < k < \infty$) which operates on the output signal r_k of the whitened matched filter. It is dimensioned so as to suppress intersymbol interference (ISI) and noise as well as possible, producing a sequence of decision variables \tilde{a}_k which is fed into a symbol-by-symbol detector, whose binary output sequence \hat{a}_k serves as an estimate of the transmitted data sequence a_k .

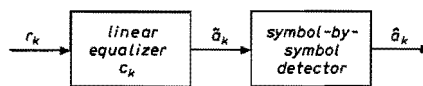


Fig. 3. Linear receiver.

To simplify the following mathematical derivation, we will initially assume the equalizer to be zero-forcing, i.e. to eliminate all ISI prior to detection. In this case its transfer function $C(\Omega)$ is given by ²²⁾

$$C(\Omega) = \frac{1}{F(\Omega)}, \quad (24)$$

where $F(\Omega)$ denotes the Fourier transform of f_k . By inserting the time domain version of eq. (24) in eq. (14), we see that \tilde{a}_k is given by

$$\tilde{a}_k = (a * (\delta + e^A))_k + (n * f^{-1})_k. \quad (25)$$

This expression reveals that the decision variable comprises a filtered noise component with variance

$$\sigma^2 = N_0 \int_{-0.5}^{0.5} \frac{d\Omega}{|F(\Omega)|^2} = N_0 \int_{-0.5}^{0.5} \frac{d\Omega}{X^0(\Omega)}. \quad (26)$$

Moreover, in the absence of sampling phase errors the overall system impulse response amounts to a Kronecker delta function, implying that the decision distance $d/2$, defined as the minimum distance between the (zero) detector threshold level and any possible value of the non-noise component $(a * (\delta + e^A))_k$ of \tilde{a}_k , equals 1. An erroneous sampling phase does not affect the noise variance of \tilde{a}_k , but decreases $d/2$ to

$$\frac{d}{2} = (1 + e_0^A) - \sum_{k \neq 0} |e_k^A|, \quad (27)$$

as expansion of eq. (25) reveals. For sufficiently large signal-to-noise ratios x_0^0/N_0 , the error probability $\Pr[E]$ achieved by the receiver assumes the form^{20, 23)}

$$\Pr[E] \propto Q\left(\frac{d}{2\sigma}\right), \quad (28)$$

where

$$Q(x) \triangleq \frac{1}{\sqrt{2\pi}} \int_x^\infty \exp\left(-\frac{y^2}{2}\right) dy. \quad (29)$$

For systems with spectral zeros (such as the one under consideration) the integral of eq. (26) diverges, and alternative methods are needed to achieve acceptable noise variances and thus bit error rates. One method is to modify slightly the dimensioning of the equalizer so as to allow some residual ISI in exchange for improved noise suppression. For the nominal channel, the minimum achievable mean-square error (MMSE) (i.e. the total power of noise and residual ISI) then amounts to

$$\varepsilon_{\min} = \int_{-0.5}^{0.5} \frac{N_0}{X^0(\Omega) + N_0} d\Omega, \quad (30)$$

and is attained by means of an equalizer transfer function ¹²⁾

$$C(\Omega) = \frac{F^*(\Omega)}{X^0(\Omega) + N_0}, \quad (31)$$

whose modulus is guaranteed to remain finite for any positive noise variance N_0 . An estimate for the transmission quality achieved in this case can be obtained by naively assuming the error signal $\tilde{a}_k - a_k$ to have a Gaussian distribution ¹²⁾. For high signal-to-noise ratios, this leads to an error probability linearly proportional to $Q(d/2\sqrt{\varepsilon_{\min}})$, with $d/2 = 1$. The system under study has zero transfer at $\Omega = 0$ only, so that the new transfer function of the equalizer (cf. eq. (31)) essentially deviates from the zero-forcing one (eq. (24)) in being finite near $\Omega = 0$, as a result of which the overall system impulse response obtains a small dc-offset. As practical full-response systems invariably use a dc-restoring circuit and/or a dc-constraint in the employed transmission code ²⁴⁾, the effect of this offset on the detection process can be disregarded, allowing the Δ -dependent decision distance $d/2$ to be approximated by its zero-forcing value (27).

4.2. Optimum zero-forcing partial response equalizer

A second means of reducing the noise enhancement entailed in full response linear equalization involves the use of partial response techniques, ^{25, 12)} which do not eliminate all ISI prior to detection, but rather create an integer-valued overall system impulse response g_k extending over a small number of symbol intervals. In digital magnetic recording systems, the responses

$$g_k = \delta_k - \delta_{k-1} \quad (32)$$

and

$$g_k = \delta_k - \delta_{k-2}, \quad (33)$$

designated Bipolar and Class IV partial response, respectively, are frequently applied ^{6, 8)}. Their respective Fourier transforms $G(\Omega)$ are given by

$$G(\Omega) = 1 - \exp(-j2\pi\Omega) = 2 \exp(j\pi(\frac{1}{2} - \Omega)) \sin \pi\Omega \quad (34)$$

and

$$G(\Omega) = 1 - \exp(-j 4\pi \Omega) = 2 \exp(j \pi(\frac{1}{2} - 2\Omega)) \sin 2\pi \Omega. \quad (35)$$

In order to create the desired correlation structure, the equalizer must have a transfer function

$$C(\Omega) = \frac{G(\Omega)}{F(\Omega)}, \quad (36)$$

and since the spectral zeros at dc of $|G|^2$ coincide with those of X^0 (cf. eq. (20)), the noise variance

$$\sigma^2 = N_0 \int_{-0.5}^{0.5} \frac{|G(\Omega)|^2}{|F(\Omega)|^2} d\Omega = N_0 \int_{-0.5}^{0.5} \frac{|G(\Omega)|^2}{X^0(\Omega)} d\Omega \quad (37)$$

will remain finite, as desired. For the Bipolar partial response, this integral can be evaluated analytically:

$$\begin{aligned} \sigma^2 &= 2N_0 \int_0^{0.5} \frac{\sinh \pi D}{\cosh(2\pi D(\frac{1}{2} - \Omega))} d\Omega \\ &= 2N_0 \frac{\sinh \pi D}{\pi D} \arctan\left(\tanh \frac{\pi D}{2}\right). \end{aligned} \quad (38)$$

This expression can be approximated for small D as

$$\sigma^2 \approx N_0 \pi D, \quad (39)$$

the approximation error being of the order $O(D^2)$. Being an estimate for the ternary data sequence

$$b_k \triangleq (a * g)_k, \quad (40)$$

the equalizer output signal \tilde{b}_k now nominally possesses three data levels, requiring a three-level symbol-by-symbol detector. (For the sake of simplicity, we will not concern ourselves with the additional precoding and square-law inverse mapping operations that are required to prevent error propagation when reconstructing \hat{a}_k from the detected ternary sequence. The presence of these operations does not affect any of the results derived here ¹²). Assuming the detector thresholds to be spaced halfway adjacent nominal data levels (i.e. at ± 1), we have a decision distance $d/2 = 1$ in the absence of timing errors, and

an error probability which is again linearly proportional to $Q(d/2\sigma)$ at high signal-to-noise ratios¹²). According to eqs (14) and (36), a non-zero sampling phase induces a decision variable $\tilde{b}_k = (r * c)_k$ of the form

$$\tilde{b}_k = (b * (\delta + e^\Delta))_k + (n * g * f)_k \quad (41)$$

whose noise content is not affected by Δ . By expanding the first term in the right-hand side of eq. (41) on the basis of eq. (40) as a weighted sum of bits a_{k-i} and next using eqs (32) and (33) to distinguish between the bits that determine b_k and the ones that do not, the decision distance $d/2$ can be seen to degrade to

$$\begin{aligned} \frac{d}{2} &= 1 - \max\{(g * e^\Delta)_l - (g * e^\Delta)_0, |(g * e^\Delta)_0 + (g * e^\Delta)_l|\} - \sum_{k \neq 0, l} |(g * e^\Delta)_k| \\ &= 1 - \max\{-(g_- * g * e^\Delta)_0, |((g - g_-) * e^\Delta)_0|\} - \sum_{k \neq 0, l} |(g * e^\Delta)_k|, \end{aligned} \quad (42)$$

where $l = 1$ and 2 for the Bipolar and Class IV partial responses, respectively. Here, the left and right braced terms are due to 'in phase' bits that give rise to $b_k = \pm 2$ and $b_k = 0$, respectively.

4.3. Raised cosine partial response equalizer

The partial response equalizers considered above are optimum in the sense that they achieve the smallest possible noise enhancement of all zero-forcing Bipolar and Class IV linear equalizers, respectively. Unfortunately, as we will see, they may be quite sensitive to sampling phase variations, particularly when the channel has a large bandwidth. We now contrast these schemes with two partial response schemes that are applied in practice^{6, 8}).

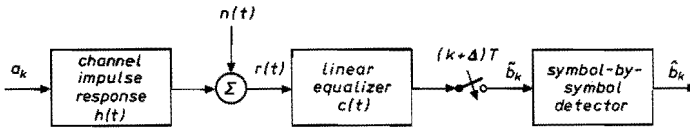


Fig. 4. Continuous-time data transmission system employing partial response linear equalization.

Unlike the other reception methods considered in this paper, these schemes cannot be decomposed in terms of a matched filter followed by a transversal filter. Instead, they explicitly limit the bandwidth of the continuous-time

received signal $r(t)$ (see fig. 4) by means of an equalizer transfer function

$$C(f) \triangleq \frac{G(f) W_\beta(f)}{H(f)} \quad (43)$$

where the partial response characteristic $G(f)$ is given by eq. (34) or eq. (35) (with f replacing Ω), while $W_\beta(f)$ is a raised cosine characteristic of the form

$$W_\beta(f) \triangleq \begin{cases} T, & \text{for } 0 \leq f \leq \frac{1-\beta}{2}, \\ \frac{1}{2}T [1 - \sin \frac{\pi}{\beta} (f - \frac{1}{2})] & \text{for } \frac{1-\beta}{2} < f < \frac{1+\beta}{2}, \\ 0, & \text{for } f \geq \frac{1+\beta}{2}. \end{cases} \quad (44)$$

Since $W_\beta(f)$ satisfies the Nyquist-1 criterion²², the system transfer function $H(f) C(f)$ corresponds to (Bipolar or Class IV) partial response system operation.

As previously, the transmission quality achieved by these schemes assumes the asymptotic form $\text{Pr}[E] \propto Q(d/2\sigma)$, where the Δ -dependent decision distance $d/2$ can be determined from the sampled system impulse response $(h * c)((k + \Delta)T)$ by decomposing it into a (Bipolar or Class IV) nominal system impulse response $f_k = g_k$ and a deviation impulse response e_k^A , as depicted in fig. 2. Making use of eqs (34), (35) and (43), it is easily verified that

$$e_k^A = w_\beta(k + \Delta) - \delta_k, \quad (45)$$

where $w_\beta(t)$ is the inverse Fourier transform of $W_\beta(f)$, equal to

$$w_\beta(t) = \frac{\sin \pi (t/T) \cos \pi \beta (t/T)}{\pi (t/T) 1 - (2\beta t/T)^2}. \quad (46)$$

Hence e_k^A is independent of the precise characteristics of the channel. In contrast, the noise variance σ^2 at the equalizer output is given by

$$\sigma^2 = \frac{N_0}{T} \int_{-\infty}^{\infty} |C(f)|^2 df, \quad (47)$$

and as $C(f)$ depends explicitly upon the channel transfer function through

eq. (34) and eq. (35), the same must be true for the noise variance. Making use of eqs (3) and (34), the integral of eq. (47) can be evaluated analytically for the recording system under study, giving

$$\sigma^2 = \frac{N_0}{\pi D} \left\{ e^{\pi D} \left[\frac{\cosh \pi \beta D}{(2\beta D)^2 + 1} - \frac{\sinh \pi \beta D}{(2\beta D)^2 + 4} \right] - 1 \right\}. \quad (48)$$

By expanding the D -dependent terms in this expression in a Taylor series, we find that for D close to zero

$$\sigma^2 \approx N_0 \left(1 - \frac{\beta}{4} \right), \quad (49)$$

the approximation error being of the order $O(D^2)$. By comparing eq. (49) with eq. (39) we see that for small D and Bipolar operation, raised cosine reception will cause a much larger noise enhancement than reception on the basis of a matched filter. There is no contradiction in this observation: a bandwidth-restricted raised cosine filter indeed manages to suppress incoming noise quite well, but at the same time it suppresses the data component of the received signal by such a large factor that its net performance is grossly inferior to the matched filter based equalizers, where a signal-to-noise ratio optimizing (and much larger) bandwidth is used.

5. Sensitivity of the decision-feedback equalizer

Instead of using a forward filter which potentially enhances the noise, the zero-forcing (ZF) decision-feedback equalizer (DFE) eliminates all intersymbol interference by means of feedback filter (FBF) which is excited by the detected data sequence (fig. 5).

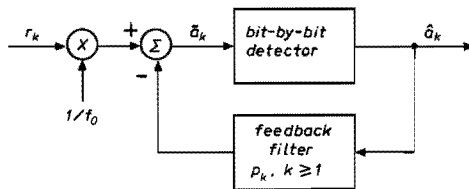


Fig. 5. Zero-forcing decision-feedback equalizer.

Because the channel impulse response f_k has minimum-phase, the forward path of the equalizer only contains a constant gain $1/f_0$ which serves to normalize the decision distance $d/2$ in the absence of timing errors to $1^{17,26}$. Provided that the FBF impulse response p_k matches the trailing part of the overall system impulse response, i.e.

$$p_k = \frac{f_k}{f_0} \text{ for } k \geq 1, \quad (50)$$

all (trailing) ISI will be eliminated prior to detection as long as the decisions fed into the FBF are correct. (The error propagation which arises if the latter condition is not met is generally not very serious at realistic signal-to-noise ratios^{26,12}.) Since even the zero-forcing DFE is perfectly capable of dealing with spectral zeros, a study of the ZF situation will reveal essentially the same information as consideration of the more complicated MMSE case.

At high signal-to-noise ratios, the error probability achieved by the ZF DFE again becomes linearly proportional to $Q(d/2\sigma)$, where $d/2$ ideally equals 1, and where the variance σ^2 of the noise contained in the decision variable \tilde{a}_k obviously equals

$$\sigma^2 = \frac{N_0}{f_0^2}. \quad (51)$$

We recall that f_k can be calculated from the log spectrum of $X^0(\Omega)$. In particular, f_0 is given by²¹)

$$f_0 = \exp\left\{\frac{1}{2} \int_{-0.5}^{0.5} \ln X^0(\Omega) d\Omega\right\}. \quad (52)$$

By using eqs (14) and (50), it is easily verified that the decision distance $d/2$ degrades to

$$\frac{d}{2} = 1 + \frac{(f * e^{\Delta})_0}{f_0} - \frac{1}{f_0} \sum_{k \neq 0} |(f * e^{\Delta})_k| \quad (53)$$

in the presence of a sampling phase error Δ .

6. Sensitivity of the maximum-likelihood sequence detector

The maximum-likelihood sequence detector (MLSD) ranks among the most

powerful receiver types conceivable¹³⁾. The MLSD, which directly operates upon the output signal (cf. (14)) of the whitened matched filter*), considers all allowable sequences a'_k , and finally selects that sequence \hat{a}_k which, after filtering by the assumed overall system impulse response f_k , best resembles its input sequence r_k (**). More specifically, the detector minimizes the Euclidian distance

$$J_{a'} \triangleq \sum_{k=-\infty}^{\infty} (r_k - (a' * f)_k)^2 = ((r - a' * f)_- * (r - a' * f))_0 \quad (54)$$

over all possible sequences a'_k . The simplest MLSD representative, viz. the Viterbi detector¹³⁾, realizes this minimization in a recursive fashion, thus omitting an exponential growth of processing effort as the message length increases. It can be seen from eqs (14) and (54) that whenever the filtered version $(a' * f)_k$ of an erroneous sequence a'_k is close (in the Euclidian sense) to the filtered version $(a * f)_k$ of the original sequence a_k , the MLSD is likely to make errors, requiring only a small amount of noise n_k or residual interference due to timing errors to cause confusion between the two. More exactly, an error will be made if $J_{a'} < J_a$, and the likeliness of this condition can be calculated by considering the difference of both distances. By making use of eqs (10), (14), (15) and (54), it is not difficult to show that

$$\begin{aligned} J_{a'} - J_a &= ((a - a')_- * x^d * (a - a'))_0 \\ &+ ((a - a')_- * (x^d - x^0) * (a + a'))_0 \\ &+ 2(n_- * (a - a') * f)_0. \end{aligned} \quad (55)$$

In the absence of parameter variations the second term in the right-hand side of this expression vanishes, causing $J_{a'} - J_a$ to depend exclusively upon the error sequence $(a - a')_k$ and no longer on the sum sequence $(a + a')_k$. By introducing the notation

$$\begin{aligned} M(a, a') &\triangleq ((a - a')_- * x^d * (a - a'))_0 \\ &+ ((a - a')_- * (x^d - x^0) * (a + a'))_0 \end{aligned} \quad (56)$$

*) There exists an MLSD variant due to Ungerboeck²⁷⁾ which operates on the sampled output of the matched filter of fig. 1. Performing an equivalent detection process, the Ungerboeck MLSD has the same sensitivity behaviour as the one analysed here.

**) It should be noted that this approach is only maximum-likelihood in the absence of timing errors, i.e. when the assumed system impulse response equals the actual one.

and

$$V(a, a') \triangleq ((a - a')_0 * x^0 * (a - a'))_0, \quad (57)$$

$J_{a'} - J_a$ is seen to be a Gaussian random variable with mean $M(a, a')$ and variance $4N_0 V(a, a')$. Hence it is smaller than zero with probability

$$\Pr[J_{a'} - J_a < 0] = Q\left(\frac{M(a, a')}{\sqrt{4N_0 V(a, a')}}\right) = Q\left(\frac{d(a, a')}{2\sigma}\right), \quad (58)$$

where

$$d^2(a, a') \triangleq \frac{M^2(a, a')}{V(a, a')} \quad (59)$$

and

$$\sigma^2 \triangleq N_0. \quad (60)$$

It is instructive to interpret the eqs (56) and (57) in the frequency domain. Making use of Parseval's relationship, we see that

$$\begin{aligned} M(a, a') &= \int_{-0.5}^{0.5} |A(\Omega) - A'(\Omega)|^2 X^d(\Omega) d\Omega \\ &+ \int_{-0.5}^{0.5} [|A(\Omega)|^2 - |A'(\Omega)|^2 + 2 \operatorname{Im}(A^*(\Omega) A'(\Omega))] \\ &\quad (X^d(\Omega) - X^0(\Omega)) d\Omega. \end{aligned} \quad (61)$$

and

$$V(a, a') = \int_{-0.5}^{0.5} |A(\Omega) - A'(\Omega)|^2 X^0(\Omega) d\Omega. \quad (62)$$

Hence both M and V can be interpreted as a frequency domain weighted measure of the dissimilarity of a_k and a'_k . We observe from eqs (61) and (62) that both M and V are insensitive to a shift of the time index k . For large signal-to-noise ratios the performance of the MLSD is dominated by the combination of a and a' which yields the smallest distance

$$d_{\min}^2 \triangleq \min_{a, a'} d^2(a, a') \quad (63)$$

of all possible combinations¹³), i.e.

$$\Pr[E] \propto Q\left(\frac{d_{\min}}{2\sigma}\right). \quad (64)$$

Since $M(a, a')$ depends not only upon the error sequence $(a - a')_k$ but also upon the sum sequence $(a + a')_k$, the traditional methods for finding d_{\min}^2 ^{22, 28}) are not applicable here, and a 'brute force' computer search seems to be the easiest way to go. Some idea of the search effort required for finding d_{\min}^2 can be obtained by taking $x_k^A - x_k^0$ to extend effectively from $-L$ to U . For an error sequence $a_k - a'_k$ which starts at $k = 0$ and has length K , it follows that $((a - a') * (x^A - x^0))_k$ then effectively equals zero outside the interval $[-L, U + K - 1]$. With the aid of eq. (56), it is clear that $M(a, a')$ is completely determined by values of a_k and a'_k in the same time interval, so that both a_k and a'_k may be taken equal to zero outside this interval for the purpose of distance calculations. For typical (high-density) values of L, U and K of 9, 10 and 5, respectively, this implies that no less than $2^{L+U} 3^{K-1} \approx 2 \cdot 10^8$ candidate pairs (a_k, a'_k) are to be considered. On a VAX 11/780 computer, this computational load requires a considerable fraction of a CPU weekend in order to generate one of the MLSD curves presented in the next section.

7. Performance comparison

A useful reference for the comparison of equalization and detection methods is the Matched Filter bound, which sets an upper limit to the performance achievable by any reception method²²). The error probability corresponding to matched filter bound performance is linearly proportional to $Q(\sqrt{\text{SNR}})$, where

$$\text{SNR} \triangleq \frac{x_0^0}{N_0} \quad (65)$$

is the signal-to-noise ratio of the output signal of the whitened matched filter. As we have seen in the previous sections, the error probability actually achieved by the reception methods considered here is linearly proportional to $Q(d/2\sigma)$, where $d/2$ and σ can be calculated from $X^A(\Omega)$ and N_0 and hence depend upon SNR. We are thus led to define a quantity

$$\mathcal{L} \triangleq \frac{\text{SNR}}{(d/2\sigma)^2} \geq 1 \tag{66}$$

to be the effective signal-to-noise ratio loss of a reception method relative to the matched filter bound. By inspecting the expressions for $d/2$ and σ^2 derived in the previous sections, it can be easily verified that \mathcal{L} is independent of SNR for all methods studied except the MMSE full response linear equalizer. Apart from the reception method, \mathcal{L} obviously depends on the normalized information density D and on the normalized sampling phase error Δ .

We now turn to the sensitivity evaluation that has been carried out on the basis of the theory developed in the preceding sections. To set the stage, fig. 6 depicts the calculated dependence of \mathcal{L} upon D in the absence of sampling phase errors and for a realistic signal-to-noise ratio SNR of 20 dB. The

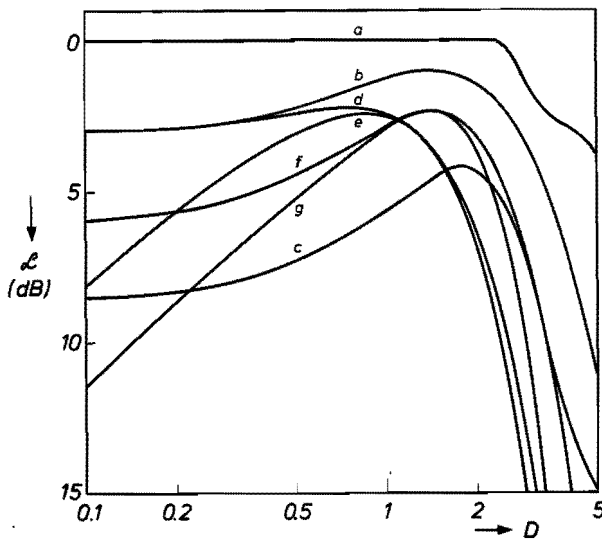


Fig. 6. Effective signal-to-noise ratio loss \mathcal{L} versus normalized information density D for various receiver types at a signal-to-noise ratio SNR of 20 dB and in the absence of a sampling phase error. a. MLSD; b. Decision feedback equalizer; c. Full response linear equalizer (integrated detection); d. Optimum zero-forcing Bipolar linear equalizer (amplitude detection); e. Raised cosine Bipolar linear equalizer (amplitude detection); f. Optimum zero-forcing Class IV linear equalizer; g. Raised cosine Class IV linear equalizer.

impressive power of the MLSD is clearly illustrated by its capability to achieve matched filter bound performance up to $D = 2.8$. Beyond this density the channel amplitude distortion becomes so large that multiple rather than single bit errors dominate, causing a rapidly increasing loss. Despite its much simpler

implementation, the DFE actually lags quite closely behind the MLSD for densities between roughly $\frac{1}{2}$ and 3. Because of its large noise enhancement, the full response linear equalizer consistently performs considerably worse than the MLSD and DFE. The Bipolar and Class IV partial response linear equalizers operating on the output of the whitened matched filter show up much better, and in fact closely approach the DFE performance at low and medium densities, respectively. As expected, up to densities of about 1, the raised cosine partial response equalizers (which use a typical value⁸) of 0.5 for β) are distinctly inferior to their whitened matched filter counterparts.

The dramatic effect of a sampling phase error of no more than 10 percent of a bit interval is depicted in fig. 7. At low densities, the large bandwidth of the

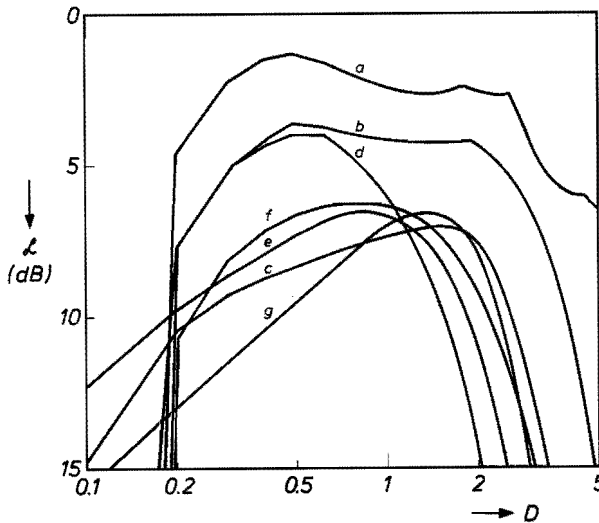


Fig. 7. As fig. 6, but in the presence of a sampling phase error of 10 percent of a bit interval.

matched filter output signal causes narrow output pulses and a consequent large susceptibility to sampling errors for all receivers which operate on a sampled version of this signal. The only (partial) exception here is the full response linear equalizer, whose familiar insensitivity to gain mismatches²⁹) complies well with the dominant effect of timing errors in this density region (cf. eq. (23)). Around $D = 0.5$, this equalizer in fact incurs a noteworthy loss of no more than 1 dB relative to the $\Delta = 0$ situation. Because of their considerable bandwidth restriction, a sensitivity-reducing pulse broadening occurs for the conventional (Bipolar and Class IV partial response) raised cosine equalizers,

allowing them to withstand a sampling phase error quite well. Nevertheless, their large noise enhancement still leads for all but the lowest densities to a performance comparable or inferior to the other receiver types. At medium densities ($1 \leq D \leq 2.5$), the mutual ranking of the receivers conforms largely to the $\Delta = 0$ situation. As they undergo about 1 dB less degradation than the approximately 4 dB incurred by the linear types of receiver, both the DFE and MLSD show up remarkably well. Finally, at the high end of the density spectrum only the Viterbi detector succeeds in establishing a performance within the scale of fig. 7, indicating a substantial performance advantage over the linear and feedback receivers.

At a fixed and relatively high density D of 2.5 (typical for the newest consumer-grade audio systems¹), we have calculated the performances of the receivers under study for sampling phase errors ranging from -25 percent to $+25$ percent of a bit interval. Fig. 8 depicts the results. Because of their large

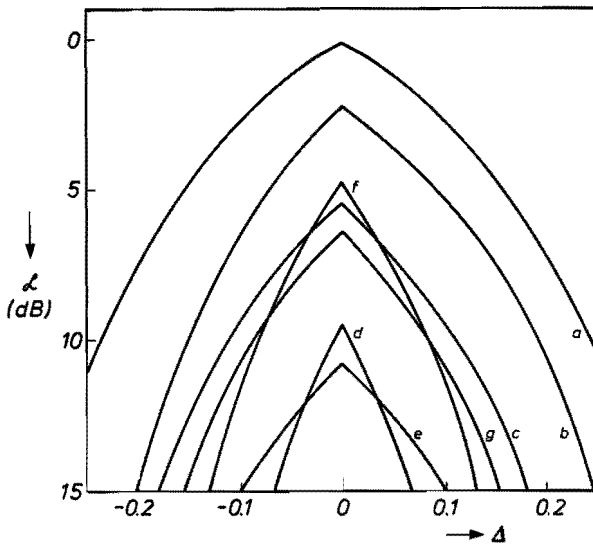


Fig. 8. Effective signal-to-noise ratio loss \mathcal{L} versus normalized sampling phase error Δ for various receiver types at a normalized information density D of 2.5 and a signal-to-noise ratio SNR of 20 dB. a. MLSD; b. Decision feedback equalizer; c. Full response linear equalizer (integrated detection); d. Optimum zero-forcing Bipolar linear equalizer (amplitude detection); e. Raised cosine Bipolar linear equalizer (amplitude detection); f. Optimum zero-forcing Class IV linear equalizer; g. Raised cosine Class IV linear equalizer.

noise enhancement, the Bipolar equalizers lag far behind the other types of receiver. The full response linear equalizer is, on the average, slightly better than its class IV counterparts, which either have a poorer nominal performance

or exhibit a larger sensitivity to phase errors. As it achieves a more than 2.5 dB better performance across the entire range of phase errors considered, the DFE clearly outperforms all linear equalizers. In turn, the MLSD consistently achieves a similar improvement over the DFE. Unlike the other methods considered, the performance of the DFE depends upon the polarity of the phase error as a consequence of the asymmetrical overall system impulse response with which it deals. On the basis of fig. 8, in order for the performance to remain within 3 dB of its nominal value, the sampling phase generated by the clock recovery circuit should, irrespective of the receiver type, always be closer than 10 percent of a bit interval to its optimum value, and for some receivers even closer than 5 percent (!).

Comparably stringent requirements can be deduced from fig. 9, which depicts a set of curves similar to fig. 8 for a (low) density D of 0.2, characteristic for e.g. disk storage systems³⁰). As observed before, only the full response and raised cosine linear equalizers have some resistance against timing errors here, while the other receivers require phase accuracies better than 8 percent of a bit interval in order to achieve a performance within 3 dB of its nominal value. Much more than at $D = 2.5$, fig. 9 clearly reflects the negative side of the insensitivity meddle, viz. the substantial penalties in terms of nominal performance that apparently accompany robustness improvements.

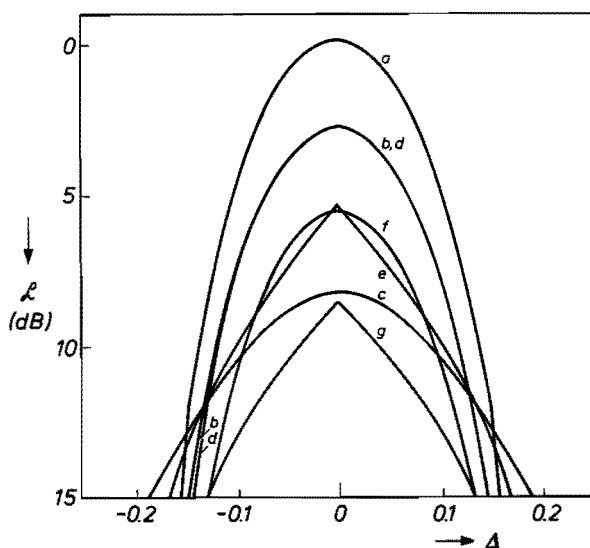


Fig. 9. As fig. 8, but at a normalized information density D of 0.2.

8. Simulations

To verify the results just described, we have performed a series of Monte Carlo simulations for normalized information densities D of 0.2 and 2.5 (figs 10 to 13). At $D = 0.2$, the error characteristics measured for both $\Delta = 0$

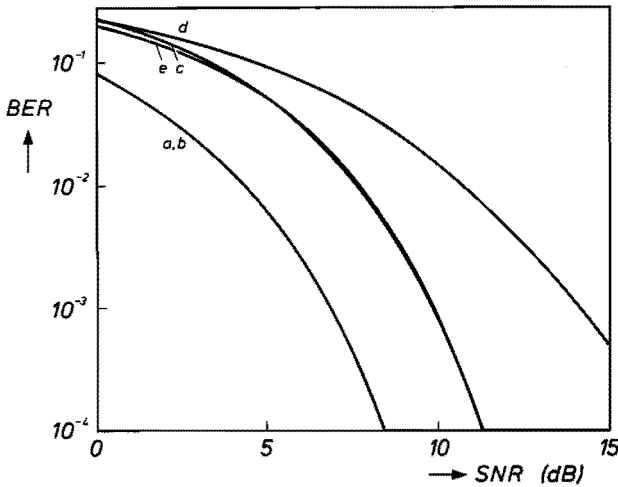


Fig. 10. Bit error rate BER plotted versus the signal-to-noise ratio SNR at a normalized information density D of 0.2 in the absence of timing errors. a. Matched filter bound; b. MLSD; c. Decision feedback equalizer; d. Full response linear equalizer; e. Optimum zero-forcing Bipolar linear equalizer.

and $\Delta = 0.1$ closely reflect the predictions of fig. 9, even though for computational efficiency all forward path filters were restricted to a length of 33 coefficients, centered around zero. Ideally having an integrating nature, which calls for a substantially longer impulse response, only the full response linear equalizer does not entirely achieve its anticipated performance. By comparing figs 10 and 11 it is seen that at $D = 0.2$ timing errors already seriously degrade the transmission quality at the smallest included signal-to-noise ratios. In contrast, at $D = 2.5$ the detrimental effects of timing errors become important much later, and in fact only reach about half of their anticipated value (expressed in decibels) at the highest SNRs included in figs 12 and 13. This phenomenon can be explained by noting that the small bandwidth of the $D = 2.5$ channel causes its impulse response to extend over many bit intervals and to change relatively slowly as a function of Δ . The residual intersymbol interference caused by timing errors will therefore typically consist of a large number of

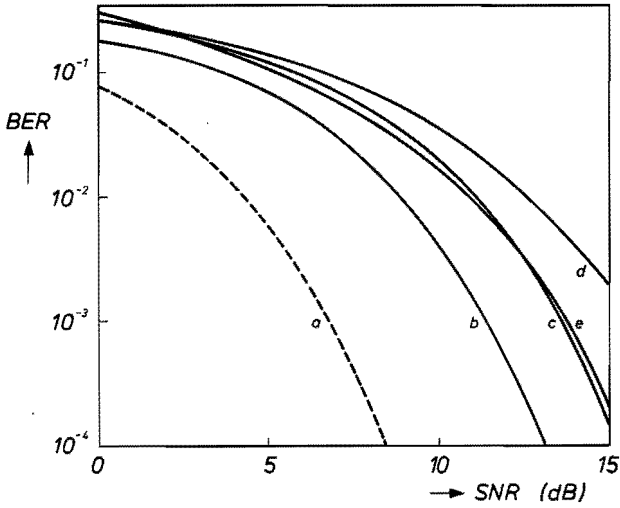


Fig. 11. As fig. 10, but in the presence of a normalized sampling phase error Δ of 10 percent.

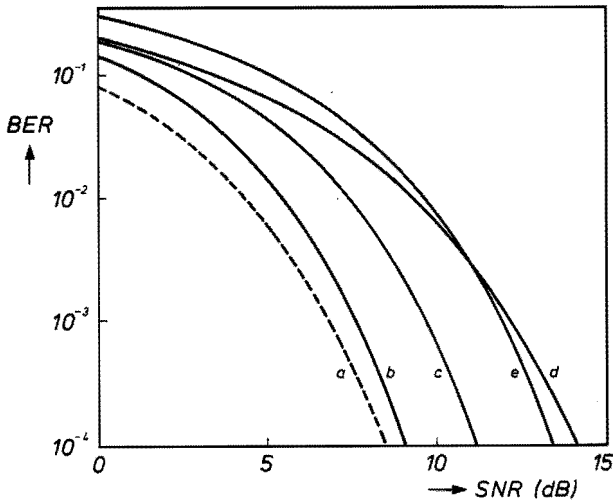


Fig. 12. As fig. 10, but at a normalized information density D of 2.5 and with curve e representing the optimum zero-forcing class IV partial response linear equalizer.

small contributions. As they are independent, these contributions only rarely

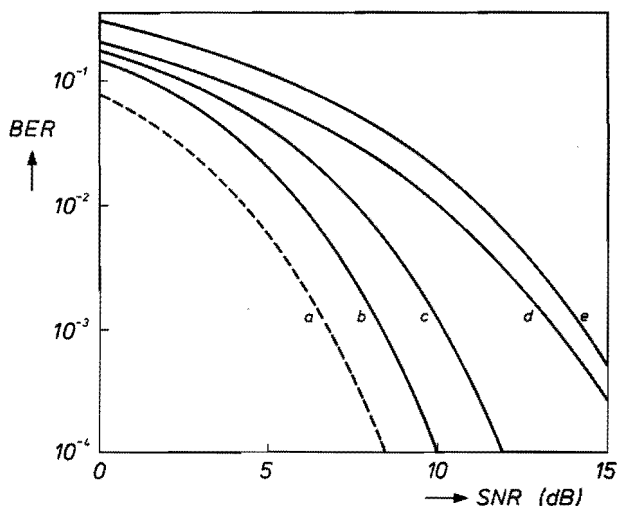


Fig. 13. As fig. 12, but in the presence of a normalized sampling phase error Δ of 10 percent.

add up to a large net interference value, and hence only become important when noise plays a background role, i.e. at high SNR's. For the same reason, the worst-case assessment of intersymbol interference employed in the effective signal-to-noise ratio loss \mathcal{L} yields overly pessimistic predictions for all but the highest SNR's, as comparison of figs 13 and 8 confirms. The MLSD curves of figs 12 and 13 have a bearing upon a reduced-state Viterbi detector of the Ungerboeck type²⁷). Using a stacksize of only 32 in order to achieve a nonprohibitive computational load, this detector sacrifices some performance relative to its full-fledged counterpart, particularly at low SNRs. As a result, its predicted matched filter bound performance for $\Delta = 0$ is only achieved for SNRs in excess of about 10 dB, while similar ratios are needed at $\Delta = 0.1$ in order to lower the influence of the stacksize reduction to negligible proportions.

9. Concluding remarks

We have investigated the performance of several equalization and detection methods in the presence of timing errors for a category of digital magnetic recording systems in which an NRZ-like transmission code is used in conjunction with differentiating playback heads. In accordance with experimental observations^{6,14}), all methods studied were invariably found to be sensitive to

such errors. For example, at most information densities none of the schemes suffered less than 3 dB signal-to-noise ratio loss in the presence of a phase error as small as 10 percent of a bit interval. At low densities, particularly the methods that make use of a whitened matched filter were found to be very vulnerable to timing errors, yet achieved good or even excellent performances when these errors did not occur. Conversely, the full response linear equalizer and the partial response schemes that shape the overall characteristics of the system in a raised cosine form were found to suffer the smallest degradation. Unfortunately, their inferior nominal performance more than offsets this advantage whenever sampling phase deviations remain within approximately 10 to 15 percent of a bit interval. Although their nominal performances may differ greatly, we observed at medium densities that all methods tend to suffer comparable losses in the presence of realistic timing errors. Quite surprisingly, the DFE and MLSD were found to withstand sampling phase errors relatively well, particularly if their considerable vulnerability to other system parameter (e.g. gain and bandwidth) variations is taken into account^{18, 29}). Nevertheless, the considerable hardware investment, required for the MLSD in particular, can only be fully exploited (and hence justified) if sophisticated timing recovery schemes are used.

These rather pessimistic findings naturally raise the question whether it is feasible to take account explicitly of sampling phase errors in the equalizer design process so as to incorporate a larger degree of tolerance, at the expense of a small performance degradation in the nominal situation. In a more general setting, this intriguing question (with an affirmative answer) is the subject of a companion paper³¹).

10. Acknowledgement

The author is indebted to Dr. K.A. Schouhamer Immink for stimulating discussions concerning the robustness of receivers.

REFERENCES

- ¹) Y. Shimpuku, S. Fukuda, H. Sugiki and K. Odaka, Proc. Sixth Int. Conf. on Video, Audio and Data Rec., Brighton, 1986, p. 67.
- ²) L.M.H.E. Driessen, W.A.L., Heijnemans, E. de Niet, J.H. Peters and A.M.A. Rijckaert, IEEE Trans. Cons. Electr., **CE-32**, 362 (1986).
- ³) T. Eguchi and J.G.S. Ive, Proc. Sixth Int. Conf. on Video, Audio and Data Rec., Brighton, 1986, p. 195.
- ⁴) M. Umemoto, S. Mita and Y. Eto, Proc. Sixth Int. Conf. on Video, Audio and Data Rec., 81-85, Brighton, England, March 1986.
- ⁵) S. Mita, Y. Eto and T. Kirino, Nat. Conv. Inst. of Electronics and Commun. Engineers of Japan, Paper no. 193, 1981.
- ⁶) S. Nakagawa, K. Yokoyama and H. Katayama, IEEE Trans. Magn., **MAG-16**, 104 (1980).

- 7) T. Schonhof and R. Price, Proc. Int. Conf. Commun., ICC-81, Denver 1981, paper 2.1.1.
- 8) H. Osawa, S. Tazaki and S. Ando, IEEE Trans. Magn., **MAG-22**, 253 (1986).
- 9) R. W. Wood and R. W. Donaldson, IEEE Trans. Magn., **MAG-14**, 218 (1978).
- 10) J. W. M. Bergmans, IEEE Trans. Magn., **MAG-22**, 157 (1986).
- 11) J. W. M. Bergmans, Proc. Sixth Int. Conf. on Video, Audio and Data Rec., Brighton, 1986, p. 141.
- 12) J. W. M. Bergmans, Philips J. Res., **42**, 209 (1987).
- 13) G. D. Forney, IEEE Trans. Inf. Theory, **IT-18**, 363 (1972).
- 14) R. W. Wood and D. A. Petersen, IEEE Trans. Commun., **COM-34**, 454 (1986).
- 15) D. D. Falconer and F. R. Magee, Jr., IEEE Trans. Commun., **COM-24**, 1130 (1976).
- 16) D. D. Falconer and F. R. Magee, Jr., IEEE Trans. Commun., **COM-24**, 1238 (1976).
- 17) S. U. Qureshi, Proc. IEEE, **73**, 1349 (1985).
- 18) J. W. M. Bergmans, Philips J. Res., **41**, 531 (1986).
- 19) K. A. Schouhamer Immink, Philips J. Res., **40**, 22 (1985).
- 20) J. Wozencraft and I. Jacobs, Principles of Communication Engineering, Wiley, New York, 1965.
- 21) A. Papoulis, Signal Analysis, McGraw-Hill, New York, 1984.
- 22) J. G. Proakis, Digital Communications, McGraw-Hill, New York, 1983.
- 23) F. E. Glave, IEEE Trans. Inf. Theory, **IT-18**, 356 (1972).
- 24) W. J. van Gestel, H. G. de Haan and T. G. J. A. Martens, Audio Engineering Handbook, Ch. 12: Digital audio on tape, to be published by McGraw-Hill, New York.
- 25) P. Kabal and S. Pasupathy, IEEE Trans. Commun., **COM-23**, 921 (1975).
- 26) C. A. Belfiore and J. H. Park, Proc. IEEE, **67**, 1143 (1979).
- 27) G. Ungerboeck, IEEE Trans. Commun., **COM-22**, 624 (1974).
- 28) R. R. Anderson and G. J. Foschini, IEEE Trans. Inf. Theory, **IT-21**, 544 (1975).
- 29) K. A. Schouhamer Immink, Philips J. Res., **41**, 410 (1986).
- 30) J. M. Harker, D. W. Brede, R. E. Pattison, G. R. Santana and L. G. Taft, IBM J. Res. Develop., **25**, 677 (1981).
- 31) J. W. M. Bergmans, Philips J. Res., **42**, 308 (1987).

A METHOD OF DESIGNING ROBUST LINEAR PARTIAL RESPONSE EQUALIZERS

Abstract

As a 'next-best' alternative for adaptive equalizers, whose application may be precluded by e.g. high data rates and power consumption restrictions, this paper develops a method for the design of fixed linear partial-response equalizers that are optimally robust relative to a mean-square performance measure which takes account of system parameter variations. The method is exemplified for a class of digital magnetic recording systems suffering from timing errors, and is in many instances found to establish significant improvements in timing margin at a modest expense to the nominal performance.

1. Introduction.

Besides intersymbol interference and noise, temporal and piece-by-piece variations of the channel characteristics are frequently an important problem in digital transmission and recording equipment¹⁻⁴). Application of adaptive equalization methods⁵) can be regarded as the most natural solution to this problem. Prior to their advent in the second half of the sixties^{6,7}), other means were sought to make data equalizers proof against channel parameter variations. After work by Tufts and Berger⁸), directed towards reduction of the influence of timing errors, Gonsalves and Tufts⁹) established the first general result in this field by deriving the full-response fixed linear data equalizer with an optimum performance (in the mean-square sense) averaged over a given probabilistic channel ensemble. Kaye¹⁰) later generalized this work to channels with nonstationary statistics. In spite of their already recognized value⁹), these findings did not cover partial response techniques, where a well-defined part of the arising intersymbol interference (ISI) is not attacked by equalization, but rather dealt with by means of residue arithmetic¹¹⁻¹⁴). In this way, significant

performance advantages may accrue relative to full-response equalization, where all ISI is eliminated prior to detection¹⁵). Apart from a recurrence to a restricted segment of the theme¹⁶), the robust data equalization problem has failed to spur research efforts in later years, partly due to the preferable alternative provided by adaptive techniques in the historically predominant application scenes of data equalization, viz. radio and line transmission⁵). Meanwhile, the related area of robust signal equalization, wherein a fully stationary environment is assumed, has continued to bear fruit¹⁷⁻¹⁹). As they neglect the cyclostationary nature of the data transmission process, the solutions concerned are of restricted value to the data equalization problem. For example, it is intrinsically impossible to make equalizers proof against timing errors on the basis of a performance measure which does not distinguish between different sampling phases.

In recent years, digital magnetic and optical recording, with their associated data equalization problems, have become increasingly important disciplines^{20,21}). Particularly in the upcoming generations of consumer-grade digital magnetic audio and video recording equipment, areal information densities are slowly increasing up to the point where ISI and noise together demand the limits of the capabilities of traditional equalization methods^{20,22,23}). While the 'nominal' recording channel is relatively well defined^{20,24}), small variations due to e.g. fluctuating tape-to-head contact and timing errors may cause the conventionally applied equalizers to induce considerable and even intolerable degradations of the transmission quality^{3,15,23,25}). Unfortunately, high data rates (in the order of tens or even hundreds of megabits per second) and power consumption restrictions not seldom preclude adaptive techniques from being applied in these systems. For this reason, a renewed interest can be accredited to the topic of robust equalization. In this context, linear partial response equalization merits special consideration in view of its widespread application and also because its sensitivity figures are generally poorer than those of its full response counterpart^{3,15,23,25}). The present paper deals with this subject. In a treatment which extends the one of Gonsalves and Tufts⁹), it develops a method to design fixed linear data equalizers which are optimally robust relative to a mean-square performance measure which takes account of both the partial response used and the potentially occurring parameter variations. *) The adopted performance measure is first optimized in a discrete-time environment, leading to an instructive closed-form frequency-domain solution. The treatment is then extended into the continuous-time domain by deriving a set of equations which uniquely determines the optimally robust continuous-time

*) To put the method on a solid mathematical basis, an appendix, contributed by A. J. E. M. Janssen, settles the arising existence and uniqueness questions.

equalizer and by outlining an efficient method for its numerical solution. To illustrate its merits, the so-identified design method is finally used to incorporate an optimum resistance to timing errors in linear data equalizers that are employed in a category of digital magnetic recording systems. Comparing the robust equalizers with their conventional counterparts, in many instances significant increments in timing margin are found to be accompanied by a modest performance degradation in the nominal situation, thus underscoring the usefulness of the method.

2. The robustness problem

Figure 1 depicts a discrete-time model of a system suffering from ISI and noise and plagued by channel parameter variations. (Though restricting the ensemble of solutions and therewith entailing some loss of optimality, this model is chosen here because of its simplicity. Later on we will be concerned with the more general continuous-time situation.)

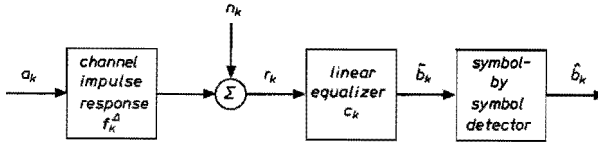


Fig. 1. Discrete-time data transmission system employing linear equalization.

A discrete-time data sequence $a_k \in \{-1, 1\}$ is applied to a discrete-time channel, which transforms a_k into an output sequence r_k of the form

$$r_k = (a * f_k^\Delta)_k + n_k, \quad (1)$$

where ‘*’ denotes linear convolution, f_k^Δ is the channel impulse response, and n_k is an additive Gaussian noise sequence. In what follows, we will assume a_k to be uncorrelated and statistically independent of n_k (the former assumption can be easily relaxed so as to accommodate the effect of correlation due to e.g. nonlinear transmission codes⁸). The channel impulse response f_k^Δ depends upon a parameter Δ belonging to an a priori known set S , which accounts for the presence of channel parameter variations. For instance, in the example to be considered later, S will be the set of all possible sampling phase errors, and f_k^Δ will be the equivalent channel impulse response corresponding to a sampling phase error $\Delta \in S$.

For the sake of simplicity, we will restrict consideration to linear reception of the received data sequence. In this case a fixed linear equalizer, having coefficients c_k , $-\infty < k < \infty$, performs a linear filtering operation upon r_k , transforming it into an output signal (see fig. 1)

$$\tilde{b}_k = (a * f^A * c)_k + (n * c)_k. \quad (2)$$

Depending upon the dimensioning of the equalizer, \tilde{b}_k can be made to resemble either the originally transmitted data sequence a_k or a simple linear transformation

$$b_k \triangleq (a * g)_k \quad (3)$$

thereof as well as possible. The latter case, referred to as partial response equalization¹⁵), involves the use of a partial response g_k , whose \mathcal{D} -transform

$$g(\mathcal{D}) \triangleq \sum_{k=-\infty}^{\infty} g_k \mathcal{D}^k \quad (4)$$

normally assumes the form

$$g(\mathcal{D}) = (1 + \mathcal{D})^m (1 - \mathcal{D})^n, \quad m, n \geq 0. \quad (5)$$

(The case $m = n = 0$ corresponds to direct estimation of a_k , referred to as full response equalization.) For small values of m and n , such as usually applied in practical systems, the transformed data sequence b_k has only few (e.g. 3) amplitude levels. The detection of its estimate \tilde{b}_k can therefore be performed by means of a relatively simple symbol-by-symbol detector, and should be followed by an inverse mapping which attempts to reconstruct a_k from its detected transformation \hat{b}_k . Since responses of the form (5) have zeros exactly on the unit circle, a precoding operation must be added at the transmitting end of the system in order for the inverse mapping to be memoryless, thereby preventing error propagation from occurring. As they are not relevant to the forthcoming analysis, neither the precoding operation nor the inverse mapping are shown in fig. 1.

Among the methods available for dimensioning the equalizer, a tractable and frequently applied one minimizes the mean-square error

$$\varepsilon(\Delta) \triangleq E[(\tilde{b} - b)_k^2] \quad (6)$$

between \tilde{b}_k and b_k^2), where E denotes expectation. The optimum transfer function

$$C(\Omega) \triangleq \sum_{k=-\infty}^{\infty} c_k \exp(-j2\pi \Omega k) \quad (7)$$

of the equalizer equals ^{2,15)}

$$C(\Omega) = \frac{F^{\Delta*}(\Omega) G(\Omega)}{|F^{\Delta}(\Omega)|^2 + N(\Omega)}, \quad (8)$$

where the superscript "*" denotes complex conjugation, $N(\Omega)$ represents the power spectral density of n_k , and $G(\Omega)$ and $F^{\Delta}(\Omega)$ represent the Fourier transforms of g_k and f_k^{Δ} , respectively. Using the nominal value for Δ results in a system that performs optimally in the absence of variations, but whose satisfactory performance is to no extent guaranteed in all other situations.

Rather than designing an equalizer to perform well for a single value of Δ , one might wish to accredit an importance measure to each possible value of $\Delta \in S$, and devise an equalizer which performs as well as possible averaged over S according to the specified distribution. In this way a well-defined degree of robustness would be incorporated in the design. Relative to a mean-square optimality criterion, we will now define this design problem mathematically, and subsequently derive its solution.

3. Optimally robust linear equalization – the discrete-time case

To accredit weight to the distinct possible values of Δ , we define a distribution function $p(\Delta)$ satisfying the usual constraints

$$p(\Delta) \geq 0 \quad \text{for all } \Delta, \quad (9)$$

and

$$\int_{\Delta \in S} p(\Delta) d\Delta = 1. \quad (10)$$

Normally, $p(\Delta)$ will be selected to attain its maximum for the nominal value of Δ , and to be smaller for other values according to their likelihood of occurrence. For a fixed equalizer, we can define an average mean-square error $\bar{\varepsilon}$ as

$$\bar{\varepsilon} \triangleq \int_{\Delta \in S} \varepsilon(\Delta) p(\Delta) d\Delta. \quad (11)$$

By expressing $\varepsilon(\Delta)$ in terms of the known system parameters as

$$\varepsilon(\Delta) = \int_{-0.5}^{0.5} [|F^{\Delta}(\Omega) C(\Omega) - G(\Omega)|^2 + N(\Omega) |C(\Omega)|^2] d\Omega \quad (12)$$

(cf. appendix A of ref. 15), this expression can equivalently be written as

$$\bar{\varepsilon} = \int_{-0.5}^{0.5} \int_{\Delta \in S} [|F^{\Delta}(\Omega) C(\Omega) - G(\Omega)|^2 + N(\Omega) |C(\Omega)|^2] p(\Delta) d\Delta d\Omega, \quad (13)$$

and we are looking for the fixed transfer function $C(\Omega)$ which optimizes $\bar{\varepsilon}$. This problem can be easily solved by adopting a calculus of variations approach. We write $C(\Omega)$ as

$$C(\Omega) \triangleq \hat{C}(\Omega) + \mu V(\Omega), \quad (14)$$

where $\hat{C}(\Omega)$ and $V(\Omega)$ represent the optimum transfer function and an arbitrary deviation thereof, respectively. To identify $\hat{C}(\Omega)$, we impose the requirement

$$\left. \frac{\partial \bar{\varepsilon}}{\partial \mu} \right|_{\mu=0} = 0 \quad \text{for all } V(\Omega). \quad (15)$$

Using eq. (14) in eq. (13), we find after the application of some elementary differentiation rules that

$$\begin{aligned} \left. \frac{\partial \bar{\varepsilon}}{\partial \mu} \right|_{\mu=0} = 2 \operatorname{Re} \int_{-0.5}^{0.5} V^*(\Omega) \left[\int_{\Delta \in S} \{ (|F^{\Delta}(\Omega)|^2 + N(\Omega)) \hat{C}(\Omega) - \right. \\ \left. - F^{\Delta*}(\Omega) G(\Omega) \} p(\Delta) d\Delta \right] d\Omega. \end{aligned} \quad (16)$$

In order for this expression to equal zero for all $V(\Omega)$ it is required that the quantity within square brackets vanishes for all Ω . Hence we conclude that

$$\hat{C}(\Omega) = \frac{\int_{\Delta \in S} F^{\Delta*}(\Omega) G(\Omega) p(\Delta) d\Delta}{\int_{\Delta \in S} (|F^{\Delta}(\Omega)|^2 + N(\Omega)) p(\Delta) d\Delta}. \quad (17)$$

According to eq. (17), the design of an optimally robust equalizer involves the calculation of an 'average matched filter' having the transfer function

$$\bar{F}^*(\Omega) \triangleq \int_{\Delta \in S} F^{\Delta*}(\Omega) p(\Delta) d\Delta \quad (18)$$

and an average power density spectrum

$$\overline{|F(\Omega)|^2} \triangleq \int_{\Delta \in S} |F^{\Delta}(\Omega)|^2 p(\Delta) d\Delta. \quad (19)$$

In this notation, the optimum equalizer transfer function assumes the simple and intuitively reasonable form (cf. eq. (8))

$$\hat{C}(\Omega) = \frac{\bar{F}^*(\Omega) G(\Omega)}{|F(\Omega)|^2 + N(\Omega)}. \quad (20)$$

Using eq. (20) in eq. (13), the corresponding minimum mean-square error $\bar{\epsilon}_{\min}$ is seen to equal

$$\bar{\epsilon}_{\min} = \int_{-0.5}^{0.5} |G(\Omega)|^2 \left[1 - \frac{|\bar{F}(\Omega)|^2}{|F(\Omega)|^2 + N(\Omega)} \right] d\Omega. \quad (21)$$

4. Optimally robust linear equalization - the continuous-time case

Due to the shift-invariance of the discrete-time problem just studied, the transfer function of the optimally robust data equalizer as given by eq. (20) has an elegant and simple appearance. Not surprisingly, a similar form was also obtained in ref. 17 using a continuous-time, stationary problem setting. As noted before, in data equalization decisions are taken at well-defined, equidistant moments, reflecting the cyclostationary nature of the data transmission process. By extending the treatment given so far into the continuous-time domain, we shall now uncover the consequences of cyclostationarity upon the resulting equalizer transfer function. To this end, we consider the continuous-time model of fig. 2, wherein a data sequence a_k (whose samples have a temporal spacing T) is filtered by a continuous-time channel impulse response $h^{\Delta}(t)$ and further corrupted by an additive Gaussian noise signal $n(t)$.

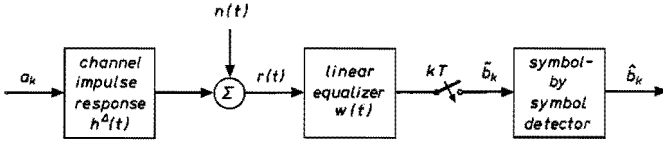


Fig. 2. Continuous-time data transmission system employing linear equalization.

The so-arising received signal $r(t)$ is applied to a linear equalizer with impulse response $w(t)$, whose output is sampled at the moments kT . This yields a sequence of decision variables \tilde{b}_k of the form

$$\tilde{b}_k = \sum_{i=-\infty}^{\infty} a_{k-i} (h^A * w)(iT) + (n * w)(kT), \quad (22)$$

where ‘*’ again denotes linear convolution, this time in its continuous-time form. As before, we assume a_k to be uncorrelated, and statistically independent of $n(t)$. Using these assumptions, the mean-square error

$$\varepsilon(\Delta) \triangleq E[(\tilde{b} - b)_k^2] \quad (23)$$

between \tilde{b}_k and $b_k = (a * g)_k$ is found to equal

$$\begin{aligned} \varepsilon(\Delta) = & \sum_{i=-\infty}^{\infty} (h^A * w)^2(iT) - 2 \sum_{i=-\infty}^{\infty} g_i (h^A * w)(iT) + \sum_{i=-\infty}^{\infty} g_i^2 \\ & + E[(n * w)^2(kT)]. \end{aligned} \quad (24)$$

To be able to express $\varepsilon(\Delta)$ in frequency-domain form, we define the Fourier transform $W(f)$ of $w(t)$ as

$$W(f) \triangleq \int_{-\infty}^{\infty} w(t) \exp\left(\frac{-j2\pi ft}{T}\right) dt, \quad (25)$$

analogously define $H^A(f)$ to be the Fourier transform of $h^A(t)$, and furthermore denote the power spectral density of $n(t)$ as $N(f)$. Chosen here because it simplifies the forthcoming formulas, the adopted Fourier transform definition is somewhat unconventional, involving a normalized and dimensionless frequency variable f . Applying Parseval’s identity and Poisson’s summation

formula²⁶⁾ to eq. (24), we can express $\varepsilon(\Delta)$ in terms of $H^\Delta(f)$, $W(f)$, $N(f)$ and $G(f)$ (as defined before, with f replacing Ω) as

$$\begin{aligned} \varepsilon(\Delta) = & \frac{1}{T^2} \sum_{n=-\infty}^{\infty} \int_{-\infty}^{\infty} H^{\Delta*}(f) W^*(f) H^\Delta(f+n) W(f+n) df \\ & - \frac{2}{T} \int_{-\infty}^{\infty} H^{\Delta*}(f) W^*(f) G(f) df + \int_{-0.5}^{0.5} |G(f)|^2 df \\ & + \frac{1}{T} \int_{-\infty}^{\infty} N(f) |W(f)|^2 df. \end{aligned} \quad (26)$$

The average mean-square error

$$\bar{\varepsilon} \triangleq \int_{\Delta \in S} \varepsilon(\Delta) p(\Delta) d\Delta \quad (27)$$

thus becomes

$$\begin{aligned} \bar{\varepsilon} = & \frac{1}{T^2} \sum_{n=-\infty}^{\infty} \int_{-\infty}^{\infty} \bar{R}_n(f) W^*(f) W(f+n) df \\ & - \frac{2}{T} \int_{-\infty}^{\infty} \bar{H}^*(f) W^*(f) G(f) df + \int_{-0.5}^{0.5} |G(f)|^2 df \\ & + \frac{1}{T} \int_{-\infty}^{\infty} N(f) |W(f)|^2 df, \end{aligned} \quad (28)$$

where the average transfer function $\bar{H}(f)$ and frequency autocorrelation function $\bar{R}_n(f)$ of the channel are defined respectively as

$$\bar{H}(f) \triangleq \int_{\Delta \in S} H^\Delta(f) p(\Delta) d\Delta \quad (29)$$

and

$$\bar{R}_n(f) \triangleq \int_{\Delta \in S} H^{\Delta*}(f) H^\Delta(f+n) p(\Delta) d\Delta. \quad (30)$$

To find the equalizer transfer function which optimizes $\bar{\varepsilon}$, we set

$$W(f) \triangleq \hat{W}(f) + \mu V(f), \quad (31)$$

where $\hat{W}(f)$ and $V(f)$ represent the optimum transfer function and an arbitrary deviation thereof, respectively. The requirement

$$\frac{\partial \bar{\epsilon}}{\partial \mu} \Big|_{\mu=0} = 0 \text{ for all } V(f) \quad (32)$$

now serves to identify $\hat{W}(f)$. Making use of elementary differentiation rules, it is easily verified that

$$\frac{\partial \bar{\epsilon}}{\partial \mu} \Big|_{\mu=0} = \frac{2}{T} \operatorname{Re} \int_{-\infty}^{\infty} V^*(f) \left[\frac{1}{T} \sum_{n=-\infty}^{\infty} \bar{R}_n(f) \hat{W}(f+n) - \bar{H}^*(f) G(f) + N(f) \hat{W}(f) \right] df. \quad (33)$$

A necessary and sufficient condition for this derivative to be zero for all $V(f)$ is that the quantity in square brackets vanishes for all f . This means that

$$\frac{1}{T} \sum_{n=-\infty}^{\infty} \bar{R}_n(f) \hat{W}(f+n) + N(f) \hat{W}(f) = \bar{H}^*(f) G(f) \text{ for all } f. \quad (34)$$

According to appendix A, this infinite set of equations has a unique solution $\hat{W}(f)$, provided that mild regularity conditions (including positivity and finiteness of $N(f)$) are met. Generalizing upon the conventional nonrobust case^{8,15}, eq. (34) indicates that the optimum equalizer can be decomposed into a continuum of matched filters (with prewhitening) and cascaded transversal filters. To see this, we define a Δ -dependent transfer function

$$C^\Delta(f) \triangleq G(f) - \frac{1}{T} \sum_{n=-\infty}^{\infty} \hat{W}(f+n) H^\Delta(f+n) \quad (35)$$

which is periodic in f with period 1 and hence describes a (symbol interval-spaced) transversal filter. Combining eqs (35), (34), (30) and (29), the ensemble average of the transfer function $H^\Delta(f)/N(f)$ of the matched filter with prewhitening in tandem with $C^\Delta(f)$ is seen to equal

$$\int_{\Delta \in S} \frac{H^\Delta(f)}{N(f)} C^\Delta(f) p(\Delta) d\Delta = \frac{1}{N(f)} [\bar{H}^*(f) G(f) - \frac{1}{T} \sum_{n=-\infty}^{\infty} \bar{R}_n(f) \hat{W}(f+n)] = \hat{W}(f), \quad (36)$$

thus proving the conjecture.

According to eq. (34), $\hat{W}(f)$ is for any frequency f completely determined by samples of \bar{R}_n , \bar{H} and G taken at f and all integer shifts thereof. For this reason, we are led to define two vectors $U(\Omega)$ and $\hat{W}(\Omega)$ and a matrix $M(\Omega)$ having components

$$U_i(\Omega) \triangleq \bar{H}^*(\Omega + i) G(\Omega + i) \quad \text{for all } i, \quad (37)$$

$$\hat{W}_i(\Omega) \triangleq \hat{W}(\Omega + i) \quad \text{for all } i, \quad (38)$$

and

$$M_{i,j}(\Omega) \triangleq \frac{1}{T} \bar{R}_{j-i}(\Omega + i) + \delta_{j-i} N(\Omega + i) \quad \text{for all } i, j, \quad (39)$$

respectively. In terms of these entities, (34) can equivalently be written as

$$M(\Omega) \hat{W}(\Omega) = U(\Omega) \quad \text{for all } \Omega. \quad (40)$$

Imposing little more than the condition $0 < N(\Omega) < \infty$ for all Ω , appendix A proves that this matrix equation has a unique solution

$$\hat{W}(\Omega) = M^{-1}(\Omega) U(\Omega) \quad \text{for all } \Omega, \quad (41)$$

where ‘ -1 ’ indicates matrix inversion. By solving $\hat{W}(\Omega)$ for all $\Omega \in [-\frac{1}{2}, \frac{1}{2}]$, $\hat{W}(f)$ is uniquely determined for all f (theorem A.2 of appendix A rigorously asserts the correspondence of $\hat{W}(\Omega)$ with $\hat{W}(f)$). When $\bar{H}(f)$ has negligible content outside the interval $[-L, L]$, then only about $2L + 1$ and $(2L + 1)^2$ components of $U(\Omega)$ and $M(\Omega)$ will essentially differ from zero, respectively. As the bandwidth restrictions responsible for intersymbol interference automatically cause L to be relatively small, the numerical solution of eq. (40) will generally be quite practicable. A further saving of computation effort can be obtained by using the prior knowledge that $\hat{w}(t)$ must be real-valued, so that $\hat{W}(f) = \hat{W}^*(-f)$ for all f . Hence \hat{W} needs to be determined for positive frequencies only, allowing the set of equations (40) to be roughly halved in size. To avoid aliasing distortion in reconstructing $\hat{w}(t)$ from $\hat{W}(\Omega)$, an appropriate spacing has to be selected for the frequencies at which \hat{W} (and hence M and U) are sampled, related to the temporal extent of $\hat{w}(t)$ as described in ref. 26, pp. 74-76. Mutatis mutandis, a similar remark applies to the reconstruction of convolved versions of $\hat{w}(t)$, such as overall system impulse responses of the form $(h^d * \hat{w})(t)$.

Finally, using eqs (34) and (41) in eq. (28), the minimum mean-square error $\bar{\epsilon}_{\min}$ achieved by the optimally robust continuous-time equalizer is found to equal

$$\begin{aligned} \bar{\epsilon}_{\min} &= \int_{-0.5}^{0.5} |G(\Omega)|^2 d\Omega - \frac{1}{T} \int_{-\infty}^{\infty} \bar{H}^*(f) G(f) \hat{W}^*(f) df \\ &= \int_{-0.5}^{0.5} [|G(\Omega)|^2 - \frac{1}{T} U^T(\Omega) M^{-1*}(\Omega) U^*(\Omega)] d\Omega, \end{aligned} \quad (42)$$

where ‘ T ’ and ‘ $*$ ’ indicate transposition and component-wise complex conjugation, respectively. This expression is reminiscent of its discrete-time counterpart eq. (21).

5. A design example: resistance to timing errors in digital magnetic recording

As a comprehensive example, we now apply the developed theory to a class of digital magnetic recording system suffering from timing errors. Conforming to a sizeable fraction of commercially available equipment, we confine ourselves to systems which use an NRZ-like transmission code, longitudinal magnetization and a differentiating playback head²⁰). When both the medium thickness and the gap size of the playback head are sufficiently small, the nominal channel transfer characteristic $H^0(f)$ of a recording system within this category assumes the form²⁴)

$$H^0(f) = [1 - \exp(-j2\pi f)] \exp(-\pi D|f|) \quad \text{for all } f, \quad (43)$$

where D is a normalized measure of the information density on the recording medium, ranging between roughly 0.1 and 3 in current systems. The noise signal $n(t)$ present in the output signal of the playback head normally has a Gaussian distribution and a relatively flat spectral density^{23, 20}), taken equal to N_0 for the purpose of the present analysis. For the partial response g_k , we will consider the popular cases

$$g(\mathcal{D}) = 1, \quad (44)$$

$$g(\mathcal{D}) = 1 - \mathcal{D}, \quad (45)$$

and

$$g(\mathcal{D}) = 1 - \mathcal{D}^2, \quad (46)$$

whose application is referred to as Integrated Detection, Amplitude Detection and Partial Response Class IV Detection, respectively^{3, 23}).

Having an optimum performance when its output is sampled at the nominal instants kT (cf. fig. 2), the conventional minimum mean-square error (MMSE) equalizer often incurs significant performance losses in the presence of sampling phase errors, i.e. when sampling erroneously takes place at the instants $(k + \Delta)T$, $\Delta \neq 0$ ²⁴). The influence of sampling phase deviations can be accounted for by incorporating the time shift ΔT in eq. (43) as

$$\begin{aligned} H^\Delta(f) &\triangleq H^0(f) \exp(j2\pi\Delta f) \\ &= [1 - \exp(-j2\pi f)] \exp(-\pi D|f|) \exp(j2\pi\Delta f) \quad \text{for all } f. \end{aligned} \quad (47)$$

To delimit the ensemble of possible channel characteristics, we define the set S to comprise the continuum of all sampling phase errors that are likely to occur in practice, i.e.

$$S \triangleq [-\Theta, \Theta], \quad (48)$$

where $0 \leq \Theta \leq \frac{1}{2}$ determines the maximum possible sampling phase deviation. A typical value of Θ would be 0.1²³). Furthermore, the phase error distribution $p(\Delta)$ is defined to be uniform, i.e.

$$p(\Delta) \triangleq \frac{1}{2\Theta} \quad \text{for all } \Delta \in S. \quad (49)$$

Hence all possible sampling phase deviations are weighed equally strongly.

Apart from the most natural continuous-time solution (to be considered shortly), one can in principle imagine the use of a discrete-time post-equalizer inserted between the sampler output and the detector input in an attempt to lower the effect of timing errors. Using the foregoing discrete-time results, we found that only for small densities D (up to about $D = 0.5$), where a timing error essentially induces a gain decrement²⁴), can some added resistance be achieved for the partial response schemes by increasing the equalizer gain as a precompensation for the expected gain decrement. In all other cases, discrete-time post-equalization turns out to be totally unrewarding, thus confirming the familiar restricted potential of (even adaptive) symbol-spaced transversal equa-

lizers to withstand timing errors, and implicitly underscoring the practical importance of fractional tap spacing to accomplish insensitivity improvements⁵).

The optimally robust continuous-time equalizer can be determined from the average transfer functions $\bar{H}(f)$ and $\bar{R}_n(f)$ defined in eqs (29) and (30) of sec. 4. Making use of eqs (47) and (49), these functions are seen to equal

$$\bar{H}(f) = [1 - \exp(-j2\pi f)] \frac{\sin 2\pi \Theta f}{2\pi \Theta f} \exp(-\pi D|f|) \quad \text{for all } f \quad (50)$$

and

$$\bar{R}_n(f) = 4 \sin^2(\pi f) \frac{\sin 2\pi \Theta n}{2\pi \Theta n} \exp[-\pi D(|f| + |f + n|)] \quad \text{for all } n \text{ and } f \quad (51)$$

in the recording situation under investigation. As a consequence, the vector $U(\Omega)$ and matrix $M(\Omega)$ defined in eqs (37) and (40) of sec. 4 have components

$$U_i(\Omega) = G(\Omega)[1 - \exp(j2\pi \Omega)] \frac{\sin 2\pi \Theta(\Omega + i)}{2\pi \Theta(\Omega + i)} \exp(-\pi D|\Omega + i|) \quad (52)$$

and

$$M_{i,j}(\Omega) = \frac{4}{T} \sin^2(\pi \Omega) \frac{\sin 2\pi \Theta(i-j)}{2\pi \Theta(i-j)} \exp[-\pi D(|\Omega + i| + |\Omega + j|)] \\ + N_0 \delta(i-j) \quad \text{for all } i \text{ and } j \text{ and for all } |\Omega| \leq \frac{1}{2}. \quad (53)$$

For large $|i|$ and $|j|$, the behaviour of these expressions is dominated by the contained exponential factors, which are smaller than about 1 percent of their maximum value 1 if $D|\Omega + i|$ and $D[|\Omega + i| + |\Omega + j|]$ are larger than about 1.5. Hence, even for a (small) density D of 0.2, the dimensions of $U(\Omega)$ and $M(\Omega)$ can be chosen as small as about 17 and (17×17) , respectively, while at a (relatively high) density D of 2.5 these figures reduce to a trivial 3 and (3×3) . The numerical identification of the optimally robust equalizer is thus a computationally straightforward undertaking. Rather than in mean-square error terms, we will assess the performance of the equalizer in terms of the more meaningful effective signal-to-noise ratio loss¹⁵). To this end, we first note that according to eqs (38) and (41), the noise variance σ^2 of the equalizer output signal can be written as

$$\sigma^2 = \frac{N_0}{T} \int_{-0.5}^{0.5} \hat{W}^T(\Omega) \hat{W}^*(\Omega) d\Omega = \frac{N_0}{T} \int_{-0.5}^{0.5} U^T(\Omega) M^{-1T}(\Omega) M^{-1*}(\Omega) U^*(\Omega) d\Omega. \quad (54)$$

The second factor relevant to the performance of the equalizer is the residual intersymbol interference, which can be assessed for any Δ by writing the transfer function $Q(\Omega)$ of the sampled overall system impulse response q_k in the form

$$Q(\Omega) = G(\Omega) + E^{\Delta}(\Omega). \quad (55)$$

Defining a vector $H^{\Delta}(\Omega)$ to have components

$$H_i^{\Delta}(\Omega) \triangleq H^{\Delta}(\Omega + i) \quad \text{for all } i, \quad (56)$$

and making use of eq. (38), eq. (55) and Poisson's summation formula²⁶⁾, the deviation transfer function $E^{\Delta}(\Omega)$ can be seen to attain the form

$$E^{\Delta}(\Omega) = H^{\Delta T}(\Omega) M^{-1}(\Omega) U(\Omega) - G(\Omega). \quad (57)$$

The inverse Fourier transform e_k^{Δ} of $E^{\Delta}(\Omega)$ determines the (Δ -dependent) residual intersymbol interference prior to detection. More specifically, it determines the minimum distance $d/2$ between any possible value of the non-noise component $(a * (g + e^{\Delta}))_k$ of the detector input signal and the nearest detector threshold level. In turn, $d/2$ directly governs the error probability at high signal-to-noise ratios as^{2, 27)}

$$\Pr [E] \propto Q\left(\frac{d}{2\sigma}\right), \quad (58)$$

where

$$Q(x) \triangleq \frac{1}{\sqrt{2\pi}} \int_x^{\infty} \exp(-y^2/2) dy. \quad (59)$$

For integrated detection ($g(\mathcal{D}) = 1$), $d/2$ can be expressed in e_k^{Δ} as

$$\frac{d}{2} = 1 + e_0^{\Delta} - \sum_{k \neq 0} |e_k^{\Delta}|, \quad (60)$$

while for amplitude and partial response class IV detection ($g(\mathcal{D}) = 1 - \mathcal{D}^l$ with $l = 1$ and 2 , respectively)

$$\frac{d}{2} = 1 - \max\{e_l^A - e_0^A, |e_0^A + e_l^A|\} - \sum_{k \neq 0, l} |e_k^A|, \quad (61)$$

provided that the detector thresholds are located at $\pm 1^{24}$.

To assess the performance of the equalizer, we normalize the effective signal-to-noise ratio $(d/2\sigma)^2$ of the decision variable on its optimum value

$$\begin{aligned} \text{SNR} &\triangleq \frac{1}{N_0 T} \int_{-0.5}^{0.5} |F^0(\Omega)|^2 d\Omega \\ &= \frac{2}{\pi N_0 T} \frac{1}{D(D^2 + 1)}, \end{aligned} \quad (62)$$

which corresponds to matched filter bound operation¹⁵). The effective signal-to-noise ratio loss

$$\mathcal{L} \triangleq \frac{\text{SNR}}{(d/2\sigma)^2} \quad (63)$$

is therefore bounded by $\mathcal{L} \geq 1$; a value of 1 indicating a performance that cannot be improved upon by any receiver.

Proceeding numerically along the lines just sketched, we have determined for various sets of system parameters the optimally robust equalizer according to (41) and the corresponding Δ -dependent effective signal-to-noise ratio loss \mathcal{L} . From these results, we shall first describe those related to the region of low information densities. For a density D of 0.2 and sampling phase errors ranging from -25 to $+25$ percent of a bit interval, fig. 3 depicts the effective signal-to-noise ratio loss \mathcal{L} incurred by several optimally robust continuous-time $1 - \mathcal{D}$ equalizers as well as by a conventional raised cosine $1 - \mathcal{D}$ scheme (the latter curve is taken from ref. 24, and has a bearing upon a transition parameter β of 0.5). The raised cosine equalizer, which in ref. 24 was judged to be relatively insensitive to timing errors, lags far behind the robust equalizers for all values of Θ within the scale of fig. 3. Combining large tolerance increments with a modest degradation of the nominal performance, the depicted characteristics convincingly demonstrate the merits of the developed design method. To illustrate their spectral properties, fig. 4 depicts the amplitude-frequency characteristics of the robust equalizers of fig. 3. Apart from having a

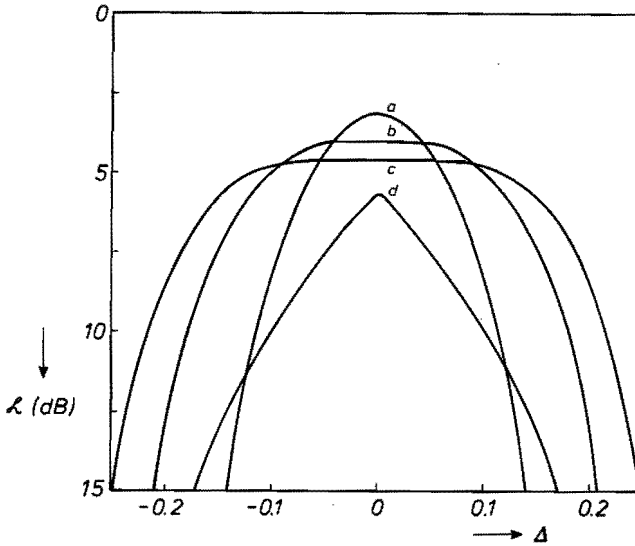


Fig. 3. Effective signal-to-noise ratio loss \mathcal{L} versus normalized sampling phase error Δ for several continuous-time bipolar $(1 - \mathcal{D})$ equalizers. Signal-to-noise ratio SNR = 25 dB; Normalized information density $D = 0.2$. a. Minimum mean-square error equalizer ($\Theta = 0$); b. Optimally robust equalizer ($\Theta = 0.1$); c. Optimally robust equalizer ($\Theta = 0.15$); d. Raised cosine equalizer ($\beta = 0.5$).

somewhat increased average transfer magnitude (and hence noise enhancement), the robust equalizers also de-emphasize frequencies onwards of roughly the bit frequency in an apparent attempt to reduce phase ambiguities of the form $\exp(j2\pi\Delta f)$, whose influence is proportional to f .

Also at a (high) density D of 2.5, the continuous-time partial response equalizer is capable of establishing a robustness improvement, though considerably smaller in magnitude than at $D = 0.2$. Figure 5 illustrates this statement for the $1 - \mathcal{D}^2$ equalizer and values of Θ ranging from 0 to 0.15. Interestingly, the $\Theta = 0.15$ equalizer virutally coincides with the $\beta = 0.5$ $1 - \mathcal{D}^2$ raised cosine scheme studied in ref. 24, whose performance characteristics are also included in fig. 5. This similarity suggests that partial response schemes such as applied in current high-density practice are close to optimally insensitive to timing errors, even though their sensitivity may still be unsatisfactory in absolute terms.

A completely different conclusion applies to the full response ($g(\mathcal{D}) = 1$)

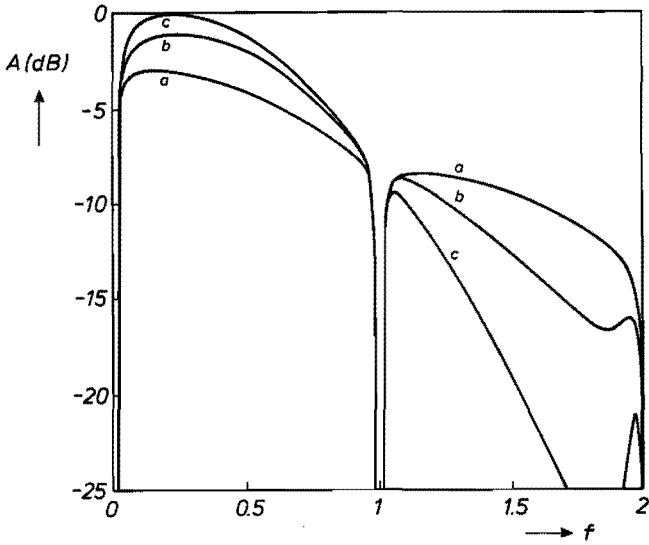


Fig. 4. Amplitude-frequency characteristics $A(f)$ of the optimally robust equalizers of fig. 3. a. $\Theta = 0$; b. $\Theta = 0.1$; c. $\Theta = 0.15$. The frequency has been normalized and the symbol rate $1/T$.

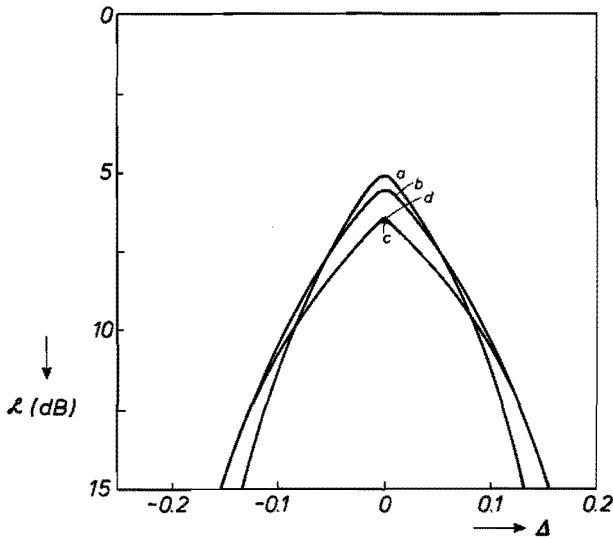


Fig. 5. Effective signal-to-noise ratio loss \mathcal{L} versus normalized sampling phase error Δ for several continuous-time partial response Class IV $(1 - \mathcal{D}^2)$ equalizers. Signal-to-noise ratio SNR = 25 dB; Normalized information density $D = 2.5$. a. Minimum mean-square error equalizer ($\Theta = 0$); b. Optimally robust equalizer ($\Theta = 0.1$); c. Optimally robust equalizer ($\Theta = 0.15$); d. Raised cosine equalizer ($\beta = 0.5$).

equalizer, whose resistance to timing errors is invariably favourable to the partial response schemes, and moreover increases significantly with increasing Θ , as fig. 6 reveals. For example, at a cost of only 0.3 dB in nominal

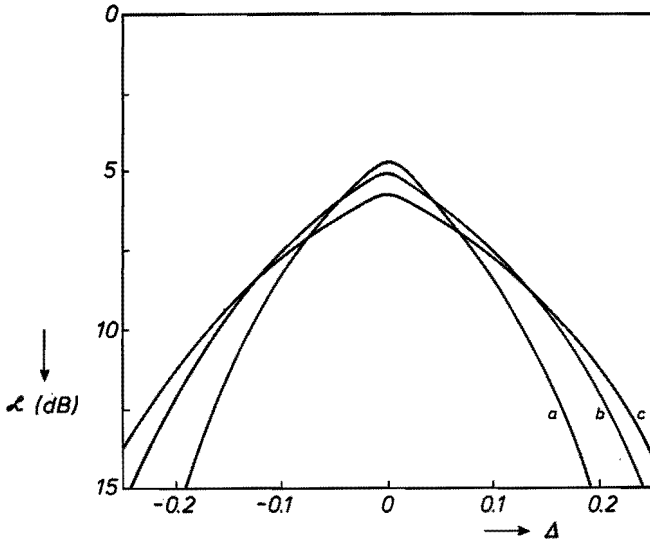


Fig. 6. Effective signal-to-noise ratio loss \mathcal{L} versus normalized sampling phase error Δ for several continuous-time optimally robust full response ($g(\mathcal{D}) = 1$) equalizers. Signal-to-noise ratio SNR = 25 dB; Normalized information density $D = 2.5$. a. $\Theta = 0$; b. $\Theta = 0.1$; c. $\Theta = 0.15$.

performance, the $\Theta = 0.1$ equalizer can withstand sampling phase variations as large as 12 percent of a bit interval before its performance decreases by more than 3 dB relative to its nominal value, as opposed to 8 percent for the conventional ($\Theta = 0$) equalizer. The spectral characteristics responsible for this robustness improvement are visualized in fig. 7. Contrary to the low-density $1 - \mathcal{D}$ situation just studied, the improved robustness is now apparently brought about by an increased transfer magnitude onwards of roughly the Nyquist frequency, just below which a decrement can be observed.

More impressively than by means of the preceding graphs, the improved resistance to timing errors of the designed robust equalizers is reflected in their eye patterns. The figs 8 and 9 depict eye patterns that were constructed by computer simulation for the equalizers of figs 3 and 6, respectively. Achieving (nearly) the same noise suppression as the conventional MMSE equalizer and an even better timing margin than the raised cosine equalizer, the robust $1 - \mathcal{D}$

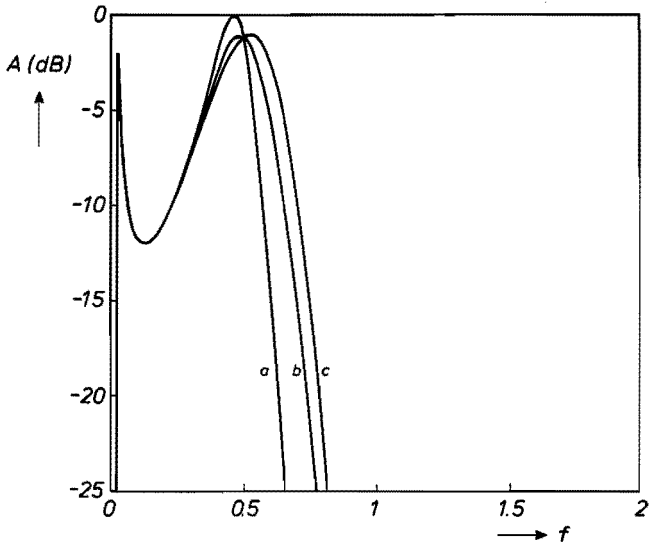


Fig. 7. Amplitude-frequency characteristics $A(f)$ of the equalizers of fig. 6. a. $\Theta = 0$; b. $\Theta = 0.1$; c. $\Theta = 0.15$. The frequency has been normalized on the symbol rate $1/T$.

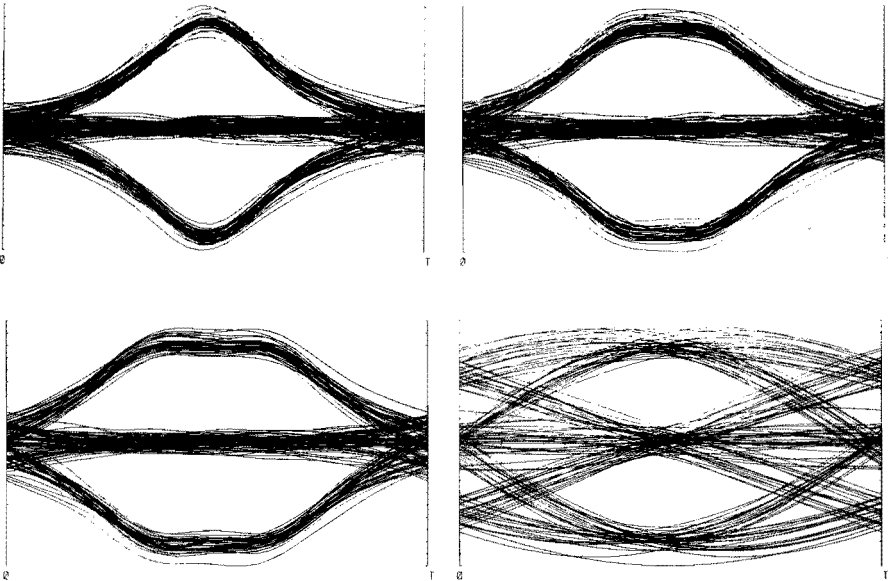


Fig. 8. Eye patterns for the equalizers of fig. 3. Signal-to-noise ratio $SNR = 20$ dB; Normalized information density $D = 0.2$. a. Minimum mean-square error equalizer ($\Theta = 0$); b. Optimally robust equalizer ($\Theta = 0.1$); c. Optimally robust equalizer ($\Theta = 0.15$); d. Raised cosine equalizer ($\beta = 0.5$).

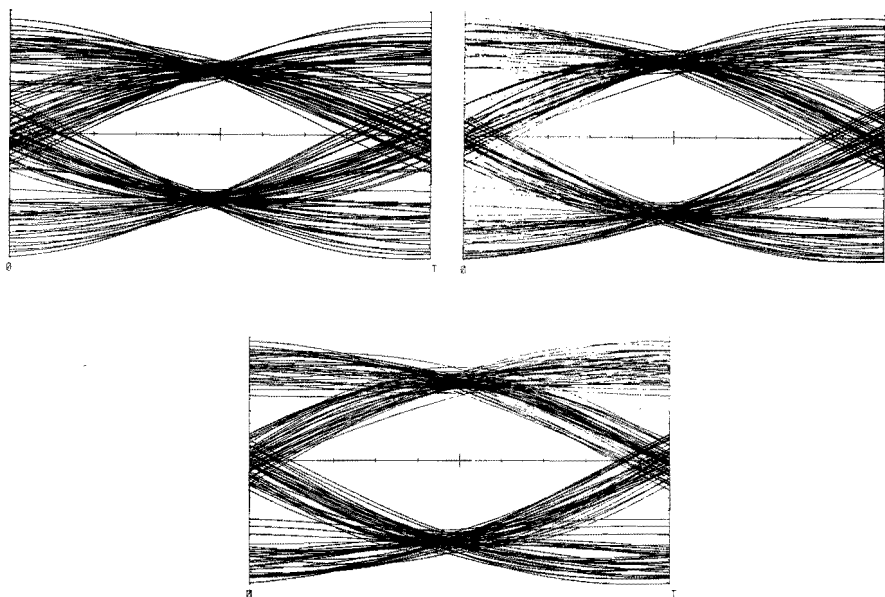


Fig. 9. Eye patterns for the equalizers of fig. 6. Signal-to-noise ratio SNR = 25 dB; Normalized information density $D = 0.2$. a. $\theta = 0$; b. $\theta = 0.1$; c. $\theta = 0.15$.

equalizers of fig. 8 apparently combine the 'best of both worlds'. Less spectacularly but clearly visible, the robust full response equalizers of fig. 9 achieve a larger timing margin at virtually no expense to the noise enhancement.

6. Concluding remarks

The preceding pages have indicated the feasibility and illustrated the usefulness of equipping both partial and full response linear data equalizers with a well-defined degree of robustness. Explicitly using prior knowledge about the ensemble of possible channel characteristics, the presented equalizer design method involves the calculation of two average channel spectra and the inversion of a set of matrices, whose dimensions are proportional to the channel bandwidth and are usually small. The method optimizes the dimensioning of the linear equalizer relative to a performance measure which takes the form of a mean-square error, averaged by means of a predefined weight function over the nominal channel and all possible deviations thereof.

To assess the merits of the design method, we have applied it to a class of digital magnetic recording systems employing an NRZ-like transmission code in conjunction with a differentiating playback head, and suffering from timing errors. For this category, we observed that considerable robustness improvements are frequently achievable at a modest cost in nominal performance. At low information densities, we found the optimally robust Bipolar (1 - \mathcal{D}) equalizer to be much less sensitive than its conventional minimum mean square error counterpart, which suffers a 3 dB loss in effective signal-to-noise ratio for sampling phase deviations as small as 8 percent of a bit interval. Sacrificing some 0.9 or 1.5 dB in the nominal situation, the optimally robust equalizers extended this range to a comfortable 15 and 19 percent, respectively. At high densities, only small robustness improvements were observed for the partial response types of equalizer, indicating that currently applied schemes are close to optimally insensitive, even though on an absolute scale their sensitivity may be unsatisfactory. In contrast, the full response linear equalizer was invariably judged to be distinctly superior to the partial response schemes in terms of robustness, while its robust versions improved the timing margin even further.

As a final remark, we note that the one-dimensional development and examples presented in this paper can be straightforwardly extended to systems in which variations of a tractable multitude of parameters occur.

Appendix A. Existence and uniqueness of solutions of the equations (34) and (40)

In this appendix we shall show that, under proper assumptions on H and N , the eq. (34) has for every $G \in L^2(\mathcal{R})$ a unique solution $\hat{W} \in L^2(\mathcal{R})$. Here $L^2(\mathcal{R})$ denotes the Hilbert space of square integrable functions on \mathcal{R} with inner product

$$(W, V)_{\mathcal{R}} \triangleq \int_{-\infty}^{\infty} W(x) V^*(x) dx \quad \text{for } W, V \in L^2(\mathcal{R}), \quad (\text{A.1})$$

and norm

$$\|W\|_{\mathcal{R}} \triangleq (W, W)_{\mathcal{R}}^{\frac{1}{2}}. \quad (\text{A.2})$$

Furthermore, we shall show that, under proper assumptions on H , G and N , the eq. (40) has for every $\Omega \in [-\frac{1}{2}, \frac{1}{2}]$ a unique solution $\hat{W}(\Omega) \in l^2(\mathcal{Z})$. Here $l^2(\mathcal{Z})$ denotes the Hilbert space of square summable sequences on \mathcal{Z} with inner product

$$(W, V)_Z \triangleq \sum_{n=-\infty}^{\infty} W(n) V^*(n) \text{ for } W, V \in l^2(\mathbb{Z}), \quad (\text{A.3})$$

and norm

$$\|W\|_Z \triangleq (W, W)_Z^{\frac{1}{2}} \quad (\text{A.4})$$

It will also be shown that the procedure outlined in eqs (40) to (44) is, under proper assumptions, a valid one to obtain the solution of the eq. (34). In theorem A.1 and theorem A.2 the main results of this appendix are given.

Before we proceed to the proofs, we develop some notation. We drop all overhead \wedge , we take T equal to one for convenience (and without loss of generality) and we use $x \in \mathbb{R}$ instead of f or Ω in eq. (34) or eq. (40). The basic operators in eqs (34) and (40) are

$$(T_H W)(x) \triangleq H^*(x) \sum_{n=-\infty}^{\infty} H(x+n) W(x+n) \text{ for } x \in \mathbb{R}, W \in L^2(\mathbb{R}), \quad (\text{A.5})$$

and

$$U_H W \triangleq (W, H^*)_Z H^* \text{ for } W \in l^2(\mathbb{Z}), \quad (\text{A.6})$$

with $H \in L^2(\mathbb{R}), H \in l^2(\mathbb{Z})$. Indeed, when we set

$$\bar{T}_H W \triangleq \int_{\Delta \in S} T_{H^\Delta} W p(\Delta) d\Delta \text{ for } W \in L^2(\mathbb{R}), \quad (\text{A.7})$$

and

$$\bar{U}_H W \triangleq \int_{\Delta \in S} U_{H^\Delta} W p(\Delta) d\Delta, \quad (\text{A.8})$$

we can write eqs (34) and (40) as

$$\bar{T}_H W + N W = \bar{H}^* G \text{ for } W \in L^2(\mathbb{R}), \quad (\text{A.9})$$

and

$$\bar{U}_H W + N_x W = \bar{H}_x G_x \text{ for } W \in l^2(\mathbb{Z}). \tag{A.10}$$

Here we have written $H_x^\Delta \triangleq (H^\Delta(x+n))_{n \in \mathbb{Z}}$, etc., and $(NW)(x) \triangleq N(x)W(x)$, for $x \in \mathbb{R}$, $(N_x W)(n) \triangleq N(x+n)W(n)$, etc.. Our aim is to find conditions on H , N and G such that eqs (A.9) and (A.10) have unique solutions $W \in L^2(\mathbb{R})$ and $W \in l^2(\mathbb{Z})$. This is achieved by requiring that the operators \bar{T}_H and U_{H_x} are bounded, self-adjoint, positive definite operators of $L^2(\mathbb{R})$ and $l^2(\mathbb{Z})$, and by getting rid in a decent way of the multiplication operators N and N_x in (A.9) and (A.10). The uniqueness and existence results follow then from the familiar fact that an equation $Tf + f = g$ in a Hilbert space \mathcal{H} has for every $g \in \mathcal{H}$ a unique solution $f \in \mathcal{H}$ whenever the linear operator T is bounded, self-adjoint and positive definite. In ref. 29 one can find a readable account of the theory of linear operators of a Hilbert space.

Proposition A.1

(i) Let $H \in L^2(\mathbb{R})$, and assume that

$$\Psi_H(x) \triangleq \sum_{n=-\infty}^{\infty} |H(x+n)|^2 \text{ for } x \in [-\frac{1}{2}, \frac{1}{2}] \tag{A.11}$$

is essentially bounded: there is an $M > 0$ such that $\{x | \Psi_H(x) > M\}$ is a null set, and the minimum of all these M is the essential supremum, *ess sup* Ψ_H , of Ψ_H . Then T_H is a bounded, self-adjoint, positive definite operator of $L^2(\mathbb{R})$. Moreover,

$$\|T_H\|_{\mathbb{R}} \triangleq \sup_{W \neq 0} \frac{\|T_H W\|_{\mathbb{R}}}{\|W\|_{\mathbb{R}}} \leq \text{ess sup } \Psi_H. \tag{A.12}$$

(ii) Let $H \in l^2(\mathbb{Z})$. Then \bar{U}_H is a bounded, self-adjoint, positive definite operator of $l^2(\mathbb{Z})$. Moreover,

$$\|\bar{U}_H\|_{\mathbb{Z}} \triangleq \sup_{W \neq 0} \frac{\|\bar{U}_H W\|_{\mathbb{Z}}}{\|W\|_{\mathbb{Z}}} = \|H\|_{\mathbb{Z}}^2. \tag{A.13}$$

Proof

(i) Let $W \in L^2(\mathbb{R})$. We shall show that $T_H W \in L^2(\mathbb{R})$. By periodicity of the series in eq. (A.5) we have

$$\int_{-\infty}^{\infty} |(T_H W)(x)|^2 dx = \int_0^1 \sum_{m=-\infty}^{\infty} |H(x+m)|^2 \left| \sum_{n=-\infty}^{\infty} H(x+n) W(x+n) \right|^2 dx. \quad (\text{A.14})$$

By the Cauchy-Schwarz inequality and the definition of Ψ_H we get

$$\int_{-\infty}^{\infty} |(T_H W)(x)|^2 dx \leq \int_0^1 \Psi_H^2(x) \sum_{n=-\infty}^{\infty} |W(x+n)|^2 dx, \quad (\text{A.15})$$

and the right-hand side is smaller than or equal to $\text{ess sup } \Psi_H^2 \cdot \|W\|^2$. This shows that $T_H W \in L^2(\mathcal{R})$, the boundedness of T_H and inequality (A.12).

We next show that T_H is self-adjoint. Let $W, V \in L^2(\mathcal{R})$. We shall show that $(T_H W, V)_R = (W, T_H V)_R$. We have

$$\begin{aligned} (T_H W, V)_R &= \int_{-\infty}^{\infty} H^*(x) V^*(x) \sum_{n=-\infty}^{\infty} H(x+n) W(x+n) dx \\ &= \sum_{n=-\infty}^{\infty} \int_{-\infty}^{\infty} H(x) W(x) H^*(x-n) V(x-n) dx \\ &= \int_{-\infty}^{\infty} W(x) [H^*(x) \sum_{n=-\infty}^{\infty} H(x-n) V(x-n)]^* dx = (W, T_H V)_R. \end{aligned} \quad (\text{A.16})$$

We finally show that T_H is positive definite. Let $W \in L^2(\mathcal{R})$. We shall show that $(T_H W, W)_R \geq 0$. We have, with $V(x) \triangleq H(x) W(x)$,

$$(T_H W, W)_R = \sum_{n=-\infty}^{\infty} \int_{-\infty}^{\infty} V(x) V^*(x+n) dx. \quad (\text{A.17})$$

If we let

$$Z(t) \triangleq \int_{-\infty}^{\infty} V(x) V^*(x+t) dx \quad \text{for } t \in \mathcal{R}, \quad (\text{A.18})$$

then we find by the Poisson summation formula (ref. 26)

$$(T_H W, W)_R = \sum_{n=-\infty}^{\infty} Z(n) = \sum_{n=-\infty}^{\infty} z(n), \quad (\text{A.19})$$

where

$$z(s) \triangleq \int_{-\infty}^{\infty} Z(t) \exp(-j2\pi s t) dt \quad (\text{A.20})$$

is the Fourier transform of Z . Since $z(s) = |v(s)|^2$, with v the Fourier transform of V , it follows that $(T_H W, W)_R \geq 0$, and the proof of (i) is complete.

(ii) This statement is completely trivial.

For the measure-theoretic intricacies in the proof of the following proposition one may consult ref. 30.

Proposition A.2

(i) Assume that $H^\Delta(x)$ is measurable as a function of $(x, \Delta) \in R \times S$, and that

$$C_H^2 \triangleq \int_{\Delta \in S} \text{ess sup } \Psi_{H^\Delta}^2 p(\Delta) d\Delta < \infty. \quad (\text{A.21})$$

Then (A.7) defines a bounded, self-adjoint, positive definite operator of $L^2(R)$. Moreover,

$$\|\bar{T}_H\|_R \leq C_H. \quad (\text{A.22})$$

(ii) Let $x \in [-\frac{1}{2}, \frac{1}{2}]$, and assume that H_x^Δ is measurable as a function of $\Delta \in S$. Furthermore, assume that

$$C_L^2(x) \triangleq \int_{\Delta \in S} \Psi_{H_x^\Delta}^2 p(\Delta) d\Delta < \infty. \quad (\text{A.23})$$

Then (A.8) defines a bounded, self-adjoint, positive definite operator of $L^2(Z)$. Moreover,

$$\|\bar{U}_{H_x}\|_Z \leq C_L. \quad (\text{A.24})$$

Proof

(i) The quantity $(T_H^\Delta W)(x)$ is measurable as a function of $(x, \Delta) \in R \times S$ when $W \in L^2(R)$. By the Cauchy-Schwarz inequality

$$\left(\int_{\Delta \in S} |(T_H^\Delta W)(x)| p(\Delta) d\Delta \right)^2 \leq \int_{\Delta \in S} |(T_H^\Delta W)(x)|^2 p(\Delta) d\Delta \quad \text{for } x \in R. \quad (\text{A.25})$$

By Fubini's theorem and proposition A.1 (i)

$$\int_{-\infty}^{\infty} \int_{\Delta \in S} |(T_{H^A} W)(x)|^2 p(\Delta) d\Delta dx \leq \|W\|_R^2 \int_{\Delta \in S} \text{ess sup } \Psi_{H^A}^2 p(\Delta) d\Delta < \infty. \quad (\text{A.26})$$

It follows from Fubini's theorem that $T_{H^A} W \in L^2(\mathcal{R})$ for almost all Δ , that

$$\int_{\Delta \in S} (T_{H^A} W)(x) p(\Delta) d\Delta \quad (\text{A.27})$$

is well-defined for almost all $x \in \mathcal{R}$ and belongs to $L^2(\mathcal{R})$ as a function of x . Hence $\bar{T}_H W$ is well-defined and belongs to $L^2(\mathcal{R})$ for $W \in L^2(\mathcal{R})$, and also the inequality (A.22) follows. The remaining facts can be shown to hold noting that for $W, V \in L^2(\mathcal{R})$

$$(\bar{T}_H W, V)_R = \int_{\Delta \in S} (T_{H^A} W, V)_R p(\Delta) d\Delta \quad (\text{A.28})$$

and using proposition A.1 (i).

(ii) The proof of this is similar to the proof of (i).

Proposition A.3

(i) Assume that $H^A(x)$ satisfies the conditions of proposition A.2 (i) and that $V \in L^2(\mathcal{R})$. There is a unique $W \in L^2(\mathcal{R})$ such that $\bar{T}_H W + W = V$. Moreover, $\|W\|_R \leq \|V\|_R$.

(ii) Let $x \in [-\frac{1}{2}, \frac{1}{2}]$, assume that H_x^A satisfies the conditions of proposition A.2 (ii) and that $V \in l^2(\mathcal{Z})$. There is a unique $W \in l^2(\mathcal{Z})$ such that $\bar{U}_H W + W = V$. Moreover, $\|W\|_Z \leq \|V\|_Z$.

Proof

(i) The existence and uniqueness result follows from general Hilbert space theory, see ref. 29. The inequality $\|W\|_R \leq \|V\|_R$ follows from $\|W\|_R^2 \leq (\bar{T}_H W, W)_R + (W, W)_R = (V, W)_R$ and the Cauchy-Schwarz inequality.

(ii) The proof of this is similar to the proof of (i).

We shall now reduce the general cases of eqs (A.9) and (A.10) to the special ones of proposition A.3. To this end we introduce the functions

$$K^A(x) \triangleq \frac{H^A(x)}{N^A(x)} \text{ and } L^A(x) \triangleq \frac{H^A(x)}{N(x)} \text{ for } x \in \mathcal{R} \quad (\text{A.29})$$

where it is assumed that $N(x)$ is measurable and $N(x) > 0$ almost everywhere.

Theorem A.1

(i) Assume that $H^\Delta(x)$ and $N(x)$ are measurable as a function of $(x, \Delta) \in \mathbb{R} \times S$, that $N(x) > 0$ almost everywhere, that $M \triangleq \text{ess sup } N < \infty$ and that $C_L < \infty$. For any $G \in L^2(\mathbb{R})$ there is a unique $W \in L^2(\mathbb{R})$ such that eq. (A.9) holds. Moreover,

$$\|W\|_{\mathbb{R}} \leq (C_L^{\frac{1}{2}} + C_L C_K^{\frac{1}{2}} M^{\frac{1}{2}}) \|G\|_{\mathbb{R}}. \tag{A.30}$$

(ii) Let $x \in [-\frac{1}{2}, \frac{1}{2}]$, assume that H_x^Δ is measurable as a function of $\Delta \in S$, that $N(x+n) > 0$, all n , that

$$M(x) \triangleq \sup_n N(x+n) < \infty \tag{A.31}$$

and that $C_L(x) < \infty$. For any $G_x \in l^2(\mathbb{Z})$ there is a unique $W_x \in l^2(\mathbb{Z})$ such that eq. (A.10) holds. Moreover,

$$\|W_x\|_{\mathbb{Z}} \leq (C_L^{\frac{1}{2}}(x) + C_L(x) C_K^{\frac{1}{2}}(x) M^{\frac{1}{2}}(x)) \|G_x\|_{\mathbb{Z}}. \tag{A.32}$$

Proof

(i) Consider the equation

$$\bar{T}_K Z + Z = Y, \tag{A.33}$$

where $Y \triangleq N^{-\frac{1}{2}} \bar{H}^* G$. We shall show that the solutions Z of (A.33) and W of (A.9) are in one-to-one correspondence by means of the transformation $Z = N^{\frac{1}{2}} W$. We first note that K satisfies the conditions of proposition A.2. (i). This is so since $C_K \leq M C_L$. We next note that $Y \in L^2(\mathbb{R})$. We have, more in particular,

$$\|Y\|_{\mathbb{R}} \leq C_K^{\frac{1}{2}} \|G\|_{\mathbb{R}}. \tag{A.34}$$

It follows that for any $G \in L^2(\mathbb{R})$ there is exactly one $Z \in L^2(\mathbb{R})$ which satisfies eq. (A.33). We shall now show that $N^{-\frac{1}{2}} Z \in L^2(\mathbb{R})$. Indeed, it holds that

$$N^{-\frac{1}{2}} Y \in L^2(\mathbb{R}), \|N^{-\frac{1}{2}} Y\|_{\mathbb{R}} \leq C_L^{\frac{1}{2}} \|G\|_{\mathbb{R}}, \tag{A.35}$$

$$N^{-\frac{1}{2}} \bar{T}_K Z = \bar{T}_L (N^{\frac{1}{2}} Z) \in L^2(\mathcal{R}), \quad (\text{A.36})$$

$$\|N^{-\frac{1}{2}} \bar{T}_K Z\|_{\mathcal{R}} \leq C_L M^{\frac{1}{2}} \|Z\|_{\mathcal{R}} \leq C_L M^{\frac{1}{2}} \|Y\|_{\mathcal{R}} \leq C_L C_K^{\frac{1}{2}} M^{\frac{1}{2}} \|G\|_{\mathcal{R}}. \quad (\text{A.37})$$

Here eq. (A.36) follows readily from the definition. Hence $N^{-\frac{1}{2}} Z \in L^2(\mathcal{R})$, and

$$\|N^{-\frac{1}{2}} Z\|_{\mathcal{R}} \leq \|N^{-\frac{1}{2}} Y\|_{\mathcal{R}} + \|N^{-\frac{1}{2}} \bar{T}_K Z\|_{\mathcal{R}} \leq (C_L^{\frac{1}{2}} + C_L C_K^{\frac{1}{2}} M) \|G\|_{\mathcal{R}}. \quad (\text{A.38})$$

By multiplying eq. (A.33) from the left by $N^{\frac{1}{2}}$ and using $N^{\frac{1}{2}} \bar{T}_K Z = \bar{T}_H (H^{\frac{1}{2}} Z)$, we see that $N^{\frac{1}{2}} Z$ is a solution of eq. (A.9). On the other hand, if W is a solution of eq. (A.9), then $N^{\frac{1}{2}} W \in L^2(\mathcal{R})$ is a solution of eq. (A.33). Together with eq. (A.38), this establishes (i).

(ii) The proof of this is similar to the proof of (i).

Our final task consists of tying the solutions W of (A.9) and the solutions W_x of eq. (A.10) together.

Theorem A.2

Let $G \in L^2(\mathcal{R})$ and assume that H and N satisfy the conditions of theorem A.1.(i). Let W be the solution of eq. (A.9). Then $G_x \in l^2(\mathcal{Z})$ for almost every $x \in [-\frac{1}{2}, \frac{1}{2}]$, and H_x, N_x satisfy the conditions of theorem A.1.(ii) for almost every $x \in [-\frac{1}{2}, \frac{1}{2}]$. Moreover, if we denote $\bar{W}_x \triangleq (W(x+n))_{n \in \mathcal{Z}}$, then $\bar{W}_x \in l^2(\mathcal{Z})$, satisfies (A.10) for almost every $x \in [-\frac{1}{2}, \frac{1}{2}]$ and $\bar{W}_x = W_x$ for almost every $x \in [-\frac{1}{2}, \frac{1}{2}]$.

Proof

We have

$$\int_0^1 \|G_x\|_{\mathcal{Z}}^2 dx = \int_0^1 \sum_{n=-\infty}^{\infty} |G(x+n)|^2 dx = \int_{-\infty}^{\infty} |G(x)|^2 dx < \infty. \quad (\text{A.39})$$

Hence $\|G_x\|_{\mathcal{Z}}^2 < \infty$ for almost every $x \in [-\frac{1}{2}, \frac{1}{2}]$. Moreover, measurability of $H^\Delta(x)$ as a function of $(x, \Delta) \in \mathcal{R} \times \mathcal{S}$ implies measurability of $H^\Delta(x+n)$ as a function of $\Delta \in \mathcal{S}$ for almost every $x \in [-\frac{1}{2}, \frac{1}{2}]$ and $n \in \mathcal{Z}$, and

$$\text{ess sup}_{\Delta \in \mathcal{S}} C_L^2(x) = \text{ess sup}_{\Delta \in \mathcal{S}} \int \Psi^{2^\Delta}(x) p(\Delta) d\Delta \leq \int \text{ess sup}_{\Delta \in \mathcal{S}} \Psi^{2^\Delta}(x) p(\Delta) d\Delta = C_L^2. \quad (\text{A.40})$$

Similarly,

$$\sup_{n \in \mathbb{Z}} N(x+n) \leq \text{ess sup } N \tag{A.41}$$

for almost all $x \in [-\frac{1}{2}, \frac{1}{2}]$. Also, $\tilde{W}_x \in L^2(\mathbb{Z})$ for almost every $x \in [-\frac{1}{2}, \frac{1}{2}]$. Finally, as the proof of proposition A.2.(i) shows,

$$(\bar{T}_H W)(x) = \bar{U}_H \tilde{W}_x \tag{A.42}$$

for almost all $x \in [-\frac{1}{2}, \frac{1}{2}]$. Now the theorem follows from the uniqueness part of theorem A.1.(ii).

Note

Theorem A.1 and theorem A.2 can be extended to cover the case where $N(x) = 0$ for x in a set of positive measure. In the assertion of theorem A.1.(i) we get the existence of a $W \in L^2(\mathbb{R})$ such that eq. (A.9) holds, and this W can be made unique by the requirement that $W(x) = 0$ whenever $N(x) = 0$. In this definition (A.29) and everywhere in the proof of theorem A.1.(i) where $N^{-\frac{1}{2}}$ is applied, we use the convention that $0/0 = 0$, $a/0 = \infty$ when $a \neq 0$. The condition $C_L < \infty$ implies that, for almost all $x \in \mathbb{R}$, $H^A(x) = 0$ for almost all $A \in S$ when $N(x) = 0$. With this convention the proof of theorem A.1.(i) can be easily adapted. We see e.g. that the solution Z of the equation $\bar{T}_K Z + Z = Y$ satisfies $Z(x) = 0$ whenever $N(x) = 0$, and that eqs (A.35) to (A.37) are still valid. In theorem A.1.(ii) the solution W_x becomes unique when we require that $W_x(n) = 0$ whenever $N(x+n) = 0$. In theorem A.2 we must take the unique solutions W and \tilde{W}_x of the adapted theorem A.1.

Acknowledgement

The author is indebted to Dr. A.J.E.M. Janssen for providing the appendix, which skilfully handles several mathematical intricacies of the problem studied here. The author also wishes to acknowledge the valuable discussions with Dr. K.A. Schouhamer Immink concerning the robustness of receivers.

REFERENCES

- 1) W. R. Bennett and J. R. Davey, Data Transmission, McGraw-Hill, New York, 1965.
- 2) J. Proakis, Digital Communications, New York, McGraw-Hill, 1963.
- 3) S. Nakagawa, K. Yokoyama and H. Katayama, IEEE Trans. Magn. **MAG-16**, 104 (1980)
- 4) R. W. Wood and D. A. Petersen, IEEE Trans. Commun., **COM-34**, 454 (1986).

- 5) S. U. Qureshi, Proc. IEEE, **73**, 1349 (1985).
- 6) R. W. Lucky, Bell Syst. Techn. J., **44**, 547 (1965).
- 7) R. W. Lucky, Bell Syst. Techn. J., **45**, 255 (1966).
- 8) D. W. Tufts and T. Berger, IEEE Trans. Inf. Theory, **IT-13**, 209 (1967).
- 9) R. A. Gonsalves and D. W. Tufts, IEEE Trans. Commun. Technol., **COM-16**, 375 (1968).
- 10) A. R. Kaye, Proc. IEEE, **56**, 1087 (1968).
- 11) A. Lender, IEEE Trans. Commun. Technol., **COM-12**, 128 (1964).
- 12) P. J. van Gerwen, Philips Res. Rept., **20**, 469 (1965).
- 13) E. R. Kretzmer, ICC Conf. Rec., 1965, p. 451, IEEE Trans. Commun. Technol., **COM-14**, 67 (1966).
- 14) P. Kabal and S. Pasupathy, IEEE Trans. Commun., **COM-23**, 921 (1975).
- 15) J. W. M. Bergmans, Philips J. Res., **42**, 209 (1987).
- 16) M. Kavehrad, Electronic Circuits and Systems, **3**, 201 (1979).
- 17) R. E. Maurer and L. E. Franks, IEEE Trans. Circuit Theory, **CT-17**, 61 (1970).
- 18) F. J. Brophy, G. J. Foschnini and R. D. Gitlin, Bell Syst. Techn. J., **52**, 1077 (1973).
- 19) G. V. Moustakides and S. A. Kassam, IEEE Trans. Commun., **COM-33**, 820 (1985).
- 20) J. C. Mallinson, Proc. IEEE, **64**, 196 (1976).
- 21) G. Bouwhuis, J. Braat, A. Huiser, J. Pasman, G. van Rosmalen and K. Schouhamer Immink, Principles of Optical Disc Systems, Adam Hilger Ltd., Bristol and Boston, 1985.
- 22) J. C. Mallinson, IEEE Trans. Magn., **MAG-21**, 1217 (1985).
- 23) H. Osawa, S. Tazaki and S. Ando, IEEE Trans. Magn., **MAG-22**, 253 (1986).
- 24) J. W. M. Bergmans, Philips J. Res., **41**, 531 (1986).
- 25) J. W. M. Bergmans, Philips J. Res., **42**, 281 (1987).
- 26) A. Papoulis, Signal Analysis, McGraw-Hill, New York, 1984.
- 27) F. E. Glave, IEEE Trans. Inf. Th., **IT-18**, 356 (1972).
- 28) J. M. Harker, D. W. Brede, R. E. Pattison, G. R. Santana and L. G. Taft, IBM J. Res. Develop., **25**, 677 (1981).
- 29) A. W. Naylor and G. R. Sell, Linear Operator Theory in Engineering and Science, Springer-Verlag, New York, 2nd edition, 1982.
- 30) A. J. E. M. Janssen and P. van der Steen, Integration Theory, Springer-Verlag, Berlin, 1984.

ROBUST DATA EQUALIZATION, FRACTIONAL TAP SPACING AND THE ZAK TRANSFORM

Abstract

To counter intersymbol interference and noise, a data equalizer must be dimensioned in accordance with the characteristics of the transmission channel that it operates upon. Adaptive techniques can be a suitable means to this end, provided that the equalizer structure is sufficiently flexible. Alternatively, prior knowledge about the ensemble of possible characteristics may be exploited to equip a non-adaptive equalizer with a sufficiently robust dimensioning to withstand all possible parameter variations. For the most commonly applied types of data equalizer, viz. the linear equalizer, its partial response variants and the decision feedback equalizer, this paper presents a unified derivation of their optimum adaptive and robust versions, using a mean-square measure of performance. The analysis is carried out by using the Zak transform, which is a linear time-frequency signal representation stemming from quantum mechanics. The comprehensive scope of the paper, which particularly for the decision feedback equalizer extends beyond previous treatments, serves to illustrate the potential of the Zak transform as a tool for use in cyclostationary environments like the one encountered here. Among other things, the paper reveals that a restricted resistance to timing errors is unavoidable in symbol interval-spaced linear equalization. Also, it demonstrates that the Zak transform matches the polyphase representation of fractionally-spaced equalizers, and as such enables one to derive the optimally robust linear and decision feedback equalizers in a convenient and elegant fashion. The latter results are quantified for a class of digital magnetic recording systems suffering from timing errors.

1. Introduction

Equalization methods serve to counter the intersymbol interference (ISI) and noise which arise in many digital transmission and recording systems¹⁻³). They involve one or more linear filters, that must be adapted to the characteristics of the channel in order to ensure a satisfactory transmission quality. In the presence of large variations or uncertainties relating to these characteristics, as encountered in voiceband modem connections²), radio channels subject to multipath fading³) and ISDN subscriber loops⁴),

it is often necessary to use adaptive techniques⁵⁾ in order to guarantee adequate performance levels. Also, to be able to cope with all possible imperfections, the structure of the equalizer must be sufficiently flexible. In this respect, the fractionally-spaced equalizer has gained increasing attention over the last decade⁵⁾. This equalizer contains a transversal filter whose taps are separated by a fraction of the symbol interval. Its main advantage over the conventional symbol interval-spaced equalizer is its ability to cope with timing errors⁶⁻⁸⁾.

Although adaptive equalization methods are beyond doubt the most natural and effective means to compensate for varying channel characteristics, it becomes difficult to incorporate adaptivity when high data rates, power consumption restrictions or limitations to costs of manufacturing are present. In situations like these, encountered in e.g. upcoming generations of consumer-grade digital audio and video recording equipment^{9,10)}, it may be more appropriate to devise a compromise equalizer dimensioning on the basis of prior knowledge about the possible channel characteristics. For the linear equalizer, the optimum mean-square solution to this design problem was found in the pre-adaptive era¹¹⁾. Recently, these results have been extended to the partial response variants of the linear equalizer, and have been applied to equip equalizers for a specific class of digital magnetic recording systems with an improved resistance to timing errors¹²⁾.

In view of their intrinsically greater sensitivity to system parameter variations¹³⁾, devising similar methods for more powerful equalizers than the linear one is more than just an academic exercise. In this respect, especially the decision feedback equalizer (DFE) merits attention in view of its relative simplicity and its increasing popularity⁴⁾. The present paper finds its roots in efforts to solve this problem. After taking stock of several conceivable approaches towards its solution, we observed that the so-called Zak transform, introduced in 1967 by J. Zak to solve certain problems in quantum mechanics¹⁴⁾, offers remarkable advantages in compactness and clarity over competing tools. The Zak transform is the Fourier transform of the sampled version of a signal, using the sampling phase as a second parameter*). As such it is a linear time-frequency signal representation, and is in between the Fourier transform for discrete-time signals and the Fourier integral for continuous-time signals. This makes it especially useful as a tool for use in data transmission, where a data stream is converted into a continuous-time signal and decisions are taken at discrete, equidistant moments, so that continu-

*) Although it has up to now not been put to systematic use in the data transmission literature, there are several examples of implicit occurrences of the Zak transform^{5,7,8,15-18)}.

ous- and discrete-time aspects are both present. It is a major aim of the present paper to ascertain these merits. We do this by showing that the Zak transform enables principal results in the area of adaptive and robust equalization to be derived in a general, compact and elegant fashion. Apart from rediscovering classical equalization wisdoms, we shall with remarkable ease add several new ones. For example, we shall use the fact that the Zak transform of any well-behaved signal has a zero somewhere in the unit square to prove in a very general way that linear equalizers are incapable of guaranteeing satisfactory performance in the presence of timing errors. Also, we shall find that the Zak transform matches the polyphase representation of fractionally-spaced equalizers, and, as a main result of the paper, we shall use the Zak transform to derive the dimensioning and performance of the optimally robust DFE relative to a mean-square performance measure which takes account of the possible parameter variations.

For the sake of clarity and conciseness, the paper will be devoid of mathematical rigor. Some basic proofs are, however, included in the appendices, and rigorous validation of the remaining results should be fairly straightforward.

The paper is organized as follows. Section 2 introduces the Zak transform and its basic properties. Section 3 rederives Nyquist's classical first criterion for distortionless transmission with the aid of the Zak transform. In sec. 4, the Zak transform is used to show that symbol interval-spaced linear equalization nearly always leads to a restricted resistance to timing errors. Section 5 elaborates a polyphase description of fractionally-spaced linear equalization, and shows that the Zak transform matches this description. In sec. 6, the optimally robust versions of the fractionally-spaced linear equalizer and its partial response variants are derived. A similar derivation is carried out in sec. 7 for the DFE. In both cases, we use a mean-square performance measure which takes account of the possible channel parameter variations. In sec. 8 the results of sec. 6 and 7 are specialized to the conventional situation where the equalizer is adapted to the instantaneous characteristics of the channel. As a second limiting case, the situation where the tap-spacing approaches zero, corresponding to equalization without prior structural restrictions, is analyzed in sec. 9. As a worked example, sec. 10 finally applies the theory to a class of digital magnetic recording systems with the object of providing non-adaptive linear and decision feedback equalizers with an optimum resistance to timing errors.

2. The Zak transform

This section provides a concise overview of definitions and properties relating to the Zak transform. A companion paper¹⁹⁾ is entirely devoted to this time-frequency signal representation, its properties and its potential applications.

The Zak transform $\mathfrak{X}_x(\tau, \Omega)$ of a continuous-time signal $x(t)$ is for all τ and $\Omega \in \mathbb{R}$ defined as

$$\mathfrak{X}_x(\tau, \Omega) \triangleq \sum_{k=-\infty}^{\infty} x((\tau + k)T) \exp(-j2\pi\Omega k). \quad (1)$$

According to this definition, the Zak transform can be interpreted as the discrete-time Fourier transform of a sampled version of $x(t)$, using a sampling interval T and a normalized sampling phase τ . Because the frequency Ω is normalized on the sampling rate $1/T$, $\mathfrak{X}_x(\tau, \Omega)$ is periodic in Ω with period 1, i.e.

$$\mathfrak{X}_x(\tau, \Omega + 1) = \mathfrak{X}_x(\tau, \Omega). \quad (2)$$

Also, $\mathfrak{X}_x(\tau, \Omega)$ is quasi-periodic in τ with period 1, i.e.

$$\mathfrak{X}_x(\tau + 1, \Omega) = \exp(j2\pi\Omega) \mathfrak{X}_x(\tau, \Omega). \quad (3)$$

Hence, $\mathfrak{X}_x(\tau, \Omega)$ is completely determined by its values on the unit square. (In fact, the Zak transform maps $L^2(\mathbb{R})$ injectively onto $L^2([0,1]^2)$.) The Zak transform is information-preserving. For example, $x(t)$ can for all $t \in \mathbb{R}$ be recovered by integrating over Ω according to

$$x(t) = \int_0^1 \mathfrak{X}_x\left(\frac{t}{T}, \Omega\right) d\Omega. \quad (4)$$

With the aid of the Poisson summation formula²⁰⁾, it is easy to show that for all τ and $\Omega \in \mathbb{R}$

$$\mathfrak{X}_x(\tau, \Omega) = \frac{1}{T} \sum_{n=-\infty}^{\infty} X(\Omega + n) \exp(j2\pi\tau(\Omega + n)). \quad (5)$$

Here $X(\Omega)$ is the Fourier integral of $x(t)$, defined as*

$$X(\Omega) \triangleq \int_{-\infty}^{\infty} x(t) \exp(-j2\pi\Omega t/T) dt. \quad (6)$$

*) Although it is somewhat unconventional in that the frequency Ω is dimensionless and normalized upon the sampling rate $1/T$, definition (6) is chosen here because it simplifies the formulas in this paper.

As its right hand side is again a Zak transform (with unit sampling interval), eq. (5) can be combined with eq. (4) to show that $X(\Omega)$ can be determined from $\mathfrak{X}_x(\tau, \Omega)$ by integrating over τ according to

$$X(\Omega) = T \int_0^1 \mathfrak{X}_x(\tau, \Omega) \exp(-j2\pi\Omega\tau) d\tau. \quad (7)$$

Remarkably, the Zak transform of any well-behaved signal has at least one zero somewhere in the unit square. This peculiar property is closely connected to the familiar sensitivity of symbol interval-spaced data equalizers to timing errors, as we will see later.

For any two signals $x(t)$ and $y(t)$, we have the Parseval-like relations

$$\int_0^1 \mathfrak{X}_z(\tau, \Omega) \mathfrak{X}_y^*(\tau, \Omega) d\Omega = \sum_{k=-\infty}^{\infty} x((\tau+k)T) y^*((\tau+k)T) \quad (8)$$

and

$$\int_0^1 \mathfrak{X}_x(\tau, \Omega) \mathfrak{X}_y^*(\tau, \Omega) d\tau = \frac{1}{T^2} \sum_{n=-\infty}^{\infty} X(\Omega+n) Y^*(\Omega+n), \quad (9)$$

where the superscript “*” indicates complex conjugation.

For any signal $x(t)$, we have that

$$\mathfrak{X}_{x_-}(\tau, \Omega) = \mathfrak{X}_x(-\tau, -\Omega) \quad (10)$$

and

$$\mathfrak{X}_{x^*}(\tau, \Omega) = \mathfrak{X}_x^*(\tau, -\Omega) \quad (11)$$

where the subscript ‘_’ indicates time-reversal, i.e. $x_-(t) \triangleq x(-t)$ for all $t \in \mathbb{R}$. When $x(t)$ is real-valued, $\mathfrak{X}_x(\tau, \Omega)$ is Hermitean in the frequency variable Ω , and

$$\mathfrak{X}_{x_-}(\tau, \Omega) = \mathfrak{X}_x(-\tau, -\Omega) = \mathfrak{X}_x^*(-\tau, \Omega). \quad (12)$$

If a signal $x(t)$ has no spectral content outside the interval $[-\frac{L}{2}, \frac{L}{2}]$ for some integer L , then both $x(t)$ and $X(\Omega)$ are completely determined by the values of $\mathfrak{X}_x(\tau, \Omega)$ on L lines in the unit square with equidistant sampling phases. In particular

$$X(\Omega) = \frac{T}{L} \sum_{l=0}^{L-1} \mathfrak{X}_x\left(\frac{l}{L}, \Omega\right) \exp(-j2\pi\frac{l}{L}\Omega) \quad \text{for all } \Omega \in \left[-\frac{L}{2}, \frac{L}{2}\right]. \quad (13)$$

Also, if both $x(t)$ and $y(t)$ have no spectral content outside the interval $[-\frac{L}{2}, \frac{L}{2}]$, then

$$\frac{T}{L} \sum_{l=0}^{L-1} \mathfrak{X}_x(-\frac{l}{L}, \Omega) \mathfrak{X}_y(\frac{l}{L}, \Omega) = T \int_0^1 \mathfrak{X}_x(-\tau, \Omega) \mathfrak{X}_y(\tau, \Omega) d\tau = \mathfrak{X}_{x*y}(0, \Omega) \quad \text{for all } \Omega \in \mathbb{R}, \quad (14)$$

where ‘*’ denotes linear convolution*). Taking $x(t) = y(-t)$ in this expression and using eq. (12), we finally have for any real-valued signal $x(t)$ with $X(\Omega) = 0$ for $|\Omega| > \frac{L}{2}$ that

$$\frac{T}{L} \sum_{l=0}^{L-1} |\mathfrak{X}_x(-\frac{l}{L}, \Omega)|^2 = T \int_0^1 |\mathfrak{X}_x(-\tau, \Omega)|^2 d\tau = \mathfrak{X}_{x*x_-}(0, \Omega) \quad \text{for all } \Omega \in \mathbb{R}, \quad (15)$$

where $(x * x_-)(t)$ is the autocorrelation function of $x(t)$.

3. Nyquist’s first criterion for distortionless transmission

For a first illustration of the role of the Zak transform in data transmission, we consider a signal $x(t)$ in the form of the classical Nyquist-1 pulse, which is tailored for distortionless transmission in that

$$x(kT) \triangleq \begin{cases} 1, & k = 0, \\ 0, & k \in \mathbb{Z}, k \neq 0. \end{cases} \quad (16)$$

Applying definition (1), we see that in order for eq. (16) to be fulfilled the Zak transform $\mathfrak{X}_x(\tau, \Omega)$ of $x(t)$ should satisfy

$$\mathfrak{X}_x(0, \Omega) = 1 \quad \text{for all } \Omega \in \mathbb{R}. \quad (17)$$

Because of eq. (7), this means that the Fourier transform $X(\Omega)$ of $x(t)$ should satisfy

$$\frac{1}{T} \sum_{n=-\infty}^{\infty} X(\Omega + n) = 1 \quad \text{for all } \Omega \in \mathbb{R}. \quad (18)$$

This is Nyquist’s celebrated first criterion for distortionless transmission²¹⁾.

This remarkably compact derivation parallels the one of ref. 16, in which no explicit use was made of the Zak transform. Nyquist’s other criteria for

) The symbol ‘’ will be used here to denote both continuous-time and discrete-time convolution. It will be clear from the context which one is meant.

distortionless transmission can be derived in a similar and comparably compact way.

4. Symbol interval-spaced linear equalization and sensitivity to timing errors

In this section, we shall use the Zak transform to study the influence of timing errors in the data transmission system of fig. 1, which uses a symbol interval-spaced linear equalizer.

A discrete-time data sequence a_k is transmitted over a noisy dispersive channel, which transforms a_k into an output signal $r(t)$ of the form

$$r(t) = \sum_{k=-\infty}^{\infty} a_k f(t - kT) + n(t), \tag{19}$$

where $f(t)$ is the impulse response of the channel, T is the symbol interval and $n(t)$ is an additive noise signal. To suppress the noise, $r(t)$ is fed into a receiving filter with impulse response $w(t)$. The output signal of the receiving filter is sampled once every symbol interval at the instants $(k + \Delta)T$, where $\Delta \in [-0.5, 0.5]$ accounts for the occurrence of timing errors. This yields a sampled signal u_k of the form

$$u_k = (a * f^\Delta)_k + n_k, \tag{20}$$

where

$$f_k^\Delta \triangleq (f * w)((k + \Delta)T) \tag{21}$$

is the sampled impulse response of the system, and

$$n_k \triangleq (n * w)((k + \Delta)T) \tag{22}$$

is the filtered and sampled noise sequence. At any instant k , u_k normally depends not only upon a_k but also on adjacent data symbols due to the fact that f_k^Δ is nonzero for several values $k \neq 0$. To eliminate this intersymbol interference (ISI), u_k is fed into a discrete-time filter with impulse response c_k , whose output signal

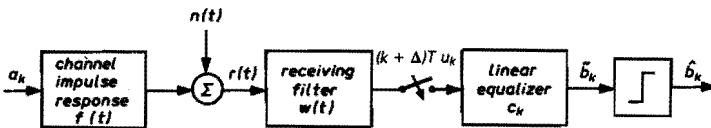


Fig. 1. Continuous-time model of a data transmission system using a symbol interval-spaced linear equalizer.

$$\tilde{b}_k = (a * f^\Delta * c)_k + (n * c)_k \quad (23)$$

ideally resembles the transmitted data a_k as well as possible. In order for \tilde{b}_k to depend only upon a_k , the convolution $(f^\Delta * c)_k$ should be a Kronecker delta-function. This means that the transfer function

$$C(\Omega) \triangleq \sum_{k=-\infty}^{\infty} c_k \exp(-j2\pi\Omega k) \quad (24)$$

should be the reciprocal of the Fourier transform

$$F^\Delta(\Omega) \triangleq \sum_{k=-\infty}^{\infty} f_k^\Delta \exp(-j2\pi\Omega k) \quad (25)$$

of the sampled system impulse response f_k^Δ . Using eq. (21) to recognize $F^\Delta(\Omega)$ as the Zak transform $\mathcal{Z}_{f * w}(\Delta, \Omega)$ of the cascade of channel and receiving filter, this condition of perfect equalization can equivalently be denoted as

$$C(\Omega) = \frac{1}{\mathcal{Z}_{f * w}(\Delta, \Omega)} \quad \text{for all } \Omega. \quad (26)$$

From sec. 2 we now recall the fact that the Zak transform $\mathcal{Z}_{f * w}(\Delta, \Omega)$ of any well-behaved function $(f * w)(t)$ has at least one zero in the unit square, say at (Δ_0, Ω_0) . If the instantaneous sampling phase error Δ happens to be close or equal to Δ_0 , then $C(\Omega)$ will be large or even infinite in modulus near $\Omega = \Omega_0$. As a direct consequence, all components of the noise signal n_k with frequencies near Ω_0 will be strongly enhanced, resulting in a poor or even inadequate transmission quality.

To a large extent, this same conclusion still applies when partial response techniques are used, as we will show now. Partial response techniques are used e.g. to achieve desired spectral characteristics or an improved noise suppression^{13,22}), and are aimed at producing faithful estimates \tilde{b}_k of a linearly transformed version

$$b_k \triangleq (a * g)_k \quad (27)$$

of the transmitted data sequence. The partial response g_k specifies the desired controlled ISI structure prior to detection. Its \mathcal{D} -transform

$$g(\mathcal{D}) \triangleq \sum_{k=-\infty}^{\infty} g_k \mathcal{D}^k \quad (28)$$

can often be factored in $(1 + \mathcal{D})$ and $(1 - \mathcal{D})$ terms. Particularly the responses $g(\mathcal{D}) = 1 + \mathcal{D}$, $g(\mathcal{D}) = 1 - \mathcal{D}$ and $g(\mathcal{D}) = (1 + \mathcal{D})(1 - \mathcal{D}) = 1 - \mathcal{D}^2$ are

frequently encountered, and all lead to a ternary signal b_k , so that a three-level symbol-by-symbol detector is needed. An inverse mapping (not shown in fig. 1) serves to reconstruct final estimates \hat{a}_k of a_k from the detector output signal \hat{b}_k^* .

By comparing eqs. (23) and (27) we see that in order to create the desired ISI structure the equalizer should be dimensioned such that

$$(f^{\Delta} * c)_k = g_k. \tag{29}$$

In frequency domain notation, this condition amounts to

$$C(\Omega) = \frac{G(\Omega)}{\mathcal{L}_{f * w}(\Delta, \Omega)}, \tag{30}$$

where

$$G(\Omega) \triangleq \sum_{k=-\infty}^{\infty} g_k \exp(-j2\pi \Omega k) \tag{31}$$

in the Fourier transform of g_k . Arguing as before, we see that excessive noise enhancement may occur whenever $G(\Omega_0) \neq 0$. For the popular partial responses $g(\mathcal{D}) = 1 + \mathcal{D}$, $g(\mathcal{D}) = 1 - \mathcal{D}$ and $g(\mathcal{D}) = 1 - \mathcal{D}^2$, $G(\Omega)$ can only be zero at $\Omega = 0$ and $\Omega = \frac{1}{2}$. Since the precise value of Ω_0 obviously depends upon the precise characteristics of both the channel and the receiving filter, $G(\Omega_0)$ can at best occasionally be zero. In zero-forcing linear equalization, where the equalizer is dimensioned to create a desired ISI structure with complete fidelity, specific timing errors therefore unavoidably lead to a significant degradation of transmission quality, irrespective of the precise characteristics of the channel, receiving filter and partial response.

The same restricted resistance to timing errors also exists when the equalizer is dimensioned according to other criteria. For example, most adaptive equalizers attempt to minimize the mean-square error ε between their output signal \tilde{b}_k and the desired data signal b_k ⁵⁾. It can be shown (by extension of eq. (88) of sec. 8) that the smallest attainable error ε_{\min} equals

$$\varepsilon_{\min} = \int_0^1 \frac{N_0 \mathcal{L}_{w * w_-}(0, \Omega) |G(\Omega)|^2}{|\mathcal{L}_{f * w}(\Delta, \Omega)|^2 + N_0 \mathcal{L}_{w * w_-}(0, \Omega)} d\Omega, \tag{32}$$

*) To make the inverse mapping memoryless and thereby prevent error propagation, one normally adds a precoder at the transmitting end of the system. More powerful (and complicated) decoding procedures, which take account of the correlation in the detector input signal, are also available but generally use the same equalizer dimensioning²³⁾. These measures are not relevant to the considerations in this paper.

provided that the noise signal $n(t)$ is white and has power spectral density N_0 , and that the data sequence a_k is uncorrelated and statistically independent of $n(t)$. This expression is a generalization of eq. (41) of ref. 5.

For realistic signal-to-noise ratio's and whenever the instantaneous sampling phase error Δ is nonproblematic, the signal power-related term $|\mathcal{E}_{f*w}(\Delta, \Omega)|^2$ will for all Ω be much larger than the noise-related term $N_0 \mathcal{E}_{w*w}(0, \Omega)$, so that ϵ_{\min} will be small. However, if Δ comes close to Δ_0 , then for $\Omega \approx \Omega_0$ $|\mathcal{E}_{f*w}(\Delta, \Omega)|^2$ rapidly vanishes relative to $N_0 \mathcal{E}_{w*w}(0, \Omega)$, provided that $\mathcal{E}_{w*w}(0, \Omega)$ strictly exceeds zero, as will normally be the case. This results in a large and possibly unacceptable increment of ϵ_{\min} .

If the equalizer is not adaptive but rather has a fixed dimensioning that has been optimized for some predetermined value of Δ (e.g. $\Delta = 0$), then eq. (32) of course gives an optimistic estimate of the true performance achieved by the equalizer. Consequently, a non-adaptive dimensioning leads to an even greater sensitivity to timing errors.

On the basis of the foregoing arguments, we may conclude that symbol interval-spaced linear equalizers are intrinsically unable to cope with timing errors. It is worth noting that this finding is much more general than previous ones^{5,8,24}) in that no restrictive conditions are imposed on e.g. $f(t)$, $w(t)$ and g_k .

Before showing how the Zak transform can be used in fractionally-spaced equalization, we note that the Zak-transform $\mathcal{E}_{f*w}(\Delta, \Omega)$ of an even function $(f*w)(t)$ has its zeros often concentrated on the line $\Delta = 0.5$ ¹⁹). This symmetry occurs e.g. when the receiving filter is a matched filter, so that $(f*w)(t)$ simply equals the channel autocorrelation function $(f*f_*)(t)$. In this case, only relatively large timing errors (for which $|\Delta| \approx 0.5$) are likely to cause a large noise enhancement (this effect was indeed observed experimentally in ref. 25). Hence, besides the fact that it preserves all information, the use of a matched filter is attractive since the harmful effects of timing errors in adaptive symbol-rate equalization tend to occur only in the more extreme (and hence less likely) misadjustment situations.

5. Fractionally-spaced linear equalization and the Zak transform

In this section we shall derive the polyphase representation of the fractionally-spaced linear equalizer, we shall show that the Zak transform of an appropriately defined equalizer impulse response is directly related to it, and we shall derive a representation in terms of Zak transforms of the output signal of the equalizer.

In the system depicted in fig. 2, transmission again takes place across a noisy dispersive channel. To account for the occurrence of parameter vari-

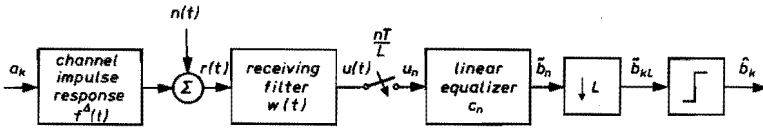


Fig. 2. Continuous-time model of a data transmission system using a fractionally-spaced linear equalizer.

ations, the channel impulse is not deterministic, but depends upon a parameter Δ whose value is selected prior to transmission according to a given distribution function.

In fractionally-spaced equalization, the output signal

$$u(t) \triangleq (r * w)(t) \tag{33}$$

of the receiving filter is sampled at an integer multiple L/T of the signalling rate $1/T^*$). Unlike the symbol interval-spaced situation just considered, this sampling rate is taken large enough to prevent aliasing distortion. To this end, L is selected such that for all possible values of Δ the channel transfer function

$$F^\Delta(\Omega) \triangleq \int_{-\infty}^{\infty} f^\Delta(t) \exp\left(-\frac{j2\pi\Omega t}{T}\right) dt \tag{34}$$

vanishes outside the interval $[-\frac{L}{2}, \frac{L}{2}]$. To reject the out-of-band noise components, the receiving filter is assumed to have the ideal low-pass characteristics

$$W(\Omega) \triangleq \begin{cases} 1, & |\Omega| \leq \frac{L}{2}, \\ 0, & \text{else,} \end{cases} \tag{35}$$

which corresponds to an impulse response

$$w(t) = \frac{L}{T} \frac{\sin\left(\frac{\pi L t}{T}\right)}{\left(\frac{\pi L t}{T}\right)}. \tag{36}$$

* For mathematical convenience, we shall confine attention to T/L -spaced equalizers in this paper. By making use of the strong time-frequency symmetries of the Zak transform¹⁹), the forthcoming analysis can with modest effort be extended to the situation where the tap spacing is a rational fraction of the symbol interval T .

Hence in particular

$$w\left(\frac{kT}{L}\right) = \frac{L}{T} \delta_k, \tag{37}$$

where δ_k is the Kronecker delta function

$$\delta_k \triangleq \begin{cases} 1, & k=0, \\ 0, & k \in \mathbb{Z}, k \neq 0. \end{cases} \tag{38}$$

Since the receiving filter does not affect the data component of the received signal, combination of eqs. (19) and (33) gives

$$u(t) = \sum_{k=-\infty}^{\infty} a_k f^\Delta(t - kT) + (n * w)(t). \tag{39}$$

The sampled version

$$u_n \triangleq u\left(\frac{nT}{L}\right) \tag{40}$$

of $u(t)$ is applied to a discrete-time linear equalizer with impulse response c_n , whose output signal \tilde{b}_n is downsampled by a factor L . In this way a detector input signal \tilde{b}_{kL} results with a sampling rate equal to the symbol rate. With eq. (40), we see that

$$\tilde{b}_{kL} = (u * c)_{kL} = \sum_{n=-\infty}^{\infty} c_n u\left(kT - \frac{nT}{L}\right). \tag{41}$$

To convert this expression into its polyphase counterpart, we subdivide the n -axis into adjacent intervals of length L . This yields

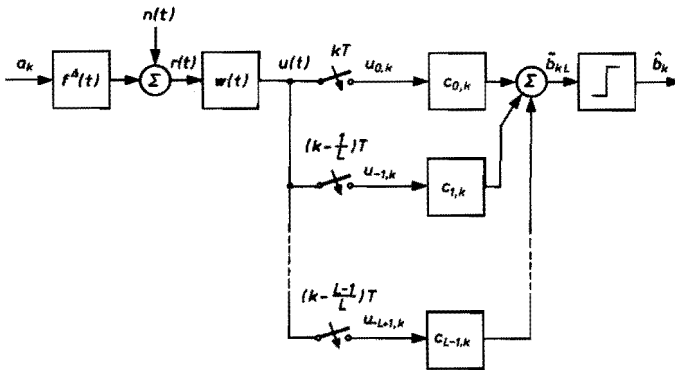


Fig. 3. Data transmission system employing a polyphase fractionally spaced linear equalizer.

$$\tilde{b}_{kL} = \sum_{l=0}^{L-1} \sum_{i=-\infty}^{\infty} c_{l+iL} u\left((k-i)T - \frac{lT}{L}\right) = \sum_{l=0}^{L-1} (u_{-l} * c_l)_k, \quad (42)$$

where the polyphase sequences $c_{l,k}$ and $u_{l,k}$ are for $l \in \{0, \dots, L-1\}$ and $k \in \mathbb{Z}$ defined as

$$c_{l,k} \triangleq c_{l+kL}, \quad (43)$$

and

$$u_{l,k} \triangleq u\left(\frac{lT}{L} + kT\right), \quad (44)$$

respectively. Expression (42) reflects the possibility of implementing the fractionally-spaced equalizer by means of a bank of L polyphase symbol interval-spaced transversal filters, as depicted in fig. 3.

Compared to the straightforward version of the fractionally-spaced equalizer as depicted in fig. 2, where $L-1$ out of L calculated output samples are neglected, the polyphase structure of fig. 3 represents an L -fold improvement of numerical efficiency²⁶.

By using eq. (39) in eq. (44), we can decompose the signals $u_{-l,k}$ of fig. 3 into their polyphase components as

$$\begin{aligned} u_{-l,k} &= \sum_{i=-\infty}^{\infty} a_i f^{\Delta}\left(-\frac{lT}{L} + (k-i)T\right) + (n * w)\left(-\frac{lT}{L} + kT\right) \\ &= (a * f_{-l}^{\Delta})_k + n_{-l,k}, \end{aligned} \quad (45)$$

where the polyphase sequences $f_{l,k}^{\Delta}$ and $n_{l,k}$ are for $l \in \{0, \dots, L-1\}$ and $k \in \mathbb{Z}$ defined as

$$f_{l,k}^{\Delta} \triangleq f^{\Delta}\left(\frac{lT}{L} + kT\right), \quad (46)$$

and

$$n_{l,k} \triangleq (n * w)\left(\frac{lT}{L} + kT\right), \quad (47)$$

respectively.

Using eq. (45) in eq. (42), we conclude that the input signal of the detector can be cast into the polyphase representation

$$\tilde{b}_{kL} = \sum_{l=0}^{L-1} (a * f_{-l}^{\Delta} * c_l)_k + \sum_{l=0}^{L-1} (n_{-l} * c_l)_k. \quad (48)$$

In frequency domain notation this gives

$$\tilde{B}(\Omega) = A(\Omega) \sum_{l=0}^{L-1} F_{-l}^{\Delta}(\Omega) C_l(\Omega) + \sum_{l=0}^{L-1} N_{-l}(\Omega) C_l(\Omega), \quad (49)$$

where $\tilde{B}(\Omega)$, $A(\Omega)$, $F_{-l}^{\Delta}(\Omega)$, $C_l(\Omega)$ and $N_{-l}(\Omega)$ represent the Fourier transforms of \tilde{b}_{kL} , a_k , $f_{-l,k}^{\Delta}$, $c_{l,k}$ and $n_{-l,k}$, respectively. In this expression, we see with eq. (46) that $F_{-l}^{\Delta}(\Omega)$ is simply the Zak transform of the channel impulse response $f^{\Delta}(t)$ evaluated at the normalized sampling phase $-\frac{l}{L}$, i.e.

$$F_{-l}^{\Delta}(\Omega) = \mathfrak{F}_{f^{\Delta}}\left(-\frac{l}{L}, \Omega\right) \quad \text{for all } l \in \{0, \dots, L-1\}. \quad (50)$$

Similarly, $C_l(\Omega)$ can be interpreted as a scaled version of the Zak transform of a continuous-time impulse response $c(t)$ representing the cascade of receiving filter and equalizer. To show this, we combine (33) and (41) and write out the continuous-time convolution explicitly. This gives

$$\tilde{b}_{kL} = \int_{-\infty}^{\infty} r(\tau) \sum_{n=-\infty}^{\infty} c_n w(kT - \tau - \frac{nT}{L}) d\tau. \quad (51)$$

By defining a continuous-time impulse response

$$c(t) \triangleq \sum_{n=-\infty}^{\infty} c_n w(t - \frac{nT}{L}) \quad (52)$$

which reflects the combined effect of the receiving filter and equalizer, eq. (51) can equivalently be denoted as

$$\tilde{b}_{kL} = (r * c)(kT). \quad (53)$$

Hence, by applying the received signal $r(t)$ to a continuous-time filter with impulse response $c(t)$ followed by a symbol-rate sampling operation we would obtain the same detector input signal as in the digital configuration presently considered. With the aid of eqs (37) and (52) we see that at the instants

$\tau = \frac{l}{L}$, $l \in \{0, \dots, L-1\}$, the Zak transform $\mathfrak{F}_c(\tau, \Omega)$ of $c(t)$ equates to

$$\begin{aligned} \mathfrak{F}_c\left(\frac{l}{L}, \Omega\right) &= \sum_{k=-\infty}^{\infty} c\left(\frac{lT}{L} + kT\right) \exp(-j2\pi\Omega k) \\ &= \frac{L}{T} \sum_{k=-\infty}^{\infty} c_{l,k} \exp(-j2\pi\Omega k) = \frac{L}{T} C_l(\Omega). \end{aligned} \quad (54)$$

Hence, by evaluating $\mathcal{X}_c(\tau, \Omega)$ at L appropriate equidistant sampling phases, we indeed obtain the transfer functions of all L polyphase equalizers. Not surprisingly, we observe with eq. (13) that these L lines also determine $c(t)$ completely.

Using eqs (50) and (54) in eq. (49), we finally have the desired Zak transform representation

$$\tilde{B}(\Omega) = A(\Omega) \frac{T}{L} \sum_{l=0}^{L-1} \mathcal{X}_{f^\Delta}(-\frac{l}{L}, \Omega) \mathcal{X}_c(-\frac{l}{L}, \Omega) + \frac{T}{L} \sum_{l=0}^{L-1} N_{-l}(\Omega) \mathcal{X}_c(\frac{l}{L}, \Omega) \quad (55)$$

of the detector input signal. This representation underlies the results of the following sections.

In the absence of noise, eq. (55) indicates that for faithful reproduction of the transmitted data at the output of the equalizer, $\mathcal{X}_c(\frac{l}{L}, \Omega)$ should for $l \in \{0, \dots, L-1\}$ be selected such that

$$\frac{T}{L} \sum_{l=0}^{L-1} \mathcal{X}_{f^\Delta}(-\frac{l}{L}, \Omega) \mathcal{X}_c(\frac{l}{L}, \Omega) = 1 \quad \text{for all } \Omega \in \mathbb{R}. \quad (56)$$

For $L > 1$, eq. (56) will be in general satisfied for a continuum of distinct choices for $\{\mathcal{X}_c(\frac{l}{L}, \Omega)\}$, $l \in \{0, \dots, L-1\}$. Hence, many different zero-forcing fractionally-spaced equalizers exist, as opposed to the unique one for $L = 1^*$. Because (by assumption and construction, respectively) both $f^\Delta(t)$ and $c(t)$ have no frequency content outside the interval $[-\frac{L}{2}, \frac{L}{2}]$, we can apply property (14) to eq. (56). This yields the equivalent condition for distortionless transmission

$$\mathcal{X}_{f^\Delta, c}(0, \Omega) = 1 \quad \text{for all } \Omega \in \mathbb{R}, \quad (57)$$

which is just the first Nyquist criterion as encountered in eq. (17) of sec. 3.

6. The optimally robust fractionally spaced linear equalizer

In this section, we derive the optimum linear equalizer relative to a mean-square error measure which accounts for channel parameter variations. Although the effect of residual ISI is more adequately described by means of

*) As a consequence, the matrix $K(\Omega)$ defined in sec. 6 and analysed in appendix A will for $N_0 = 0$ in general be singular.

an L_1 -norm than by the L_2 -norm in this measure, reasons of analytical tractability motivate this choice. In sec. 10, we shall numerically elaborate a recording example wherein the relevance of the adopted quality measure is assessed (and largely confirmed). To facilitate the analysis, we shall assume (without loss of generality²⁷) that the noise signal $n(t)$ has a frequency-independent power spectral density N_0 and also that $n(t)$, a_k and Δ are statistically independent. Since the receiving filter is cf. eq. (35) an ideal anti-aliasing filter, the former assumption implies that the noise signals $n_{-l,k}$, $l \in \{0, \dots, L-1\}$, entering the L polyphase equalizer branches of fig. 3 are uncorrelated, and are moreover statistically independent of each other. Furthermore, their variance equals

$$E[(n_{l,k})^2] = \frac{1}{T} \int_{-L/2}^{L/2} N_0 d\Omega = \frac{L}{T} N_0. \quad (58)$$

In an appropriate dimensioning, the sampled output sequence \bar{b}_{kL} of the equalizer resembles the linearly transformed version $b_k = (a * g)_k$ of a_k as well as possible. As motivated before, we shall be concerned in this paper with the optimization of the mean-square error

$$\varepsilon \triangleq E_{a,n,\Delta} [(\bar{b}_{kL} - b_k)^2] \quad (59)$$

between \bar{b}_{kL} and b_k , where the expectation is taken over the data, the noise and the ensemble of channel impulse responses. In frequency domain form, ε can be written as

$$\varepsilon = E_{a,n,\Delta} \left[\int_0^1 |\bar{B}(\Omega) - B(\Omega)|^2 d\Omega \right]. \quad (60)$$

Making use of eqs (27) and (55), eq. (60) can be written as

$$\begin{aligned} \varepsilon = \int_0^1 E_a [|A(\Omega)|^2] E_\Delta \left[\left| \frac{T}{L} \sum_{l=0}^{L-1} \mathfrak{F}_{f\Delta} \left(-\frac{l}{L}, \Omega \right) \mathfrak{F}_c \left(\frac{l}{L}, \Omega \right) - G(\Omega) \right|^2 \right] d\Omega \\ + \int_0^1 \frac{T^2}{L^2} \sum_{l=0}^{L-1} E_n [|N_{-l}(\Omega)|^2] \left| \mathfrak{F}_c \left(\frac{l}{L}, \Omega \right) \right|^2 d\Omega, \quad (61) \end{aligned}$$

where use has been made of the statistical independence of the data, the L noise components and the channel parameter Δ . Denoting the power spectral density of the data as $M(\Omega)$ and concluding from eq. (58) that the power spectral density of the noise components equals LN_0 , we can expand eq. (61) into

$$\varepsilon = \int_0^1 M(\Omega) \left[\frac{T^2}{L^2} \sum_{k=0}^{L-1} \sum_{l=0}^{L-1} \mathfrak{F}_c \left(\frac{k}{L}, \Omega \right) \mathfrak{F}_c^* \left(\frac{l}{L}, \Omega \right) \mathcal{K}(k,l,\Omega) \right]$$

$$-2 \operatorname{Re} \left\{ \frac{T}{L} \sum_{k=0}^{L-1} \mathfrak{X}_c \left(\frac{k}{L}, \Omega \right) \overline{\mathfrak{X}_f \left(-\frac{k}{L}, \Omega \right)} G^*(\Omega) \right\} + |G(\Omega)|^2 \Big] d\Omega, \quad (62)$$

where the kernel $\mathcal{H}(k, l, \Omega)$ is defined as

$$\mathcal{H}(k, l, \Omega) \triangleq \overline{\mathfrak{X}_f \left(-\frac{k}{L}, \Omega \right) \mathfrak{X}_f^* \left(-\frac{l}{L}, \Omega \right)} + \frac{L}{TM(\Omega)} \frac{N_0}{L} \delta_{k-l}$$

for all $k, l \in \mathbb{Z}$ and $\Omega \in \mathbb{R}$, (63)

and where the overline denotes averaging with respect to the ensemble of channel impulse responses. Obtained here in a heuristic fashion, this expression can actually be derived in a mathematically rigorous way.

To optimize the Zak transform $\mathfrak{X}_c(\tau, \Omega)$ of the equalizer with respect to ε , standard variational arguments²⁸⁾ can be applied to eq. (62), which lead to the L conditions of optimality

$$\frac{T}{L} \sum_{k=0}^{L-1} \mathfrak{X}_c \left(\frac{k}{L}, \Omega \right) \mathcal{H}(k, l, \Omega) = \overline{\mathfrak{X}_f^* \left(-\frac{l}{L}, \Omega \right)} G(\Omega)$$

for all $l \in \{0, \dots, L-1\}$. (64)

To solve eq. (64), we define an $L \times L$ matrix $K(\Omega)$ having entries

$$K_{k,l}(\Omega) \triangleq \mathcal{H}(k, l, \Omega) \quad \text{for all } k, l \in \{0, \dots, L-1\} \quad (65)$$

and two L -vectors $\mathfrak{X}_c(\Omega)$ and $\overline{\mathfrak{X}_f}(\Omega)$ having entries

$$\mathfrak{X}_{c,k}(\Omega) \triangleq \mathfrak{X}_c \left(\frac{k}{L}, \Omega \right) \quad \text{for all } k \in \{0, \dots, L-1\} \quad (66)$$

and

$$\overline{\mathfrak{X}_{f,k}}(\Omega) \triangleq \overline{\mathfrak{X}_f} \left(-\frac{k}{L}, \Omega \right) \quad \text{for all } k \in \{0, \dots, L-1\}, \quad (67)$$

respectively. In terms of these entities, eqs (62) and (64) can be represented more compactly as

$$\varepsilon = \int_0^1 M(\Omega) \left[\frac{T^2}{L^2} \mathfrak{X}_c^T(\Omega) K(\Omega) \mathfrak{X}_c^*(\Omega) - 2 \frac{T}{L} \operatorname{Re} \{ \mathfrak{X}_c^T(\Omega) \overline{\mathfrak{X}_f}(\Omega) G^*(\Omega) \} + |G(\Omega)|^2 \right] d\Omega \quad (68)$$

and

$$\frac{T}{L}K(\Omega)\mathfrak{X}_c(\Omega) = \overline{\mathfrak{X}_f^*}(\Omega)G(\Omega), \quad (69)$$

respectively, where the superscripts ‘ T ’ and ‘ $*$ ’ denote transposition and component-wise complex conjugation, respectively. Appendix A shows that $K(\Omega)$ is nonsingular, provided that $N_0 > 0$ and that the data sequence has finite power (so that $M(\Omega)$ is bounded for all $\Omega \in \mathbb{R}$). In this case $\mathfrak{X}_c(\Omega)$ can be solved for as

$$\mathfrak{X}_c(\Omega) = \frac{L}{T}K^{-1}(\Omega)\overline{\mathfrak{X}_f^*}(\Omega)G(\Omega). \quad (70)$$

Using eq. (70) in eq. (68), the corresponding mean-square error ε_{\min} is found to equal

$$\varepsilon_{\min} = \int_0^1 M(\Omega)|G(\Omega)|^2[1 - \overline{\mathfrak{X}_f^T}(\Omega)K^{-1}(\Omega)\overline{\mathfrak{X}_f^*}(\Omega)]d\Omega, \quad (71)$$

where the superscript ‘ -1 ’ indicates matrix inversion.

Because of eq. (14), which holds since both $f^\Delta(t)$ and $c(t)$ have zero spectral content outside the interval $\left[-\frac{L}{2}, \frac{L}{2}\right]$, we see that the cascade of channel and equalizer satisfies

$$\mathfrak{X}_{f^\Delta * c}(0, \Omega) = \frac{T}{L}\mathfrak{X}_{f^\Delta}^T(\Omega)\mathfrak{X}_c(\Omega) = \mathfrak{X}_{f^\Delta}^T(\Omega)K^{-1}(\Omega)\overline{\mathfrak{X}_f^*}(\Omega)G(\Omega), \quad (72)$$

where the last equality sign follows from eq. (70). According to eqs (3) and (4), the inverse Fourier transform of this expression specifies the system impulse response $(f^\Delta * c)(t)$ at the nominal sampling instants $t = kT$.

Although the calculation of $K^{-1}(\Omega)$ can (as we shall see later) in certain cases be performed analytically, it will generally involve the use of numerical techniques. Computational effort can be cut by a factor of nearly two by making use of the prior knowledge that the optimum impulse response $c(t)$ is real-valued, so that $\mathfrak{X}_c(\tau, \Omega)$ must satisfy the symmetry condition (11). Hence the set of equations (69) can be roughly halved in size.

For the nonrobust case, a precursor of the above results was obtained in ref. 8. By applying an appropriate transformation, the findings can be represented in terms of Fourier rather than Zak transforms. This is shown in appendix B. In cases (as encountered in sec. 9) where an analytic description of the Δ -dependent channel transfer function is available, this representation will be directly applicable and hence more useful for computational purposes.

For future reference, we note that the factor

$$Z(\Omega) \triangleq [1 - \bar{\mathcal{F}}_f^T(\Omega) K^{-1}(\Omega) \bar{\mathcal{F}}_f^*(\Omega)]^{-1}, \quad (73)$$

the inverse of which is contained in eq. (71), should be nonnegative for all Ω , since otherwise it would be possible to make a choice for $G(\Omega)$ that would lead to a negative mean-square error. A somewhat stronger version of this fact is proved to hold in appendix A, and will turn out to be important in the DFE analysis in the next section.

7. The optimally robust fractionally-spaced decision feedback equalizer

We now augment the polyphase model of fig. 4 with a feedback filter (FBF) which enables previous decisions to assist in taking subsequent ones (fig. 4).

Since only past decisions can effect the detection of the current symbol, the impulse response p_k of the FBF must satisfy the causality constraint

$$p_k = 0 \quad \text{for all } -\infty < k \leq 0. \quad (74)$$

Assisted by the FBF, the DFE attempts to form faithful estimates \hat{a}_k of the transmitted data a_k , which are then applied to a bit-by-bit detector*). To facilitate the analysis, we make the usual assumption that all decisions propagating in the FBF are correct. On the basis of this assumption, which is mostly satisfied under normal operating conditions⁵), eq. (48) can be augmented to yield

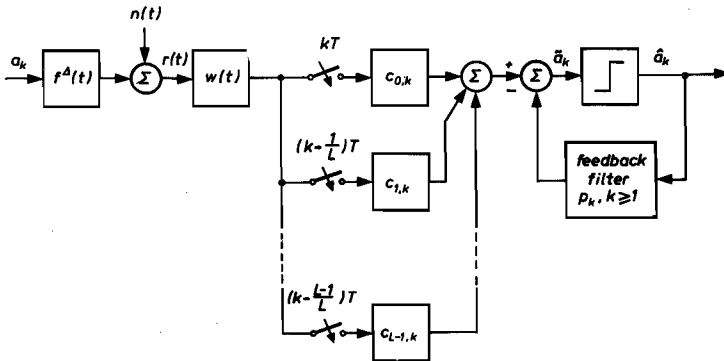


Fig. 4. Data transmission system employing a fractionally spaced polyphase decision-feedback equalizer.

*) Although it is in principle conceivable to reconstruct a linearly transformed version of a_k , it can be shown that this partial response approach can essentially never lead to a better transmission quality than is achievable by direct reconstruction of a_k ¹³).

$$\bar{a}_k = \sum_{l=0}^{L-1} (a * f_{-l}^\Delta * c)_k - (a * p)_k + \sum_{l=0}^{L-1} (n_{-l} * c)_k. \quad (75)$$

Proceeding along the same lines as before, and denoting the Fourier transform of p_k as $P(\Omega)$, it is easy to show that the new mean-square error ε can be denoted in terms of the vectorial Zak transforms $\mathfrak{F}_c(\Omega)$ and $\mathfrak{F}_f(\Omega)$ (as defined in eqs (66) and (67), respectively) as

$$\varepsilon = \int_0^1 M(\Omega) \left[\frac{T^2}{L^2} \mathfrak{F}_c^T(\Omega) K(\Omega) \mathfrak{F}_c^*(\Omega) - 2\text{Re} \left\{ \frac{T}{L} \mathfrak{F}_f^T(\Omega) \mathfrak{F}_c(\Omega) (1 + P^*(\Omega)) \right\} + |1 + P(\Omega)|^2 \right] d\Omega. \quad (76)$$

Except for the factor $1 + P(\Omega)$ which replaces $G(\Omega)$, this expression agrees with expression (68) for the partial response linear equalizer. Consequently, the feedback filter can be thought of as realizing an a priori unknown partial response, and from this point of view our present objective is the joint optimization of the forward part of the equalizer and the partial response determined by the feedback filter.

Identification of the optimally robust DFE amounts to finding the functions $\mathfrak{F}_c(\Omega)$ and $P(\Omega)$ which, subject to eq. (74), minimize ε^*). The solution of this optimization problem is reproduced in appendix C, and centers around the spectral factorization of the function $Z(\Omega)$ as defined in eq. (73). This factorization is possible because $Z(\Omega)$ is real-valued, strictly greater than one, and bounded for all $\Omega \in \mathbb{R}$, as appendix A proves when $N_0 > 0$ and when $M(\Omega)$ is bounded for all $\Omega \in \mathbb{R}$. It results in a representation for $Z(\Omega)$ of the form

$$Z(\Omega) = |\Gamma(\Omega)|^2, \quad (77)$$

where $\Gamma(\Omega)$ is the causal minimum-phase root of $Z(\Omega)$, which is uniquely determined by $Z(\Omega)$ and can be easily determined numerically^{20,29}). According to appendix C, the optimum receiving and feedback filters can for all $\Omega \in \mathbb{R}$ be represented in terms of $\Gamma(\Omega)$ as

$$\mathfrak{F}_c(\Omega) = \frac{L \Gamma(\Omega)}{T \gamma_0} K^{-1}(\Omega) \mathfrak{F}_f^*(\Omega) \quad (78)$$

*) In many instances where an adaptive implementation of the receiving filter is beyond reach, it may still be feasible to implement the feedback filter adaptively, e.g. by making use of the table look-up structure⁴). In deriving the optimum fixed receiving and feedback filters relative to a performance measure accounting for channel parameter variations, we are thus establishing a pessimistic estimate of the truly achievable transmission quality when an adaptive FBF is used.

and

$$P(\Omega) = \frac{\Gamma(\Omega)}{\gamma_0} - 1, \quad (79)$$

where γ_0 is the zeroth term of the inverse Fourier transform γ_k of $\Gamma(\Omega)$, given by

$$\gamma_0 = \exp \left\{ \frac{1}{2} \int_0^1 \ln Z(\Omega) d\Omega \right\} \quad (80)$$

(ref. 29, p. 161). As in the nonrobust situation⁵), the minimum mean-square error ε_{\min} is found to be related to γ_0 as

$$\varepsilon_{\min} = \frac{P_m}{\gamma_0^2}, \quad (81)$$

where P_m is the power of the transmitted data sequence, given by

$$P_m \triangleq \int_0^1 M(\Omega) d\Omega. \quad (82)$$

By comparing eqs (78) and (70), we see that $1 + P(\Omega) = \frac{\Gamma(\Omega)}{\gamma_0}$ can indeed be interpreted as the optimum partial response that we were implicitly looking for.

Because $c(t)$ and the average channel impulse response $\bar{f}(t)$ have zero spectral content outside the interval $\left[-\frac{L}{2}, \frac{L}{2}\right]$, we have from eq. (14) that the average system impulse response satisfies

$$\mathfrak{F}_{\bar{f} * c}(0, \Omega) = \frac{T}{L} \overline{\mathfrak{F}_f^T(\Omega)} \mathfrak{F}_c(\Omega) = \frac{1}{\gamma_0} \left[\Gamma(\Omega) - \frac{1}{\Gamma^*(\Omega)} \right], \quad (83)$$

where the second equality sign follows from (C.11) of appendix C. The inverse Fourier transform of this expression specifies the average system impulse response $(\bar{f} * c)(t)$ at the nominal sampling instants $t = kT$.

Like for the linear equalizer, appendix B shows that these results can be cast into an equivalent Fourier transform representation, which offers computational advantages when an analytic description of the Δ -dependent channel transfer function is available.

Before considering the limiting case $L \rightarrow \infty$, we will first specialize the results obtained so far to the adaptive situation.

8. Fractionally-spaced equalization in the absence of channel parameter variations

The presence of an adaptation mechanism enables the equalizer to be dimensioned in accordance with the instantaneous impulse response $f(t)$ of the channel. This situation can be accounted for in the foregoing sections by dropping all overbars and expectations with respect to the channel ensemble. In this case, the matrix $K(\Omega)$ of eq. (63) is the sum of a full rank matrix $\frac{LN_0}{TM(\Omega)}I$ (with inverse $\frac{TM(\Omega)}{LN_0}I$) and a rank 1 matrix $\mathfrak{F}_f^*(\Omega)\mathfrak{F}_f^T(\Omega)$. Thus the matrix inversion lemma (in the mathematical literature also known as the Sherman-Morrison formula, ref. 30, p. 3) can be applied and we get

$$K^{-1}(\Omega) = \frac{TM(\Omega)}{LN_0} \left[I - \frac{\frac{T}{L}\mathfrak{F}_f^*(\Omega)\mathfrak{F}_f^T(\Omega)}{\frac{T}{L}\sum_{k=0}^{L-1} |\mathfrak{F}_f(-\frac{k}{L}, \Omega)|^2 + \frac{N_0}{M(\Omega)}} \right]. \quad (84)$$

Because $|F(\Omega)| = 0$, $|\Omega| \geq \frac{L}{2}$, we can use eq. (15) to simplify the sum contained in this expression as

$$\frac{T}{L}\sum_{l=0}^{L-1} |\mathfrak{F}_f(-\frac{l}{L}, \Omega)|^2 = \mathfrak{F}_{f*f_-}(0, \Omega), \quad (85)$$

where $(f*f_-)(t)$ is the autocorrelation function of the channel impulse response $f(t)$. With eqs (84) and (85), the function $Z(\Omega)$ cf. (73) can also be evaluated explicitly:

$$Z(\Omega) = 1 + \frac{M(\Omega)\mathfrak{F}_{f*f_-}(0, \Omega)}{N_0} \quad (86)$$

Now the optimum fractionally-spaced linear and decision feedback equalizers as well as their performance can be determined explicitly. Using eqs (84) to (86) in eqs (70), (71), (78), (80) and (81), we have that for the linear equalizer

$$\mathfrak{E}_c\left(\frac{l}{L}, \Omega\right) = \frac{G(\Omega)\mathfrak{F}_f^*\left(-\frac{l}{L}, \Omega\right)}{\mathfrak{F}_{f*f_-}(0, \Omega) + \frac{N_0}{M(\Omega)}} \quad \text{for all } l \in \{0, \dots, L-1\} \text{ and } \Omega \in \mathbb{R}, \quad (87)$$

and

$$\varepsilon_{\min} = \int_0^1 \frac{N_0 |G(\Omega)|^2}{\mathfrak{X}_{f^*f}(0, \Omega) + \frac{N_0}{M(\Omega)}} d\Omega, \quad (88)$$

while for the DFE

$$\mathfrak{X}_c\left(\frac{l}{L}, \Omega\right) = \frac{\frac{1}{\gamma_0} \Gamma(\Omega) \mathfrak{X}_f^*\left(-\frac{l}{L}, \Omega\right)}{\mathfrak{X}_{f^*f}(0, \Omega) + \frac{N_0}{M(\Omega)}} \quad \text{for all } l \in \{0, \dots, L-1\} \text{ and } \Omega \in \mathbb{R}, \quad (89)$$

and

$$\varepsilon_{\min} = P_m \exp \left\{ \int_0^1 \ln \left[\frac{\frac{N_0}{M(\Omega)}}{\mathfrak{X}_{f^*f}(0, \Omega) + \frac{N_0}{M(\Omega)}} \right] d\Omega \right\}. \quad (90)$$

To convert these expressions into Fourier transform notation, we first apply eq. (7) to show that

$$\mathfrak{X}_{f^*f}(0, \Omega) = \frac{1}{T} \sum_{n=-\infty}^{\infty} |F(\Omega + n)|^2 \quad \text{for all } \Omega. \quad (91)$$

We next note that besides $F(\Omega)$, the Fourier transform $C(\Omega)$ of $c(t)$ is (by construction) also bandlimited to $\left[-\frac{L}{2}, \frac{L}{2}\right]$. Thus eq. (13) can be applied after multiplying the left and right hand sides of eqs (87) and (89) by $\exp(-j2\pi\frac{l}{L}\Omega)$ and summing over all l . Together with eq. (91), this yields the conventional expressions

$$C(\Omega) = \frac{F^*(\Omega) G(\Omega)}{\frac{1}{T} \sum_{n=-\infty}^{\infty} |F(\Omega + n)|^2 + \frac{N_0}{M(\Omega)}} \quad \text{for all } \Omega \in \mathbb{R}, \quad (92)$$

and

$$C(\Omega) = \frac{\frac{1}{\gamma_0} F^*(\Omega) \Gamma(\Omega)}{\frac{1}{T} \sum_{n=-\infty}^{\infty} |F(\Omega + n)|^2 + \frac{N_0}{M(\Omega)}} \quad \text{for all } \Omega \in \mathbb{R} \quad (93)$$

for the linear and the decision feedback equalizer, respectively^{3,31,13}). Because of eq. (91), we see at once that the performance expressions (88) and (90) coincide with the familiar ones for the continuous-time MMSE linear and decision feedback equalizers^{3,31,13}). Hence fractionally-spaced equalization yields the same performance as equalization without prior structural restrictions, provided that the tap spacing L is chosen sufficiently large to guarantee that $|F(\Omega)| = 0$, $|\Omega| \geq \frac{L}{2}$. Since ε_{\min} does not directly depend upon $f(t)$ but only on its autocorrelation function $(f * f_{-})(t)$, which is not affected by time shifts of $f(t)$ as induced by timing errors, we conclude that, unlike the symbol interval-spaced situation considered before, timing errors can be compensated for without loss of performance.

9. Optimum equalization without prior structural restrictions

For the adaptive fractionally-spaced equalizers, we have just shown that beyond a certain oversampling factor L , determined by the characteristics of the channel, performance and dimensioning expressions arise which coincide with their continuous-time counterparts. The optimally robust continuous-time equalizers can be obtained on the basis of the results of secs 7 and 8 by letting L grow infinitely large. This limiting operation turns sums into integrals, because for any continuous function $\mathcal{X}(\tau, \Omega)$

$$\lim_{L \rightarrow \infty} \frac{T}{L} \sum_{l=0}^{L-1} \mathcal{X}\left(-\frac{l}{L}, \Omega\right) = T \int_0^1 \mathcal{X}(-\tau, \Omega) d\tau. \quad (94)$$

By way of example, we shall for the linear equalizer briefly review the consequences of this limiting operation for the preceding analysis. Using eq. (94), we see that expression (62) now becomes

$$\varepsilon = \int_0^1 M(\Omega) \left[T^2 \int_0^1 \int_0^1 \mathcal{X}_c(\mu, \Omega) \mathcal{X}_c^*(\tau, \Omega) \mathcal{H}_{\infty}(\mu, \tau, \Omega) d\mu d\tau - 2\text{Re} \left\{ T \int_0^1 \mathcal{X}_c(\tau, \Omega) \overline{\mathcal{X}_f(-\tau, \Omega)} G^*(\Omega) d\tau \right\} + |G(\Omega)|^2 \right] d\Omega, \quad (95)$$

where the kernel

$$\mathcal{H}_{\infty}(\mu, \tau, \Omega) \triangleq \overline{\mathcal{X}_f(-\mu, \Omega) \mathcal{X}_f^*(-\tau, \Omega)} + \frac{N_0}{TM(\Omega)} \delta(\tau - \mu), \quad (96)$$

in which $\delta(\tau)$ is the Dirac delta function, is the continuous-time counterpart of $\mathcal{H}(k, l, \Omega)$ as defined in eq. (63). The associated condition of optimality (cf. eq. (69)) can be denoted in operator notation as

$$T(K_\infty \mathfrak{L}_c)(\tau, \Omega) = G(\Omega) \overline{\mathfrak{L}_f^*}(-\tau, \Omega), \tag{97}$$

where $K_\infty(\Omega)$ is the integral operator associated with $\mathcal{H}_\infty(\mu, \tau, \Omega)$, operating on the time variable only. For an account of the theory of linear operators in a Hilbert space the reader is referred to ref. 28. Because (cf. appendix A) $\mathcal{H}_\infty(\mu, \tau, \Omega)$ is positive definite if $N_0 > 0$ and if $M(\Omega)$ is bounded for all $\Omega \in \mathbb{R}$, $\mathfrak{L}_c(\tau, \Omega)$ can (cf. eq. (70)) be solved as

$$\mathfrak{L}_c(\tau, \Omega) = \frac{1}{T} G(\Omega) (K_\infty^{-1} \overline{\mathfrak{L}_f^*})(\tau, \Omega). \tag{98}$$

Like eq. (71), this solution leads to a minimum mean-square error

$$\varepsilon_{\min} = \int_0^1 M(\Omega) |G(\Omega)|^2 Z^{-1}(\Omega) d\Omega, \tag{99}$$

where the function $Z(\Omega)$ (cf. eq. (73)) is now given by

$$Z(\Omega) = \left[1 - \int_0^1 \overline{\mathfrak{L}_f}(\tau, \Omega) (K_\infty^{-1} \overline{\mathfrak{L}_f^*})(\tau, \Omega) d\tau \right]^{-1} \tag{100}$$

To specialize eqs (98) and (99) to their nonrobust versions, it suffices to drop the overbars in eqs (95), (96) and (97). For $\mathfrak{L}_c(\tau, \Omega)$ this yields the integral equation

$$T \mathfrak{L}_f^*(-\tau, \Omega) \int_0^1 \mathfrak{L}_f(-\mu, \Omega) \mathfrak{L}_c(\mu, \Omega) d\mu + \frac{N_0}{M(\Omega)} \mathfrak{L}_c(\tau, \Omega) = G(\Omega) \mathfrak{L}_f^*(-\tau, \Omega), \tag{101}$$

which should be satisfied for all $\tau \in [0, 1]$ and all $\Omega \in \mathbb{R}$. It can be confirmed by inspection that the continuous-time version

$$\mathfrak{L}_c(\tau, \Omega) = \frac{G(\Omega) \mathfrak{L}_f^*(-\tau, \Omega)}{\mathfrak{L}_{f^*f}(0, \Omega) + \frac{N_0}{M(\Omega)}} \tag{102}$$

of eq. (87) provides the desired (and expected) solution, which can be used in eq. (95) to re-assert that the corresponding minimum mean-square error is given by eq. (88).

The DFE analysis of secs 7 and 8 can also be extended to $L \rightarrow \infty$ by incorporating minor modifications, similar to the ones above. Although for didactic reasons we have presented the continuous-time analysis here as a limiting case of the fractionally-spaced analysis, it is by no means necessary to take this somewhat lengthy detour. This is exemplified in ref. 32, where the optimally robust continuous-time DFE is derived in a direct and compact way.

10. Improvement of resistance to timing errors in digital magnetic recording

For a class of digital magnetic recording systems suffering from timing errors, we shall in this section compare the merits of the robust equalizers found in secs 8 and 9 with those of their conventional counterparts.

We first describe the transfer characteristics of the systems, which use an NRZ-like transmission code, longitudinal magnetization and a differentiating playback head. When both the thickness of the magnetic recording medium and the gap size of the playback head are sufficiently small, the nominal transfer characteristic $F(\Omega)$ of a system within this class assumes the form³³⁾

$$F(\Omega) = (1 - \exp(-j2\pi\Omega)) \exp(-\pi D|\Omega|), \quad (103)$$

where D is normalized measure of the information density of the system, ranging from roughly 0.1 for low-density (e.g. rigid disk-drive) systems to about 3 for high density (e.g. R-DAT³⁴⁾) systems.

For numerical convenience, we shall take the recorded data sequence a_k to be uncorrelated, so that $M(\Omega) = 1$. For the purpose of the present comparison, this assumption is sufficiently valid in e.g. R-DAT-systems, where an 8-to-10 transmission code³⁵⁾ is applied.

In the presence of timing errors (i.e. when sampling erroneously takes place at the instants $(k + \Delta)T$ with $k \neq 0$, cf. sec. 4), conventional MMSE equalizers often incur significant performance losses^{36,37)}. The influence of sampling phase errors can be accounted for by incorporating the normalized sampling phase Δ in eq. (103) as

$$\begin{aligned} F^\Delta(\Omega) &\triangleq F(\Omega) \exp(j2\pi\Delta\Omega) \\ &= [1 - \exp(-j2\pi\Omega)] \exp(-\pi D|\Omega|) \exp(j2\pi\Delta\Omega) \quad \text{for all } \Omega. \end{aligned} \quad (104)$$

For mathematical convenience, we shall assume the values of Δ to be uniformly distributed in the interval $[-\Theta, \Theta]$, where $\Theta \in [0, \frac{1}{2}]$ determines the maximum possible sampling phase deviation. A typical value of Δ would be 0.1³⁷⁾.

Because in this case an explicit description of the Δ -dependent system transfer characteristics is available, the optimally robust data equalizers can be most easily identified in their Fourier transform representation as described in appendix B. It is easy to see that the vector $\bar{F}(\Omega)$ and the matrix $\bar{K}(\Omega)$ of appendix B have components

$$\bar{F}_i(\Omega) = [1 - \exp(-j2\pi\Omega)] \frac{\sin 2\pi\Theta(\Omega + i)}{2\pi\Theta(\Omega + i)} \exp(-\pi D|\Omega + i|) \quad (105)$$

and

$$\bar{K}_{i,j}(\Omega) = 4 \frac{1}{T} \sin^2(\pi\Omega) \frac{\sin 2\pi \Theta(i-j)}{2\pi \Theta(i-j)} \exp(-\pi D[|\Omega+i| + |\Omega+j|]) + N_0 \delta_{i-j}, \quad (106)$$

respectively¹²). The components of $\bar{K}(\Omega)$ are real-valued, which facilitates numerical effort.

For a given density D , the minimally required oversampling factor L can be determined by imposing the condition that the energy outside the band $\left[-\frac{L}{2}, \frac{L}{2}\right]$ of $F(\Omega)$ is an insignificant fraction of the total energy. On the basis of eq. (103) it can be seen that for even L this fraction equals $\exp(-\pi D L)$. Hence a suitable even value of L can be determined as

$$L = 2 \left\lceil -\frac{\ln 10}{20\pi} \frac{\alpha}{D} \right\rceil, \quad (107)$$

where $\lceil \cdot \rceil$ denotes the integer ceiling function, while α is the maximum fraction of out-of-band energy expressed in dB, fixed at -40 in the forthcoming calculations. Thus, at a high density D of 2.5 it suffices to take $L = 2$, while for a (very small) density D of 0.2 a relatively large oversampling factor of about 16 is needed. Involving the inversion of a set of 16×16 matrices, even the latter value of D does not pose insurmountable numerical problems.

Using the results of appendix B, we have determined for various values of D and Θ the optimally robust data equalizers and their performance. In our calculations, we have assumed a fixed signal-to-noise ratio

$$\text{SNR} \triangleq \frac{(f * f_-)(0)}{N_0} \quad (108)$$

of 25 dB. To assess the performance of the equalizers we have used the effective signal-to-noise ratio loss \mathcal{L} as defined in refs 12 and 36. This measure, which can be easily determined numerically, quantifies the performance loss of a receiver relative to the matched filter (zero ISI) bound³), assessing residual ISI in terms of its L_1 norm. As such, it is more meaningful than the Δ -dependent mean-square error, which reflects the power of the residual ISI. For realistic signal-to-noise ratios, an improvement of \mathcal{L} of one dB corresponds to an improvement of the bit error rate of roughly an order of magnitude.

At a (medium) density D of 1, the performance of the full response linear equalizer (having $g(\mathcal{D}) = 1$) is distinctly inferior to its partial response coun-

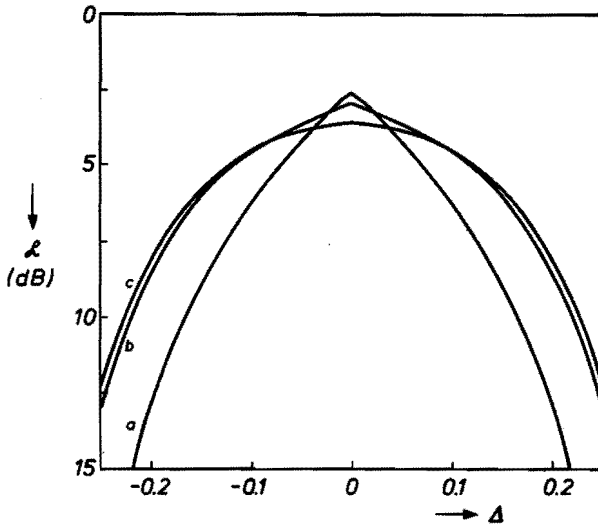


Fig. 5. Effective signal-to-noise ratio loss \mathcal{L} versus normalized sampling phase error Δ for the Bipolar linear equalizer ($g(\mathcal{D}) = 1 - \mathcal{D}$). Signal-to-noise ratio SNR = 25 dB; Normalized information density $D=1$; a) $\theta = 0$; b) $\theta = 0.05$; c) $\theta = 0.1$.

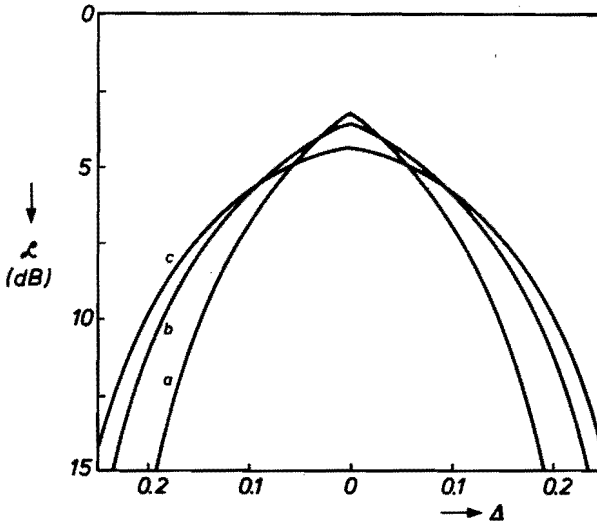


Fig. 6. Effective signal-to-noise ratio loss \mathcal{L} versus normalized sampling phase error Δ for the Class IV partial response linear equalizer ($g(\mathcal{D}) = 1 - \mathcal{D}^2$). Signal-to-noise ratio SNR = 25 dB; Normalized information density $D=1$; a) $\theta = 0$; b) $\theta = 0.05$; c) $\theta = 0.1$.

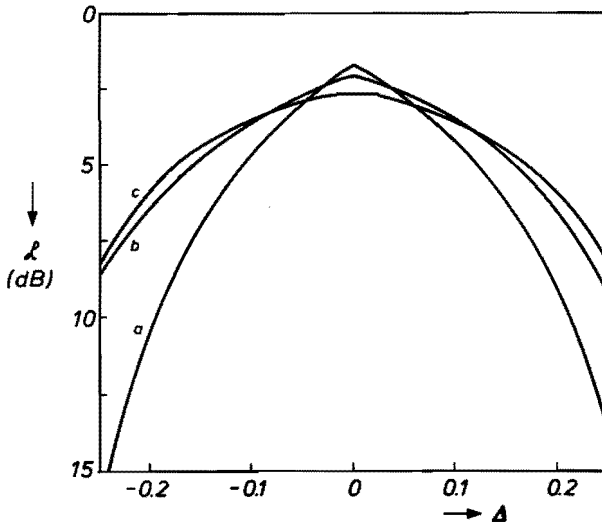


Fig. 7. Effective signal-to-noise ratio loss \mathcal{L} versus normalized sampling phase error Δ for the decision feedback equalizer (DFE). Signal-to-noise ratio SNR=25 dB; Normalized information density $D=1$; a) $\Theta = 0$; b) $\Theta = 0.05$; c) $\Theta = 0.1$.

terparts and the DFE¹³). For conventional and optimally robust versions of the latter equalizers we have evaluated the effective signal-to-noise ratio loss when sampling phase variations occur ranging from -25 percent to $+25$ percent of a bit interval T (figs 5 to 7). Comparing the $\Theta = 0$ curves of figs 5 to 7, we see that the Bipolar and Class IV partial response linear equalizers (having $g(\mathcal{D}) = 1 - \mathcal{D}$ and $g(\mathcal{D}) = 1 - \mathcal{D}^2$, respectively) have comparable performances and that the DFE is some 1 dB better. For the $\Theta = 0$ equalizers, timing errors apparently induce significant performance losses, which amount to some 4.5 dB for realistic sampling phase errors with $|\Delta| \approx 0.1$. At an expense of some 0.4 dB to the nominal performance, the robust equalizers with $\Theta = 0.05$ manage to restrict these losses to 3 dB for the $1 - \mathcal{D}^2$ LE (fig. 6), to 2 dB for the $1 - \mathcal{D}$ LE (fig. 5), and to a mere 1.5 dB for the DFE (fig. 7). At a further expense of 0.6 to 0.8 dB, the $\Theta = 0.1$ equalizers maintain a useful performance level over an even wider range of operating conditions. For example, under adverse conditions with $|\Delta| \approx 0.15$, the $\Theta = 0.1$ equalizers outperform their conventional counterparts by 2.5 to 3 dB, corresponding to a bit error rate which is several orders of magnitude smaller.

To show the reason for the decreased performance in the nominal situation, figs 8 and 9 depict the amplitude-frequency characteristics $|C(\Omega)|$ of the $1 - \mathcal{D}$ and $1 - \mathcal{D}^2$ equalizers of figs 5 and 6, respectively. Similarly, fig. 10

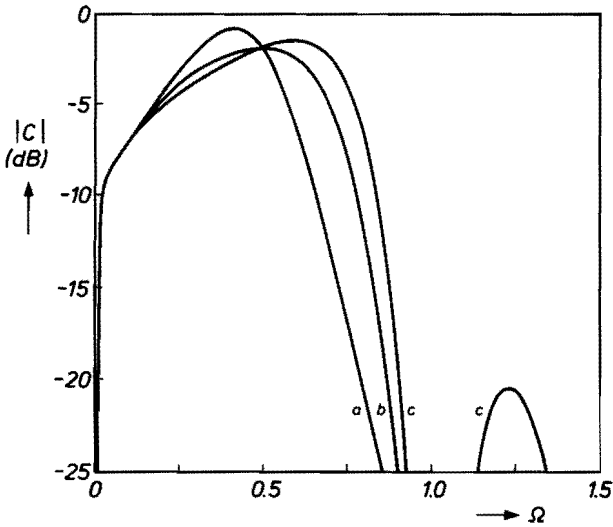


Fig. 8. Amplitude frequency characteristics $|C(\Omega)|$ of the Bipolar $(1 - \mathcal{D})$ linear equalizers of fig. 5. a) $\theta = 0$; b) $\theta = 0.05$; c) $\theta = 0.1$.

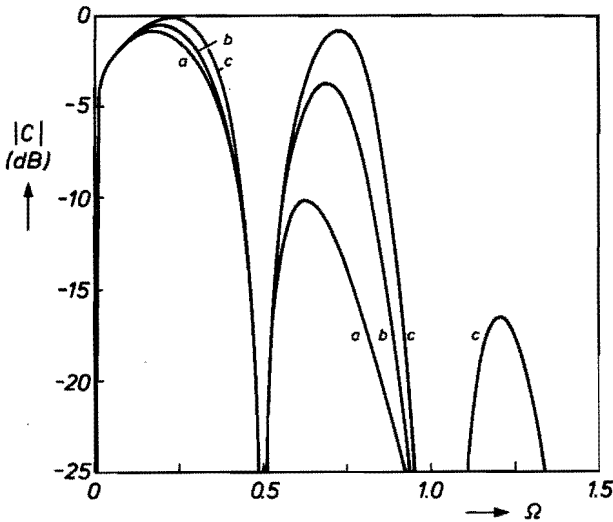


Fig. 9. Amplitude frequency characteristics $|C(\Omega)|$ of the Class IV partial response $(1 - \mathcal{D}^2)$ linear equalizers of fig. 6. a) $\theta = 0$; b) $\theta = 0.05$; c) $\theta = 0.1$.

depicts the receiving filter amplitude-frequency characteristics $|C(\Omega)|$ of the DFE's of fig. 7. In order to enable a direct comparison these figures have the same 0dB level. Compared to the $\theta = 0$ characteristics, the reduced

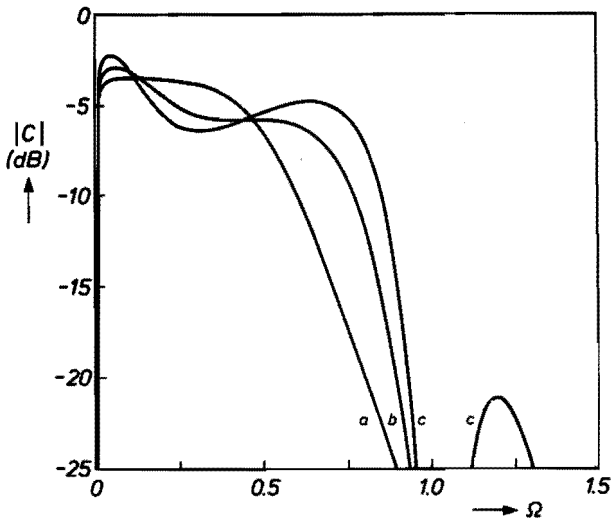


Fig. 10. Receiving filter amplitude-frequency characteristics $|C(\Omega)|$ of the decision feedback equalizers (DFE's) of fig. 7. a) $\Theta = 0$; b) $\Theta = 0.05$; c) $\Theta = 0.1$.

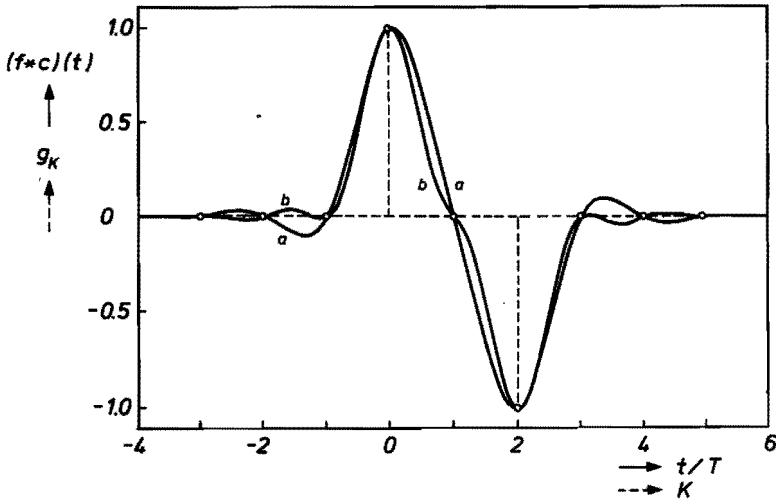


Fig. 11. Nominal system impulse response $(f+c)(t)$ created by the Class IV partial response $(1 - \mathcal{D}^2)$ linear equalizers of fig. 6. a) $\Theta = 0$; b) $\Theta = 0.1$; The desired sampled impulse response g_k is also depicted (dashed).

transfer magnitude of the $\Theta = 0.05$ and $\Theta = 0.1$ characteristics at frequencies roughly below the Nyquist frequency $\Omega = 0.5$ is traded off against a considerably larger transfer magnitude at higher frequencies, so that a net incre-

ment of the noise enhancement results. Apart from a degradation of the nominal performance, this high-frequency emphasis leads to a significantly smaller quantity of residual ISI in the presence of timing errors. This is clarified in fig. 11 for the Class IV partial response LE and in fig. 12 for the DFE.

From fig. 11, we see that for $\Theta = 0$ the overall system impulse response $(f * c)(t)$ indeed approximates the desired $1 - \mathcal{D}^2$ response (shown dashed) accurately when sampling takes place at the nominal instants $t/T = k$. However, the resemblance rapidly deteriorates in the presence of sampling phase errors (which amount to a shift of $(f * c)(t)$ relative to g_k). This causes increased residual ISI and thus a decreased transmission quality. In contrast, for $\Theta = 0.1$ the system impulse response $(f * c)(t)$ has a considerably smaller slope in the vicinity of the nominal sampling instants $t/T = k$, so that the effect of modest sampling phase errors is less detrimental. Similar remarks apply to the $\Theta = 0$ and $\Theta = 0.1$ curves of fig. 12. In this figure, we see that in the absence of timing errors, the post-cursive ISI which shows up in the trailing part of the system impulse response $(f * c)(t)$ is perfectly compensated by the action of the feedback filter (with impulse response p_k). While for the $\Theta = 0$ DFE a small shift of the timebase already leads to significant compensation errors (and hence residual ISI), the small slope of $(f * c)(t)$ around the post-cursive nominal sampling instants causes these errors to be much smaller for the $\Theta = 0.1$ DFE.

The combined effect of increased noise enhancement and decreased re-

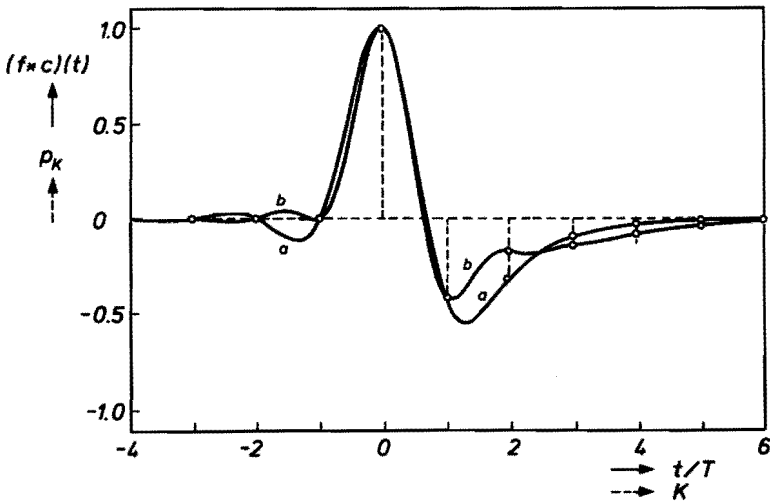


Fig. 12. Nominal system impulse response $(f * c)(t)$ created by the DFE's of fig. 7. a) $\Theta = 0$; b) $\Theta = 0.1$; The corresponding feedback filter impulse responses p_k are also depicted (dashed).

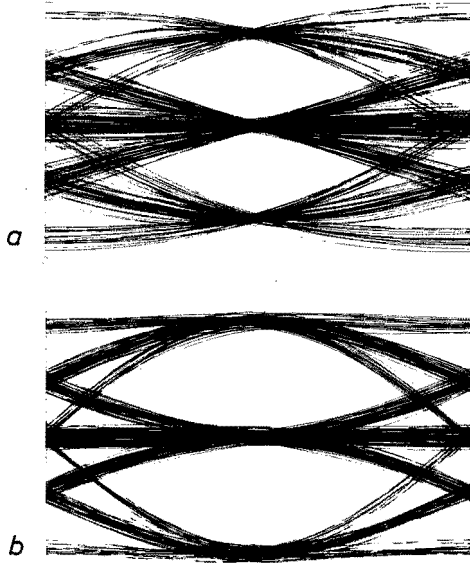


Fig. 13. Eye patterns for the Class IV partial response linear equalizers of fig. 6. Signal-to-noise ratio SNR=25 dB; Normalized information density $D = 1$. a) $\theta = 0$; b) $\theta = 0.1$.

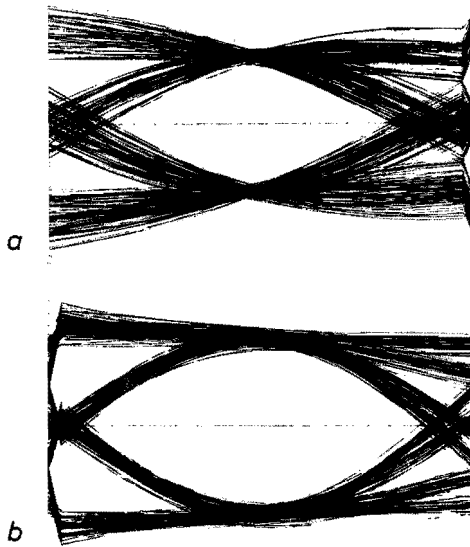


Fig. 14. Eye patterns for the decision feedback equalizers of fig. 7. Signal-to-noise ratio SNR=25 dB; Normalized information density $D = 1$. a) $\theta = 0$; b) $\theta = 0.1$.

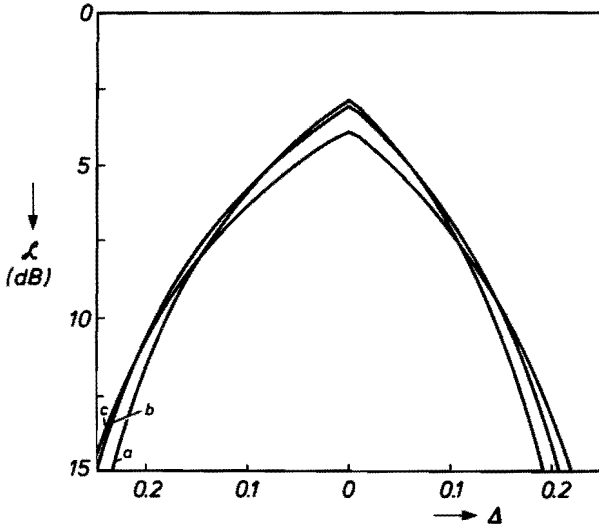


Fig. 15. Effective signal-to-noise ratio loss \mathcal{L} versus normalized sampling phase error Δ for the decision feedback equalizer (DFE). Signal-to-noise ratio SNR=25 dB; Normalized information density $D=2.5$; a) $\theta = 0$; b) $\theta = 0.05$; c) $\theta = 0.1$.

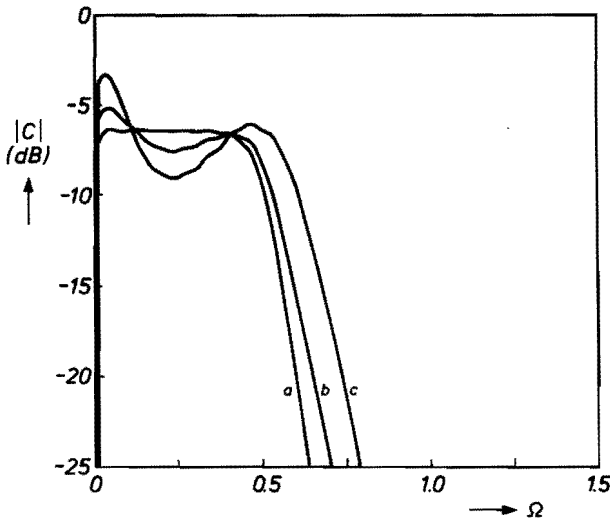


Fig. 16. Receiving filter amplitude-frequency characteristics $|C(\Omega)|$ of the decision feedback equalizers of fig. 15. a) $\theta = 0$; b) $\theta = 0.05$; c) $\theta = 0.1$.

sidual ISI in the presence of timing errors is most clearly illustrated by means of eye patterns. Figs 13 and 14 depict eye patterns that were constructed by

computer simulation for the equalizers of figs 5 and 7, respectively. For maximum visual clarity, the DFE used for the construction of fig. 14 contains a hold function which causes changes of the FBF output signal to occur only midway the nominal sampling instants $t/T = k$. Looking at figs 13 and 14, we see that the $\Theta = 0.1$ eye patterns are indeed somewhat more noisy, but clearly more robust to timing errors than their $\Theta = 0$ counterparts.

For a high density D of 2.5, it was shown in ref. 12 that among the linear equalizers only the full-response variant could for $\Theta \neq 0$ be equipped with an appreciably better resistance to timing errors. For the sake of brevity, we shall not review these results here. For both the conventional DFE and its robust version, fig. 15 depicts the effective signal-to-noise ratio loss incurred at $D = 2.5$ in the presence of sampling phase errors. Although some margin against timing errors can be added by choosing $\Theta > 0$, fig. 15 clearly indicates that significant improvements are beyond reach. Interestingly, the Δ -dependent mean-square error does exhibit significant improvements for $\Theta > 0$. This observation confirms our initial doubts about the ability of the adopted quality measure to quantify residual ISI accurately. Nevertheless, the robust DFE still outperforms its linear counterparts, as can be seen from figs 5 and 6 of ref. 12. Like for $D = 1$ (fig. 10), the main difference between the receiving filter amplitude-frequency characteristics of the robust DFE and the conventional one is the increased emphasis of the lowest and highest frequencies. This is illustrated in fig. 16, whose 0dB level coincides with that

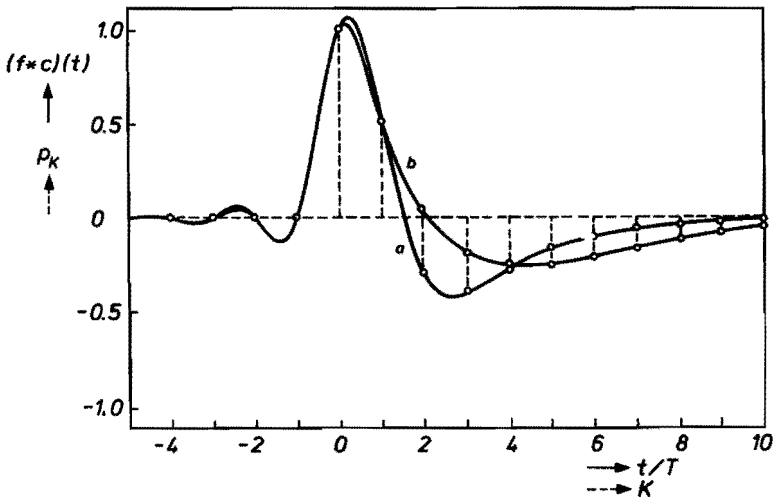


Fig. 17. Nominal system impulse response $(f*c)(t)$ created by the DFE's of fig. 15. a) $\Theta = 0$; b) $\Theta = 0.1$; The corresponding feedback filter impulse responses p_k are also depicted (dashed).

of fig. 7 of ref. 12, so that a comparison is allowed. The system impulse response $(f * c)(t)$ of the robust $\Theta = 0.1$ equalizer differs particularly for $t \geq 0$ significantly from its $\Theta = 0$ counterpart, as shown in fig. 17. As before, the $\Theta = 0.1$ equalizer achieves a favourable reduction of the slope of $(f * c)(t)$ at the post-cursive nominal sampling instants $t/T = k$. Unfortunately, this advantage is largely offset by the significantly increased duration of the trailing part of $(f * c)(t)$, which leads to a larger number of residual ISI components in the presence of timing errors.

11. Concluding remarks

The quadratic performance measure used in this paper makes the problem of finding the optimally robust linear and decision feedback equalizers analytically tractable, but has the disadvantage that the residual intersymbol interference is quantified in terms of its power rather than the more relevant L_1 -norm. Thus, while the foregoing results will often lead to significant improvements of robustness (cf. figs. 5 to 7), it may happen (as indeed observed in sec. 10 and fig. 15) that significant improvements in mean-square terms lead to a negligible actual improvement of robustness.

Although we have confined attention to the reception part of the data transmission problem in this paper, one might expect from the preceding pages that the Zak transform can be comparably useful for analyzing other aspects of data transmission. In fact, it seems reasonable to conjecture that the Zak transform is a natural tool for use in any environment where both continuous-time and discrete-time aspects play a role, digital audio and video systems perhaps being major examples. For further reading on the Zak transform, its properties and its relations with the Fourier integral, the Wigner distribution and other signal representations we refer the reader to a companion paper¹⁹⁾.

As a final remark, we note that the Zak transform bears some similarity to the eye pattern, which is often used in data transmission as a display tool and also maps a continuous-time signal by means of a periodic overlap procedure onto a unit interval in which only sampling phases can be distinguished. In view of this similarity and its information lossless nature (as opposed to the non-invertible nature of the eye pattern), it seems rewarding to explore the value of the Zak transform as a display tool in data transmission.

Appendix A. Regularity of $K(\Omega)$; positiveness and boundedness of $Z(\Omega)$

In this appendix we shall show that, under proper conditions on N_0 and

$M(\Omega)$, the inverse $K^{-1}(\Omega)$ of the matrix $K(\Omega)$ as defined in eq. (65) exists. Subject to slightly stronger conditions, we shall furthermore show that the function $Z(\Omega)$ as defined in eq. (73) is positive and bounded. We shall neither in this appendix nor in the following ones question ourselves whether the functions under consideration are well-behaved, rapidly decaying, and the like. Such properties can be readily guaranteed by casting the treatment into a (more voluminous) Hilbert space framework and imposing some weak additional conditions of regularity (cf. e.g. the appendix of ref. 12).

We first develop some notation. We shall denote the inner product of two L -vectors U and V as

$$(U, V) \triangleq U^T V^*, \quad (\text{A.1})$$

and the norm of an L -vector U as

$$\|U\| \triangleq \sqrt{(U, U)}. \quad (\text{A.2})$$

Let $\mathfrak{X}_{f\Delta}(\Omega)$ be the L -vector with components

$$\mathfrak{X}_{f\Delta}(\Omega) \triangleq \mathfrak{X}_{f\Delta}(-\frac{l}{L}, \Omega) \quad \text{for all } l \in \{0, \dots, L-1\}. \quad (\text{A.3})$$

In terms of $\mathfrak{X}_{f\Delta}(\Omega)$, the matrix $K(\Omega)$ as defined in eq. (65) can equivalently be defined as

$$K(\Omega) \triangleq E_{\Delta}[\mathfrak{X}_{f\Delta}^*(\Omega)\mathfrak{X}_{f\Delta}^T(\Omega)] + \frac{LN_0}{TM(\Omega)}I, \quad (\text{A.4})$$

where I is the $L \times L$ identity matrix, and $E_{\Delta}[\cdot]$ denotes averaging with respect to the ensemble of channel impulse responses. Let the vector $\overline{\mathfrak{X}}_f(\Omega)$ be as defined in eq. (67), and let the $L \times L$ matrix $Q(\Omega)$ be defined as

$$Q(\Omega) \triangleq \overline{\mathfrak{X}}_f^*(\Omega)\overline{\mathfrak{X}}_f^T(\Omega). \quad (\text{A.5})$$

Proposition A.1

Let $N_0 > 0$ and let $M(\Omega)$ be bounded for all $\Omega \in \mathbb{R}$. Then the matrix $K(\Omega) - Q(\Omega)$ is for all $\Omega \in \mathbb{R}$ positive definite with eigenvalues no smaller than $\frac{LN_0}{TM(\Omega)}$.

Proof

It can be observed from eqs (A.4) and (A.5) that the matrices $K(\Omega)$ and

$Q(\Omega)$ are both Hermitian. Hence the same must be true for their difference. From eqs (A.4), (73) and (A.5), we have that for any L -vector x

$$x^T[K(\Omega) - Q(\Omega)]x^* = E[x, \mathfrak{F}_{f\Delta}(\Omega)]^2 - (x, E[\mathfrak{F}_{f\Delta}(\Omega)])^2 + \frac{LN_0}{TM(\Omega)} \|x\|^2. \quad (\text{A.6})$$

Since the variance of any stochastic variable can never be smaller than the square of its average, it follows that for all x

$$x^T[K(\Omega) - Q(\Omega)]x^* \geq \frac{LN_0}{TM(\Omega)} \|x\|^2, \quad (\text{A.7})$$

and because $\frac{N_0}{M(\Omega)}$ is strictly positive, it follows that $K(\Omega) - Q(\Omega)$ must be positive definite. For any Hermitian matrix $K(\Omega) - Q(\Omega)$,

$$\min_{x \neq 0} x^T [K(\Omega) - Q(\Omega)]x^* = \lambda_{\min}(\Omega) \|x\|^2, \quad (\text{A.8})$$

where $\lambda_{\min}(\Omega)$ is the smallest eigenvalue of $k(\Omega) - Q(\Omega)$. From eqs (A.7) and (A.8), we conclude that $\lambda_{\min}(\Omega)$ is at least equal to $\frac{L N_0}{TM(\Omega)}$.

Proposition A.2

Let the conditions of proposition A.1 apply. Then $K(\Omega)$ is non-singular.

Proof

By repeating the argument of proposition A.1 for the quadratic form $x^T K(\Omega) x^*$ it follows that $K(\Omega)$ is positive definite with smallest eigenvalue at least equal to $\frac{L N_0}{TM(\Omega)} > 0$. Thus $K(\Omega)$ must be non-singular.

Proposition A.3

Let the vector $\overline{\mathfrak{F}}_f(\Omega)$ for all $\Omega \in \mathbb{R}$ have a nonzero norm $\|\overline{\mathfrak{F}}_f(\Omega)\|$. Let $N_0 > 0$ and let $M(\Omega)$ be bounded for all $\Omega \in \mathbb{R}$. Then the quadratic form $\overline{\mathfrak{F}}_f^T(\Omega) K^{-1}(\Omega) \overline{\mathfrak{F}}_f^*(\Omega)$ assumes a value in the interval (0,1), i.e.

$$0 < \overline{\mathfrak{F}}_f^T(\Omega) K^{-1}(\Omega) \overline{\mathfrak{F}}_f^*(\Omega) < 1. \quad (\text{A.9})$$

Proof

Since $K^{-1}(\Omega)$ exists, $\|\overline{\mathfrak{F}}_f(\Omega)\| \neq 0$ and $\frac{N_0}{M(\Omega)} > 0$, we have that

$$\begin{aligned}
 0 < \frac{LN_0}{TM(\Omega)} \|K^{-1}(\Omega) \bar{\mathfrak{F}}_f^*(\Omega)\|^2 \\
 &= \frac{LN_0}{TM(\Omega)} (K^{-1}(\Omega) \bar{\mathfrak{F}}_f^*(\Omega), K^{-1}(\Omega) \bar{\mathfrak{F}}_f^*(\Omega)). \quad (\text{A.10})
 \end{aligned}$$

According to proposition A.1, $K(\Omega) - Q(\Omega)$ is positive definite with eigenvalues at least equal to $\frac{L}{TM(\Omega)} N_0 > 0$. For this reason, the right hand side of eq. (A.10) can be lower bounded as

$$\begin{aligned}
 \frac{LN_0}{TM(\Omega)} \|K^{-1}(\Omega) \bar{\mathfrak{F}}_f^*(\Omega)\|^2 &\leq ([K(\Omega) - Q(\Omega)] K^{-1}(\Omega) \bar{\mathfrak{F}}_f^*(\Omega), K^{-1}(\Omega) \bar{\mathfrak{F}}_f^*(\Omega)) \\
 &= (\bar{\mathfrak{F}}_f^*(\Omega), K^{-1}(\Omega) \bar{\mathfrak{F}}_f(\Omega)) \\
 &\quad - (Q(\Omega) K^{-1}(\Omega) \bar{\mathfrak{F}}_f^*(\Omega), K^{-1}(\Omega) \bar{\mathfrak{F}}_f^*(\Omega)) \\
 &= \bar{\mathfrak{F}}_f^T(\Omega) K^{-1}(\Omega) \bar{\mathfrak{F}}_f^*(\Omega) \\
 &\quad - \|\bar{\mathfrak{F}}_f^T(\Omega) K^{-1}(\Omega) \bar{\mathfrak{F}}_f^*(\Omega)\|^2 \quad (\text{A.11})
 \end{aligned}$$

where the last equality follows from eq. (A.5). Since the function $f(x) = x(1 - x)$ is positive only in the interval (0,1), we conclude from eqs (A.10) and (A.11) that eq. (A.9) must hold.

Corollary

The function $Z(\Omega) \triangleq [1 - \bar{\mathfrak{F}}_f^T(\Omega) K^{-1}(\Omega) \bar{\mathfrak{F}}_f^*(\Omega)]^{-1}$ is, subject to the conditions of proposition A.3, strictly greater than one and bounded for all $\Omega \in \mathbb{R}$.

Appendix B. Frequency domain representation of the optimally robust equalizers

In this appendix we derive the frequency domain representation of the optimally robust equalizers from their Zak transform representations derived before. For mathematical convenience, we shall take L to be an even integer, so that $L/2$ is an integer. The case of odd L can be similarly handled by using a set $\left\{-\frac{L+1}{2}, \dots, \frac{L+1}{2}\right\}$ and an interval $\left[-\frac{1}{2}, \frac{1}{2}\right]$ instead of $\left\{-\frac{L}{2}, \dots, \frac{L}{2}-1\right\}$ and $[0,1]$, respectively, in what follows. Before stating and proving the results, we first introduce the frequency domain entities of interest.

Let $C(\Omega)$ and $F^A(\Omega)$ be the Fourier transforms of the receiving filter and channel impulse responses $c(t)$ and $f^A(t)$, respectively, and let the L -vectors $C(\Omega)$ and $F^A(\Omega)$ be defined as

$$C_i(\Omega) \triangleq C(\Omega + i) \quad \text{for all } i \in \left\{-\frac{L}{2}, \dots, \frac{L}{2} - 1\right\} \text{ and } \Omega \in [0, 1], \quad (\text{B.1})$$

and

$$F_i^A(\Omega) \triangleq F^A(\Omega + i) \quad \text{for all } i \in \left\{-\frac{L}{2}, \dots, \frac{L}{2} - 1\right\} \text{ and } \Omega \in [0, 1], \quad (\text{B.2})$$

respectively. It can be observed from these definitions that $C(\Omega)$ and $F^A(\Omega)$ describe the potentially nonzero components (for which $|\Omega| < \frac{L}{2}$) of $W(\Omega)$ and $F^A(\Omega)$. Denote

$$\bar{F}(\Omega) \triangleq E_{\Delta}[F^A(\Omega)] \quad \text{for all } \Omega \in [0, 1], \quad (\text{B.3})$$

where $E_{\Delta}[\cdot]$ denotes averaging with respect to the ensemble of channel characteristics. Similarly, let $\bar{K}(\Omega)$ be the $L \times L$ matrix

$$\bar{K}(\Omega) \triangleq \frac{1}{T} E_{\Delta}[F^{A*}(\Omega) F^{AT}(\Omega)] + \frac{N_0}{M(\Omega)} I \quad \text{for all } \Omega \in [0, 1], \quad (\text{B.4})$$

with I the $L \times L$ identity matrix. Finally, let $R(\Omega)$ be the $L \times L$ matrix with entries

$$R_{l,n}(\Omega) \triangleq \exp(-j2\pi(n + \Omega)\frac{l}{L}) \quad \text{for all } l \in \{0, \dots, L-1\},$$

$$n \in \left\{-\frac{L}{2}, \dots, \frac{L}{2} - 1\right\} \text{ and } \Omega \in \mathbb{R}. \quad (\text{B.5})$$

Proposition B.1

Let $K(\Omega)$ be defined as in eq. (65). Let $N_0 > 0$ and let $M(\Omega)$ be bounded for all $\Omega \in \mathbb{R}$. Then $\bar{K}(\Omega)$ as defined above is nonsingular, and we have for $\Omega \in [0, 1]$ that

$$R^T(\Omega) K^{-1}(\Omega) R^*(\Omega) = T \bar{K}^{-1}(\Omega). \quad (\text{B.6})$$

Proof

By making use of the fact that for integer n

$$\sum_{l=0}^{L-1} \exp(j2\pi n \frac{l}{L}) = \begin{cases} L, & n = 0 \text{ mod } L, \\ 0, & \text{else,} \end{cases} \quad (\text{B.7})$$

it can be easily verified that $R(\Omega)$ is nonsingular for all $\Omega \in \mathbb{R}$, and that

$$R^{-1}(\Omega) = \frac{1}{L} R^T(\Omega) \quad \text{for all } \Omega \in \mathbb{R}. \quad (\text{B.8})$$

Thus we have that

$$\begin{aligned} A(\Omega) &\triangleq [R^T(\Omega) K^{-1}(\Omega) R^*(\Omega)]^{-1} \\ &= \frac{1}{L^2} R^T(\Omega) K(\Omega) R(\Omega) \quad \text{for all } \Omega \in [0,1]. \end{aligned} \quad (\text{B.9})$$

This inversion is always possible because $K(\Omega)$ is nonsingular according to appendix A under the given conditions. Applying eq. (B.5) to expand the right hand side of this expression, we see that the components $A_{i,n}(\Omega)$ of $A(\Omega)$ are given by

$$\begin{aligned} A_{i,j}(\Omega) &= \frac{1}{L^2} \sum_{l=0}^{L-1} \sum_{n=0}^{L-1} \exp(j2\pi(\Omega+i)\frac{l}{L}) K_{l,n}(\Omega) \exp(-j2\pi(\Omega+j)\frac{n}{L}) \\ &\quad \text{for all } i,j \in \left\{ -\frac{L}{2}, \dots, \frac{L}{2} - 1 \right\} \text{ and } \Omega \in [0,1]. \end{aligned} \quad (\text{B.10})$$

By making use of eqs (7), (63), (65) and (B.7), and the fact that $F^A(\Omega) = 0$, $|\Omega| > \frac{L}{2}$, it can be easily verified that

$$\begin{aligned} A_{i,j}(\Omega) &= \frac{1}{T^2} E[F^A(\Omega+i) F^{A*}(\Omega+j)] + \frac{1}{T} \frac{N_0}{M(\Omega)} \delta_{i-j} \\ &\quad \text{for all } i,j \in \left\{ -\frac{L}{2}, \dots, \frac{L}{2} - 1 \right\} \text{ and } \Omega \in [0,1]. \end{aligned} \quad (\text{B.11})$$

Comparing eq. (B.11) and eq. (B.4), we see that

$$A(\Omega) = \frac{1}{T} \tilde{K}(\Omega), \quad (\text{B.12})$$

and by combining eq. (B.12) with eq. (B.9), eq. (B.6) follows.

Proposition B.2

Let $N_0 > 0$ and let $M(\Omega)$ be bounded for all $\Omega \in \mathbb{R}$. Let $K(\Omega)$ and $\bar{\mathcal{F}}_f(\Omega)$ be defined as in eq. (65) and (67), and let $Z(\Omega)$ for $\Omega \in [0,1]$ be given

by (see eq. (73))

$$Z(\Omega) \triangleq [1 - \overline{\mathfrak{F}}_f^T(\Omega) K^{-1}(\Omega) \overline{\mathfrak{F}}_f^*(\Omega)]^{-1}. \quad (\text{B.13})$$

Then $Z(\Omega)$ can alternatively be written as

$$Z(\Omega) = [1 - \frac{1}{T} \overline{F}^T(\Omega) \check{K}^{-1}(\Omega) \overline{F}^*(\Omega)]^{-1} \quad \text{for all } \Omega \in [0,1]. \quad (\text{B.14})$$

Proof

By applying eq. (5) to the Zak transform $\overline{\mathfrak{F}}_f(\tau, \Omega)$ evaluated at the instants $\tau = -\frac{l}{L}$, $l \in \{0, \dots, L-1\}$, it follows that

$$\overline{\mathfrak{F}}_f(-\frac{l}{L}, \Omega) = \frac{1}{T} \sum_{n=-\infty}^{\infty} \overline{F}(\Omega + n) \exp(-j2\pi(\Omega + n)\frac{l}{L}) \quad \text{for all } \Omega \in \mathbb{R}, \quad (\text{B.15})$$

where $\overline{F}(\Omega) = E_{\Delta}[F^A(\Omega)]$, compare eq. (B.3). Because $\overline{F}(\Omega)$ vanishes outside the interval $[-\frac{L}{2}, \frac{L}{2}]$, this expression can be more compactly written as

$$\overline{\mathfrak{F}}_f(\Omega) = \frac{1}{T} R(\Omega) \overline{F}(\Omega) \quad \text{for all } \Omega \in [0,1], \quad (\text{B.16})$$

where $R(\Omega)$, $\overline{F}(\Omega)$ and $\overline{\mathfrak{F}}_f(\Omega)$ are defined in eqs (B.5), (B.3) and (67), respectively. Using eq. (B.16) in eq. (B.13), we now have that

$$Z(\Omega) = [1 - \frac{1}{T^2} \overline{F}^T(\Omega) R^T(\Omega) K^{-1}(\Omega) R^*(\Omega) \overline{F}^*(\Omega)]^{-1}, \quad (\text{B.17})$$

and with proposition B.1 (B.14) is established.

Proposition B.3

Let $N_0 > 0$ and let $M(\Omega)$ be bounded for all $\Omega \in \mathbb{R}$. Let $K(\Omega)$ and $\overline{\mathfrak{F}}_f(\Omega)$ be defined as in eqs (65) and (67). Then the optimally robust linear equalizer satisfies

$$C(\Omega) = G(\Omega) \check{K}^{-1}(\Omega) \overline{F}^*(\Omega) \quad \text{for all } \Omega \in [0,1]. \quad (\text{B.18})$$

Proof

By translating eq. (52) to the frequency domain and making use of eq. (54), we see that

$$C(\Omega) = W(\Omega) \frac{T}{L} \sum_{l=0}^{L-1} \mathfrak{X}_c\left(\frac{l}{L}, \Omega\right) \exp(-j2\pi\Omega\frac{l}{L}) \quad \text{for all } \Omega \in \mathbb{R}. \quad (\text{B.19})$$

Since $W(\Omega)$ equals zero outside the interval $\left[-\frac{L}{2}, \frac{L}{2}\right]$, $C(\Omega)$ can only inside this interval assume nonzero values. These can be grouped into the L -vector $C(\Omega)$ as defined in eq. (B.1), so that the nontrivial part with $|\Omega| \leq \frac{L}{2}$ of eq. (B.19) can be denoted more compactly as

$$C(\Omega) = \frac{T}{L} R^T(\Omega) \mathfrak{X}_c(\Omega) \quad \text{for all } \Omega \in [0,1]. \quad (\text{B.20})$$

By combining this expression with the one for the Zak transform of the optimally robust linear equalizer (70), we see that

$$C(\Omega) = G(\Omega) R^T(\Omega) K^{-1}(\Omega) \bar{\mathfrak{X}}_f^*(\Omega) \quad \text{for all } \Omega \in [0,1], \quad (\text{B.21})$$

and by applying eq. (B.16) and proposition B.1 the proof is complete.

Note

The expressions (B.6) and (B.18) have previously been derived in ref. 12 without the aid of the Zak transform.

Proposition B.4

Let $N_0 > 0$ and let $M(\Omega)$ be bounded for all $\Omega \in \mathbb{R}$. Let $K(\Omega)$ and $\bar{\mathfrak{X}}_f(\Omega)$ be defined as in eqs (65) and (67). Then the optimally robust DFE satisfies

$$C(\Omega) = \frac{\Gamma(\Omega)}{\gamma_0} \tilde{K}^{-1}(\Omega) \bar{F}^*(\Omega) \quad \text{for all } \Omega \in [0,1]. \quad (\text{B.22})$$

and

$$P(\Omega) = \frac{\Gamma(\Omega)}{\gamma_0} - 1, \quad (\text{B.23})$$

where $\Gamma(\Omega)$ is the unique causal minimum-phase root of $Z(\Omega)$ as given in proposition B.2, and γ_k is the inverse Fourier transform of $\Gamma(\Omega)$.

Proof

The proof of this proposition is similar to the one of proposition B.3.

Appendix C. Identification of the optimally robust decision feedback equalizer

In this appendix we shall determine the vectorial Zak transform $\mathfrak{X}_c(\Omega)$ of the receiving filter and the Fourier transform $P(\Omega)$ of the feedback filter which minimize the mean-square error

$$\varepsilon \triangleq \int_0^1 M(\Omega) \left[\frac{T^2}{L^2} \mathfrak{X}_c^T(\Omega) K(\Omega) \mathfrak{X}_c^*(\Omega) - 2\text{Re} \left\{ \frac{T}{L} \overline{\mathfrak{X}}_f^T(\Omega) \mathfrak{X}_c(\Omega) \right. \right. \\ \left. \left. (1 + P^*(\Omega)) \right\} + |(1 + P(\Omega))|^2 \right] d\Omega, \quad (\text{C.1})$$

subject to the causality constraint

$$p_k = 0 \quad \text{for all } k \leq 0 \quad (\text{C.2})$$

on the inverse Fourier transform p_k of $P(\Omega)$.

Before stating and proving the results, we outline the notation used in this appendix. Apart from the vectorial Zak transform $\mathfrak{X}_c(\Omega)$, we shall use the polyphase impulse responses $c_{l,k}$ as defined in eq. (43) to describe the receiving filter. The feedback filter will be described by means of its Fourier transform $P(\Omega)$ or, equivalently, by its impulse response p_k . Finally, the average channel will be described in terms of both its vectorial Zak transform $\overline{\mathfrak{X}}_f(\Omega)$ and its polyphase impulse responses

$$\tilde{f}_{-l,k} \triangleq E_{\Delta} [f^{\Delta}((-\frac{l}{L} + k)T)] \quad \text{for all } l \in \{0, \dots, L-1\}, \quad (\text{C.3})$$

where $E_{\Delta}[\cdot]$ denotes averaging with respect to the channel ensemble.

Proposition C.1

The conditions

$$\frac{T}{L} K(\Omega) \mathfrak{X}_c(\Omega) = \overline{\mathfrak{X}}_f^*(\Omega) (1 + P(\Omega)) \quad \text{for all } \Omega \in \mathbb{R}, \quad (\text{C.4})$$

and

$$p_k = \sum_{l=0}^{L-1} (\tilde{f}_l * c_l)_k \quad \text{for all } k \geq 1, \quad (\text{C.5})$$

are necessary for the receiving and feedback filters to minimize ε .

Proof

Condition (C.4) follows immediately from eq. (C.1) by variation with re-

spect to the components $\mathfrak{X}_c(\frac{l}{L}, \Omega)$, $l \in \{0, \dots, L - 1\}$, of $\mathfrak{X}_c(\Omega)$. Condition (C.5) follows by translating eq. (C.1) into the equivalent time domain expression and variation with respect to the coefficients p_j , $j \geq 1$.

Proposition C.2

Let $Z(\Omega)$ be defined as in eq. (73), i.e.

$$Z(\Omega) = [1 - \overline{\mathfrak{X}}_f^T(\Omega) K^{-1}(\Omega) \overline{\mathfrak{X}}_f^*(\Omega)]^{-1}, \quad (\text{C.6})$$

and let $\Gamma(\Omega)$ be the causal minimum-phase root of $Z(\Omega)$, for which

$$Z(\Omega) = |\Gamma(\Omega)|^2. \quad (\text{C.7})$$

Then $\Gamma(\Omega)$ exists when $N_0 > 0$ and when $M(\Omega)$ is bounded for all $\Omega \in \mathbb{R}$, and the receiving and feedback filters which optimize ε cf. eq. (C.1) have

$$\mathfrak{X}_c(\Omega) = \frac{L \Gamma(\Omega)}{T \gamma_0} K^{-1}(\Omega) \overline{\mathfrak{X}}_f^*(\Omega) \quad \text{for all } \Omega \in \mathbb{R} \quad (\text{C.8})$$

and

$$P(\Omega) = \frac{\Gamma(\Omega)}{\gamma_0} - 1 \quad \text{for all } \Omega \in \mathbb{R}, \quad (\text{C.9})$$

where γ_0 is the zeroth term of the inverse Fourier transform γ_k of $\Gamma(\Omega)$.

Proof

The existence of a causal minimum-phase root $\Gamma(\Omega)$ of $Z(\Omega)$ is governed by the Paley-Wiener condition²⁰⁾

$$\int_0^1 \ln \dot{Z}(\Omega) d\Omega > -\infty, \quad (\text{C.10})$$

which is certainly satisfied when $Z(\Omega)$ is strictly greater than one and bounded for all Ω . According to appendix A, this is so when $N_0 > 0$ and when $M(\Omega)$ is bounded for all $\Omega \in \mathbb{R}$. Thus having ascertained the existence of $\Gamma(\Omega)$ (which can be calculated from $Z(\Omega)$ by means of e.g. the recursive procedure described in ref. 38), we next express $\Gamma(\Omega)$ in eq. (C.8) with the aid of eq. (C.9) in terms of $P(\Omega)$. This demonstrates that $\mathfrak{X}_c(\Omega)$ and $P(\Omega)$ as given by eqs (C.8) and (C.9) jointly satisfy eq. (C.4). These functions also satisfy eq. (C.5), as we shall now demonstrate. To this end, we first combine eqs (C.8), (C.9), (C.6) and (C.7) to show that

$$\frac{T}{L} \mathfrak{F}_f^T \mathfrak{F}_c(\Omega) = \frac{1}{\gamma_0} [\Gamma(\Omega) - \frac{1}{\Gamma^*(\Omega)}] = 1 + P(\Omega) - \frac{1}{\gamma_0 \Gamma^*(\Omega)}. \quad (\text{C.11})$$

Making use of eqs. (50), (54), (66) and (67), the inverse Fourier transform of this expression is seen to equal

$$\sum_{l=0}^{L-1} (\hat{f}_l * c_l)_k = \delta_k + p_k - \frac{1}{\gamma_0} \gamma_k^{-1} \quad \text{for all } k, \quad (\text{C.12})$$

where γ_k^{-1} is the inverse Fourier transform of $\frac{1}{\Gamma(\Omega)}$. Because $\Gamma(\Omega)$ has minimum-phase, the sequence γ_k^{-1} must be anticausal. Thus for $k \geq 1$, eq. (C.12) coincides with eq. (C.5). This concludes the proof.

Proposition C.3

The minimum mean-square error ε_{\min} achieved by the optimally robust DFE equals

$$\varepsilon_{\min} = \frac{P_m}{\gamma_0^2} = P_m \exp \left\{ - \int_0^1 \ln Z(\Omega) d\Omega \right\}, \quad (\text{C.13})$$

where P_m is the power of the transmitted data sequence, i.e.

$$P_m \triangleq \int_0^1 M(\Omega) d\Omega. \quad (\text{C.14})$$

Proof

Combination of (C.8) and (C.6) ascertains that

$$\mathfrak{F}_c^T(\Omega) K(\Omega) \mathfrak{F}_c^*(\Omega) = \frac{L^2 |\Gamma(\Omega)|^2}{T^2 \gamma_0^2} \left[1 - \frac{1}{Z(\Omega)} \right] = \frac{L^2}{T^2} \frac{1}{\gamma_0^2} [Z(\Omega) - 1]. \quad (\text{C.15})$$

Using eqs (C.15), (C.11), (C.9), (C.7) and (C.14) in eq. (C.1) we obtain the first equality of eq. (C.13). The second one is a standard result from spectral factorization theory (ref. 29, pp. 161-162).

REFERENCES

- ¹⁾ W.R. Bennett and J.R. Davey, Data Transmission, McGraw-Hill, New York, 1965.
- ²⁾ R.W. Lucky, J. Salz and E.J. Weldon, Jr., Principles of Data Communication, McGraw-Hill, New York, 1968.
- ³⁾ J.G. Proakis, Digital Communications, New York, McGraw-Hill, 1983.
- ⁴⁾ P.J. van Gerwen, N.A.M. Verhoeckx and T.A.C.M. Claassen, IEEE J. Selected Areas Commun. SAC-2, 314 (1984).

- 5) S.U. Qureshi, Proc. IEEE, **73**, 1349 (1985).
- 6) L. Guidoux, L'Onde Electronique **55**, 9 (1975).
- 7) G. Ungerboeck, IEEE Trans. Commun. **COM-24**, 856 (1976).
- 8) R.D. Gitlin and S.B. Weinstein, Bell Syst. Tech. J. **60**, 275 (1981).
- 9) G. Bouwhuis, J. Braat, A. Huijser, J. Pasman, G. van Rosmalen and K. Schouhamer Immink, Principles of Optical Disc Systems, Adam Hilger Ltd., Bristol and Boston, 1985.
- 10) R.W. Wood, Proc. IEEE **74**, 1557 (1986).
- 11) R.A. Gonsalves and D.W. Tufts, IEEE Trans. Commun. Technol. **COM-16**, 375 (1968).
- 12) J.W.M. Bergmans, Philips J. of Res. **42**, 310 (1987).
- 13) J.W.M. Bergmans, Philips J. of Res. **42**, 208 (1987).
- 14) J. Zak, Physical Review Letters **19**, 1385 (1967).
- 15) G. D. Forney, Jr., IEEE Trans. Inf. Th. **IT-18**, 363 (1972).
- 16) P. van der Wurf and O. Rikkert de Koe, Proc. IEEE **57**, 701 (1969).
- 17) W. A. Gardner, IEEE Trans. Commun. **COM-34**, 1089 (1986).
- 18) D. G. Messerschmitt, IEEE Trans. Commun. **COM-34**, 1209 (1986).
- 19) A. J. E. M. Janssen, Philips J. of Res. **42**, to appear (1987).
- 20) A. Papoulis, Signal Analysis, McGraw-Hill, New York, 1984.
- 21) H. Nyquist, Trans. AIEE (Commun. and Electronics) **47**, 617 (1928).
- 22) P. Kabal and S. Pasupathy, IEEE Trans. Commun. **COM-23**, 921 (1975).
- 23) D.D. Falconer and F.R. Magee, Jr., Bell Syst. Tech. J. **55**, 1541 (1973).
- 24) J.E. Mazo, Bell Syst. Tech. J. **54**, 189 (1975).
- 25) F.R. Magee, Jr., IEEE Trans. Commun. **COM-23**, 361 (1975).
- 26) R.E. Crochiere and L.R. Rabiner, Multirate Digital Signal Processing, Prentice-Hall Inc., Englewood Cliffs, New Jersey 07632, 1983.
- 27) J.M. Wozencraft and I.M. Jacobs, Principles of Communication Engineering, Wiley, New York, 1965.
- 28) L.A. Ljusternik and W.I. Sobolew, Elemente der Funktionsanalyse, Akademie-Verlag, Berlin, 1955.
- 29) J.L. Doob, Stochastic Processes, New York, Wiley, 1953.
- 30) G.H. Golub and Charles F. van Loan, Matrix Computations, North Oxford Academic, John Hopkins University Press, Baltimore, Maryland, 1983.
- 31) P. Monsen, IEEE Trans. Inf. Th. **IT-17**, 55 (1971).
- 32) J.W.M. Bergmans and A.J.E.M. Janssen, Proc. Int. Symp. Mathematical Theory of Networks and Systems, Phoenix, Arizona, June 15-19, 1987; also in Proc. Eighth Symp. on Information Theory in the Benelux, Deventer, the Netherlands, May 21-22, 1987.
- 33) J.W.M. Bergmans, Philips J. of Res. **41**, 531 (1986).
- 34) H. Nakajima and M. Kosaka, IEEE Trans. Cons. Electr. **CE-32**, 404 (1986).
- 35) K.A. Schouhamer Immink, Philips J. of Res. **42**, 22 (1985).
- 36) J.W.M. Bergmans, Philips J. of Res. **42**, 283 (1987).
- 37) H. Osawa, S. Tazaki and S. Ando, IEEE Trans. Magn. **MAG-22**, 253 (1986).
- 38) D.G. Messerschmitt, Rec. Int. Conf. Commun. **ICC-74**, (Minneapolis, MN), pp. 37D1-37D5.

Biography

Jan W. M. Bergmans was born in Tilburg, The Netherlands, on August 15, 1957. He received the Ingenieur degree in electrical engineering from Eindhoven University of Technology, Eindhoven, The Netherlands, in 1981. After spending his military service as manager for communication projects in the Royal Netherlands Navy, he joined Philips Research Laboratories, Eindhoven, in 1982. There, he has been engaged in research on digital transmission and recording, with special emphasis on algorithmic design tools, smearing filters, and equalization and detection methods. He is a member of the IEEE, of the executive board of the Nederlands Electronica- en Radio Genootschap (NERG) and of the URSI committee of The Netherlands.

Samenvatting

Systemen voor transmissie of registratie van digitale informatie hebben vaak te kampen met intersymboolinterferentie (ISI) en ruis. Data-egalisatoren dienen om de ongewenste gevolgen van deze verschijnselen te minimaliseren. Met behulp van één of meer filters vormen zij schattingen van de verzonden datasymbolen, waaruit beslissingen genomen worden met behulp van een detector.

Dit proefschrift handelt over de toepassing van partiële-responsie technieken in data-egalisatie. Deze technieken behelzen het introduceren van beperkte en bekende ISI en het detecteren van gecorrleerde datasymbolen met een toegenomen aantal data-niveau's, waaruit de oorspronkelijke datasymbolen worden teruggevonden door middel van een deterministische terugtransformatie. Het proefschrift toont aan dat deze indirecte aanpak kan leiden tot systemen die beter bestand zijn tegen ruis en minder lijden aan foutvoortplanting.

Bij de beschouwingen over data-egalisatie wordt vervolgens de robuustheid van data-egalisatoren betrokken, dat wil zeggen hun capaciteit om naar behoren te functioneren bij variaties van de systeem-parameters. Deze eigenschap is in het bijzonder van belang wanneer data-egalisatoren niet adaptief kunnen worden uitgevoerd, zoals het geval kan zijn bij hoge datasnelheden, of wanneer de toelaatbare vermogens-dissipatie beperkt is. Bij deze beschouwingen wordt de robuustheid van diverse conventionele egalisatie- en detectiemethoden geanalyseerd en worden geoptimaliseerde robuuste versies van de meest gangbare data-egalisatoren afgeleid, waarbij als kwaliteitscriterium een gemiddelde kwadratische foutmaat geldt.

De resultaten van de analyse worden geïllustreerd met kwaliteitsvergelijkingen voor een klasse van digitale magnetische registratie-systemen. Daartoe wordt allereerst een eenvoudige tijddiscrete karakterisatie van deze systemen afgeleid. Naast conventionele egalisatiemethoden worden ook ISI-compensatie en detectie van de meest waarschijnlijke reeks van verzonden datasymbolen in deze vergelijkingen betrokken.

STELLINGEN

**bij het proefschrift van J. W. M. Bergmans
8 september 1987, Technische Universiteit, Eindhoven**

I

De zienswijze dat toepassing van partiële responsie-technieken niet kan leiden tot een verbetering van de transmissiekwaliteit is onjuist.

- P. Kabal and S. Pasupathy, *IEEE Trans. Commun.* **COM-23**, 921 (1975).
E. R. Kretzmer, *IEEE Trans. Commun. Technol.* **COM-14**, 67 (1966).
R. W. Lucky, J. Salz, and E. J. Weldon, Jr., *Principles of Data Communication*, McGraw-Hill, New York, 1968, pp. 83-90.

II

De beperkte decodeervertraging van de door Gersho en Lim geïntroduceerde 'canceller of intersymbol interference' is een belangrijke oorzaak voor de vaak teleurstellende kwaliteit van dit ontvangertype.

- A. Gersho and T. Lim, *Bell Syst. Tech. J.* **60**, 1997 (1981).

III

Bij het bestrijden van de gevolgen van overspraak van digitale signalen is het aantrekkelijk om gebruik te maken van hun cyclostationaire karakter.

- S. Nakagawa, K. Yokoyama and H. Katayama, *IEEE Trans. Magn.* **MAG-16**, 104 (1980).
G. Bouwhuis, J. Braat, A. Huijser, J. Pasman, G. van Rosmalen and K. Schouhamer Immink, *Principles of Optical Disc Systems*, Adam Hilger Ltd., Bristol, U.K., 1985, pp. 49-53.
J. C. Campbell, A. J. Gibbs and B. M. Smith, *IEEE Trans. Commun.* **COM-33**, 629 (1983).

IV

De door Zak voor toepassingen in de kwantummechanica geïntroduceerde signaaltransformatie is bij uitstek geschikt voor het analyseren van cyclostationaire signalen en systemen.

J. Zak, *Physical Review Letters* **19**, 1385 (1967).

V

Het getuigt van onzorgvuldigheid om de impulsresponsie van een lineair tijdinvariant systeem voor te stellen als een signaal.

M. L. Meade and C. R. Dillon, *Signals and Systems (Models and Behaviour)*, v. Nostrand-Reinhold, U.K., 1986, p. 28.

A. B. Carlson, *Communication Systems*, McGraw-Hill, Tokyo, 1975, p. 59.

A. P. Clark, *Advanced Data-Transmission Systems*, Pentech Press, London, 1977, p. 13.

VI

Voor data-ontvangers waarin adaptatie aan de systeemp parameters plaatsvindt op basis van een gemiddelde kwadratische foutmaat, kan een vergroting van het aantal vrijheidsgraden door toevoeging van niet-lineaire filters, zoals voorgesteld door o.a. Falconer, onbedoeld leiden tot een beduidend slechtere transmissiekwaliteit.

D. D. Falconer, *Bell Syst. Tech. J.* **57**, 2589 (1978).

VII

De door Vry en door Ehrenbard en Tompsett beschreven adaptatie-algoritmes kunnen leiden tot een ongewenste filter-instelling.

M. G. Vry, Proc. ISSLS'84, Nice, France, pp. 259-263, 1984.

C. A. Ehrenbard and M. F. Tompsett, Proc. GLOBECOM'82, Miami, USA, pp. D.8.4.1-D.8.4.5, 1982.

VIII

De praktische verwezenlijking van de voordelen van recursieve digitale filters wordt ernstig gehinderd door het ontbreken van krachtige en gebruikersvriendelijke ontwerpprogramma's.

A. V. Oppenheim and R. W. Schaffer, Digital Signal processing, Prentice-Hall, Inc., Englewood Cliffs, New Jersey, 1975, pp. 268-269.

L. R. Rabiner and B. Gold, Theory and Application of Digital Signal Processing, Prentice-Hall, Inc., Englewood Cliffs, New Jersey, 1975, pp. 40-46.

R. E. Crochiere and L. R. Rabiner, Multirate Digital Signal processing, Prentice-Hall, Inc., Englewood Cliffs, New Jersey, 1983, pp. 130-131.

IX

Het verleden is haast net zo onzeker als de toekomst.